Approaches towards Molecular Construction of a Synthetic Vaccine against Hepatitis C Virus

Theodorus Joannes Meuleman, M.Sc.

Submitted in fulfilment of the requirements for the degree of Doctor of Philosophy (PhD)

School of Chemistry
College of Science and Engineering
University of Glasgow

December 2019

I dedicate this thesis to my fellow Knights of the Rectangular Table

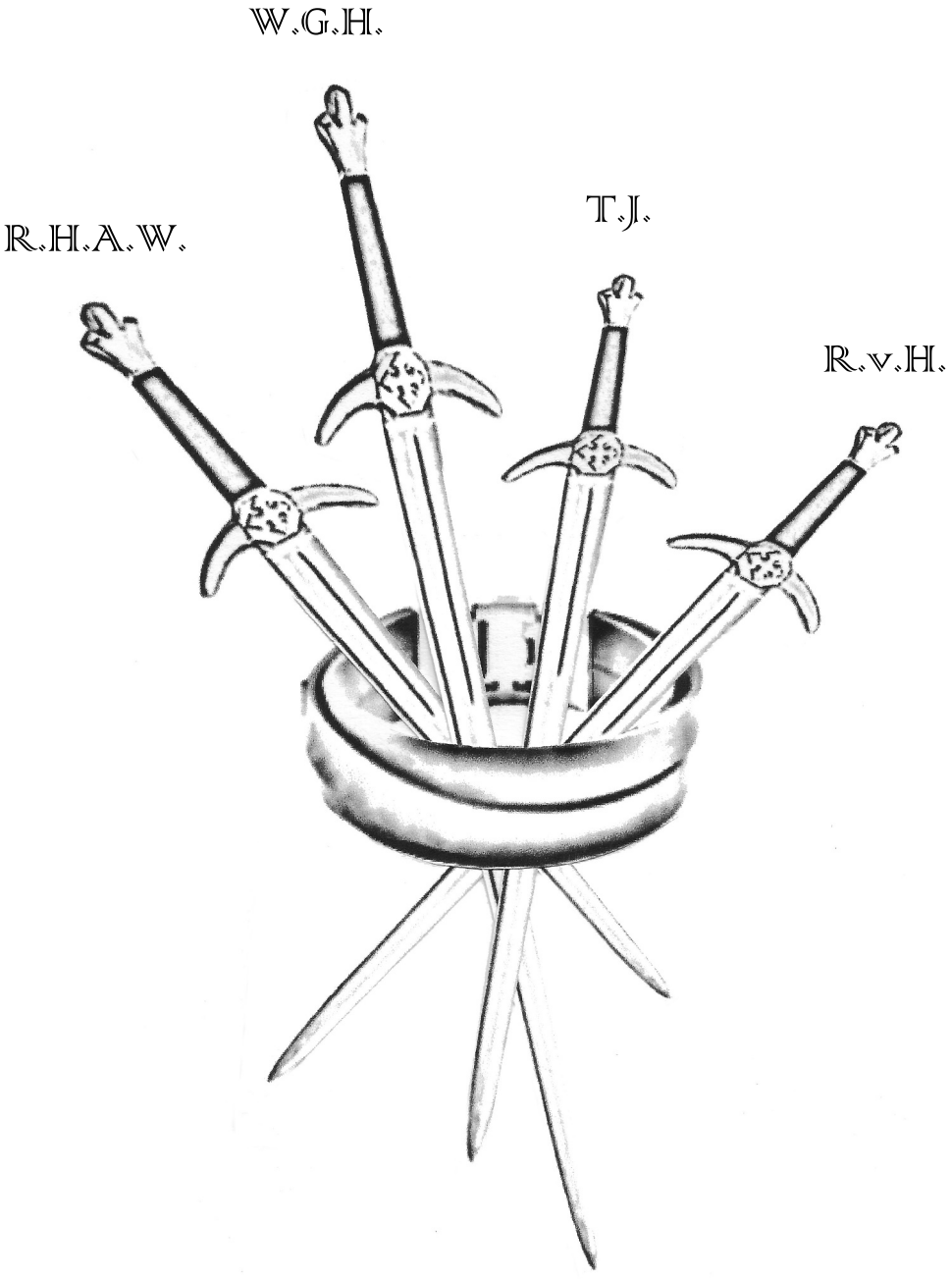

Abstract

In this work, an alternative strategy involving a fully synthetic approach is being investigated toward structure-based vaccine design against HCV. The main focus is being put on the HCV envelope E2 glycoprotein, which is a viral protein that is present on the outside of the virus particle and essential in establishing infection. Extensive research on the E2 glycoprotein has yielded an enormous amount of information dictating highly conserved domains to which the immune system can efficiently respond in order to neutralize the virus and even naturally cure infection. These highly conserved and neutralizing domains, together with the availability of antibodies binding these regions, will be exploited to design synthetic peptide-based modulators (*i.e.* epitope mimics) towards a prophylactic vaccine against hepatitis C virus. This methodology is based on a modular approach that allows for fast and easily modifiable vaccines that can quickly respond to the rapidly mutating nature of HCV and predicted outbreaks of specific strains. The difficulty of identifying a generic consensus epitope that shows effective antigenicity and immunogenicity across the diverse range of HCV variants could be bypassed this way. The design of epitope mimics is highly influenced by the spatial configuration and structural conformation of the native epitope within the overall protein structure. Synthetic peptides on molecular scaffolds can take a desired epitope out of the context of the viral protein, while maintaining its correct structural and spatial conformation. Therefore, the major bulk of the protein can be omitted to circumvent unwanted incorporation of potential immune-evasive domains in the vaccine.

This thesis starts by providing a general introduction of HCV in the context of its global burden, life cycle, impact on the immune system, and considerations with respect to vaccine design (Chapter 1). This is followed by investigation of the impact of introducing conformational constraints on synthetic epitope mimics, by peptide cyclization, on antibody binding (Chapter 2). Next, epitope mimics were synthesized using novel polar hinges to improve their aqueous solubility and re-validated their biological activity (Chapter 3). Then, the work presented culminates in the construction of a complex fully synthetic epitope mimic presenting three individual epitopes conjugated onto a molecular scaffold and its potential for vaccination was investigated (Chapter 4).

Table of Contents

CHAPTER 1 – In a world of direct-acting antivirals, vaccination remains the only option towards true control and eradication of the hepatitis C virus 19-70

1.1 Vaccination: Global control and eradication of the hepatitis C virus 21

1.2 Hepatitis C virus and the immune system 22-32
- 1.2.1 HCV life cycle 22
- 1.2.2 The immune system strikes back to control and resolve viral infection 25
- 1.2.3 HCV employs immune-evasive strategies to counteract the immune system 31

1.3 Present day approaches of vaccine design for hepatitis C virus 33-42
- 1.3.1 T-cell vaccines: Protective immunity by stimulating the cellular response 33
- 1.3.2 B-cell vaccines: Protective immunity by stimulating the humoral response 34
- 1.3.3 Structural information of antibody-E2 interaction drives vaccine design forward 35

1.4 Chemistry provides valuable tools towards epitope-focused vaccine design 43-52
- 1.4.1 Structural conservation of the epitope is essential for effective mimicry 45
- 1.4.2 Mimicry of continuous epitopes exhibiting a high degree of flexibility 47
- 1.4.3 Mimicry of continuous epitopes associated with a distinct secondary structure 47
- 1.4.4 Mimicry of discontinuous epitopes 51

1.5 References 53-70

CHAPTER 2 – Immobilization by surface conjugation of cyclic peptide for effective mimicry of the HCV-envelope E2 glycoprotein as a strategy towards synthetic vaccines 71-105

2.1 Introduction 73-75

2.2 Results and discussion 76-88

2.2.1 Synthesis of the peptide cyclization and linear linker with a maleimide reactive tetraethylene glycol (TEG) spacer 76

2.2.2 Synthesis of cysteine containing peptides for cyclization or alkylation 77

2.2.3 Synthesis of the epitope mimics for surface conjugation 79

2.2.4 Immobilization by surface conjugation to immobilized maleimide residues 80

2.2.5 Impact of peptide cyclization for adequate mimicry of E2 peptide loops 83

2.2.6 Employing epitope mimic coated surfaces for identification of key binding residues 86

2.3 Conclusions 89

2.4 Experimental section 90-101

2.5 References 102-105

CHAPTER 3 – Improving the aqueous solubility of HCV-E2 glycoprotein epitope mimics by cyclization using polar hinges 106-144

3.1 Introduction 108-111

3.2 Results and discussion 112-123

3.2.1 Synthesis of the polar triazine (TBMT) and triazinane (TATB) cyclization hinges and subsequent azide functionalization 112
3.2.2 Synthesis of an alkyne-functionalized tetraethylene glycol monotrityl thioether 113
3.2.3 Synthesis of cysteine containing peptides and subsequent cyclization 114
3.2.4 Assembling the cyclic epitope mimics 118
3.2.5 Validating the biological activity of cyclic epitopes based on different cyclization hinges 120

3.3 Conclusions 124

3.4 Experimental section 125-140

3.5 References 141-144

CHAPTER 4 – Construction of HCV-E2 glycoprotein continuous and discontinuous epitope mimics and investigating their potential as synthetic vaccines to elicit an anti-HCV E2 glycoprotein antibody response 145-197

4.1 Introduction 147-150

4.2 Results and discussion 151-167

4.2.1 Synthesis of the triazacyclophane (TAC) scaffold 151
4.2.2 Synthesis and subsequent instalment of a triethylene glycol monotrityl thioether ethylamine linker on the TAC-scaffold 154
4.2.3 Synthesis of cysteine containing peptides based on HCV-E2 glycoprotein epitopes and subsequent cyclization 155
4.2.4 Assembling continuous epitope mimics via CuAAC on the developed alkyne linker 157
4.2.5 Assembling a discontinuous epitope mimic by combining cyclic peptides on the monotrityl thioether modified TAC-scaffold 158
4.2.6 Synthesis and subsequent instalment of a triethylene glycol Boc-amide ethylamine linker on the TAC-scaffold 158
4.2.7 Assembling a discontinuous epitope mimic by combining cyclic peptides on the Boc-amide modified TAC-scaffold 159
4.2.8 Elicitation of anti-HCV E2 glycoprotein antibodies 161

4.3 Conclusions 168

4.4 Future work 169-170

4.5 Experimental section 171-193

4.6 References 194-197

List of Tables

Table 1.1	Co-crystalized synthetic epitope I-based peptides	37
Table 2.1	Synthesized peptidic antigen sequences of HCV-E2 glycoprotein	78
Table 2.2	Tabulated yields and purities of epitope mimics **21-31**	80
Table 2.3	Synthesized epitope IIa and IIb based chimera sequence	87
Table 3.1	Synthetic peptide sequences corresponding to epitopes I-III of HCV-E2 glycoprotein	115
Table 4.1	Synthetic peptide sequences corresponding to epitopes I-III of HCV-E2 glycoprotein	156

List of Figures

Figure 1.1	Overview of the HCV life cycle	23
Figure 1.2	Overview of the HCV polyprotein	24
Figure 1.3	Cytokine secretion ‘’warns’’ neighbouring cells of infection	26
Figure 1.4	Overview of MHC-II and antigen processing and presentation	28
Figure 1.5	Overview of the adaptive immune response	29
Figure 1.6	Overview of MHC-I loading and presentation	30
Figure 1.7	HCV envelope E2 glycoprotein core structure	36
Figure 1.8	Co-crystalized synthetic epitope I (412-423)	38
Figure 1.9	Co-crystalized synthetic epitope II (434-446)	40
Figure 1.10	Illustration of molecular mimetic designed by Van Dongen *et al.*[137]	43
Figure 1.11	Conceptual illustration of epitope mimicry	44
Figure 1.12	Representation of two different structural classes of epitopes	45
Figure 1.13	Overview of SPPS using Fmoc chemistry	46
Figure 1.14	Representation of peptide cyclization	48
Figure 1.15	Overview of ‘’*peptide stapling*’’	49
Figure 1.16	Overview of β-hairpin stabilization	50
Figure 1.17	Discontinuous epitope mimicry using molecular scaffolds	52
Figure 2.1	Epitope mimicry: Assembly of peptides on a scaffold molecule	74
Figure 2.2	Chemoselective approach for covalent immobilization	75
Figure 2.3	ELISA of immobilized cyclic epitope I mimic **21**	81
Figure 2.4	ELISA of immobilized cyclic epitope IIa mimics **23** and **24**	82
Figure 2.5	ELISA of immobilized cyclic epitope IIb mimics **26** and **27**	82
Figure 2.6	ELISA of immobilized cyclic epitope IIa **24** and IIb **27** mimics	83
Figure 2.7	ELISA of immobilized cyclic epitope III mimics **29** and **30**	83
Figure 2.8	ELISA comparing immobilized cyclic (**21**, **24**, **27**) versus immobilized linear (**22**, **25**, **28**) epitope mimics	85
Figure 2.9	Identification of key-binding residues by ELISA	88

Figure 3.1	Cyclization hinges for preparation of bicyclic peptides	109
Figure 3.2	Covalent and uniform surface of epitope mimics for ELISA	111
Figure 3.3	Overview of cyclization hinges **8**, **9**, **10**, and **11**	113
Figure 3.4	Overlay of HPLC traces indicating improved aqueous solubility	117
Figure 3.5	Overview of epitope mimics described in Chapter 2	121
Figure 3.6	ELISA comparing immobilized epitope I mimics **31**, **32**, and **42**	122
Figure 3.7	ELISA comparing immobilized epitope II mimics **34**, **35**, and **43**	123
Figure 3.8	ELISA comparing immobilized epitope III mimics **38** and **44**	123
Figure 4.1	Continuous epitope mimics based on HCV-E2 glycoprotein	148
Figure 4.2	Discontinuous epitope mimic based on HCV-E2 glycoprotein	149
Figure 4.3	Continuous epitope mimics **39-41** conjugated on mcKLH	163
Figure 4.4	Discontinuous epitope mimic **53** conjugated on mcKLH	164
Figure 4.5	ELISA of immunized sera against HCV-E2 glycoprotein	165

List of Schemes

Scheme 2.1	Synthesis of cyclization linker **7** and linear linker **9**	77
Scheme 2.2	Alkylation of precursor peptides with the linker constructs **7** or **9**	79
Scheme 3.1	Synthesis of cyclization hinges TBMT **3** and TATB **6**	112
Scheme 3.2	Synthesis of azide-functionalized cyclization hinges DBMT-N_3 **8**, TADB-N_3 **9**, and DBMB-N_3 **10**	113
Scheme 3.3	Synthesis of alkyne functionalized TEG monotrityl thioether **14**	114
Scheme 3.4	Synthesis and overview of cyclic azido-peptides **19-30**	116
Scheme 3.5	Synthesis and overview of epitope mimics **31-41**	119
Scheme 4.1	Synthesis of alkyne containing TAC-scaffold **14**	152
Scheme 4.2	Synthesis of orthogonally protected pentynoic acids **22** and **23**	153
Scheme 4.3	Synthesis of orthogonally protected TAC-scaffold **25**	154
Scheme 4.4	Synthesis of monotrityl thioether equipped TAC-scaffold **30**	155
Scheme 4.5	Synthesis and overview of cyclic azido-peptides **35-37**	156
Scheme 4.6	Synthesis and overview of continuous epitope mimics **39-41**	157
Scheme 4.7	Synthesis of Boc-amide equipped TAC-scaffold **48**	159
Scheme 4.8	Instalment of a first cyclic azido-peptide to TAC-scaffold **49**	160
Scheme 4.9	Instalment of a second cyclic azido-peptide to TAC-scaffold **51**	160
Scheme 4.10	Instalment of a third cyclic azido-peptide to TAC-scaffold **53**	161

Acknowledgements

I like to start by thanking the esteemed reader that is about to embark upon a journey that I have travelled in these last four years. However, we cannot get started without thanking the numerous people that made this journey possible.

From start to finish I have been able to rely on the excellent supervision and extensive experience of my supervisors Prof. Rob M. J. Liskamp and Prof. Arvind H. Patel whom have guided me throughout the PhD.

At least as important were Dr. Sarah Cole, Dr. Vanessa Cowton, Dr. Susan Gannon, Dr. Mohammed Hezwani, Dr. Alex Hoose, and Dr. Helmus van de Langemheen whom all provided invaluable support on the chemistry and/or biology sides of the project.

I would like to specifically mention and thank the following people that have provided significant help during the project. Including: Dr. Helmus van de Langemheen and Joachim Bijl, M.Sc. for performing the synthesis of 1,1',1''-(1,3,5-triazinane-1,3,5-triyl)tris(2-bromoethanone) (**6**; described in Chapter 3) and providing me with ample material during the project; Dr. Anna Mickowska for the synthesis of pentynoic acid amidated TAC-scaffold (**11**; described in Chapter 4) and providing me with ample material during the project; Dr. Vanessa Cowton for her contribution in performing a final biological assay while I was fully focussed on writing during the last moments of the PhD (described in Chapter 4).

During my time I have met many highly competent people on whom I could rely on with respect to professional and personal advice. Without the friendship of the following people: Hallam Davis, Valerijs Korotkov, Jake McGuire, Dan Mills, Alin Pirvan, Mike Shipman, Alex Wallace, David Ward, and many others, I am sure I would not have been able to complete the PhD.

Lastly, I would like to thank my father W. G. H. Meuleman, mother G.A.M. Ossendrijver, brother R. H. A. W. Meuleman, and dearest friend Rob van Horsen for their continuing support and discussion that carried well throughout many a nights. All hail the Knights of the Rectangular Table.

Author's Declaration

I, Theodorus Joannes Meuleman, hereby declare that this thesis and the work presented herein is the sole product of my own original research. Contributions provided by joint effort with others have been clearly stated. Consultation of published work of others has been appropriately referenced throughout this thesis. The work presented here has not been submitted towards any other degree within the University of Glasgow or other institutions.

Parts of the work presented within this thesis have been published:

- Meuleman, T. J., Dunlop, J. I., Owsianka, A. M., Van de Langemheen, H., Patel, A. H., Liskamp, R. M. J. (2018) Immobilization by surface conjugation of cyclic peptides for effective mimicry of the HCV-envelope E2 protein as a strategy toward synthetic vaccines. *Bioconjug. Chem. 29*(4):1091-1101.
  DOI: 10.1021/acs.bioconjchem.7b00755

- Meuleman T, J., Cowton, V. M., Patel, A. H., Liskamp, R. M. J. (*in press*) Improving the aqueous solubility of HCV-E2 glycoprotein epitope mimics by cyclization using polar hinges. *J. Pep. Sci. X*(X):XXX-XXX

Theodorus J. Meuleman, M.Sc.

Prof. Rob M. J. Liskamp

Prof. Arvind H. Patel

Abbreviations

Ac	acetyl
AcOH	acetic acid
aq	aqueous
Boc	*tert*-butyloxycarbonyl
BOP	(benzotriazol-1-yloxy)tris(dimethylamino)phosphonium hexafluorophosphate
CD4	cluster of differentiation 4
CD8	cluster of differentiation 8
CD81	cluster of differentiation 81
CEPS	chemo-enzymatic peptide synthesis
CLDN1	claudin-1
cp	cyclic precursor
CTV	cyclotriveraltrylene
CuAAC	copper(I) catalyzed alkyne-azide cycloaddition
d	doublet
DAA	direct-antiviral agent
DBMB-N_3	1-(azidomethyl)-3,5-bis(bromomethyl)benzene
DBMT-N_3	1-(azidomethyl)-3,5-bis(bromomethyl)-s-triazine
DBU	1,8-diazabicyclo[5.4.0]undec-7-ene
DC	dendritic cell
DCE	1,2-dichloroethane
D*i*PEA	*N*,*N*-diisopropylethylamine
DMA	dimethylacetamide
DMF	*N,N*-dimethylformamide
E1	envelope glycoprotein 1
E2	envelope glycoprotein 2
EDC	1-ethyl-3-[3-dimethylaminopropyl]carbodiimide hydrochloride
EDT	1,2-ethanedithiol
EDTA	ethylene diamine tetraacetic acid
ELISA	enzyme-linked immunosorbent assay

equiv.	equivalents
EtOAc	ethylacetate
Et_2O	diethylether
FB	final bleed
Fmoc	fluorenylmethyloxycarbonyl
Fmoc-OSu	9-fluorenylmethyloxycarbonyl *N*-hydroxysuccinimide ester
g	gram
GFP	green fluorescent protein
GNA	*Galanthus nivalis* lectin
HA	hemagglutinin
HCC	hepatocellular carcinoma
HCTU	*N*,*N*,*N*′,*N*′-tetramethyl-*O*-(6-chloro-1*H*-benzotriazol-1-yl)uranium hexafluorophosphate
HCV	hepatitis C virus
HCV-E2	hepatitis C virus envelope glycoprotein 2
HCVpp	hepatitis C virus pseudo-particles
HFIP	hexafluoro-2-propanol
HIV	human immunodeficiency virus
HPLC	high performance liquid chromatography
HRMS	high resolution mass spectrometry
HRP	horse radish peroxidase
HSPG	heparan sulfate proteoglycans
HVR1	hyper variable region 1
HVR2	hyper variable region 2
igVR	intergenotypic variable region
IRES	internal ribosomal entry site
LCMS	liquid chromatography mass spectrometry
LDA	lithium diisopropylamine
LDLR	low-density lipoprotein receptor
lp	linear precursor

m	multiplet
M	molar
mAb	monoclonal antibody
mcKLH	mariculture keyhole limpet hemocyanin
MeCN	acetonitrile
MeOH	methanol
MHC-I	major histocompatibility complex I
MHC-II	major histocompatibility complex II
MLV	murine leukemia virus
mRNA	messenger ribonucleic acid
MTBE	methyl-*tert*-butylether
nAb	neutralizing antibody
n-BuLi	butyl lithium
NK	natural killer cell
NMR	nuclear magnetic resonance
NS2	non-structural protein 2
NS3	non-structural protein 3
NS4A	non-structural protein 4A
NS4B	non-structural protein 4B
NS5A	non-structural protein 5A
NS5B	non-structural protein 5B
OCLN	occludin
*o*NBS	*ortho*-nitrobenzenesulfonyl
PAMP	pathogen-associated molecular patterns
PB	pre-immunization bleed
PBS	phosphate-buffered saline
PBST	phosphate-buffered saline supplemented with 0.05% Tween®-20
PEG	polyethylene glycol
PG	protection group
PKR	protein kinase R
ppm	parts per million
PRR	pattern-recognition receptor

q	quartet
quant.	quantitative
RAM	rink amide
R_f	retention factor
RNA	ribonucleic acid
s	singlet
sE2	soluble envelope glycoprotein 2
SPPS	solid phase peptide synthesis
SR-BI	scavenger receptor class I type B
t	triplet
TAAB	*N,N',N''*-benzene-1,3,5-triyltrisprop-2-enamide
TAC	triazacyclophane
TADB-N_3	azido triazinane-tris(2-bromoethanone)
TATA	1,3,5-triacryloyl-1,3,5-triazinane
TABT	1,1',1''-(1,3,5-triazinane-1,3,5-triyl)tris(2-bromoethanone)
TBAB	*N,N',N''*-(benzene-1,3,5-triyl)-tris(2-bromoacetamide)
TBAF	terta-*n*-butylammonium fluoride
TBMB	1,3,5-tris(bromomethyl)benzene
TBMT	2,4,6-tris(bromomethyl)-s-triazine
TBTA	tris[(1-benzyl-1H-1,2,3-triazol-4-yl)methylamine
*t*BuOH	*tert*-butanol
TCR	T cell receptor
TEA	triethylamine
TEG	tetraethylene glycol
TES	triethylsilyl
TFA	trifluoroacetic acid
THF	tetrahydrofuran
TIS	triisopropylsilane
TIPS	triisopropylsilyl
TLC	thin layer chromatography
TMB	3, 3', 5, 5' tetramethylbenzidine
TMS	trimethylsilane
t_R	retention time
Ts	toluenesulfonyl

UV	ultraviolet
UV/VIS	ultraviolet visible spectroscopy
δ	chemical shift
m	milli-
μ	micro-
m	meta-
n	nano-
o	ortho-
ρ	para-

Amino acids

Ala	A	Alanine
Asn	N	Asparagine
Asp	D	Aspartic acid
Arg	R	Arginine
Cys	C	Cysteine
Gln	Q	Glutamine
Glu	E	Glutamic acid
Gly	G	Glycine
His	H	Histidine
Ile	I	Isoleucine
Leu	L	Leucine
Lys	K	Lysine
Met	M	Methionine
Phe	F	Phenylalanine
Pro	P	Proline
Ser	S	Serine
Thr	T	Threonine
Trp	W	Tryptophan
Tyr	Y	Tyrosine
Val	V	Valine

CHAPTER 1

In a world of direct-acting antivirals, vaccination remains the only option towards true control and eradication of the hepatitis C virus

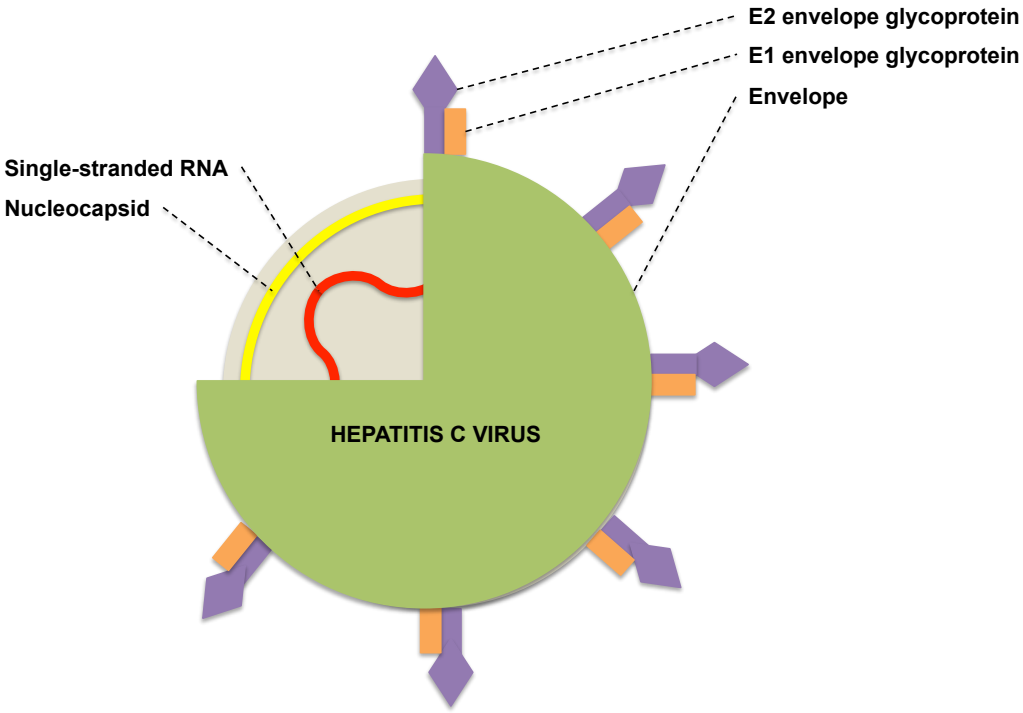

Abstract

Hepatitis C virus remains a significant burden on global health care with millions of people being infected and that number increases by the thousands annually. Despite the amazing feat of modern medicine having produced highly potent direct-acting antivirals capable of curing the majority of patients there is still a need for a prophylactic vaccine capable of protecting the population. This need has not been met to this day. The development of a therapeutic or prophylactic vaccine requires a thorough understanding of the virus. This includes the virus life cycle and the way the virus interacts with the host's immune system. Furthermore, a thorough understanding of the concept of vaccination is required to devise the most prominent strategy (*i.e.* T-cell or B-cell vaccine). Capitalizing on extensive research with respect to neutralizing antibodies and their corresponding epitopes provides essential information that drives the development of a functional vaccine. The overarching aim for the work presented in this thesis is to approach vaccine design from a chemistry point of view using epitope mimicry. To this end, a general introduction will be provided with respect to these essential topics.

1.1 Vaccination: Global control and eradication of the hepatitis C virus

Hepatitis C virus (HCV) infection is the causative agent of chronic hepatitis C in 70% of cases, leading to overall liver damage (fibrosis and cirrhosis) and liver cancer (hepatocellular carcinoma, HCC).[1] Worldwide, 400 000 infected patients die on a yearly basis due to the complications involved with chronic hepatitis C, which include non-liver (extra-hepatic) based diseases.[2] Despite the availability of direct-antiviral agents (DAAs) and combination therapies, which reach cure rates greater than 95%, approximately 71 million people are still chronically infected and 1.7 million new infections occur annually.[1]

HCV infection can be established and transmitted by a blood-borne route and can be classified into two stages, the acute phase followed by the chronic phase. Both stages are typically clinically silent and asymptomatic, until liver damage is advanced.[3] Indeed, many chronically infected people may be unaware of their infection and therefore remain untreated.[4,5] In addition, the cost for diagnosis and treatment remains a large obstacle. The importance of diagnosis is further highlighted by the fact that HCV shows a remarkable genetic variability (7 genotypes, including 67 different subtypes), and optimal treatment varies for specific genotypes.[6,7]

Without taking away the fact that the development of highly effective DAAs and their remarkable cure-rates (≥95%) is an enormous feat of modern medicine, the fight for global control and potential eradication of HCV is far from over.[8] Even after successful DAA therapy, re-infection is common.[9] Furthermore, evidence shows that regardless of successful HCV elimination there is an increased risk of developing HCC in patients.[10] Thus, despite the high efficacy of current DAA therapy, development of a prophylactic vaccine that induces protective immunity remains crucial to truly move forward in controlling HCV.

1.2 Hepatitis C virus and the immune system

A minority of patients (15% according to most clinical reviews) is capable of launching a successful immune response and naturally clear HCV infection.[11] This suggests that the immune system should be capable of controlling HCV infection, but why does this occur for only a fraction of patients? The answer to that question lies within the complicated relationship between HCV and the host immune system.

1.2.1 HCV life cycle

Understanding HCV infection starts by understanding its life cycle. A detailed description of the HCV life cycle is beyond the scope of the research presented here, instead a brief overview is provided. However, excellent reviews on the topic are available.[12-17] The HCV life cycle can be distinguished in several steps including: (1) attachment and entry of virus particles; (2) translation of released viral RNA; (3) replication of viral RNA; (4) assembly and release of virus particles (Figure 1.1). HCV attaches to its host cell membrane via sequential binding of HCV envelope proteins E1 and E2 to various cellular receptors, which results in its internalization into the cytoplasm. In turn, the viral genome, a positive sense single-stranded RNA, is released and readily translated by cellular host proteins into a viral polyprotein precursor that contains all respective viral proteins (Figure 1.2). Cellular proteases then continue to proteolytically process the polyprotein, thereby freeing non-structural (NS) proteins 3 and 4A that form a serine-protease complex. The NS3/4A protease continues to liberate the remaining structural core, envelope E1 and E2 glycoproteins, NS2, NS4B, NS5A, and NS5B. The latter non-structural viral proteins are responsible for the subsequent replication stage and, together with the structural core and envelope glycoproteins E1 and E2 for the assembly and release stage.

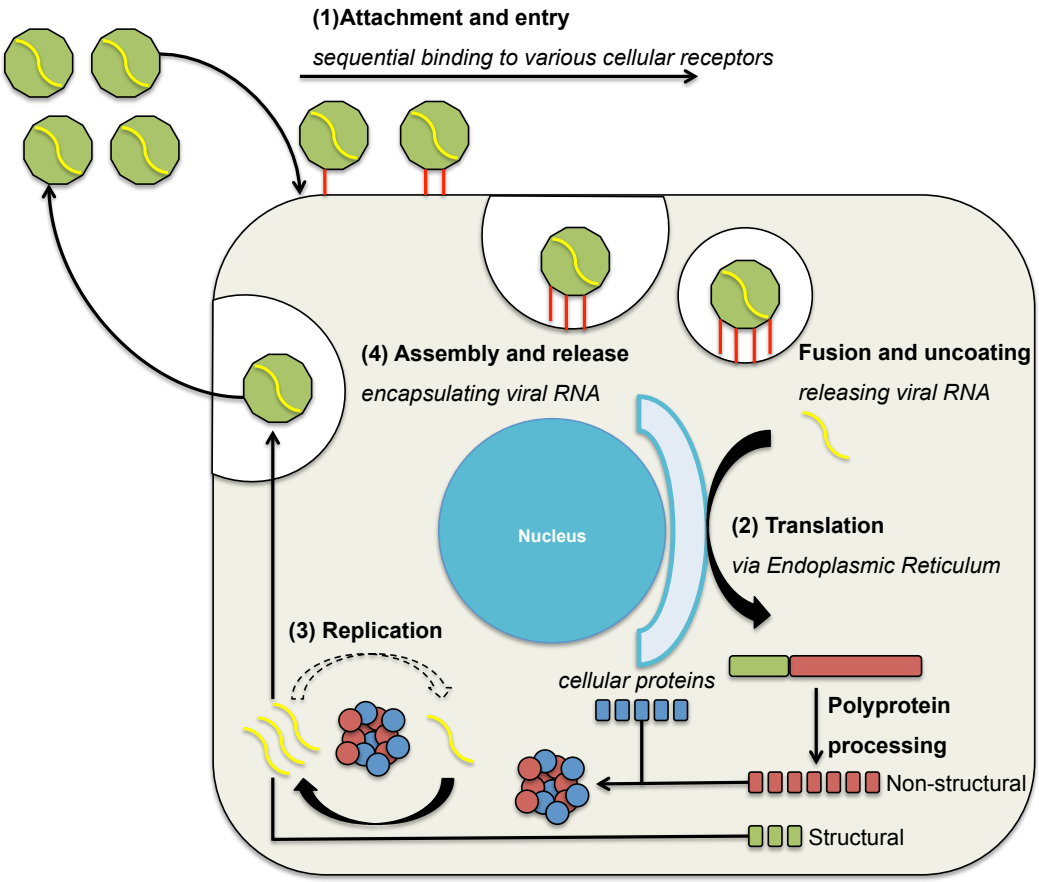

Figure 1.1. Overview of the HCV life cycle, including: (1) attachment and entry; (2) translation; (3) replication; (4) assembly and release. HCV attaches and infects by sequential binding of HCV envelope proteins E1 and E2 to various cellular receptors (1). Next, viral RNA is freed and readily translated into a viral polyprotein precursor from which the viral proteins are released by proteolytic processing (2). The liberated non-structural viral proteins recruit cellular proteins to form a replication complex to generate new virus RNA (3). Lastly, the liberated structural viral proteins package the new virus RNA and assemble new virus particles that are released from the cell (4).

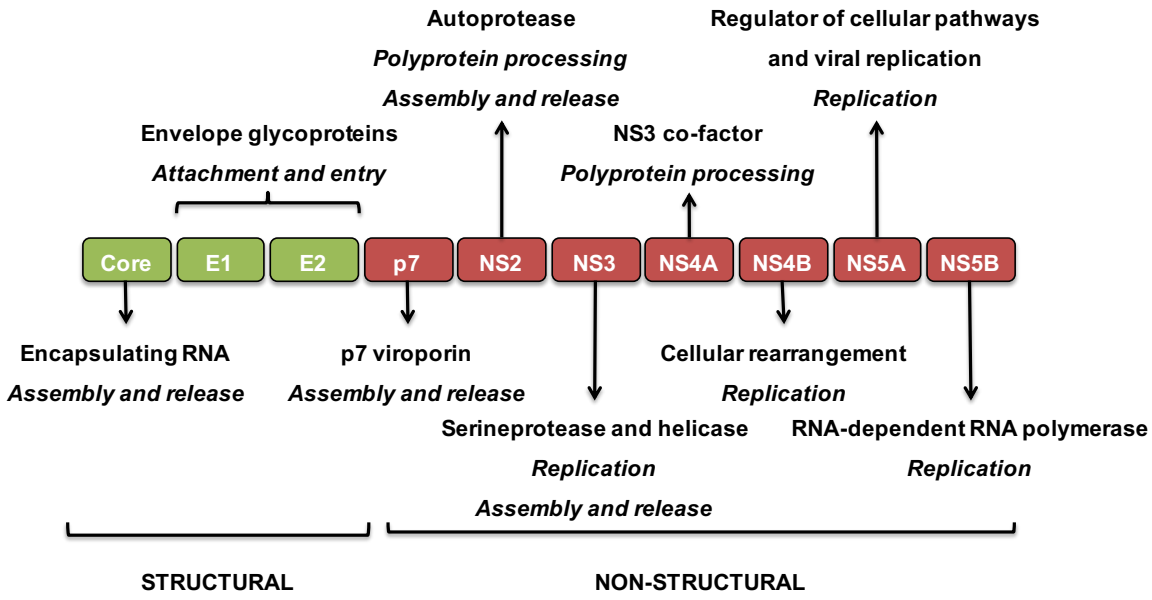

Figure 1.2. Overview of the polyprotein containing the structural (green) and non-structural (red) viral proteins and their involvement in the life cycle. The core protein packages viral RNA and assembles new virus particles; Envelope E1 and E2 glycoproteins bind and enter cells to establish infection; p7 viroporin is involved in assembling and releasing new virus particles, although how is not fully understood; NS2, NS3, and NS4A proteins process the polyprotein to generate the individual viral proteins; NS4B, NS5A, and NS5B proteins form the replication complex by scaffolding and recruitment of cellular host proteins to generate new viral RNA; NS2 protein coordinates assembly by recruiting E1E2 heterodimers, p7 viroporin, and Core packaged RNA to successfully assemble new functional virus particles; NS3 and NS5A are important for assembly and release, but the mechanism is not fully understood. This Figure has been adapted from Dubuisson *et al.*[13]

To appreciate the work presented within this thesis, it is important to have a more in depth understanding of the entry and attachment phase of the HCV infection.[12-14] As mentioned previously, the entry and attachment phase of the life cycle involves sequential binding to various cellular receptors. These receptors include, at the very least, the scavenger receptor class B type I (SR-BI), human cluster of differentiation 81 (CD81), claudin-1 (CLDN1), and occludin (OCLN).

HCV particles are typically associated with host lipoproteins[18] that facilitate initial attachment to the host cell via heparin sulfate proteoglycans (HSPGs).[19] HSPGs are involved in the metabolism of lipoproteins and are thought to modify the lipoproteins associated with the HCV particle.[14,20] Binding of HCV associated lipoproteins to HSPGs results in sequential binding to low-density lipoprotein receptor (LDLR)[21] and SR-BI[22], both of which are involved in lipoprotein metabolism.[14,23] Lipoproteins associated with the HCV particles are suggested to shield the E1E2 glycoprotein heterodimers on the virus surface, which is liberated upon transfer to SR-BI to facilitate binding of E2 to CD81.[13,14] Binding of CD81 mediates a conformational rearrangement within the E1E2 heterodimer that primes the virus particles for internalization and pH-dependent fusion.[13,14,24] In addition, HCV binding to CD81 activates multiple host regulatory mechanisms involving lateral diffusion within the plasma membrane, receptor clustering, cytoskeletal rearrangement, and energy production necessary for internalization of HCV.[13,14] Downstream events of HCV entry involve the formation of a co-receptor complex of CD81 with tight junction proteins CLDN1[25] and OCLN[26]. Evidently, the CD81 receptor is the key-player in the entry and attachment phase of the HCV life cycle.[27]

1.2.2 The immune system strikes back to control and resolve viral infection

All information regarding the immune system as discussed below has been obtained from the textbook ‘*’Flint, S. J., Enquist, L. W., Racaniello, V. R., Skalka, A. M. Principles of virology, third edition, volume II pathogenesis and control, chapter 4 immune defences, pp. 87-132*’’.[28]

Innate immune response – Upon infection, the infected cells recognize various pathogen-associated molecular patterns (PAMPs) via pattern-recognition receptors (PRRs) in the cell. In turn, this induces the production of a wide-variety of signalling proteins (cytokines) that have important functions in generating an overall antiviral environment in the host cell

that inhibit viral replication (Figure 1.3). In an attempt to contain infection cytokines are also secreted to warn neighbouring cells that then generate a similar antiviral state, and recruit additional immune cells including dendritic cells (DCs), macrophages, and natural killer cells (NKs) to the infected tissue.

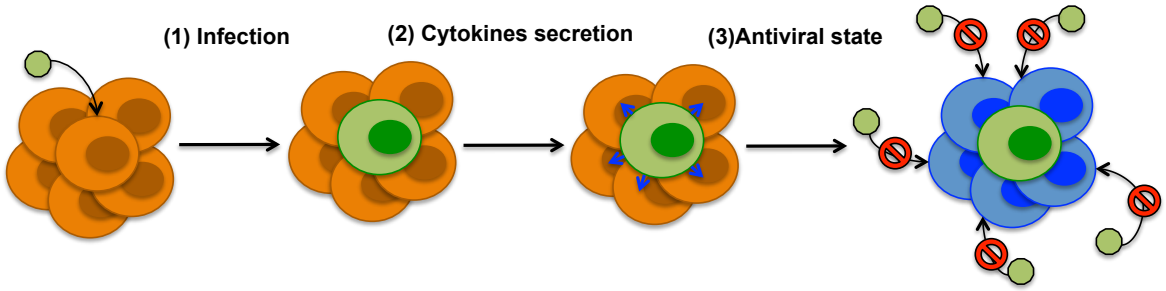

Figure 1.3. Cytokine secretion ''warns'' neighbouring cells of infection. Upon infection by a virus particle (in **green**), the innate immune response is triggered and cytokines are produced to hinder virus replication. In addition, the infected cell secretes cytokines to induce a similar preventive antiviral environment in neighbouring cells to control virus spread.

NKs form the immediate front line of protection by the innate immune system and are ready to recognize and kill virus-infected cells. NKs recognize infected cells by scanning the plasma membrane for major histocompatibility complex I (MHC-I). Infected cells generally have decreased levels of major histocompatibility complex I (MHC-I). The absence of MHC-I activates NKs, which then kills the infected cell.

DCs are crucial in classifying the infectious agent and stimulate further immune responses accordingly and specifically. DCs are present all throughout the body, including the liver and become activated early in the infection by cytokines secreted by infected cells. Activation of DCs can also occur from uptake of viral proteins from dead and dying cells. DCs perform two essential roles in the antiviral response: Inhibition of virus replication by producing large quantities of cytokines and stimulation of the subsequent adaptive immune response (discussed below).

Adaptive immune response – The adaptive immune response is made up of two complex actions, the cell-mediated response (helper and cytotoxic cells) and humoral response (antibodies). Both responses are vital in antiviral defence and function in tandem.

After uptake of viral proteins and virus genome, DCs migrate from the site of infection to lymphoid tissue. Once there, DCs cleave the viral protein into small peptide fragments that are loaded onto MHC-II proteins and these complexes are presented on the plasma membrane (Figure 1.4). T-helper cells (often denoted as CD4+ T cells) subsequently scan these MHC-II–viral peptide complexes with their T cell receptor (TCR) and become activated upon recognition (Figure 1.5). Activation causes the T-helper cells to multiply and, produce and secrete cytokines that activate cytotoxic T-killer cells (often denoted as CD8+ T cells) (Figure 1.5). The T-killer cells are then recruited to the infected tissue and patrol for viral markers presented on infected cells. Recognition of infected cells occurs through the MHC-I–complexes that are present on all nucleated cells. All cells present their protein 'household' on their plasma membrane in the form of small peptide fragments loaded onto MHC-I proteins (Figure 1.6).

In the case of an infected cell, viral proteins are produced and proteolytically cleaved, which results in presentation of MHC-I–viral peptide complexes on their plasma membrane (Figure 1.6). T-killer cells patrol the infected tissue with their TCR and become activated upon recognition of viral peptide presented by these MHC-I proteins (Figure 1.5 and 1.6). Activation of T-killer cells causes them to multiply, produce and secrete cytokines to create a local antiviral environment, and directly kill the infected cells (Figure 1.5).

The humoral response is mediated by B-cells, but is tightly linked to T-helper cells. Inactivated B-cells become activated by binding virus particles or viral protein via membrane bound antibodies on their plasma membrane. Binding causes internalization of the virus-antibody complex, which is then processed in a similar fashion as in DCs (Figure 1.4). Activated B-cells migrate to lymphoid tissue and proteolytically cleave viral material into small peptide fragments loaded in MHC-II and presented on their plasma membrane (Figure 1.4 and 1.5). T-helper cells scan these MHC-II–viral peptide complexes with their TCR and become activated upon recognition. Again, this causes production and secretion of cytokines that stimulate the B-cells to multiply and differentiate into plasma cells that become antibody-producing factories (Figure 1.5).

Activation of T-helper, T-killer, and B-cells also induces specific differentiation into a small population of memory cells. These memory cells are long lived and are important in providing protective immunity by facilitating a faster immune response upon re-infection. Priming the immune system using a non-harmful artificial virus infection and producing memory cells that prevent infection of the actual virus is the concept of vaccination.

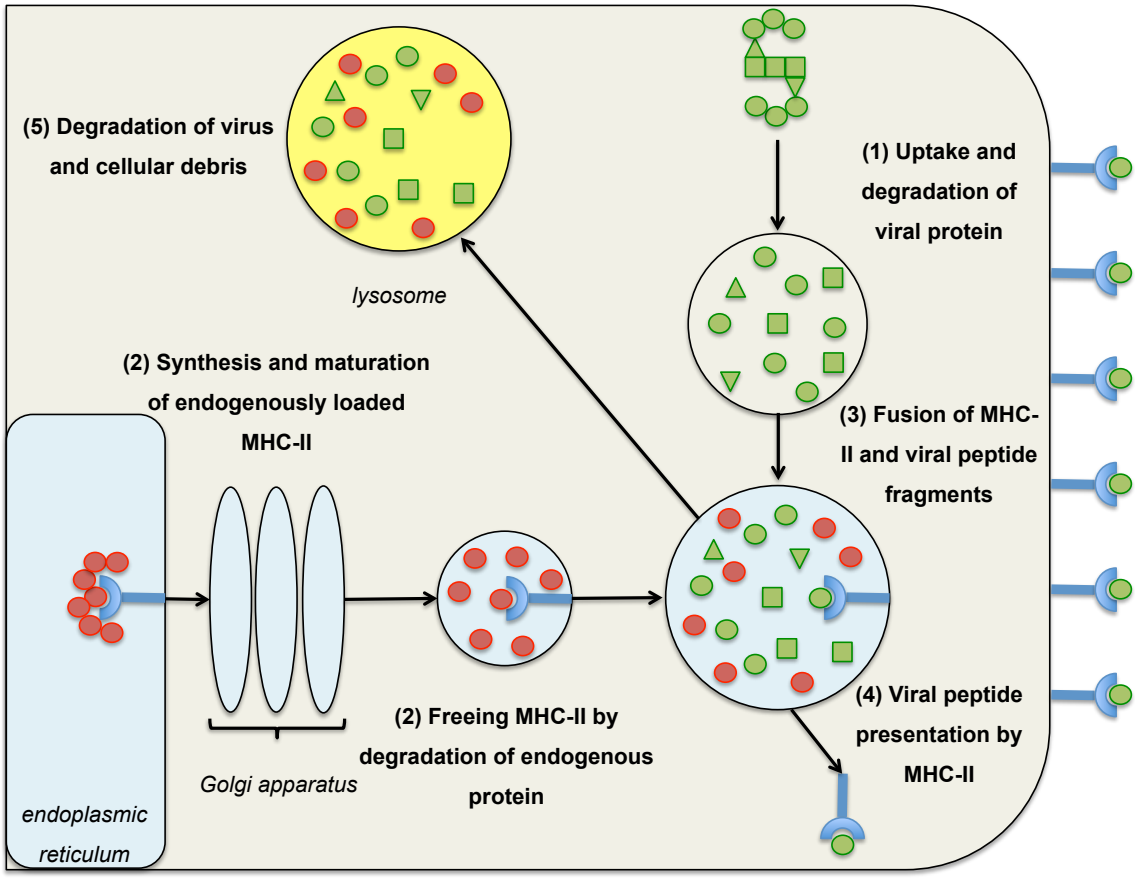

Figure 1.4. Overview of MHC-II and antigen processing and presentation in antigen-presenting cells (DCs, B-cells). (1) Intracellular viral proteins are degraded into small peptide fragments; (2) MHC-II is continuously translated in a pre-loaded state in the endoplasmic reticulum and processed by the Golgi-apparatus, followed by unloading the MHC-II by degrading the loaded protein; (3) MHC-II and viral peptide fragments are combined to allow loading of viral peptide into the MHC-II; (4) The resulting MHC-II–viral peptide complex is transported onto the plasma membrane for extracellular presentation; (5) Residual debris that originated from cleaved pre-loaded and viral proteins are transported to the lysosome where it is degraded. This Figure has been adapted from ''*Flint, S. J., Enquist, L. W., Racaniello, V. R., Skalka, A. M. Principles of virology, third edition, volume II pathogenesis and control, chapter 4 immune defences, pp. 87-132*''.[28]

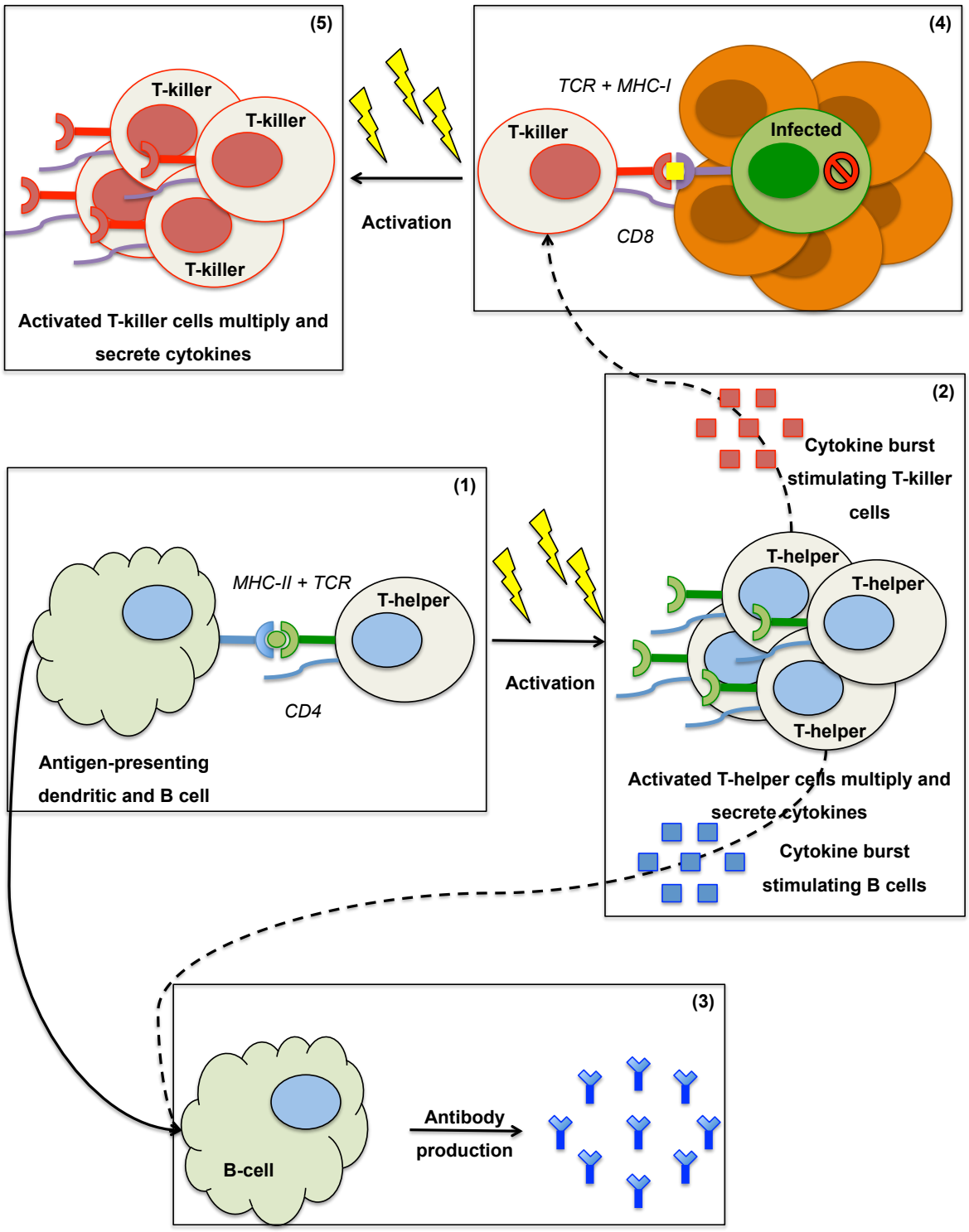

Figure 1.5. Overview of the adaptive immune response, including the cellular and humoral response. (1) Recognition of MHC-II–viral peptide complex (see Figure 1.4) by T-helper cells results in their activation; (2) The activated T-helper cells secrete cytokines to stimulate the B-cells (3) and T-killer cells (4); (3) Stimulation of the B-cells results in them to multiply and increase production and secretion of antibodies (3); (4) Stimulation of the T-cells results in them to find and kill infected cells; (5) Identification of infected cells relies on viral peptides being presented on the cell surface by MHC-I proteins (see Figure 1.6), which when successful activates the T-killer cells to multiply.

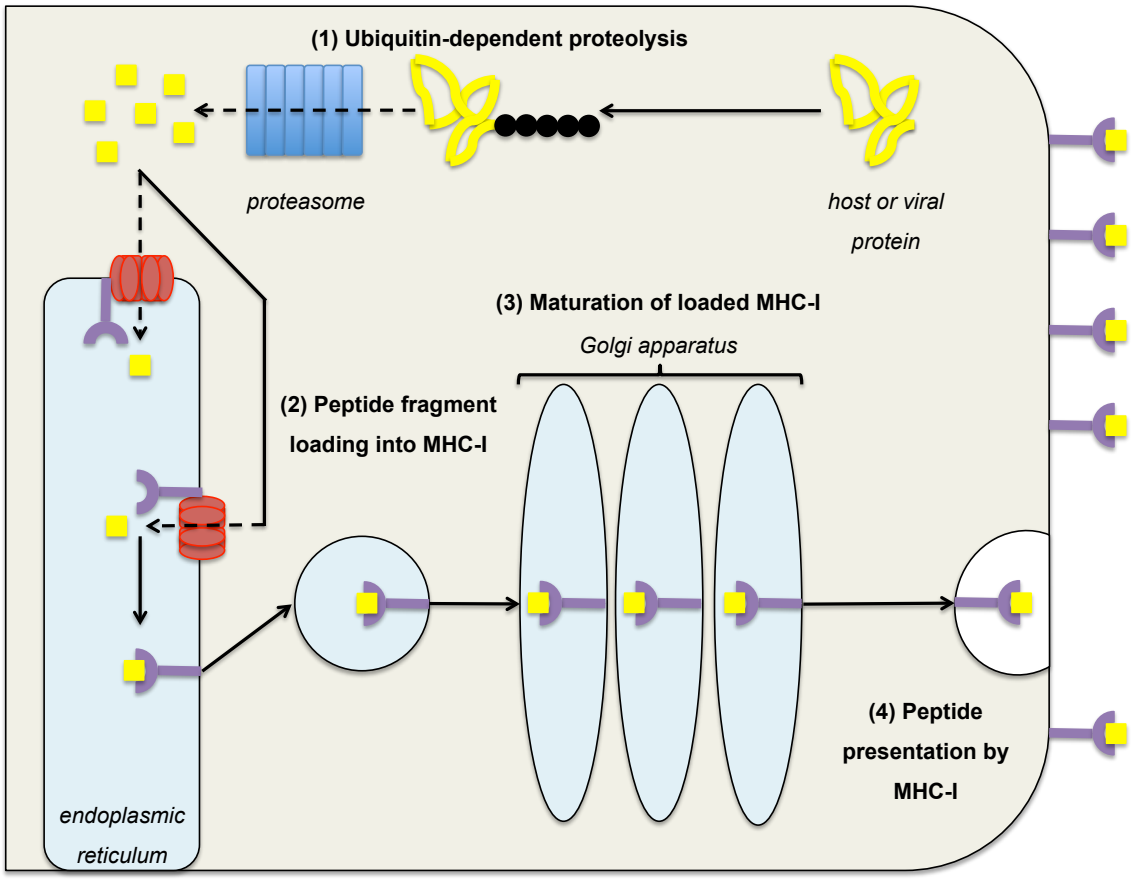

Figure 1.6. Overview of MHC-I loading and presentation. (1) Intracellular proteins become ubiquitinated to some extent, which triggers degradation by the proteasome; (2) The resulting peptide fragments move to the endoplasmic reticulum and get loaded into MHC-I; (3) The loaded MHC-I is post-translationally modified by the Golgi apparatus; (4) The resulting MHC-I–viral peptide complex is transported to the plasma membrane to present the peptide fragment. Infected cells are recognized by producing viral proteins that also get processed through this pathway and presented on the plasma membrane. This Figure has been adapted from ''*Flint, S. J., Enquist, L. W., Racaniello, V. R., Skalka, A. M. Principles of virology, third edition, volume II pathogenesis and control, chapter 4 immune defences, pp. 87-132*''.[28]

1.2.3 HCV employs immune-evasive strategies to counteract the immune system

HCV manipulates the immune system actively during the innate immune response and the following cytokine production.[29] Disrupting cytokines production has far-reaching consequences by preventing induction of an overall antiviral state and more importantly communication with and coordination of the subsequent adaptive immune response that comes after. HCV rearranges intracellular membranes to form enclosed microenvironments of double-membrane vesicles called the membranous web in which replication of viral RNA occurs.[16,30] These enclosed microenvironments shield viral PAMPs from recognition and thereby preventing initiation of the innate immune response. Even when PAMPs are recognized, HCV NS3/4A protease plays a major role in disrupting downstream signaling cascades that trigger cytokine production by proteolytically cleaving antiviral signaling proteins.[31,32]

One antiviral mechanism of the cell is initiated upon recognition of double-stranded viral RNA by protein kinase R (PKR). In turn, this suppresses cap-dependent translation of host mRNA and overall protein production, but induces cytokine production.[33,34] Suppressing cellular protein production should also result in a decrease in viral protein production of an infected cell. However, HCV RNA translation occurs using an internal ribosome entry site (IRES) that circumvents cap-dependent translation.[35] Although the mechanism is not fully understood, HCV NS5A and envelope E2 glycoprotein have been shown to bind and modulate PKR activity.[36,37]

Although not covered here, the complement system consists of a tightly regulated network of cellular proteins involved in a wide variety of functions in host defense.[38-40] HCV envelope E2 glycoprotein and structural core protein have been shown to also manipulate the complement system by a mechanism that is not fully understood.[41-43]

HCV infection does not seem to have a direct effect on the adaptive immune response, as immune cells do not seem to be susceptible to HCV infection.[44] It is more likely that HCV influences the adaptive immune response indirectly by sabotaging cytokine driven communication and stimulation between the innate and adaptive immune system. Immunological escape of HCV is another mechanism that the virus uses to evade the adaptive immune response. HCV NS5B is an error-prone RNA-dependent RNA polymerase responsible for synthesis of new progeny RNA. The lack of a proofreading

mechanism in NS5B results in a high degree of mutations in HCV progeny, which in turn accounts for multiple amino-acid changes in viral proteins.[45,46] This yields a highly diverse pool of antigens that are presented to stimulate the adaptive immune response, thereby exhausting the immune system.[47-52] The high genetic diversity of HCV ensures that despite a large pool of antigens, there is a high chance that one or more variants will remain unaffected, which may lead to establishing a chronic infection.

Indeed, the host antibody response lags behind the ever-changing HCV.[53,54] Antibodies capable of neutralizing one HCV variant will soon be overcome by a next new variant, demonstrating the continued evolution and escape of HCV. The antibody response is mainly targeted towards envelope E2 glycoprotein, which evades neutralization by employing dominant immunogenic decoys, masking neutralizing domains by glycosylation, and concealing itself by associating with host lipoprotein.[18,55-57]

Despite extensive manipulation and evasion by HCV, infection is still met with an immune response in all patients, but still progresses to a chronic infection in the majority of the patients.[29,58,59] Attenuation, rather than elimination, of the immune response by HCV might provide the appropriate balance between host and virus to ensure a long lasting partnership. The small population that naturally clears HCV might be associated with a rare un-attenuated, perfectly coordinated, targeted, and fast immune response capable of striking before and/or managing the diverse pool of HCV variants.

1.3 Present day approaches of vaccine design for hepatitis C virus

The principle of vaccination is to provide a lasting, protective, and sterilizing immunity towards a pathogen by stimulating the immune system to be able to generate a coordinated, strong, fast, and specific response upon infection. Achieving immunity to hepatitis C virus seems possible, as studies in previously infected chimpanzees and human patients that naturally resolved HCV infection showed a lower chance of HCV re-infection.[60,61] However, sterilizing immunity is not always achieved after natural clearance of HCV.[62]

Vaccination has achieved considerable success in global control of and protection against viruses such as smallpox virus, measles, and poliovirus.[63-65] However, vaccination against more present and challenging viruses such as human immunodeficiency virus (HIV)[66,67] and HCV[68,69] remains elusive. These viruses continue to threaten public health and the development of effective vaccines is essential in controlling these viruses globally. Strategies of vaccine design typically include an inactivated or dead virus (inactivated vaccine), a weakened virus that does not induce disease (attenuated vaccine), viral proteins or subunits (subunit vaccine), and genetically engineered virus (recombinant vaccine).[70] Most of the effort to develop a HCV vaccine leans towards design of a recombinant vaccine. Recombinant vaccines are specifically constructed using non-pathogenic genomes that produce selected viral proteins to immunize a host against the actual pathogenic virus. Currently there are two main vaccine strategies that are moving towards human clinical trials.

1.3.1 T-cell vaccines: Protective immunity by stimulating the cellular response

The first vaccination strategy targets the T-cells to stimulate the T-helper and cytotoxic T-killer cells using HCV NS3, NS4A, NS4B, NS5A, and NS5B viral proteins. Typically, T-cell vaccines are recombinant vaccines that deliver an engineered recombinant viral genome into the cell using a viral vector (*i.e.* adenovirus). Upon internalization, the viral genome is translated and processed to produce the viral proteins *in vivo*. It is important to note that the viral vector is specifically engineered to be replication-defective and does not result in actual virus production. One major benefit of genetic vaccines is that there is a possibility to induce an innate immune response by recognition of intracellular viral PAMPs of the HCV proteins. Stimulation of the innate immune response can occur along

side and be beneficial to the main strategy of inducing a protective T-cell response and long-term memory thereof, and thus establishing protective immunity. The selectivity of recombinant vaccines towards T-cells comes from the fact that HCV NS3, NS4A, NS4B, NS5A, and NS5B viral proteins are mainly intracellular (with the exception of possible extracellular debris from dead or dying cells) and will be processed and presented via MHC-I, which subsequently activates T-killer cells. Extracellular viral debris from dead or dying cells might be taken up by antigen presenting DCs and, processed and presented via MHC-II to activate T-helper cells.

A developed recombinant adenovirus containing HCV NS3, NS4A, NS4B, NS5A, and NS5B viral proteins was shown to be capable of priming a HCV specific and cross-reactive T-killer cell response in chimpanzees and subsequent development of T-killer cell memory.[71] Re-infection resulted in expansion of this HCV specific and cross-reactive T-killer cell population and reduced the amount of HCV virus particles in the blood in 4 of the 5 vaccinated chimpanzees.[71] In turn, testing of this recombinant HCV vaccine using adenoviral and vaccinia Ankara vectors in healthy human volunteers induced a similar promising broad, multifunctional, and cross-reactive HCV-specific T-helper and T-killer cell response.[72-74] The induced T-helper and T-killer cell population was maintained for up to a year after vaccination and exhibited T-cell memory function.[72-74] Clinical trials using the vaccination regiment developed by Swadling *et al.*[73] continued in a phase II clinical trial as a prophylactic vaccine in high-risk intravenous drug users [NCT01436357]. The outcome of which (*not yet published*) should provide information if the vaccine will be able to provide protection during real-life exposure to HCV.

1.3.2 B-cell vaccines: Protective immunity by stimulating the humoral response

The second vaccination strategy targets the B-cells to stimulate anti-HCV antibody production. In contrast to T-cell activation that relies on recognition of proteolytically processed viral peptide fragments by antigen-presenting and infected cells. B-cell activation starts with recognition of epitopes comprised by (a) peptide-sequence(s) with specific conformations of the intact protein. B-cell vaccines are therefore generally based on accessible viral proteins present on the virus particle. Design of a HCV B-cell vaccine is typically focussed on the envelope E2 glycoprotein, which is an accessible protein

present on the surface of HCV virus particles with an essential role in binding to and entering host cells.[75]

A recombinant HCV envelope E1/E2 subunit vaccine has been shown to induce a strong cross-reactive humoral response in vaccinated chimpanzees that provided protection and in some cases even sterilizing immunity upon re-infection.[76,77] Preclinical evaluation of a HCV E1-E2 heterodimer based subunit vaccine stimulated both production of neutralizing antibodies (nAbs) and activation of T-helper cells.[78,79] The resulting nAbs were found to target multiple-epitopes of HCV E1/E2 across different genotypes.[80,81] A subunit HCV vaccine based on recombinant soluble envelope E2 glycoprotein elicited antibodies in rhesus macaques that neutralized a broad panel of different genotypes of HCV and also stimulated a T-cell response.[82]

Despite the general distinction between T-cell and B-cell vaccines, it is common that a specific vaccine induces both a cellular as well as a humoral response to some extent. This can be explained by the tight regulation and cooperation between these two immune responses. Next generation vaccine design will likely attempt to capitalize on both the cellular and humoral immune response by combining T-cell and B-cell type vaccination approaches.[83]

1.3.3 Structural information of antibody-E2 interaction drives vaccine design forward

The two strategies described above have demonstrated promising immunogenicity in animals and healthy human volunteers. However, to our knowledge, protective immunity against real-life HCV exposure has not been demonstrated.

Inducing a broad and cross-reactive immune response that is capable of being effective across the high genetically diverse landscape associated with HCV, is an essential aspect for a functional vaccine. Therefore, many research efforts have focussed on identification, characterization, and isolation of neutralizing antibodies from immunized animals and human patients. In turn, these antibodies allow identification and provide information on the structural relevance of B-cell epitopes in the envelope E2 glycoprotein. This could be an important driver for successful vaccine design. Especially antibodies isolated from patients that have naturally cleared HCV provide a wealth of information to guide rational

vaccine design. A similar strategy is pursued towards identification and characterization of promising T-cell epitopes. For T-cell epitopes this requires isolated T-cells, which are integrated in specific tissue and difficult to obtain. In contrast to antibodies, which are small proteins that circulate in the blood and can be isolated relatively easily.

Currently all licensed viral vaccines rely on the production of neutralizing antibodies (B-cell vaccines).[84] HCV infected patients that naturally clear the infection have been found to be able to generate a broad neutralizing antibody response early in the infection and thus HCV clearance correlates with inducing a humoral immune response.[54,85,86] Protective immunity upon re-infection has also been correlated to a broad humoral immune response during the first infection.[87] Furthermore, passive transfer of broad neutralizing antibodies into experimental animals provided protection against HCV infection.[88-90]

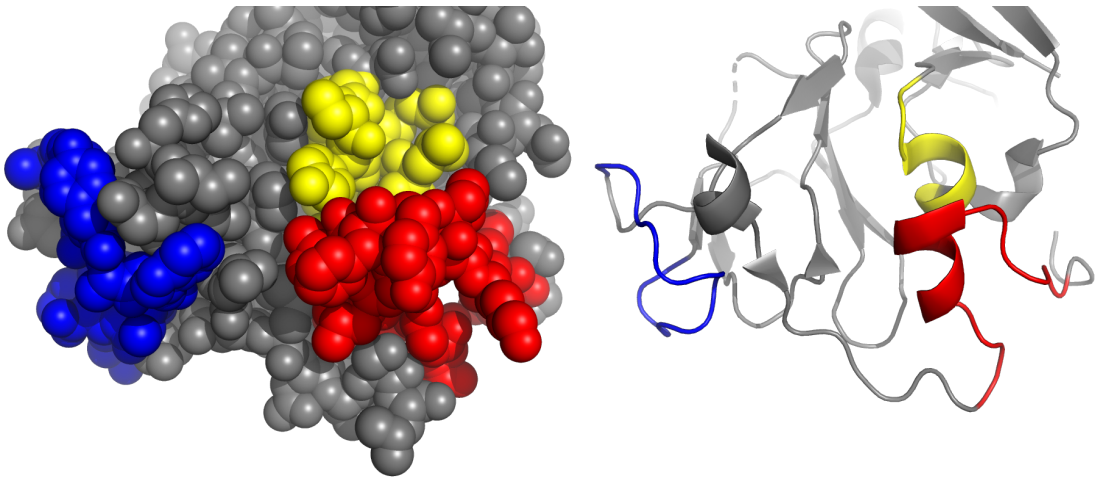

Figure 1.7. HCV envelope E2 glycoprotein core structure obtained by Kong *et al.*[99] [PDB 4MWF]. Epitope II (434-446) in **red**; Epitope III (523-535) in **blue;** Epitope IV (611-617) in **yellow**.

The majority of HCV-neutralizing antibodies target a specific region in the HCV envelope E2 glycoprotein, denoted as the CD81 binding site.[91,92] Cellular CD81 is the host cellular receptor that is essential in initiating the attachment and entry phase of the virus life cycle via interaction with HCV-E2.[12-14] Binding of E2 to CD81 is essential for infection by all HCV strains and therefore the E2 glycoprotein contains highly conserved domains, making this envelope protein an ideal target for use in vaccine design.[93-98] These conserved CD81 binding domains of E2 glycoprotein are associated with a wide variety of neutralizing antibodies and have been denoted in literature using several different nomenclatures, here we will refer to them as epitope I, II, III, and IV. A crystal structure of a truncated HCV

envelope E2 glycoprotein, referred to as E2 core structure, has been obtained including epitopes II, III, and IV (Figure 1.7).[99] Epitope I could not be resolved in the crystal structure because of a high degree of flexibility.

To guide rational vaccine design, it is vital to understand the structural relevance of the four prominent immunogenic epitopes (I, II, III, and IV) bound to promising broadly neutralizing antibodies.

Epitope I – Encompasses a highly conserved region in the envelope E2 glycoprotein between amino acid residues 412 and 423 that is recognized by a number of monoclonal antibodies (mAbs).[93] One such antibody AP33, a mouse mAb, was isolated from an immunization experiment with a recombinant E1E2 heterodimer.[100] mAb AP33 was capable of neutralizing infection in cell culture models of HCV as well as HCV pseudoparticles based on all genotypes, signifying epitope I to be highly conserved.[101,102] Desombere *et al.*[103] has shown that mAb AP33 provided passive protection *in vivo* in human liver chimeric mice when challenged with patient derived HCV. The key-binding residues for antibody recognition have been identified by alanine-scanning mutagenesis and X-ray crystallography, and include: Leucine-413, Asparagine-415, Glycine-418, and Tryptophan-420.[102,104-106] Specifically, Tryptophan-420 is a contact residue for all broadly neutralizing antibodies that recognize epitope I and is crucial for the E2-CD81 interaction.[95,102,104-108] Other mAbs that bind epitope I are HCV1[109], 3/11[110], and HC33.1[111]. Structural relevance of epitope I was obtained by co-crystallization of synthetic peptides based on epitope I bound by different monoclonal antibodies (Table 1.1).

Table 1.1. Synthetic epitope I-based peptides co-crystalized with neutralizing mAbs.

Synthetic peptide	**mAb**	**Structure**	**Reference**
L^{413}INTNGSWHVN^{423}	AP33	β-hairpin	Potter *et al.*[104]
R^{411}QLINTNGSWHIN^{423}	HCV1	β-hairpin	Kong *et al.*[107]
Q^{412}LINTNGSWHVN^{423}	3/11	Extended	Meola *et al.*[108]
R^{411}QLINTNGSWHIN^{423}	HC33.1	Extended / β-hairpin / coil	Li *et al.*[106]

Binding by mAb AP33 (Figure 1.8A; green)[104] and HCV1 (Figure 1.8B; cyan)[107] showed that epitope I adopts a β-hairpin structure. In contrast, binding by mAb 3/11[108] (Figure 1.8C; gray) showed a very different extended conformation for epitope I. Another different intermediate β-hairpin / coil conformation of epitope I was showed by binding mAb

HC33.1[106] (Figure 1.8D; magenta). Taken together, this would suggest that epitope I exhibits a degree of structural flexibility and adopts multiple conformations *in vivo*. Indeed, epitope I could not be resolved in the HCV envelope E2 core structure because of its flexibility.[99] The high degree of structural flexibility of epitope I might be responsible for the low levels of high affinity antibodies targeting this region being found in patient sera.[112]

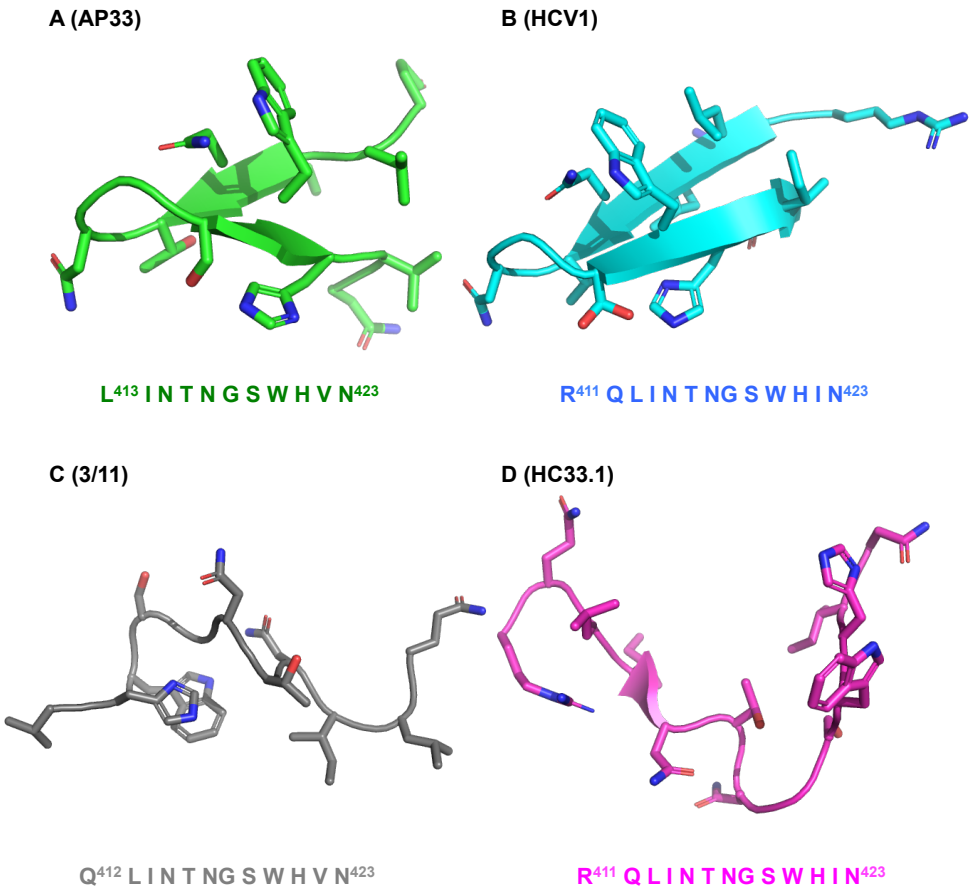

Figure 1.8. Co-crystalized linear short synthetic peptides based on epitope I (412-423) bound to four different antibodies. (**A**) mAb AP33 binding induced a β-hairpin conformation, shown in **green** [PDB 4GAG];[104] (**B**) mAb HCV1 binding induced a β-hairpin conformation, shown in **cyan** [PDB 4DGV];[107] (**C**) mAb 3/11 binding induced an extended conformation, shown in **gray** [PDB 4WHT];[108] (**D**) mAb HC33.1 binding induced an intermediary β-hairpin / coil conformation, shown in **magenta** [PDB XVJ].[106]

Epitope II – Consists of HCV-E2 amino acids 434-446 and contains the highly conserved Phenylalanine-442 and Tyrosine-443 residues involved in binding to CD81.[96,113,114] This epitope II structure has been resolved in the E2 core crystal structure (Figure 1.7; red) and adopted a loop–α-helix–loop structure.[99] A promising series of broadly neutralizing antibodies (HC84 series) have been isolated from a chronically infected patient and show

resistance against immune-escape variants.[115] The HC84 series included monoclonal antibodies that were shown to neutralize a panel of different genotypic cell culture models of HCV, which indicated epitope II as highly conserved.[115] Continued replication of cell-culture models of HCV in the presence of low levels of HC84.xx antibodies did not result in viral variants that escaped neutralization.[115] Taken together, this highlights the HC84 series as excellent drivers of HCV vaccine design. Antibody recognition of E2 envelope glycoprotein involves binding to several key residues that is dependent on the antibody HC84.xx type.[115] These key-residues consistently include Leucine-441, Phenylalanine-442, and Tyrosine-443 for all antibodies in the HC84 series.[115] Other neutralizing antibodies that target epitope II are mAb≠8 and mAb♯41.[116-118]

Structures of synthetic epitope II based peptides co-crystalized with different mAbs that bind epitope II, including: HC84.1 (Figure 1.9A; green)[119], HC84.27 (Figure 1.9B; cyan)[119], mAb♯8 (Figure 1.9C; gray)[117], and mAb♯12 (Figure 1.9D; magenta)[118] highlight a degree of flexibility in epitope II. Krey *et al.*[119] showed that a synthetic peptide (N^{434}TGWLAGLFYQHK^{446}) adopted a N-terminal α-helix and C-terminal loop structure upon co-crystallization with neutralizing mAbs HC84.1 (bound to residues between Asparagine-434 to Lys-446) or HC84.27 (bound to residues between Asparagine-434 to Lys-446). In contrast to Deng *et al.*[117,118], which showed a synthetic epitope I/II based peptide (H^{421}INSTALNCNESLNTGWLAGLFYQHK^{446}) to adopt a N-terminal loop and C-terminal α-helix structure when co-crystalized with neutralizing mAb♯8 (bound to residues Asparagine-430 to Phenylalanine-442) or non-neutralizing mAb♯12 (bound to Asparagine-434 to Phenylalanine-442). Neutralizing mAbs HC84.1, HC84.27, and mAb♯8 showed strong binding across the epitope II sequence. In contrast to mAb♯12, which showed strong binding to the C-terminus and weak binding to the N-terminus of the epitope II sequence. Dengue *et al.*[118] continued to suggest that the flexibility of epitope II influences the affinity of antibodies to epitope II, which reflects neutralization versus non-neutralization of HCV.

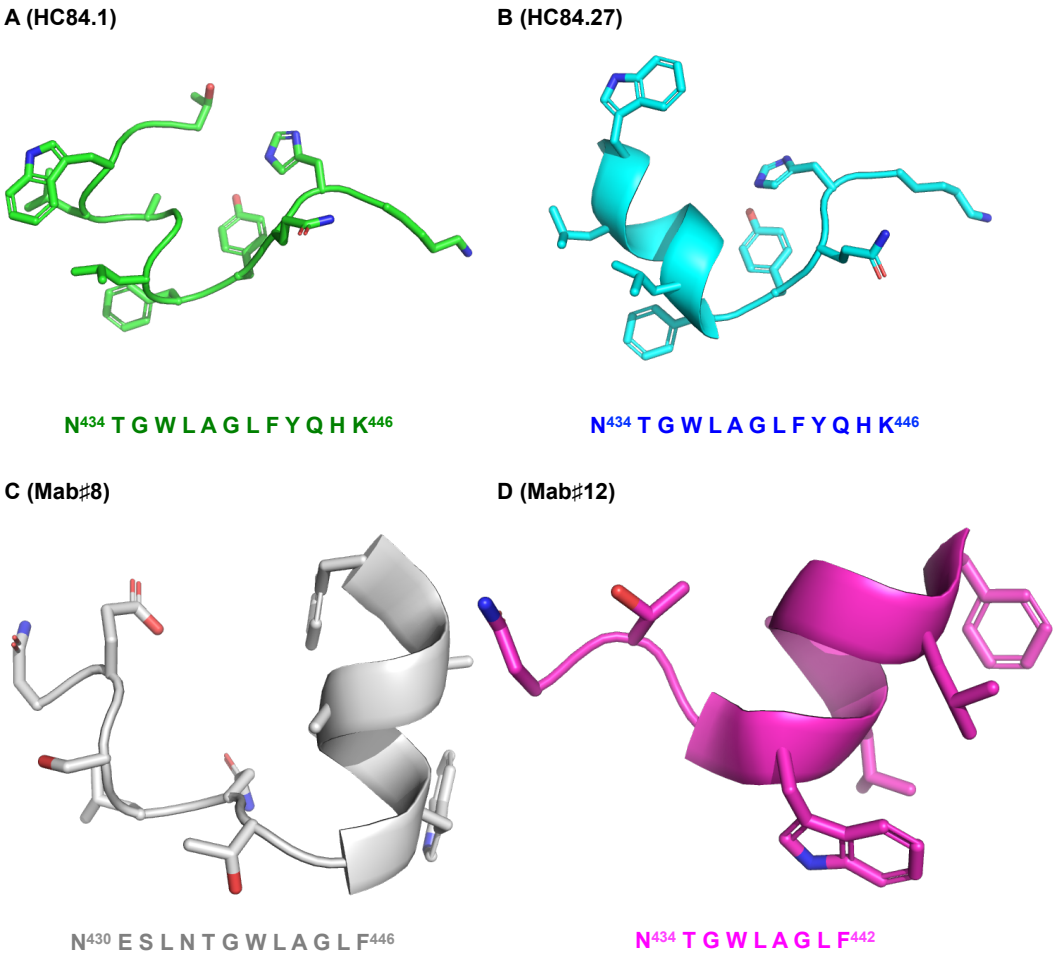

Figure 1.9. Co-crystalized linear short synthetic peptides based on epitope II (434-446) bound to four different antibodies. (**A**) mAb HC84.1 binding induced a N-terminal α-helix conformation, shown in **green** [PDB 4JZN];[119] (**B**) mAb HC84.27 binding induced a N-terminal α-helix conformation, shown in **cyan** [PDB 4JZO];[119] (**C**) mAb♯8 binding induced a C-terminal α-helix conformation, shown in **gray** [PDB 4HZL];[117] (**D**) mAb♯12 binding induced a C-terminal α-helix conformation, shown in **magenta** [PDB XVJ].[118]

Epitope III – Covers a region from 523 to 535 that is proposed as a major site for binding the CD81 receptor and as such has been found to be intolerant to neutralization escape mutations.[120] Highly conserved residues that are essential for CD81 binding within epitope III are Tyrosine-527, Tryptophan-529, Gly-530, and Asp-535 and have been identified by alanine-scanning mutagenesis.[95] Several different broadly neutralizing antibodies have been isolated that target epitope III.[93,120,121] Evaluation of several broadly neutralizing antibodies (1:7[98], A8[98], J6.27[122], H77.31[122]) has shown binding to some of these essential amino acid residues, which included: Glycine-523, Alanine-524, Threonine-526, Tyrosine-527, Trp-529, Glycine-530, Aspartic acid-533, and Aspartic acid-535.[94,123] The structure of epitope III has been resolved in the E2 core crystal structure and consists of a long loop

like structure (Figure 1.7; blue).[99] In the HCV-E2 envelope glycoprotein, epitope III has been associated with multiple conformations that influences antibody affinity and HCV neutralization.[124]

Epitope IV – Consists of a small region covering amino acids 611 to 617 involved in binding the CD81 receptor.[125] The epitope IV structure has been resolved in the crystal structure of the HCV-E2 core and formed a short α-helix (Figure 1.7; yellow).[99] A few key-binding residues, including: Tyrosine-613 and Tryptophan-616, are present in this region involved in binding neutralizing antibodies.[123] These residues of epitope IV are only recognized together with residues that lie in epitope I, II, and III. It seems that epitope IV is not recognized on its own.[115,126,127]

In view of the mapped structure-activity relationships between epitopes I, II, III, and IV and promising broadly neutralizing antibodies, it should be possible to engineer a vaccine candidate against HCV. The interest in using the HCV envelope E2 glycoprotein towards vaccine design is attractive since it is an accessible target on the virus particle. However, there are a number of factors that need to be considered that could impact on the suitability of using the entire E2 glycoprotein as a vaccine.[91,92] First, the HCV envelope E2 glycoprotein contains three hypervariable regions (HVR1, HVR2, and igVR) that modulate binding of the CD81 receptor and prevent recognition by neutralizing antibodies on E2.[125,127-129] Second, HVR1 is an immunodominant epitope and has been proposed as an immunogenic decoy that rapidly evolves under immunogenic pressure to facilitate continuous immune evasion.[130-134] Third, HCV envelope E2 glycoprotein contains an extensive glycan shield that provides protection to conserved neutralizing epitopes.[135] Fourth, the HCV envelope E2 glycoprotein is shielded by host lipoprotein associated to the virus particle.[18] Lastly, the HCV-E2 envelope glycoprotein and its promising epitopes I[104,106-108], II[117-119], and III[124] are associated with a high degree of flexibility. The dynamic nature of E2 results in many different conformations at a given time that influences the affinity of antibodies and could benefit escape of the immune system.[136]

In summary, the epitopes I, II, III, and IV represent important targets for vaccine design with many mAbs available that neutralize HCV *in vitro*. These mAbs provide excellent tools to specifically engineer and validate a vaccine candidate based on their epitopes alone. Purified HCV-E2 envelope glycoprotein or subunit vaccines are likely not the most efficient strategy, because they still present shielding factors and immunodominant decoy

epitopes that elicit non-neutralizing antibodies. These non-functional epitopes rapidly mutate to escape the immune system and result in exhaustion, giving HCV the upper hand.

A more focussed immune response is necessary, using a vaccine that does not include the tools employed by HCV to deceive the immune system. A largely unexplored strategy is to use small conserved epitopes of the HCV-E2 envelope glycoprotein in a vaccine. The advantages of chemistry could be made evident in such a strategy. Synthetic peptides would provide an outcome to selectively present epitopes known to only target neutralizing antibodies. Chemical modifications on these synthetic peptides, for example cyclization or linking to a molecular or protein scaffold, could enhance their efficiency as a vaccine.

1.4 Chemistry provides valuable tools towards epitope-focused vaccine design

Development of synthetic epitopes that exhibit desirable activity depends on understanding important epitope-antibody interactions. Recently, a proof of concept has been presented for antibody-guided discovery of medium-sized molecules that prevented influenza infection *in vitro* and *in vivo*.[137] Design of this medium-sized antibody-mimetic was based on a well-characterized and neutralizing anti-influenza antibody. The resulting mimetic showed anti-influenza properties similar to the antibody. Highlighting the advantage of considering epitope-specific binding activity, function, and mode of action when designing a mimetic.

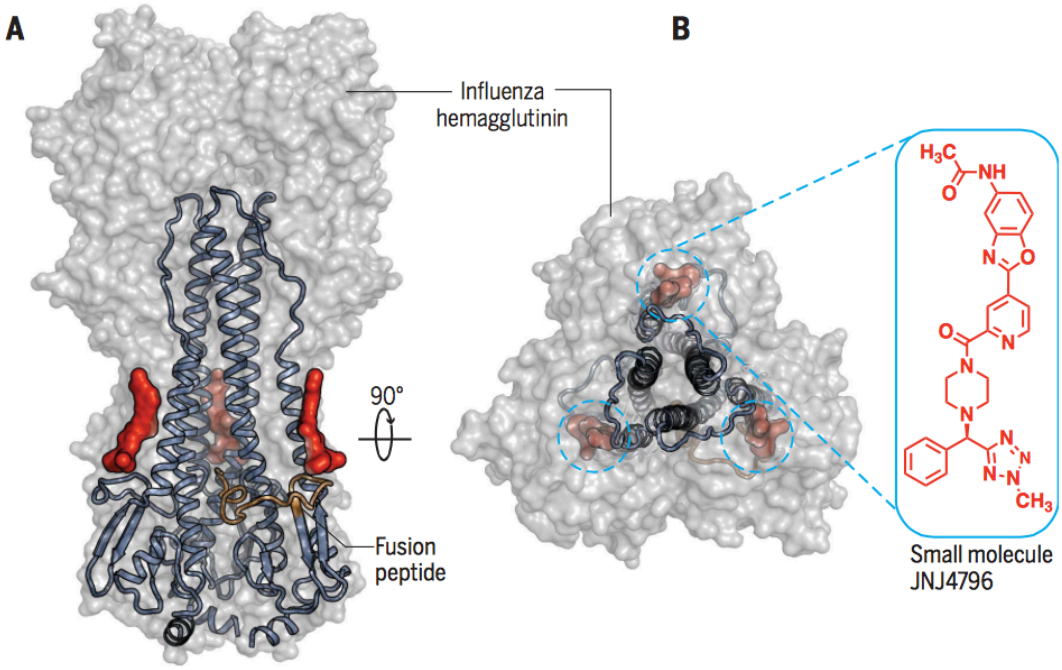

Figure 1.10. Influenza A virus hemagglutinin (HA) in complex with a molecular fusion inhibitor JNJ4796 developed by Van Dongen *et al.*[137] (**A**) Crystal structure of influenza A virus HA (**gray**) in complex with JNJ4796 (**red**) binding and blocking the fusion peptide (**orange**). (**B**) View along the threefold axis of the HA trimer, highlighting three identical binding sites of JNJ4796 (**cyan**) as well as the chemical structure of JNJ4796 (enlarged view). Permission to republish this Figure was granted by the publisher.[137]

The concept presented by Van Dongen *et al.*[137] (Figure 1.10) can be readily adapted towards vaccine design. Development of an effective HCV vaccine can be guided by structural and functional activity of promising epitope-antibody interactions. Conserved epitopes could be presented outside of the HCV-E2 envelope glycoprotein by synthetic modulators such as peptides (Figure 1.11). The benefit of this strategy is that no immunogenic decoys or glycan shields are presented. Specific presentation of only functional epitopes could increase the efficiency of the immune system.

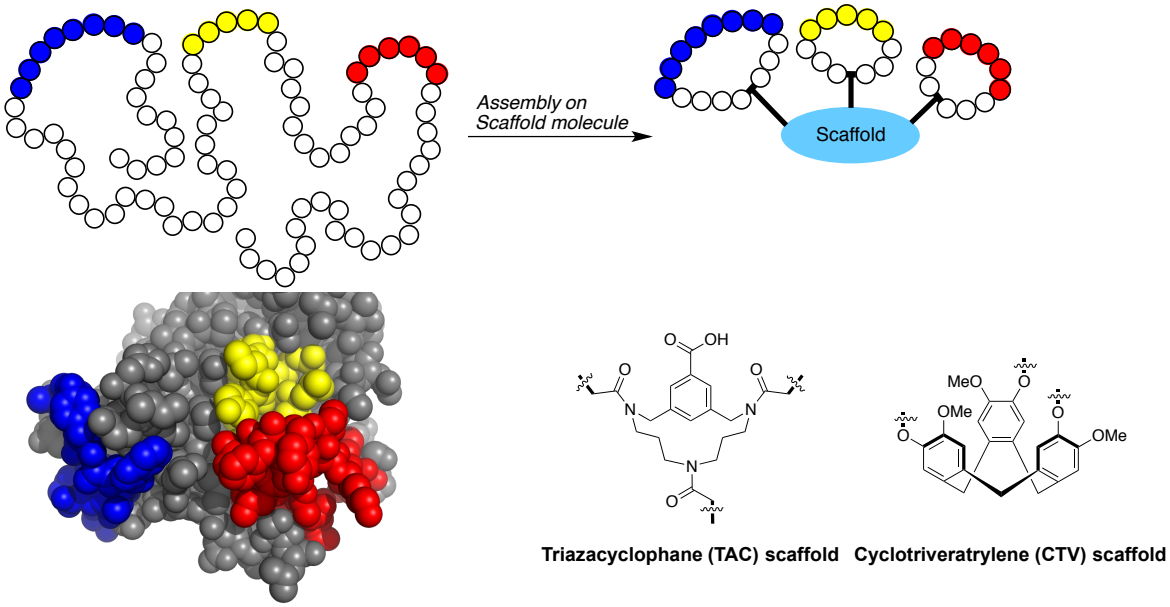

Figure 1.11. Conceptual illustration of epitope mimicry. HCV-E2 epitopes **II in red**, **III in blue**, and **IV in yellow** from the E2 core structure obtained by Kong *et al.*[99] can be taken out of the context of the viral protein using synthetic peptides and chemically conjugated on a fully synthetic molecular scaffold (CTV[138] or TAC[139] developed by Liskamp *et al.*) to maintain the proper spatial configuration of the synthetic epitopes with respect to each other. Thereby, generating a fully synthetic epitope of the HCV-E2 glycoprotein presenting only essential immunogenic information.

1.4.1 Structural conservation of the epitope is essential for effective mimicry

The aim of structure-based vaccine design is conserving or inducing the correct native conformation of (the) epitope(s) of the parent (E2) protein in a synthetic protein mimic. The first step in devising a strategy for epitope mimicry is determining whether the target epitope is continuous or discontinuous (Figure 1.12). Continuous epitopes are recognized as a stand-alone continuous row of amino acids (Figure 1.12A). Discontinuous epitopes are recognized as parts of multiple amino-acid residues that lay farther apart and form a binding pocket by the overall folding of the protein (Figure 1.12B).

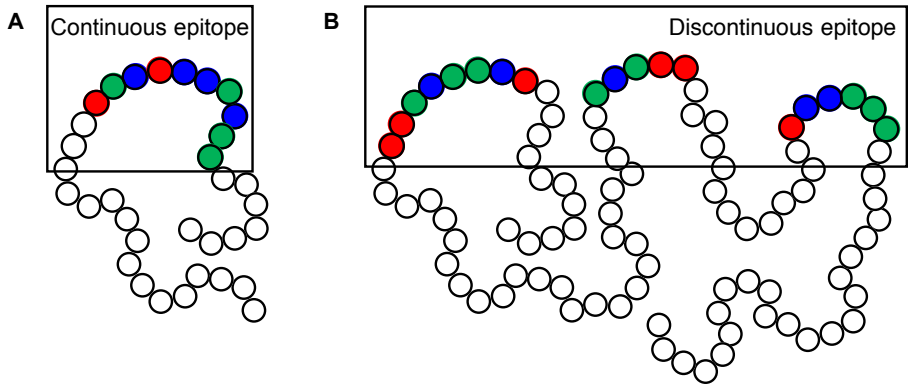

Figure 1.12. Representation of two different structural classes of epitopes. (**A**) Stand alone continuous row of amino acids making up an individual continuous epitope; (**B**) Multiple peptide segments that form a discontinuous epitope by the overall folding of the protein structure. This Figure was adopted from Werkhoven and Liskamp.[140]

The CD81 binding site of HCV envelope E2 glycoprotein, containing epitopes I, II, III, and IV, is a prime example of a discontinuous epitope. Peptides with corresponding sequences towards these epitopes can be readily synthesized by solid phase peptide synthesis (SPPS).[141,142] Using this method the peptide is synthesized on a solid support[143,144] by iterative cycles of a 9-fluorenylmethoxycarbonyl (Fmoc) deprotection step[145-148], followed by a coupling step[149-151] (Figure 1.13). Upon completion of the peptide sequence it is cleaved from the resin and simultaneously fully deprotected at its side chain residues.[143,144,152-156] The N-terminus is often acetylated to form an N-terminal amide bond to improve proteolytic stability and have a better resemblance to a native peptide sequence.[157] Depending on the resin a C-terminal amide can be introduced to further improve upon the proteolytic stability and mimicry of a native peptide sequence.[158] The major challenge in mimicry of a discontinuous epitope is combining the individual

synthetic peptides in a correct spatial orientation. In addition to forming a discontinuous epitope, the individual epitopes I, II, and III are recognized by several antibodies as continuous epitopes. Mimicry of continuous epitopes is relatively simple as a single synthetic peptide could be enough. Mimicry of both continuous and discontinues epitopes will be covered below.

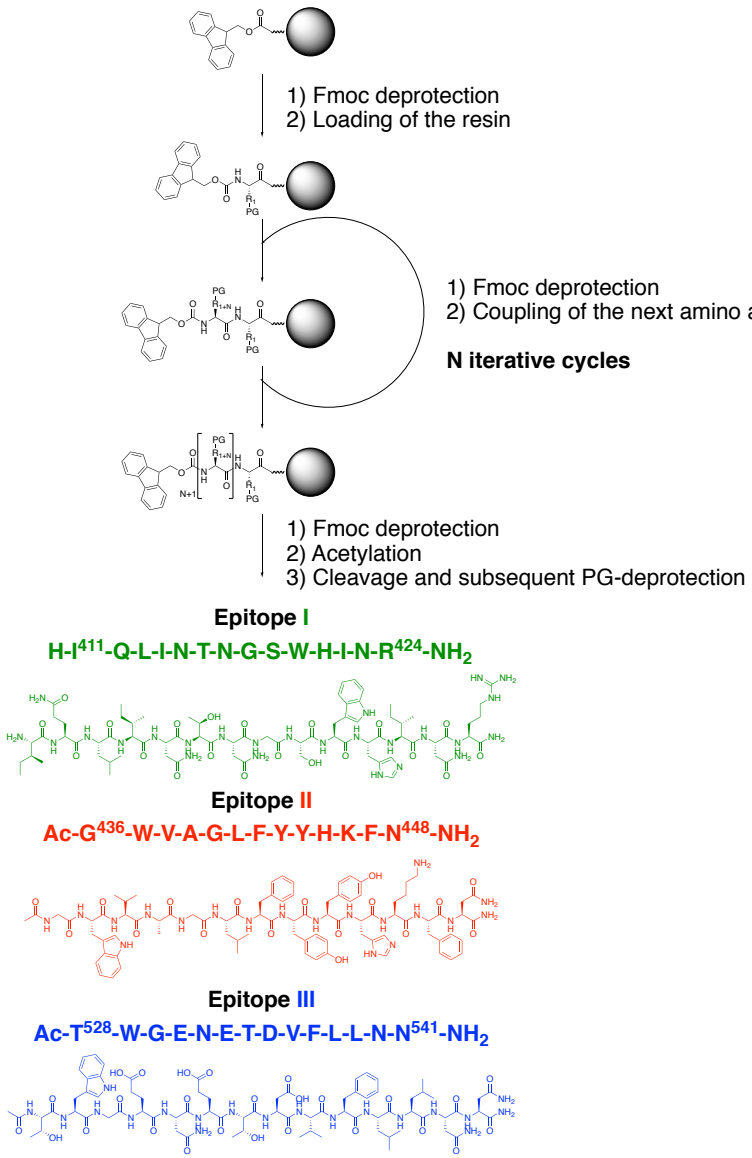

Figure 1.13. Overview of SPPS[141,142] using Fmoc[145-148] chemistry. The synthetic peptide is synthesized on a solid phase resin[143,144] by Fmoc[145-158] deprotection, followed by coupling of an amino acid residue[149-151]. Cycles of deprotection and subsequent coupling afford the peptide with the desired sequence and length. After which, the N-terminus is acetylated and the peptide is cleaved from the resin with subsequent removal of protection groups (PG).[152-156] Affording synthetic peptides based on epitope **I in green**, **II in red**, and **III in blue**.

1.4.2 Mimicry of continuous epitopes exhibiting a high degree of flexibility

In essence, mimicry of continuous epitopes can be achieved by a single synthetic peptide. Depending on the flexibility of the epitope, a simple linear synthetic peptide would be sufficient to represent the native epitope. To provide context with respect to HCV, epitope I could not be resolved in the HCV-E2 core crystal structure and is thus associated with a high degree of flexibility.[99,159] In addition, a linear synthetic peptide representing the epitope has been co-crystalized with four different antibodies, in which the peptide adopted four different structural conformations. (Figure 1.8).[104,106-108] This would suggest that mimicry of epitope I might be as straightforward as a short linear synthetic peptide.

One example of successful epitope mimicry using a short linear peptide (15-mer) led to one of the first peptide vaccines that provided protection against parvovirus.[160] Another example, a longer linear peptide (>60-mer) provided protection against influenza in mice.[161] Nordstrom *et al.*[162] has demonstrated the potential of improving upon an already promising peptide (20-mer) vaccine against *Streptococcus pyogenes* through optimization of the amino-acid sequence. The optimized peptide vaccine showed protection against bacterial infection in mice using a single immunization.[162] In contrast to the original peptide vaccine that required three immunizations to provide protection.[162] Recent research of synthetic linear peptides and their immunogenic potential include, among others, *Mycobacterium tuberculosis*[163], human papilloma virus[164], and *Candida albicans*[165].

1.4.3 Mimicry of epitopes associated with a distinct secondary structure

Most continuous epitopes possess a secondary structure including loop, α-helix or β-strand. Depending on the length and sequence of a synthetic peptide, it might already adopt the native secondary structure of the peptide segment of the epitope naturally. However, the secondary structure often has to be approached by chemical modification(s). The proper secondary structures might be essential for antibody binding and thus will have to be introduced in the epitope mimic.

Loop-like structures are the most often encountered and could be readily mimicked by peptide cyclization. Epitopes within the native protein could be considered to always have, at the very least, a cyclic conformation as they are incorporated in a protein and thus are

flanked by many additional amino acid residues. The synthesis of cyclic peptides and their therapeutic potential is extensively researched.[166-175]

One attractive method and the most widely used for synthesizing cyclic peptides is based on thioether-formation with Cysteine-containing peptides (Figure 1.14).[166-177] Other examples include, the use of copper(I) catalyzed alkyne-azide cycloaddition (CuAAC)[172], oxime ligation[174], and chemo-enzymatic peptide synthesis (CEPS)[173,174].

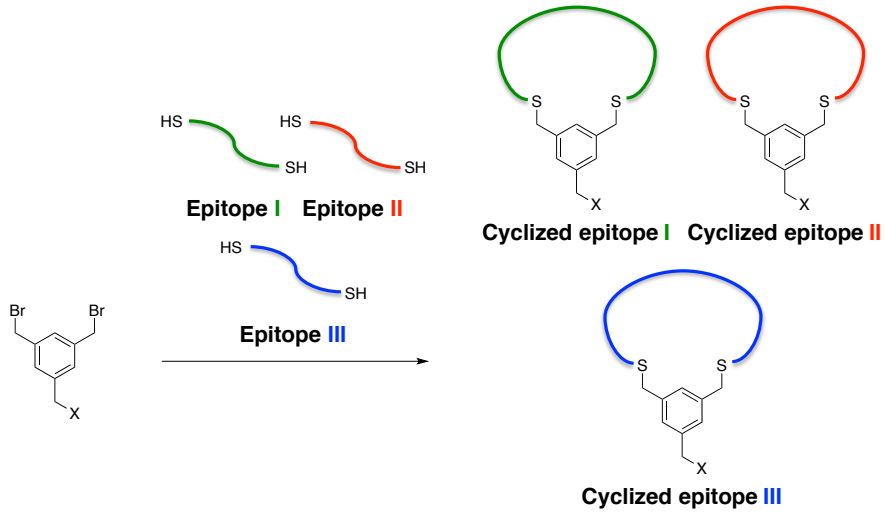

Figure 1.14. Representation of peptide cyclization. Synthetic peptide based on epitopes **I in green**, **II in red**, and **III in blue**, are equipped with one Cysteine residue at the N-terminus and C-terminus to allow for cyclization by thioether bond formation on a benzylic-bromide derivative. The shown benzylic-bromide derivative can have a variety of additional functionalities (X) installed on its ring to allow further chemical modification of the cyclic peptides.[175-177]

Indeed, cyclic peptides have been explored as a strategy toward vaccination against HCV with contrasting outcomes. Sandomenico *et al.*[178] used cyclic peptides based on HCV epitope I that were able to induce antibodies in an immunization experiment, but were unable to neutralize infection. In contrast, success was obtained by Pierce *et al.*[179] when using mono-glycosylated cyclic peptides based on epitope I as well as recombinant E2 glycoprotein containing one or two copies of the epitope I region that elicited neutralizing antibodies in immunized mice. Thereby, Pierce *et al.*[179] demonstrated that engineered epitope-based peptide vaccines can induce neutralizing anti-HCV antibodies *in vivo*. Antibodies obtained by Pierce *et al.*[179] showed neutralization *in vitro*, but are unknown to provide protection against HCV infection *in vivo*.

The neutralization capacity of vaccine-elicited antibodies is typically tested *in vitro* using cell culture models or pseudo particles of HCV. To truly assess the potential of a vaccine candidate, it is essential to show that vaccination results in protection from HCV infection *in vivo*. These experiments are rare, due to limited animal models.[180] Vercauteren *et al.*[181] has developed a human liver chimeric mice model that is susceptible to HCV infection. Thereby providing a platform in which vaccine-induced protection against HCV infection can be validated *in vivo*.

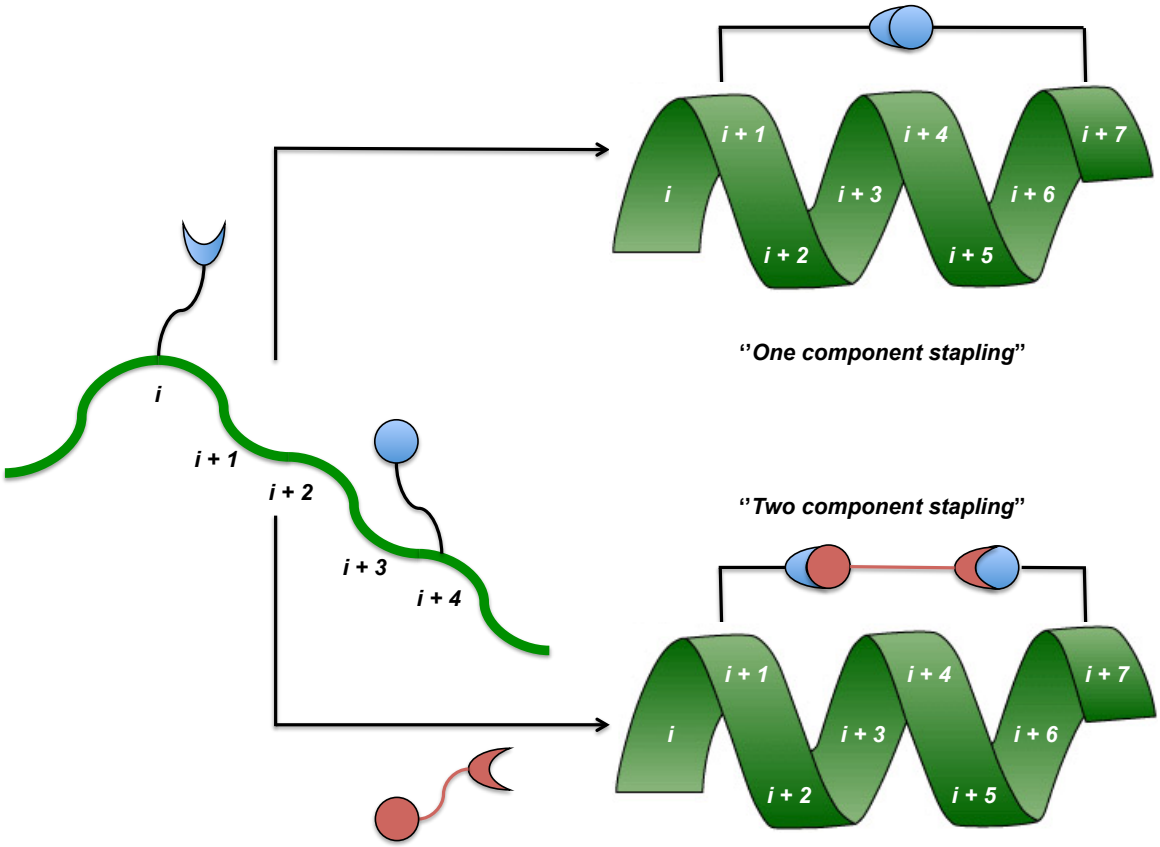

Figure 1.15. Overview of ''*peptide stapling*'' using a ''*one component*'' versus ''*two component*'' strategies. Side chains of properly spaced amino acids (*i*, *i*+4, *i*+7, *i*+11) are chemically linked to each other by, for example amide bond formation between lysine and glutamic acid residues (''*one component*''); Side chains of properly spaced amino acids (*i*, *i*+4, *i*+7, *i*+11) are chemically linked to each other by, for example thioether bond formation using Cysteine residues and benzylic-bromide derivatives (also see Figure 1.14). This Figure was adapted from Lau *et al.*[182]

A wide variety of chemical modifications allow for the stabilization of α-helices and β-strands, but will not be discussed in detail, as these strategies were not attempted in this research. Chemically linking the side chains of appropriately spaced (*i*, *i+4, i+7, i*+11)

amino acid residues in a peptide, often referred to as ''*peptide-stapling*'' is a widely used strategy to form α-helical structures (Figure 1.15).[182] Both ''*one component''* as well as ''*two component*'' strategies can be employed, in which the ''*two component*'' is based on intermolecular stabilization by conjugation onto a second molecule. This could be preferred as additional chemical handles can be installed through conjugation with the second molecule for further modification. Especially, the ''*two component*'' is reminiscent of peptide cyclization via thioether bond formation that was discussed earlier. Combining strategies of peptide cyclization, inducing a turn using an appropriate template (*i.e.* D-Proline-L-Proline), and reinforcing side-chain interactions by π-stacking, disulfide bond formation, or ''*Hydrogen Bond Surrogates*'' can contribute towards mimicry of a β-turn or β-hairpin conformation (Figure 1.16).[183]

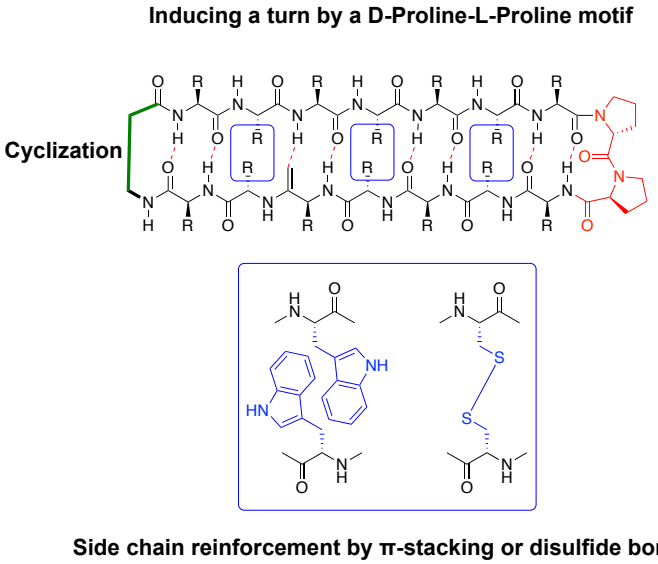

Figure 1.16. Overview of β-hairpin stabilization. Combining cyclization of a synthetic peptide in **green**, together with inducing a turn-motif by for example D-Proline-L-Proline in **red** allow for hydrogen-bonds of the primary peptide chain to stabilize a β-hairpin structure. Stabilization could be further enhanced by side-chain interactions in **blue** by for example Tryptophan induced π-stacking or formation of disulfide bonds using Cysteines. This Figure was adapted from Sawyer *et al.*[183]

1.4.4 Mimicry of discontinuous epitopes

Many epitopes are discontinuous and require presentation of multiple peptide sequences with the correct spatial orientation to resemble the native protein. The major strategy towards discontinuous epitope mimics relies on fully engineered fusion proteins based on a patchwork of recombinant peptide sequences associated with promising neutralizing epitopes that are linked by flexible amino-acid sequences.[184-187] The idea is that these engineered fusion proteins are large enough and exhibit the right amount of rigidity in the epitopes compared to flexibility in the linker sequences to adopt the desired folding and presentation of the epitopes as they are found in the protein. Another, more promising strategy is based on scaffold proteins that share structural similarity to the target protein in which the desired epitopes are recombinantly expressed.[188] However, these approaches have rarely been tested outside of a computational setting and remain to be validated experimentally.[184,185] With the exception provided by Guo *et al.*[186] and Singh *et al.*[187] which have shown that their designed vaccines indeed provided protection against infection *in vivo*. As an example in the work for HCV, He *et al.*[188] investigated proteins exhibiting structural similarities to HCV envelope E1 and E2 glycoproteins as scaffolds to incorporate recombinant HCV epitopes towards vaccine design. He *et al.*[188] continued to validate the designed vaccine towards antibody binding *in vitro*, but has yet to show whether it induces neutralizing antibodies and subsequent protection *in vivo*.

Full synthetic mimicry of discontinuous epitopes is met with significant challenges and is rarely described in the literature. Liskamp *et al.*[138,139,176,177,189-193] have developed several molecular scaffolds capable of orthogonally introducing cyclic peptides to adopt a three-dimensional configuration and are leading figures within the field. These scaffolds are the cyclotriveratrylene (CTV)[138] and triazacyclophane (TAC)[139] scaffolds that have been equipped with orthogonally protected alkyne-moieties that allow for the sequential conjugation of azide modified cyclic peptides (Figure 1.17). Design of the CTV and TAC scaffolds, including the TAC precursors, have paved the way toward fully synthetic artificial receptors[189], antibodies[138,190], and vaccines.[139,176,177,191-193]

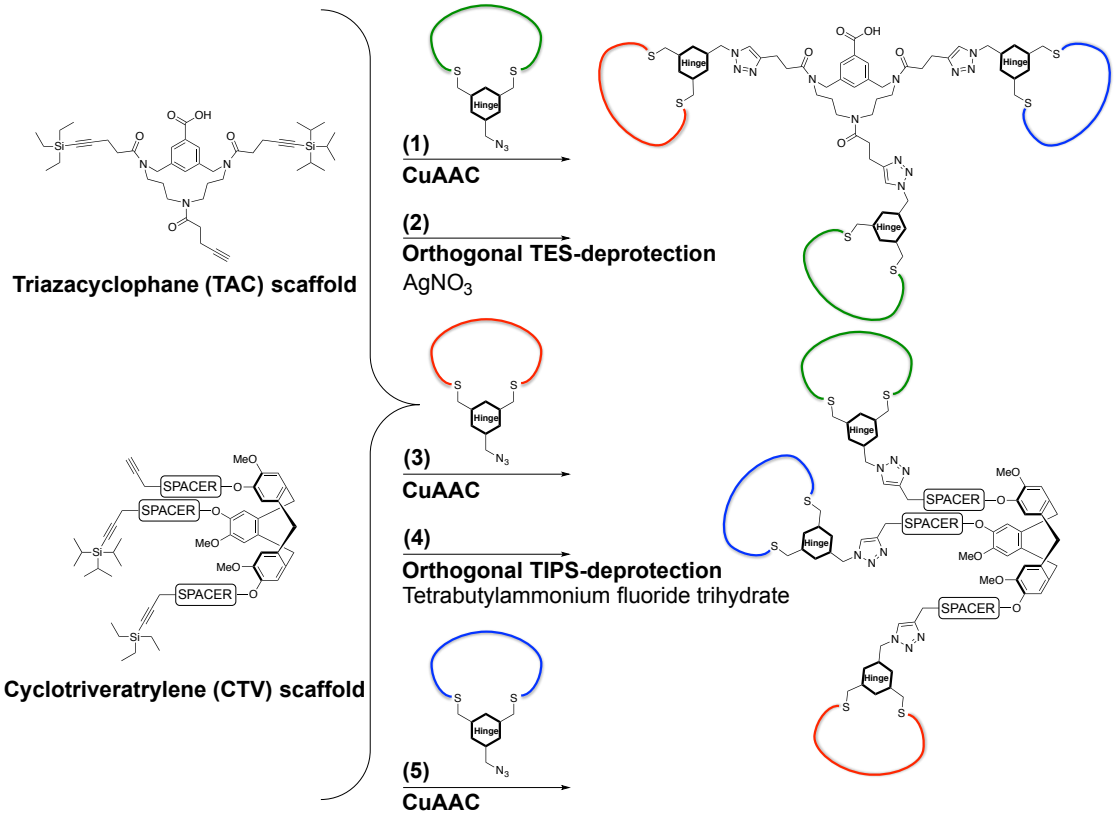

Figure 1.17. Step for step instalment towards a discontinuous epitope mimic using molecular scaffolds. Sequential conjugation of azide-derivatized cyclic peptides on the TAC scaffold or CTV scaffold, via the use of orthogonal silyl protection groups. This Figure was adopted from Longin *et al.*[138] and Werkhoven *et al.*[139]

1.5 References

1. WHO (2017) *Global Hepatitis Report, 2017, WHO*
2. Negro, F., Forton, D., Craxí, A., *et al.* (2015) Extrahepatic morbidity and mortality of chronic hepatitis C. *Gastroenterology. 149*(6):1345–1360. DOI: 10.1053/j.gastro.2015.08.035
3. Lee, M. H., Yang, H. I., Yuan, Y., *et al.* (2014) Epidemiology and natural history of hepatitis C virus. *World J. Gastroenterol. 20*(28):9270–9280. DOI: 10.3748/wjg.v20.i28.9270
4. Bruggmann, P., Berg, T., Ovrehus, A. L., *et al.* (2014) Historical epidemiology of hepatitis C virus (HCV) in selected countries. *J. Viral. Hepat. 21* Suppl 1:5-33. DOI: 10.1111/jvh.12247
5. Gower, E., Estes, C., Blach, S., *et al.* (2014) Global epidemiology and genotype distribution of the hepatitis C virus infection. *J. Hepatol. 61*(1 Suppl):S45-57. DOI: 10.1016/j.hep.2014.07.027
6. Janiak, M., Caraballo Cortez, K., Demkow, U., *et al.* (2018) Spontaneous elimination of hepatitis C virus infection. *Adv. Exp. Med. Biol. 2018*(1039):45-54. DOI: 10.1007/5584_2017_76
7. European association for the study of the liver. (2017) EASL recommendations on treatment of hepatitis C 2016. *J. Hepatol. 66*(1):153–194. DOI: 10.1016/j.hep.2016.09.001
8. Bartenschlager, R., Baumert, T. F., Buhk, J., *et al.* (2018) Critical challenges and emerging opportunities in hepatitis C virus research in an era of potent antiviral therapy: Considerations for scientists and funding agencies. *Virus Res. 248*:53–62. DOI: 10.1016/j.virusres.2018.02.016
9. Midgard, H., Weir, A., Palmateer, N., *et al.* (2016) HCV epidemiology in high-risk groups and the risk of reinfection. *J. Hepatol. 65*(1 Suppl):S33–S45. DOI: 10.1016/j.hep.2016.07.012
10. Baumert, T. F., Juhling, F., Ono, A., *et al.* (2017) Hepatitis C-related hepatocellular carcinoma in the era of new generation antivirals. *BMC Med. 15*(1):52. DOI: 10.1186/s12916-017.0815-7
11. Micallef, J. M., Kaldor, J. M., Dore, G. J. (2006) Spontaneous viral clearance following acute hepatitis C infection: a systematic review of longitudinal studies. *J. Viral. Hepat. 13*(1):34–41. DOI: 10.1111/j.1365-2893.2005.00651.x

12. Kim, C. W., Chang, K. M. (2013) Hepatitis C virus: Virology and life cycle. *Clin. Mol. Hepatol. 19*(1):17–25. DOI: 10.3350/cmh.2013.19.1.17. DOI: 10.3350/cmh.2013.19.1.17
13. Dubuisson, J., Cosset, F. L. (2014) Virology and cell biology of the hepatitis C virus life cycle: An update. *J. Hepatol. 61* (1 Suppl):S3–S13. DOI: 10.1016/j.hep.2014.06.031
14. Miao, Z., Zhenrong, X., Miao, J., *et al.* (2019) Regulated entry of hepatitis C virus into hepatocytes. *Viruses. 9*(5):100. DOI: 10.3390/v9050100
15. Lindenbach, B. D., Rice, C. M. (2013) The ins and outs of hepatitis C virus entry and assembly. *Nat. Rev. Microbiol. 11*(10):688–700. DOI: 10.1038/nrmicro3098
16. Paul, D., Madan, V., Bartenschlager, R. (2014) Hepatitis C virus RNA replication and assembly: Living on the fat of the land. *Cell Host Microbe. 16*(5):569-579. DOI: 10.1016/j.chom.2014.10.008
17. Scheel, T. K., Rice, C. M., (2013) Understanding the hepatitis C virus life cycle paves the way for highly effective therapies. *Nat. Med. 19*(7):837–849. DOI: 10.1038/nm.3248
18. Catanese, M. T., Uryu, K., Kopp, M., *et al.* (2013) Ultra-structural analysis of hepatitis C virus particles. *Proc. Natl. Acad. Sci. USA. 110*(23):9505-9510. DOI:10.1073/pnas.1307527110
19. Jiang, J., Wu, X., Tang, H., *et al.* (2013) Apoliprotein E mediates attachment of clinical hepatitis C virus to hepatocytes by binding to cell surface heparin sulphate proteoglycan receptors. *PLoS One. 8*(7):e67982. DOI: 10.1371/journal.pone.0067982
20. Mahley, R. W., Ji, Z. S. (1999) Remnant lipoprotein metabolism: Key pathways involving cell-surface heparan sulfate proteoglycans and apolipoprotein E. *J. Lipid Res. 40*(1):1-16. DOI: unavailable
21. Agnello, V., Abel, G., Elfahal, M., *et al.* (1999) Hepatitis C virus and other flaviviridae viruses enter cells via low density lipoprotein receptor. *Proc. Natl. Acad. Sci. USA. 96*(22):12766-12771. DOI: 10.1073/pnas.96.22.12766
22. Dao Thi, V. L., Granier, C., Zeisel, M. B., *et al.* (2012) Characterization of hepatitis C virus particle sub-populations reveals multiple usage of the scavenger receptor BI for entry steps. *J. Biol. Chem. 287*(37):31242-31257. DOI: 10.1074/jbc.m112.365924
23. Eck, M. V., Hoekstra, M., Out, R., *et al.* (2008) Scavenger receptor BI facilitates the metabolism of VLDL lipoproteins *in vivo*. *J. Lipid Res. 49*(1):136-146. DOI: 10.1194/jlr.m700355-jlr200

24. Sharma, N. R., Mateu, G., Dreux, M., *et al.* (2011) Hepatitis C virus is primed by CD81 protein for low pH-dependent fusion. *J. Biol. Chem. 286*(35):30361-30376. DOI: 10.1074/jbc.m111.263350
25. Evans, M. J., von Hahn, T., Tscherne, D. M., *et al.* (2007) Claudin-1 is a hepatitis C virus co-receptor required for a late step in entry. *Nature. 446*(7137):801-805. DOI: 10.1038/nature05654
26. Benedicto, I., Molina-Jimenez, F., Bartosch, B., *et al.* (2009) The tight junction-associated protein occluding is required for a postbinding step in hepatitis C virus entry and infection. *J. Virol. 83*(16):8012-8020. DOI: 10.1128/jvi.00038-09
27. Feneant, L., Levy, S., Cocquerel, L. (2014) CD81 and hepatitis C virus (HCV) infection. *Viruses. 6*(2):535-572. DOI: 10.3390/v6020535
28. Flint, S. J., Enquist, L. W., Racaniello, V. R., Skalka, A. M. (2009) Immune defenses. *ASM Press. Third edition.* (Flint, S. J., Enquist, L. W., Racaniello, V. R., Skalka, A. M., Eds.) pp. 87-132, Chapter 4, American Society for Microbiology, Washington, DC
29. Horner, S. M., Gale, M. Jr. (2013) Regulation of hepatic innate immunity by hepatitis C virus. *Nat. Med. 19*(7):879–888. DOI: 10.1038/nm.3253
30. Lohmann, V. (2013) Hepatitis C virus RNA replication. *Curr. Top. Microbiol. Immunol. 369*:167-198. DOI: 10.1007/978-3-642-27340-7_7
31. Foy, E., Li, K., Sumpter, R. Jr., *et al.* (2005) Control of antiviral defenses through hepatitis C virus disruption of retinoic acid-inducible gene-I signaling. *Proc. Natl. Acad. Sci. USA. 102*(8):2986-2991. DOI: 10.1073/pnas.0408707102
32. Li, K., Foy, E., Ferreon, J. C. *et al.* (2005) Immune evasion by hepatitis C virus NS3/4A protease-mediated cleavage of the Toll-like receptor 3 adaptor protein TRIF. *Proc. Natl. Acad. Sci. USA. 102*(8):2992-2997. DOI: 10.1073/pnas.0408824102
33. McAllister, C. S., Samuel, C. E. (2009) The RNA-activated protein kinase enhances the induction of interferon-beta and apoptosis mediated by cytoplasmic RNA sensors. *J. Biol. Chem. 284*(3):1644-1651. DOI: 10.1074/jbc.M807888200
34. Arnaud, N., Dabo, S., Maillard, P., *et al.* (2010) Hepatitis C virus controls interferon production through PKR activation. *PLoS One. 5*(5):e10575. DOI: 10.1371/journal.pone.0010575
35. Shimoike, T., McKenna, S. A., Lindhout, D. A., *et al.* (2009) Translation insensitivity to potent activation of PKR by HCV IRES RNA. *Antiviral Res. 83*(3):228-237. DOI: 10.1016/j.antiviral.2009.05.004

36. Gale, M. J. Jr., Korth, M. J., Tang, N. M., *et al.* (1997) Evidence that hepatitis C virus resistance to interferon is mediated through repression of the PKR protein kinase by the non-structural NS5A protein. *Virology. 230*(2):217-227. DOI: 10.1006/viro.1997.8493
37. Taylor, D. R., Shi, S. T., Romano, P. R., *et al.* (1999) Inhibition of the interferon-inducible protein kinase PKR by HCV E2 protein. *Science. 285*(5424):107-110. DOI: 10.1126/science.285.5424.107
38. Varela, J. C., Tomlinson, S. (2015) Complement: an overview for the clinician. *Hematol. Oncol. Clin. North. Am. 29*(3):409-427. DOI: 10.1016/j.hoc.2015.02.001
39. Sarma, J. V., Ward, P. A. (2011) The complement system. *Cell Tissue Res. 343*(1):227-235. DOI: 10.1007/s00441-010-1034-0
40. Trouw, L. A., Daha, M. R. (2011) Role of complement in innate immunity and host defence. *Immunol. Lett. 138*(1):35-37. DOI: 10.1016/j.imlet.2011.02.014
41. Kwon, Y. C., Meyer, K., Peng, G., *et al.* (2019) Hepatitis C virus E2 envelope glycoprotein induces an immunoregulatory phenotype in macrophages. *Hepatology. 69*(5):1873-1884. DOI: 10.1002/hep.29843
42. Saito, K., Ait-Goughoulte, M., Truscott, S. M., *et al.* (2008) Hepatitis C virus inhibits cell surface expression of HLA-DR, prevents dendritic cell maturation, and induces interleukin-10 production. *J. Virol. 82*(7):3320-3328. DOI: 10.1128/jvi.02547-07
43. Kwon, Y. C., Kim, H., Meyer, K., *et al.* (2016) Distinct CD55 isoform synthesis and inhibition of complement-dependent cytolysis by hepatitis C virus. *J. Immunol. 197*(4):1127-1136. DOI: 10.4049/jimmunol.1600631
44. Ding, Q., Von Schaewen, M., Ploss, A. (2014) The impact of hepatitis C virus entry on viral tropism. *Cell Host Microbe. 16*(5):562-568. DOI: 10.1016/j.chom.2014.10.009
45. Neumann, A. U., Lam, N. P., Dahari, H., *et al.* (1998) Hepatitis C viral dynamics in vivo and the antiviral efficacy of interferon-alpha therapy. *Science. 282*(5386):103-107. DOI: 10.1126/science.282.5386.103
46. Rong, L., Dahari, H., Ribeiro, R. M., *et al.* (2010) Rapid emergence of protease inhibitor resistance in hepatitis C virus. *Sci. Transl. Med. 2*(30):30ra32. DOI: 10.1126/scitranslmed.3000544
47. Schulze Zur Wiesch, J., Ciuffreda, D., Lewis-Ximenez, L., *et al.* (2012) Broadly directed virus-specific CD4+ T cell responses are primed during acute hepatitis C virus, but rapidly disappear from human blood with viral persistence. *J. Exp. Med. 209*(1):61-75. DOI: 10.1084/jem.20100388

48. Bengsch, B., Seigel, B., Ruhl, M., *et al.* (2010) Coexpression of PD-1, 2B4, CD160 and KLRG1 on exhausted HCV-specific CD8+ T cells is linked to antigen recognition and T cell differentiation. *PLoS Pathog. 6*(6):e1000947. DOI: 10.1371/journal.ppat.1000947
49. Radziewicz, H., Ibegbu, C. C., Fernandez, M. L., *et al.* (2007) Liver-infiltrating lymphocytes in chronic human hepatitis C virus infection display an exhausted phenotype with high levels of PD-1 and low levels of CD127 expression. *J. Virol. 81*(6):2545-2553. DOI: 10.1128/jvi.02021-06
50. Golden-Mason, L., Palmer, B. E., Kassam, N., *et al.* (2009) Negative immune regulator Tim-3 is overexpressed on T cells in hepatitis C virus infection and its blockade rescues dysfunctional CD4+ and CD8+ T cells. *J. Virol. 83*(18):9122-9130. DOI: 10.1126/jvi.00639-09
51. Kroy, D. C., Ciuffreda, D., Cooperrider, J. H., *et al.* (2014) Liver environment and HCV replication affect human T-cell phenotype and expression of inhibitory receptors. *Gastroenterology. 146*(2):550-561. DOI: 10.1053/j.gastro.2013.10.022
52. Wherry, E. J. (2011) T cell exhaustion. *Nat. Immunol. 12*(6):492-499. DOI: 10.1038/ni.2035
53. Von Hahn, T., Yoon, J. C., Alter, H., *et al.* (2007) Hepatitis C virus continuously escapes from neutralizing antibody and T-cell responses during chronic infection in vivo. *Gastroenterology. 132*(2):667-678. DOI: 10.1053/j.gastro.2006.12.008
54. Dowd, K. A., Netski, D. M., Wang, X. H., *et al.* (2009) Selection pressure from neutralizing antibodies drives sequence evolution during acute infection with hepatitis C virus. *Gastroenterology. 136*(7):2377-2386. DOI: 10.1053/j.gastro.2009.02.080
55. Helle, F., Duverlie, G., Dubuisson, J. (2011) The hepatitis C virus glycan shield and evasion of the humoral response. *Viruses. 3*(10):1909-1932. DOI: 10.3390/v3101909
56. Cashman, S. B., Marsden, B. D., Dustin, L. B. (2014) The humoral immune response to HCV: Understanding is key to vaccine development. *Front. Immunol. 5*:550. DOI: 10.3389/fimmu.2014.00550
57. Ball, J. K., Tarr, A. W., McKeating, J. A. (2014) The past, present and future of neutralizing antibodies for hepatitis C virus. *Antiviral Res. 105*:100-111. DOI: 10.1016/j.antiviral.2014.02.013
58. Dustin, L. B. (2017) Innate and adaptive immune responses in chronic HCV infection. *Curr. Drug Targets. 18*(7):826-843. DOI: 10.2174/1389450116666150825110532

59. Ray, R. B., Ray, R. (2019) Hepatitis C virus manipulates humans as its favorite host for a long-term relationship. *Hepatology. 69*(2):889-900. DOI: 10.1002/hep.30214
60. Mehta, S. H., Cox, A., Hoover, D. R., *et al.* (2002) Protection against persistence of hepatitis C virus. *Lancet. 359*(9316):1478-1483. DOI: 10.1016/S0140-6736(02)08435-0
61. Lanford, R. E., Guerra, B., Chavez, D., *et al.* (2004) Cross-genotype immunity to hepatitis C virus. *J. Virol. 78*(3):1575-1581. DOI: 10.1128/jvi.78.3.1575-1581.2004
62. Buhk, J. Thimme, R., Meunier, J. C., *et al.* (2008) Previously infected chimpanzees are not consistently protected against reinfection or persistent infection after reexposure to the identical hepatitis C virus strain. *J. Virol. 82*(16):8183-8195. DOI: 10.1128/jvi.00142-08
63. Eyler, J. K. (2003) Smallpox in history: the birth, death, and impact of a dread disease. *J. Lab. Clin. Med. 142*(4):216-220. DOI: 10.1016/S0022-2143(03)00102-1
64. Goodson, J. L., Seward, J. F. (2015) Measles 50 years after use of measles vaccine. *Infect. Dis. Clin. North. Am. 29*(4):725-743. DOI: 10.1016/j.idc.2015.08.001
65. Bandyopadhyay, A. S., Garon, J., Seib, K., *et al.* (2015) Polio vaccination: past, present, and future. *Future Microbiol. 10*(5):791-808. DOI: 10.2217/fmb.15.19
66. Rios, A. (2018) Fundamental challenges to the development of a preventive HIV vaccine. *Curr. Opin. Virol. 29*:26-32. DOI: 10.1016/j.coviro.2018.02.004
67. Stephenson, K. E. (2018) Therapeutic vaccination for HIV: hopes and challenges. *Curr. Opin. HIV. AIDS. 13*(5):408-415. DOI: 10.1097/COH.0000000000000491
68. Honegger, J. R., Zhou, Y., Walker, C. M. (2014) Will there be a vaccine to prevent HCV infection? *Semin. Liver Dis. 34*(1):79-88. DOI: 10.1055/s-0034-1371081
69. Baily, J. R., Barnes, E., Cox, A. L. (2019) Approaches, progress, and challenges to hepatitis C vaccine development. *Gastroenterology. 156*(2):418-430. DOI: 10.1053/j.gastro.2018.08.060
70. Flint, S. J., Enquist, L. W., Racaniello, V. R., Skalka, A. M. (2009) Immune defenses. *ASM Press. Third edition.* (Flint, S. J., Enquist, L. W., Racaniello, V. R., Skalka, A. M., Eds.) pp. 250-277 Chapter 8, American Society for Microbiology, Washington, DC
71. Folgori, A., Capone, S., Ruggeri, L., *et al.* (2006) A T-cell HCV vaccine eliciting effective immunity against heterologous virus challenge in chimpanzees. *Nat. Med. 12*(2):190-197. DOI: 10.1038/nm1353

72. Barnes, E., Folgori, A., Capone, S., *et al.* (2012) Novel adenovirus-based vaccines induce broad and sustained T cell responses to HCV in man. *Sci. Transl. Med. 4*(115):115ra1. DOI: 10.1126/scitranslmed.3003155
73. Swadling, L., Capone, S., Antrobus, R. D., *et al.* (2014) A human vaccine strategy based on chimpanzee adenoviral and MVA vectors that primes, boosts, and sustains functional HCV-specific T cell memory. *Sci. Transl. Med. 6*(261):261ra153. DOI: 10.1126/scitranslmed.3009185
74. Kelly, C., Swadling, L., Brown, A., *et al.* (2015) Cross-reactivity of hepatitis C virus specific vaccine-induced T cells at immunodominant epitopes. *Eur. J. Immunol. 45*(1):309-316. DOI: 10.1002/eji.201444686
75. Feneant, L., Levy, S., Cocquerel, L. (2014) CD81 and hepatitis C virus (HCV) infection. *Viruses. 6*(2):535-572. DOI: 10.3390/v6020535
76. Choo, Q. L., Kuo, G., Ralston, R., *et al.* (1994) Vaccination of chimpanzees against infection by the hepatitis C virus. *Proc. Natl. Acad. Sci. USA. 91*(4):1294-1298. DOI: 10.1073/pnas.91.4.1294
77. Meunier, J. C., Gottwein, J. M., Houghton, M., *et al.* (2011) Vaccine-induced cross-genotype reactive neutralizing antibodies against hepatitis C virus. *J. Infect. Dis. 204*(8):1186-1190. DOI: 10.1093/infdis/jir511
78. Frey, S. E., Houghton, M., Coates, S., *et al.* (2010) Safety and immunogenicity of HCV E1E2 vaccine adjuvanted with MF59 administered to healthy adults. *Vaccine. 28*(38):6367-6373. DOI: 10.1016/j.vaccine.2010.06.084
79. Ray, R., Meyer, K., Banerjee, A., *et al.* (2010) Characterization of antibodies induced by vaccination with hepatitis C virus envelope glycoproteins. *J. Infect. Dis. 2020*(6):862-866. DOI: 10.1086/655902
80. Law, J. L., Chen, C., Wong, J., *et al.* (2013) A hepatitis C virus (HCV) vaccine comprising envelope glycoprotein gpE1/gpE2 derived from a single isolate elicits broad cross-genotype neutralizing antibodies in humans. *PLoS One. 8*(3):e0059776. DOI: 10.1371/journal.pone.0059776
81. Wong, J. A., Bhat, R., Hockman, D., *et al.* (2014) Recombinant hepatitis C virus envelope glycoprotein vaccine elicits antibodies tartgeting multiple epitopes on the envelope glycoprotein associated with broad cross-neutralization. *J. Virol. 88*(24):14278-14288. DOI: 10.1128/jvi.01911-14
82. Li, D., Wang, X., Von Schaewen, M., *et al.* (2017) Immunization with a subunit HCV vaccine elicits pan-genotypic neutralizing antibodies and intrahepatic T-cell responses in nonhuman primates. *J. Infect. Dis. 215*(12):1824-1831. DOI: 10.1093/infdis/jix180

83. Shoukry, N. H. (2018) Hepatitis C vaccines, antibodies, and T cells. *Front. Immunol. 9*:1480. DOI: 10.3389/fimmu.2018.0148

84. Lambert, P. H., Liu, M., Siegrist, C. A. (2005) Can successful vaccines teach us how to induce efficient protective immune responses? *Nat. Med. 11*(4 Suppl):S54-S62. DOI:10.1038/nm1216

85. Lavilette, D., Morice, Y., Germanidis, G., *et al.* (2005) Human serum facilitates hepatitis C virus infection, and neutralizing responses inversely correlate with virus replication kinetics at the acute phase of hepatitis C virus infection. *J. Virol. 79*(10):6023-6034. DOI: 10.1128/jvi.79.10.6023-6034.2005

86. Pestka, J. M., Zeisel, M. B., Blaser, E., *et al.* (2007) Rapid induction of virus-neutralizing antibodies and viral clearance in a single-source outbreak of hepatitis C. *Proc. Natl. Acad. Sci. USA. 104*(14):6025-6030. DOI: 10.1073/pnas.0607026104

87. Osburn, W. O., Fischer, B. E., Dowd, K. A., *et al.* (2010) Spontaneous control of primary hepatitis C virus infection and immunity against persistent reinfection. *Gastroenterology. 138*(1):315-324. DOI: 10.1053/j.gastro.2009.09.017

88. Law, M., Maruyama, T., Lewis, J., *et al.* (2008) Broadly neutralizing antibodies protect against hepatitis C virus quasispecies challenge. *Nat. Med. 14*(1):25-27. DOI: 10.1038/nm1698

89. Vanwolleghem, T., Bukh, J., Meuleman, P., *et al.* (2008) Polyclonal immunoglobulins from a chronic hepatitis C virus patient protect human liver-chimeric mice from infection with a homologous hepatitis C virus strain. *Hepatology. 47*(6):1846-1855. DOI: 10.1002/hep/.22244

90. Morin, T. J., Broering, T. J., Leav, B. A., *et al.* (2012) Human monoclonal antibody HCV1 effectively prevents and treats HCV infection in chimpanzees. *PLoS Pathog. 8*(1):e1002895. DOI: 10.1371/journal.ppat.1002895

91. Drummer, H. E. (2014) Challenges to the development of vaccines to hepatitis C virus that elicit neutralizing antibodies. *Front. Microbiol. 5*:329. DOI: 10.3389/fmicb.2014.00329

92. Dunlop, J. I., Owsianka, A. M., Cowton, V. M., *et al.* (2015) Current and future prophylactic vaccines for hepatitis C virus. *Vaccine Dev. Ther. 5*:31-44. DOI: 10.2147/vdt.S48437

93. Sautto, G., Tarr, A. W., Mancini, N., *et al.* (2013) Structural and antigenic definition of hepatitis C virus E2 glycoprotein epitopes targeted by monoclonal antibodies. *Clin. Dev. Immunol.* 2013:450963. DOI: 10.1155/2013/450963

94. Angus, A. G., Patel, A. H. (2011) Immunotherapeutic potential of neutralizing antibodies targeting conserved regions of the HCV envelope glycoprotein E2. *Fut. Microbiol. 6*(3):279-294/ DOI: 10.2217/fmb.11.9

95. Owsianka, A. M., Timms, J. M., Tarr, A. W., *et al.* (2006) Identification of conserved residues in the E2 envelope glycoprotein of the hepatitis C virus that are critical for CD81 binding. *J. Virol. 80*(17):8695-8704. DOI: 10.1128/jvi.00271-06

96. Drummer, H. E., Boo, I., Maerz, A., *et al.* (2006) A conserved Gly436-Trp-Leu-Ala-Gly-Leu-Phe-Tyr motif in hepatitis C virus glycoprotein E2 is a determinant of CD81 binding and viral entry. *J. Virol. 80*(16):7844-7853. DOI: 10.1128/jvi.00029-06

97. Keck, Z. Y., Op De Beeck, A., Hadlock, K. G., *et al.* (2004) Hepatitis C virus e2 has three immunogenic domains containing conformational epitopes with distinct properties and biological functions. *J. Virol. 78*(17):9224-9232. DOI: 10.1128/jvi.78.17.9224-9232.2004

98. Johansson, D. X., Voisset, C., Tarr, A. W., *et al.* (2007) Human combinatorial libraries yield rare antibodies that broadly neutralize hepatitis C virus. *Proc. Natl. Acad. Sci. USA. 104*(41):16269-16274. DOI: 10.1073/pnas.0705522104

99. Kong, L., Giang, E., Nieusma, T., *et al.* (2013) Hepatitis C virus E2 envelope glycoprotein core structure. *Science. 342*(6162):1090-1094. DOI: 10.1126/science.1243876

100. Clayton, R. F., Owsianka, A., Aitken, J., *et al.* (2002) Analysis of antigenicity and topology of E2 glycoprotein present on recombinant hepatitis C virus-like particles. *J. Virol. 76*(15), 7672-7682. DOI: 10.1128/jvi.76.15.7672-7682.2002

101. Owsianka, A., Tarr, A. W., Juttla, V. S., *et al.* (2005) Monoclonal antibody AP33 defines a broadly neutralizing epitope on the hepatitis C virus E2 envelope protein. *J. Virol. 79*(17):11095-11104. DOI: 10.1128/jvi.79.17.11095-11104.2005

102. Tarr, A. W., Owsianka, A. M., Timms, J. M., *et al.* (2006) Characterization of the hepatitis C virus epitope defined by the broadly neutralizing monoclonal antibody AP33. *Hepatology. 43*(3):592-601. DOI: 10.1002/hep.21088

103. Desombere, I., Fafi-Kremer, S., Van Houtte, F., *et al.* (2016) Monoclonal anti-envelope antibody AP33 protects humanized mice against a patient-derived hepatitis C virus challenge. *Hepatology. 63*(4):1120-1134. DOI: 10.1002/hep.28428

104. Potter, J. A., Owsianka, A. M., Jeffrey, N., *et al.* (2012) Toward a hepatitis C virus vaccine: the structural basis of hepatitis C virus neutralization by AP33, a

broadly neutralizing antibody. *J. Virol.* *86*(23):12923-12932. DOI:10.1128/jvi.02052-12

105. Kong, L., Giang, E., Nieusma, T., *et al.* (2012) Structure of hepatitis C virus envelope glycoprotein E2 antigenic site 412 to 423 in complex with AP33. *J. Virol.* *86*(23):13085-13088. DOI: 10.1128/jvi.01939-12

106. Li, Y., Pierce, B. G., Wang, Q., *et al.* (2015) Structural basis for penetration of the glycan shield of hepatitis C virus E2 glycoprotein by a broadly neutralizing human antibody. *J. Biol. Chem.* *290*(16):10117-10125. DOI: 10.1074/jbc.m115.64352

107. Kong, L., Giang, E., Robbins, J. B., *et al.* (2012) Structural basis of hepatitis C virus neutralization by broadly neutralizing antibody HCV1. *Proc. Natl. Acad. Sci. USA. 109*(24):9499-9504. DOI: 10.1073/pnas.1202924109

108. Meola, A., Tarr, A. W., England, P., *et al.* (2015) Structural flexibility of a antigenic region in hepatitis C virus glycoprotein E2 recognized by broadly neutralizing antibodies. *J. Virol. 89*(4):2170-2180. DOI: 1128/jvi.02190-14

109. Broering, T. J., Garrity, K. A., Boatright, N. K., *et al.* (2009) Identification and characterization of broadly neutralizing human monoclonal antibodies directed against the E2 envelope glycoprotein if hepatitis C virus. *J. Virol.* 83(23):12473-12482. DOI: 10.1128/jvi.01138-09

110. Flint, M., Maidens, C., Loomis-Price, L. D., *et al.* (1999) Characterization of hepatitis C virus E2 glycoprotein interaction with a putative cellular receptor, CD81. *J. Virol. 73*(8):6235-6244. DOI: unavailable

111. Keck, Z., Wang, W., Wang, Y., *et al.* (2013) Cooperativity in virus neutralization by human monoclonal antibodies to two adjacent regions located at the amino terminus of hepatitis C virus E2 glycoprotein. *J. Virol. 87*(1):37-51. DOI: 10.1128/jvi.01941-12

112. Tarr, A. W., Owsianka, A. M., Jayaraj, D., *et al.* (2007) Determination of the human antibody response to the epitope defined by the hepatitis C virus-neutralizing monoclonal antibody AP33. *J. Gen. Virol. 88*(Pt 11):2991-3001. DOI: 10.1099/vir.0.83065-0

113. Drummer, H. E., Wilson, K. A., Poumbourios, P. (2002) Identification of the hepatitis C virus E2 glycoprotein binding site on the large extracellular loop of CD81. *J. Virol. 76*(21):11143-11147. DOI: 10.1128/jvi.76.21.11143-11147.2002

114. Harman, C., Zhong, L., Ma, L., *et al.* (2015) A view of the E2-CD81 interface at the binding site of a neutralizing antibody against hepatitis C virus. *J. Virol. 89*(1):492-501. DOI: 10.1128/jvi.01661-14

115. Keck, Z. Y., Xia, J., Wang, Y., *et al.* (2012) Human monoclonal antibodies to a novel cluster of conformational epitopes on HCV E2 with resistance to neutralization escape in a genotype 2a isolate. *PLoS Pathog. 8*(4):e1002653. DOI: 10.1371/journal.ppat.1002653

116. Duan, K., Kacho, A., Zhong, L., *et al.* (2012) Amino acid residue-specific neutralization and nonneutralization of hepatitis C virus by monoclonal antibodies to the E2 protein. *J. Virol. 86*(23):12686-12694

117. Deng, L., Zhong, L., Struble, E., *et al.* (2013) Structural evidence for a bifurcated mode of action in the antibody-mediated neutralization of hepatitis C virus. *Proc. Natl. Acad. Sci. USA. 110*(18):7418-7422. DOI: 10.1073/pnas.1305306110

118. Deng, L., Ma, L., Virata-Theimer, M. L., *et al.* (2014) Discrete conformations of epitope II on the hepatitis C virus E2 protein for antibody-mediated neutralization and nonneutralization. *Proc. Natl. Acad. Sci. USA. 111*(29):10690-10695. DOI: 10.1073/pnas.1411317111

119. Krey, T., Meola, A., Keck, Z. Y., Damier-Piolle, L., *et al.* (2013) Structural basis of HCV neutralization by human monoclonal antibodies resistant to viral neutralization escape. *PLoS Pathog. 9*(5):e1003364. DOI: 10.1371/journal.ppat.1003364

120. Keck, Z. Y., Saha, A., Xia, J., *et al.* (2011) Mapping a region of hepatitis C virus E2 that is responsible for escape from neutralizing antibodies and a core CD81-binding region that does not tolerate neutralization escape mutations. *J. Virol. 85*(20):10451-10463. DOI: 10.1128/jvi.05259-11

121. Owsianka, A. M., Tarr, A. W., Keck, Z. Y., *et al.* (2008) Broadly neutralizing human monoclonal antibodies to the hepatitis C virus E2 glycoprotein. *J. Gen. Virol. 89*(Pt 3):653-659. DOI: 10.1099/vir.0.83386-0

122. Sabo, M. C., Luca, V. C., Prentoe, J., *et al.* (2011) Neutralizing monoclonal antibodies against hepatitis C virus E2 protein bind discontinuous epitopes and inhibit infection at a post attachment step. *J. Virol. 85*(14):7005-7019. DOI: 10.1128/jvi.005586-11

123. Cowton, V. M., Singer, J. B., Gifford, R. J., *et al.* (2018) Predicting the effectiveness of hepatitis C virus neutralizing antibodies by bioinformatics analysis of conserved epitope residues using public sequence data. *Front. Immunol. 9*:1470. DOI: 10.3389/fimmu.2018.01470

124. Vasiliauskaite I, Owsianka A, England P, *et al.* (2017) Conformational flexibility in the immunoglobulin-like domain of the hepatitis C virus glycoprotein E2. *MBio. 8*(3):e00382-17. DOI: 10.1128/mbio.00382-17

125. Roccasecca, R., Ansuini, H., Vitelli, A., *et al.* (2003) Binding of the hepatitis C virus E2 glycoprotein to CD81 is strain specific and is modulated by a complex interplay between hypervariable regions 1 and 2. *J. Virol. 77*(3):1856-1867. DOI: 10.1128/jvi.77.3.1856-1867.2003

126. Pierce, B. G., Keck, Z. Y., Lau, P., *et al.* (2016) Global mapping of antibody recognition of the hepatitis C virus E2 glycoprotein: Implications for vaccine design. *Proc. Natl. Acad. Sci. USA. 113*(45):E6946-E6954. DOI: 10.1073/pnas.1614942113

127. Alhammad, Y., Gu, J., Boo, I., *et al.* (2015) Monoclonal antibodies directed toward the hepatitis C virus glycoprotein E2 detect antigenic differences modulated by the N-terminal hypervariable region 1 (HVR1), HVR2, and intergenotypic variable region. *J. Virol. 89*(24):12245-12261. DOI: 10.1128/jvi.02070-15

128. Bankwitz, D., Steinmann, E., Bitzegeio, J., *et al.* (2010) Hepatitis C virus hypervariable region 1 modulates receptor interactions, conceals the CD81 binding site, and protects conserved neutralizing epitopes. *J. Virol. 84*(11):5751-5763. DOI: 10.1128/jvi.02200-09

129. McCaffrey, K., Boo, I., Poumbourios, P., *et al.* (2007) Expression and characterization of a minimal hepatitis C virus glycoprotein core domain that retains CD81 binding. *J. Virol. 81*(17): 9584-9590. DOI: 10.1128/jvi.02782-06

130. Kato, N., Sekiya, H., Ootsuyama, Y., *et al.* (1993) Humoral immune response to hypervariable region 1 of the putative envelope glycoprotein (gp70) of hepatitis C virus. *J. Virol. 67*(7):3923-3930. 0022-538X/93/073923-08$02.00/0

131. Kato, N., Nakazawa, T., Ootsuyama, Y., *et al.* (1994) Virus isolate-specific antibodies against hypervariable region 1 of the hepatitis C virus second envelope glycoprotein, gp70. *Jpn. J. Cancer. Res. 85*(10):987-991. DOI: 10.1111/j.1349-7006.1994.tb02894.x

132. Zibert, A., Schreier, E., Roggendorf, M. (1995) Antibodies in human sera specific to hypervariable region of hepatitis C virus can block viral attachment. *Virology. 208*(2):653-661. DOI: 10.1006/viro.1995.1196

133. Mondelli, M. U., Cerino, A., Segagni, L., *et al.* (2001) Hypervariable region 1 of hepatitis C virus: Immunological decoy or biologically relevant domain? *Antiviral Res. 52*(2):153-159. DOI: 10.1016/SO166-3542(01)00180-2

134. Liu, L., Fischer, B. E., Dowd, K. A., *et al.* (2010) Acceleration of hepatitis C virus envelope evolution in humans is consistent with progressive humoral immune selection during the transition from acute to chronic infection. *J. Virol. 84*(10):5067-5077. DOI: 10.1128/jvi.02265-09

135. Anjum, S., Wahid, A., Afzal, M. S., *et al.* (2013) Additional glycosylation within a specific hypervariable region of subtype 3a of hepatitis C virus protects against virus neutralization. *J. Infect. Dis. 208*(11):1888-1897. DOI: 10.1093/infdis/jit376

136. Prentoe, J., Velásquez-Moctezuma, R., Augestad, E.H., *et al.* (2019) Hypervariable region 1 and N-linked glycans of hepatitis C regulate virion neutralization by modulating envelope conformations. *Proc. Natl. Acad. Sci. USA. 116*(20):10039-10047. DOI: 10.1073/pnas.1822002116

137. Van Dongen, M. J. P., Kadam, R. U., Juraszek, J., *et al.* (2019) A small-molecule fusion inhibitor of influenza virus is orally active in mice. *Science. 363*(6431). DOI: 10.1126/science.aar6221

138. Longin, O., Van de Langemheen, H., Liskamp, R. M. J. (2017) An orthogonally protected cyclotriveratrylene (CTV) as a highly pre-organized molecular scaffold for subsequent ligation of different cyclic peptides towards protein mimics. *Bioorg. Med. Chem. 25*(18):5008-5015. DOI:10.1016/j.bmc.2017.05.038

139. Werkhoven, P. R., Elwakiel, M., Meuleman, T. J., *et al.* (2016) Molecular construction of HIV-gp120 discontinuous epitope mimics by assembly of cyclic peptides on an orthogonal alkyne functionalized TAC-scaffold. *Org. Biolmol. Chem. 14*,(2):701-710. DOI: 10.1039/c5ob02014j

140. Werkhoven, P. R., Liskamp, R. M. J. (2013) Chemical approaches for localization, characterization and mimicry of peptide loops. *RSC Drug Discovery Series No. 36. Biotherapeutics: Recent Developments using Chemical and Molecular Biology* (Jones, L. H. and McKnight, A. J., Eds.) pp. 263–284, Chapter 10, The Royal Society of Chemistry, Cambride.

141. Merriflied, R. B. (1963) Solid phase peptide synthesis. I. The synthesis of a tetrapeptide. *J. Am. Chem. Soc. 85*(14):2149-2154. DOI: 10.1021/ja00897a025]

142. Merrifield, B. (1986) Solid phase Synthesis. *Science. 232*(4748):341-347. DOI: 10.1126/science.3961484

143. Rink, H. (1987) Solid-phase synthesis of protected peptide fragments using a trialkoxy-diphenyl-methylester resin. *Tetrahedron Lett. 28*(33):3787-3790. DOI: 10.1016/S0040-4039(00)96384-6

144. Wang, S. S. (1973) p-alkoxybenzyl alcohol resin and p-alkoxybenzyloxycarbonylhydrazine resin for solid phase synthesis of protected peptide fragments. *J. Am. Chem. Soc. 95*(4):1328-1333. DOI: 10.1021/ja00785a602

145. Carpino, L.A., Han, Y. G. (1970) 9-Fluorenylmethoxycarbonyl function, a new base-sensitive amino-protecting group. *J. Am. Chem. Soc. 92*(19):5748-5749. DOI: 10.1021/ja00722a043

146. Carpino, L.A., Han, G. Y. (1972) 9-Fluorenylmethoxycarbonyl amino-protecting group. *J. Org. Chem. 37*(22):3404-3409. DOI: 10.1021/jo00795a005

147. Atherton, E., Fox, H., Harkiss, D., *et al.* (1978) A mild procedure for solid phase peptide synthesis: Use of fluorenylmethoxycarbonylamino-acids. *J. Chem. Soc. Chem. Comm.* (13):537-539. DOI: 10.1039/C39780000537

148. Chang, C. D., Meienhofer, J. (1978) Solid-phase peptide synthesis using mild base cleavage of N alpha-fluorenylmethyloxycarbonylamino acids, exemplified by a synthesis of dihydrosomatostatin. *Int. J. Pept. Protein Res. 11*(3):246-249. DOI: 10.1111/j.1399-3011.1978.tb02845.x

149. Sheehan, J. C., Hess, G. P. (1955) A new method of forming peptide bonds. *J. Am. Chem. Soc. 77*(4):1067-1068. DOI: 10.1021/ja01609a099

150. Konig, W., Geiger, R. (1970) A new method for synthesis of peptides: Activation of the carbonyl group with dicyclohexylcarbodiimide using 1-hydroxybenzotriazoles as additives. *Chem. Ber. 103*(3):788-798. DOI: 10.1002/cber.197010303319

151. Carpino, L. A., El-Faham, A. (1999) The diisopropylcarbodiimide/1-hydroxyl-7-azabenzotriazole system: Segment coupling and stepwise peptide assembly. *Tetrahedron. 55*(22):6813-6830. DOI: 10.1016/S0040-4020-(99)00344-0

152. Sieber, P., Riniker, B. (1991) Protection of carboxamide functions by the trityl residue. Applications to peptide synthesis. *Tetrahedron Lett. 32*(6):739-742. DOI: 10.1016/S0040-4039(00)74872-6

153. Sieber, P., Riniker, B. (1987) Protection of Histidine in peptide synthesis: A reassessment of the trityl group. *Tetrahedron Lett. 28*(48):6031-6034. DOI: 10.1016/S0040-4039(00)96856-4

154. Carpino, L. A., Shroff, H., Triolo, S. A., *et al.* (1993) The 2,2,4,6,7-pentamethyldihydrobenzofurazan-5-sulfonyl group (Pbf) as arginine side chain protectant. *Tetrahedron Lett. 34*(49):7829-7832. DOI: 10.1016/S0040-4039(00)61487-9

155. Pearson, D. A., Blanchette, M., Baker, M. L., *et al.* (1989) Trialkylsilanes as scavengers for the trifluoroacetic acid deblocking of protection groups in peptide

synthesis. *Tetrahedron. Lett. 30*(21):2739-2742. DOI: 10.1016/S0040-4039(00)99113-5

156. Mehta, A., Jaouhari, R., Benson, T. J., *et al.* (1992) Improved efficiency and selectivity in peptide synthesis: Use of triethylsilane as a carbocation scavenger in deprotection of t-butyl esters and t-butoxycarbonyl-protected sites. *Tetrahedron Lett. 33*(37):5441-5444. DOI: 10.1016/S0040-4039(00)79116-7

157. Greenfield, N. J., Stafford, W. F., Hitchcock-DeGregori, S. E. (1994) The effect of N-terminal acetylation on the structure of an N-terminal tropomyosin peptide and alpha alpha-tropomyosin. *Protein Sci. 3*(3):402-410. DOI: 10.1002/pro.5560030304

158. Brinckerhoff, L. H., Kalashnikov, V. V., Thompson, L. W., *et al.* (1999) Terminal modifications inhibit proteolytic degradation of an immunogenic MART-1(27-35) peptide: Implications for peptide vaccines. *Int. J. Cancer. 83*(3):326-334. DOI: 10.1002/(sici)1097-0215(19991029)83:3<326::aid-ijc7>3.0.co;2-x

159. Khan, A. G., Whidby, J., Miller, M. T., *et al.* (2014) Structure of the core ectodomain of the hepatitis C virus envelope glycoprotein 2. *Nature. 509*(7500):381-384. DOI: 10.1038/naute13117

160. Langeveld, J. P., Casal, J. I., Osterhaus, A. D., *et al.* (1994) First peptide vaccine providing protection against viral infection in the target animal: studies of canine parvovirus in dogs. *J. Virol. 68*(7):4506-4513. 0022-538X/94/$04.00+0

161. Wang, T. T., Tan, G. S., Hai, R., *et al.* (2010) Vaccination with a synthetic peptide from the influenza virus hemagglutinin provides protection against distinct viral subtypes. *Proc. Natl. Acad. Sci. USA. 107*(44):18979-18984. DOI: 10.1073/pnas.1013387107

162. Nordstrom, T., Pandey, M., Calcutt, A., *et al.* (2017) Enhancing the efficacy by engineering a complex synthetic peptide to become a super immunogen. *J. Immunol. 199*(8)|:2794-2802. DOI: 10.4049/jimmunol.1700836

163. Singh, M., Bhatt, P., Sharma, M., *et al.* (2019) Immunogenicity of late stage specific peptide antigens of *Mycobacterium tuberculosis*. *Infect. Genet. Evol. 74*:103930. DOI: 10.1016/j.meegid.2019.103930

164. Maynard, S. K., Marshall, J. D., Macgill, R. S., *et al.* (2019) Vaccination with synthetic long peptide formulated with CpG in an oil-in-water emulsion induces robust E7-specific CD8 T cell responses and TC-1 tumor eradication. *BMC Cancer. 19*(1):540. DOI: 10.1186/s12885-019-5725-y

165. Xin, H., Glee, P., Adams, A., *et al.* (2019) Design of a mimotope-peptide based double epitope vaccine against disseminated candidiasis. *Vaccine. 37*(18):2430-2438. DOI: 10.1016/j.vaccine.2019.03.061

166. Zorzi, A., Deyle, K., Heinis, C. (2017) Cyclic peptide therapeutics: Past, present, and future. *Curr. Opin. Chem. Biol. 38*:24-29. DOI: 10.1016/j.cbpa.2017.02.006

167. Chen, S., Morales-Sanfrutos, J., Angelini, A., *et al.* (2012) Structurally diverse cyclisation linkers impose different backbone conformations in bicyclic peptides. *ChemBioChem. 13*(7):1032-1038. DOI: 10.1002/cbic.201200049

168. Angelini, A., Cendron, L., Chen, S., *et al.* (2012) Bicyclic peptide inhibitors reveals large contact interface with a protease target. *ACS Chem. Biol. 7*(5):817-821. DOI: 10.1021/cb200478t

169. Chen, S., Bertoldo, D., Angelini, A., *et al.* (2014) Peptide ligands stabilized by small molecules. *Angew. Chem. Int. Ed. Engl. 53*(6):1602-1606. DOI: 10.1002/anie.201309459

170. Deyle K, Kong XD, Heinis C. (2017) Phage selection of cyclic peptides for application in research and drug development. *Acc. Chem. Res. 50*(8):1866-1874. DIO: 10.1021/acs.accounts.7b00184

171. Kale, S. S., Villequey, C., Kong, X. D., *et al.* (2018) Cyclization of peptides with two chemical bridges affords large scaffold diversities. *Nat. Chem. 10*(7):715-723. DOI: 10.1038/s41557-018-0042-7

172. Richelle, G. J. J., Ori, S., Hiemstra, H., *et al.* (2018) General and facile route to isomerically pure tricyclic peptides based on templated tandem CLIPS/CuAAC cyclizations. *Angew. Chem. Int. Ed. Engl. 57*(2):501-505. DOI:10.1002/anie.201709127

173. Streefkerk, D. E., Schmidt, M., Ippel, J. H., *et al.* (2019) Synthesis of constrained tetracyclic peptides by consecutive CEPS, CLIPS, and oxime ligation. *Org. Lett.* 2019;*21*(7):2095-2100. DOI: 10.1021/acs.orglett.9b00378

174. Richelle, G. J. J., Schmidt, M., Ippel, H., *et al.* (2018) A one pot ‘’triple-C’’ multicyclization methodology for the synthesis of highly constrained isomerically pure tetracyclic peptides. *ChemBioChem. 19*(18):1934-1938. DOI: 10.1002/cbic.201800346

175. Van de Langemheen, H., Korotkovs, V., Bijl, J., *et al.* (2017) Polar hinges as functionalized conformational constraints in (bi)cyclic peptides. *ChemBioChem. 18*(4):387-395. DOI: 10.1002/cbic.201600612

176. Werkhoven, P. R., Van de Langemheen, H., Van der Wal, S., Kruijtzer, J. A. W, Liskamp, R. M. J. (2014) Versatile convergent synthesis of a three peptide loop containing protein mimic of whooping cough pertactin by successive Cu(I)-catalyzed azide alkyne cycloaddition on an orthogonal alkyne functionalized TAC-scaffold. *J. Pept. Sci*. *20*(4):235-239. DOI: 10.1002/psc.2624

177. Meuleman, T. J., Dunlop, J. I., Owsianka, A. M., Van de Langemheen, H., Patel, A. H., Liskamp, R. M. J. (2018) Immobilization by surface conjugation of cyclic peptides for effective mimicry of the HCV-envelope E2 protein as a strategy toward synthetic vaccines. *Bioconjug. Chem. 29*(4):1091-1101. DOI: 10.1021/acs.bioconjchem.7b00755

178. Sandomenico, A., Leonardi, A., Berisio, R., *et al.* (2016) Generation and characterization of monoclonal antibodies against a cyclic variant of hepatitis C virus E2 epitope 412-422. *J. Virol. 90*(7):3745-3759. DOI: 10.1128/jvi.02397-15

179. Pierce, B. G., Boucher, E. N., Piepenbrink, K. H., *et al.* Structure-based design of hepatitis C virus vaccines that elicit neutralizing antibodies responses to a conserved epitope. *J. Virol. 91*(20):e01032-17. DOI: 10.1128/jvi.01032-17

180. Meuleman, P., Leroux,-Roels, G. (2009) HCV animal models: a journey of more then 30 years. *Viruses. 1*(2):222-240. DOI: 10.3390/v1020222

181. Vercauteren. K., De Jong, Y. P., Meuleman, P. (2014) HCV animal models and liver disease. *J. Hepatol. 61*(1 Suppl):S26-S33. DOI: 10.1016/j.hep.2014.07.013

182. Lau, Y. H., De Andrade, P., Wu, Y., *et al.* (2015) Peptide stapling techniques based on different macrocyclisation chemistries. *Chem. Soc. Rev. 44*(1):91-102. DOI: 10.1039/c4cs00246f

183. Sawyer, N., Arora, P.S. (2018) Hydrogen bond surrogate stabilization of β-hairpins. *ACS Chem. Biol. 13*(8):2027-2032. DOI: 10.1021/acschembio.8b00641

184. Urrutia-Baca, V. H., Gomez-Flores, R., De La Garza-Ramos, M. A., *et al.* (2019) Immunoinformatics approach to design a novel epitope-based oral vaccine against *Helicobacter pylori*. *J. Comput. Biol. 26*:1-14. DOI: 10.1089/cmb.2019.0062

185. Kesherwani, V., Tarang, S. (2019) An immunoinformatic approach to universal therapeutic vaccine design against BK virus. *Vaccine. 37*(26):3457-3463. DOI: 10.1016/j.vaccine.2019.04.096

186. Guo, L., Hong, D., Wang, S., *et al.* (2019) Therapeutic protection against *H. pylori* infection in Mongolian gerbils by oral immunization with a tetravalent

epitope-based vaccine with polysaccharide adjuvant. *Front. Immunol. 10*:1185. DOI: 10.3389/fimmu.2019.01185

187. Singh, G., Zholobko, O., Pillatzki, A., *et al.* (2019) An amphiphilic invertible polymer as a delivery vehicle for a M2e-HA2-HA1 peptide vaccine against an influenza A virus in pigs. *Vaccine. 37*(31):4291-4301. DOI: 10.1016/j.vaccine.2019.06.030

188. He, L., Cheng, Y., Kong, L., *et al.* (2015) Approaching rational epitope vaccine design for hepatitis C virus with meta-server and multivalent scaffolding. *Sci. Rep. 5*:12501. DOI: 10.1038/srep12501

189. Opatz, T., Liskamp, R. M. J. (2001) A selectively deprotectable triazacyclophanescaffold for the construction of artificial receptors. *Org. Lett.* 3(22):3499–3502. DOI: 10.1021/oi0101741

190. Longin, O., Hezwani, M., Van de Langemheen, H., *et al.* (2018) Synthetic antibody protein mimics of infliximab by molecular scaffolding on novel CycloTriVeratrilene (CTV) derivatives. *Org. Biomol. Chem. 16*(29):5254-5274. DOI: 10/1039/c8ob01104d

191. Hijnen, M., Van Zoelen, D. J., Chamorro, C., *et al.* (2007) A novel strategy to mimic discontinuous protective epitopes using a synthetic scaffold. *Vaccine. 25*(37-38):6807-6817. DOI: 10.1016/j.vaccine.2007.06.027

192. Mulder, G. E., Kruijtzer, J. A. W., Liskamp, R. M. J. (2012) A combinatorial approach toward smart libraries of discontinuous epitopes of HIV gp120 on a TAC synthetic scaffold. Chem. Commun. *48*(80):10007-10009. 10.1039/c2cc35310e

193. Mulder, G. E., Van Ufford, H. L., Van Ameijde, J., *et al.* (2013) Scaffold optimization in discontinuous epitope containing protein mimics of gp120 using smart libraries. Org. Biomol.Chem. *11*(16): 2676–2684. DOI: 10.1039/c3ob27470e

CHAPTER 2

Immobilization by surface conjugation of cyclic peptide for effective mimicry of the HCV-envelope E2 glycoprotein as a strategy towards synthetic vaccines

Parts of the work presented here has been published in:

- Meuleman, T. J., Dunlop, J. I., Owsianka, A. M., Van de Langemheen, H., Patel, A. H., Liskamp, R. M. J. Immobilization by surface conjugation of cyclic peptides for effective mimicry of the HCV-envelope E2 protein as a strategy toward synthetic vaccines. *Bioconjug. Chem.* 2018;*29*(4):1091-1101.
  DOI: 10.1021/acs.bioconjchem.7b00755

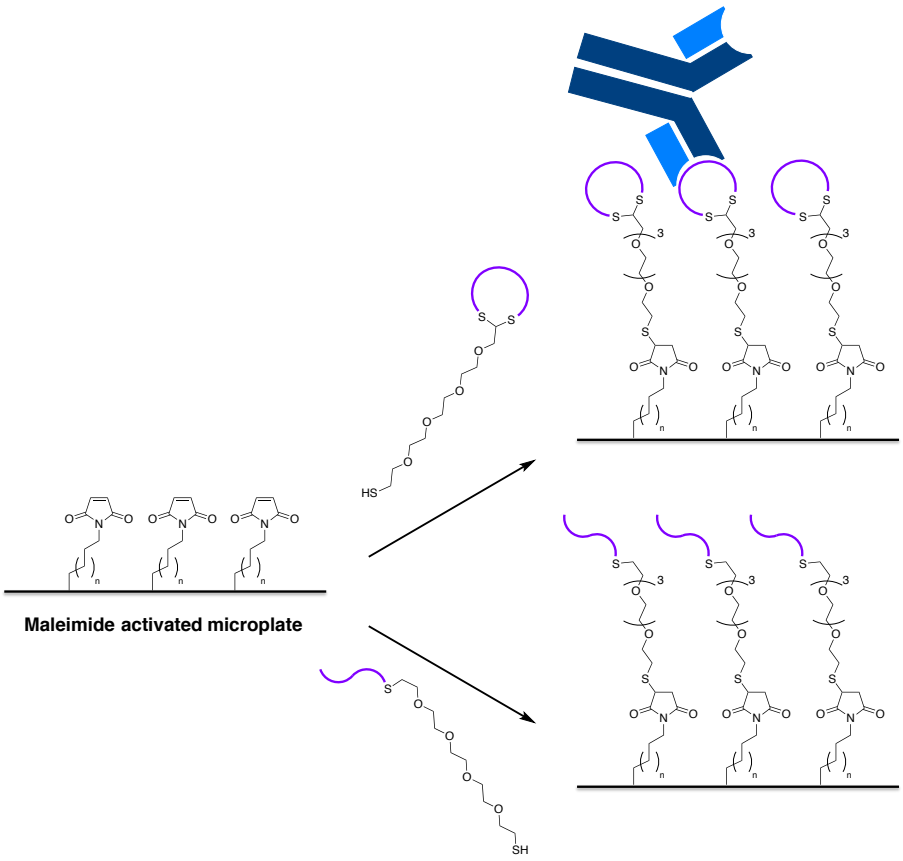

Abstract

Mimicry of the binding interface of antibody-antigen interactions using peptide-based modulators (*i.e.* epitope mimics) has promising applications for vaccine design. These epitope mimics can be synthesized in a streamlined and straightforward fashion, thereby allowing for high-throughput analysis. The design of epitope mimics is highly influenced by their spatial configuration and structural conformation. It is widely assumed that for proper mimicry sufficient conformational constraints have to be implemented. This chapter describes the synthesis of bromide derivatives functionalized with a flexible TEG linker equipped with a thiol-moiety that could be used to support cyclic or linear peptides. The cyclic and linear epitope mimics were covalently conjugated via the free thiol-moiety on maleimide-activated plate surfaces. The resulting covalent, uniform, and oriented coated surface of cyclic or linear epitope mimics were subjected to an ELISA to investigate the effect of peptide cyclization with respect to mimicry of an antigen-antibody interaction of the HCV-E2 glycoprotein. To our knowledge, the benefit of cyclized peptides over linear peptides has been clearly demonstrated here for the first time. Cyclic epitope mimics, and not the linear epitope mimics, demonstrated specificity towards their monoclonal antibodies HC84.1 and V3.2, respectively. However, monoclonal antibody AP33 bound both the cyclic and linear epitope mimic, which is probably due to the flexible nature associated to its epitope in the protein. The described strategy for the construction of epitope mimics shows potential for high-throughput screening of key-binding residues by simply changing the amino-acid sequences within synthetic peptides. In this way, Tryptophan-Leucine sequence at position 437-438 has been identified as key-binding residues for binding monoclonal antibody V3.2.

2.1 Introduction

Hepatitis C Virus (HCV) poses a global threat and is estimated to have infected over 3% of the world's population.[1] So far, its high mutation rate and intrinsic immune evasive strategies have hampered development of therapeutic and prophylactic vaccines. Despite this and the availability of novel antivirals[2] there is an urgent need for the development of HCV vaccines[3], since drugs do not prevent reinfection[4] and their treatment is expensive.[3] The potential of these possible future vaccines is underlined by the existence of antibodies capable of preventing viral infection (*i.e.* neutralizing antibodies (nAbs)).[5]

Evidently, the HCV-E2 envelope glycoprotein is of major importance for development of HCV vaccines[6] as it is involved in viral attachment and entry, and is therefore an accessible target located on the surface of the virion. However, generating nAbs against this glycoprotein is not straightforward as it contains highly variable immunogenic domains. Antibodies against these regions tend to be strain-specific and unable to prevent infection by a different strain of HCV. These variable epitopes serve as decoys to distract the immune system. In addition, HCV-E2 contains 11 *N*-linked glycans that can shield certain epitopes, thereby preventing binding of antibodies.[7] Nevertheless, numerous nAbs have been isolated from patient sera that are able to inhibit infection by a broad range of HCV isolates. Most of these broadly-neutralizing antibodies bind to conserved, discontinuous regions within the HCV-E2 glycoprotein and block its interaction with the CD81 receptor.[8] These regions are designated as broadly neutralizing epitopes.[5,9-11] The availability of structural information on these HCV-E2 neutralizing epitope-antibody interactions might be crucial for future vaccine design.[5,10,12,13]

In the past Liskamp *et al.*[14,15] have introduced a chemical biology perspective for designing synthetic vaccines by describing a strategy for mimicry of discontinuous protective epitopes using a synthetic scaffold for obtaining a 'PEPTAC' molecular construct, which acted as a synthetic vaccine and protected mice against infection with *B. Pertussis*. Although this was a very promising result, in order to further improve chances for ultimately a successful synthetic HCV vaccine, it would be necessary to mimic neutralizing epitopes present in E2 as closely as possible and ligate them on a diversity of suitable scaffold molecules.[16-18]

The required scaffold molecule should mimic the structural integrity that is normally provided for by the majority of a protein (Figure 2.1). Thus, the resulting epitope containing protein mimic will only present the essential epitope(s) and will not contain any shielding or immunogenic decoy domains. Consequently, these protein mimics have the potential to lead to synthetic and more efficient vaccines.[19,20]

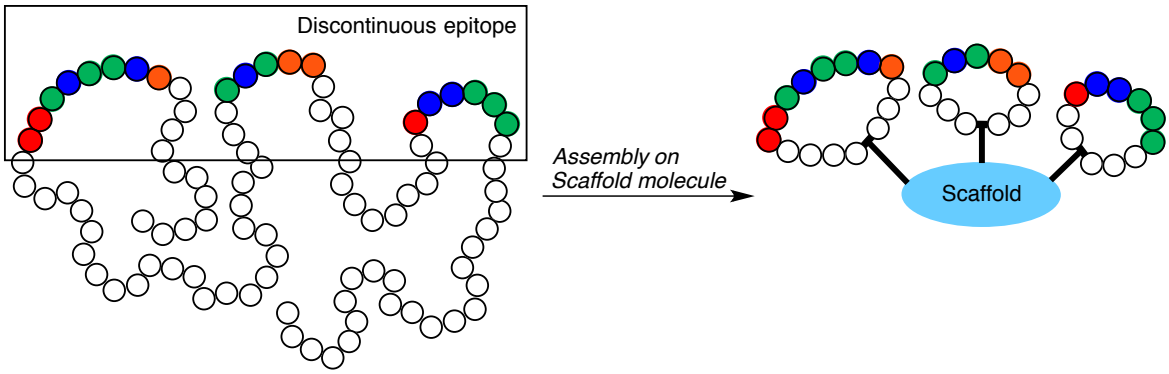

Figure 2.1. Epitope mimicry, in which essential peptide loops of a discontinuous epitope are ligated on a molecular scaffold.

Conformational constraints are probably very important in the design of epitope mimics, since they can induce or enforce conformations of epitopes as they are present in the native protein.[16] Many epitopes are comprised of loop-like structures and mimicry of loop-like peptide sequences is best achieved by cyclization. Furthermore, introduction of conformational constraints by cyclization has been found to improve rigidity, stability, bioavailability, and biological activity of peptide-based therapeutics.[14,15,18] Therefore, constrained peptides are to be preferred in the design of adequate and effective epitope mimics.[21-26] However, to our knowledge, this favourable effect on epitope mimicry by the introduction of conformational constraints by cyclization has not been rigorously investigated so far.

The cornerstone of studying antigen-antibody interactions and the identification of promising neutralizing epitopes is the enzyme-linked immunosorbent assay (ELISA). With respect to this, novel isolated nAbs, obtained from immunization studies or patients, are tested by ELISA to verify binding.[9,27-30] Key binding residues of antigen-antibody interactions are identified (*i.e.* epitope mapping) using mutagenesis studies, in which ELISA is used to assess the altered binding affinity of antibodies towards different mutants.[9,31-33] Conventional ELISA involves non-covalent adsorption of antigen(s) on polystyrene plates, which likely results in a heterogeneous surface of differently adsorbed

antigen molecules. Thus, these will probably interact with different affinities with antibodies.[34] In addition, adsorption of antigens on polystyrene plates could potentially perturb the structure of the antigen, thereby also influencing antibody binding. Gori *et al.*[35] have shown the importance of accurate control of covalent immobilization and generating a uniform and oriented surface for proper gauging of antigen-antibody interactions using peptide sequences.

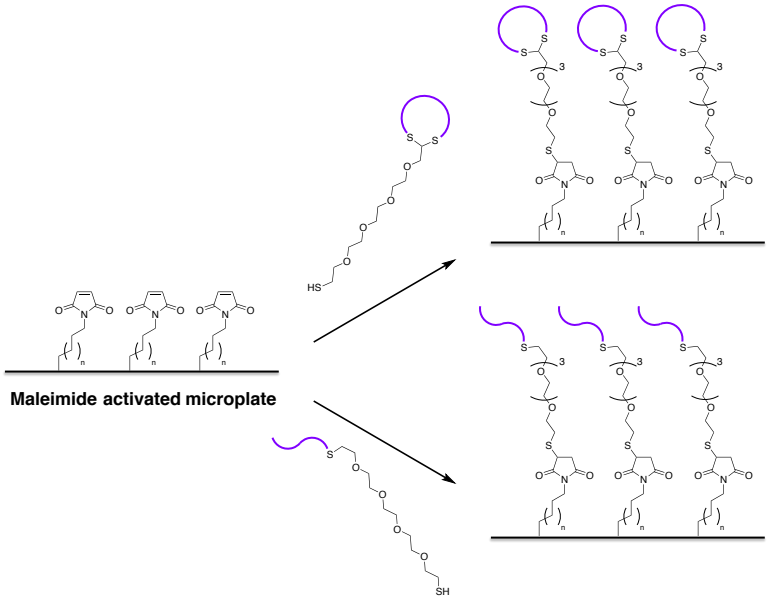

Figure 2.2. Chemoselective approach for covalent immobilization of epitope mimics in a uniform and specifically oriented fashion via thiol addition to maleimide.

In this research the importance of cyclization of peptides as a conformational constraint for effective mimicry of neutralizing epitopes from HCV-E2 is investigated. To this end, more flexible, linear peptides were compared with their constrained, cyclic counterparts. These peptide constructs were obtained via benzylic bromide derivatives equipped with a tetraethylene glycol (TEG) spacer containing a trityl-protected thiol-moiety (**9** and **7**, respectively). After liberation of the thiol moiety, instead of random non-covalent adsorption, a covalent coating of epitope mimics on polystyrene plates was obtained using commercially available Pierce® maleimide activated 96-well plates (Figure 2.2).

The availability of a mouse antibody AP33[27], a human/mouse antibody variant of the broadly neutralizing human monoclonal antibody (mAb) HC84.1[9], a weakly neutralizing mouse antibody V3.2 (to be published), and a non-neutralizing antibody DAO5[30], enabled us to evaluate our epitope mimics using ELISA and the impact of peptide cyclization for effective mimicry.

2.2 Results and Discussion

2.2.1 Synthesis of the peptide cyclization and linear linker with a maleimide reactive tetraethylene glycol (TEG) spacer

Recently, Werkhoven *et al.*[15,18] introduced a bisbromobenzyl azide derivative for cyclization of dicysteine containing peptides and subsequent Cu-catalyzed azide-alkyne cyclo-addition to alkyne containing scaffold molecules. Here a related bisbromobenzyl derivative was required, having instead of an azide functionality a TEG moiety for improved water solubility and a (protected) thiol group for reaction with maleimide moieties present on the surface of an ELISA plate.[36]

Thus, TEG **1** was monotosylated with ρ-toluenesulfonyl chloride **2** to tosylate **3** (64 %), followed by substitution using crude trityl-thiol **4** leading to trityl-TEG-sulfide **5** (*quant.*). Next, the cyclization linker moiety was introduced in a reaction with 1,3,5-tris(bromomethyl)benzene **6** and trityl protected cyclization linker **7** was obtained in a moderate yield (32%) (Scheme 2.1). Similarly, trityl-TEG-sulfide **5** was reacted with 1,3-bis(bromomethyl)benzene **8**, to provide trityl protected linear linker **9** also in a moderate yield (42%). Di- and tri-substituted products were observed during the reaction of cyclic linker **7** and linear linker **9**, which at least partially explained the lower yields of the mono substituted products. The availability of both scaffolds supporting cyclized or linear peptide constructs was essential for a rigorous evaluation of the constraining effects by peptide cyclization.

Scheme 2.1. Synthesis of PEG-based thiol linkers for peptides cyclization/attachment and conjugation to plates.

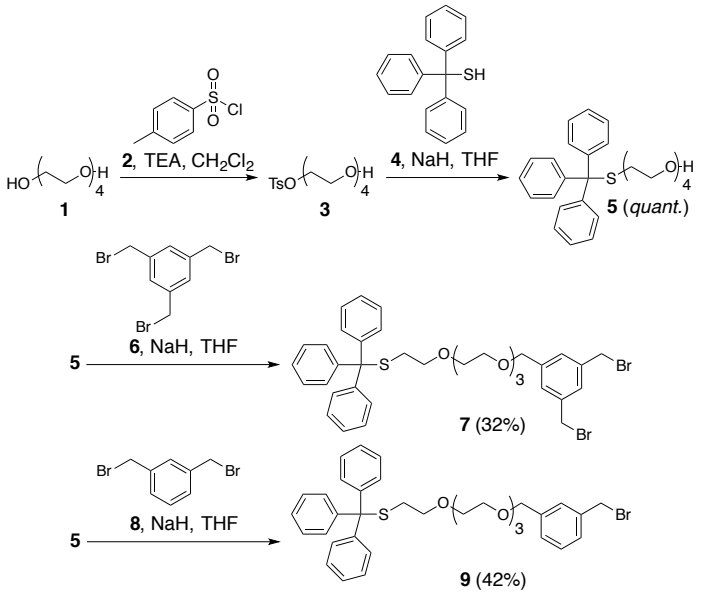

2.2.2 Synthesis of cysteine containing peptides for cyclization or alkylation

The required peptides containing one or two cysteines were obtained by solid phase peptide synthesis (SPPS).[37,38] Their amino acid sequences originated from epitopes I (I^{411} Q**LI**NTN**GS**W**H**INR^{424}; residues in bold are highly conserved across different HCV genotypes)[31,33], II (N^{434} **TG**WL**A**G**LFY**QHK^{446}; residues in bold are highly conserved across genotypes)[9,10,33,39], and III (**G**^{523} A**PTY**S**WG**ANDT**D**^{535}; residues in bold are highly conserved across genotypes)[33] present in HCV-E2 glycoprotein.

The cysteine residues were installed at the termini to maintain the native amino acid sequence of the epitopes. Thereby creating a better chance at preserving their ability for antibody binding. Optimization of the epitope mimics by varying the loop length and/or position of the non-native cysteine residues could potentially result in better structural mimicry. However, when introducing a more complex design the comparison between cyclic versus linear might become more complex as well. Therefore, for this research, a simpler design was pursued to allow for a more complete comparison of cyclic versus linear peptides with respect to mimicry.

Epitope I consist of a flexible region that is recognized by nAb AP33 as a neutralizing immunogenic domain and has been mapped to residues 411-423.[27,40,41] Epitope II is a neutralizing immunogenic domain recognized by nAb HC84.1[9,10] and by a weak nAb V3.2

(to be published). Epitopes of mAb HC84.1 and V3.2 have been mapped to HCV-E2 residues 439 to 446[9,10] and residues 435 to 442 (to be published), respectively. Epitope III contains a sequence recognized by non-neutralizing antibody DAO5 that has been mapped to residues 532 to 540.[30] Although antibody DAO5 is non-neutralizing, it will allow for validation of epitope mimicry. The available sequence information of the different HCV genotypes/strains allowed for the optimization of epitopes I, II, and III towards consensus sequences corresponding to residues 411 to 424, 436 to 448 and 430 to 444, and 528 to 541 of peptides shown in Table 2.1, which cover the multiple genotypes of HCV. These consensus sequences led to one peptide sequence for epitope I, however, for epitopes IIa and IIb, and III it resulted in two peptide sequences with one or two amino-acid substitutions that are equally represented within the available sequence information of the epitopes.

Table 2.1. Overview of synthesized peptidic antigen sequences of HCV-E2 glycoprotein with: Epitope **I in green**; **IIa in red**; **IIb in purple**; **III in blue**; **scrambled in black.** * Indicates equally represented amino-acid substitutions within the available sequence information of the epitopes.

			Antibodies
Epitope I	**10** (cp)	H – C I^{411} Q L I N T N G S W H I N R^{424} C – NH_2	AP33 [ref.38]
	11 (lp)	H – I^{411} Q L I N T N G S W H I N R^{424} C – NH_2	
Epitope IIa	**12** (cp)	Ac – C G^{436} F* V A G L F Y Y H K F N^{448} C – NH_2	
	13 (cp)	Ac – C G^{436} W* V A G L F Y Y H K F N^{448} C – NH_2	HC84.1 [ref.9]
	14 (lp)	Ac – G^{436} W* V A G L F Y Y H K F N^{448} C – NH_2	
Epitope IIb	**15** (cp)	Ac – C N^{430} E S L N T G F* V* A G L F Y Y^{444} C – NH_2	
	16 (cp)	Ac – C N^{430} E S L N T G W* L* A G L F Y Y^{444} C – NH_2	V3.2
	17 (lp)	Ac – N^{430} E S L N T G W* L* A G L F Y Y^{444} C – NH_2	
Epitope III	**18** (cp)	Ac – C T^{528} W G E N E T D V F L* L N N^{541} C – NH_2	DAO5 [ref.30]
	19 (cp)	Ac – C T^{528} W G E N E T D V F V* L N N^{541} C – NH_2	
Scrambled	**20** (cp)	Ac – C H F G K Y A F W L G N Y L C – NH_2	None

Peptides **10** (cp), **12** (cp), **13** (cp) **15** (cp), **16** (cp), **18** (cp) and **19** (cp) served as cyclization precursor (cp) peptides for the preparation of the cyclic peptide constructs **21**, **23**, **24**, **26**, **27**, **29**, and **30**, respectively, and were synthesized with a cysteine residue at both N- and C-termini. Linear precursor (lp) peptides **11** (lp), **14** (lp), and **17** (lp) containing one

cysteine residue were synthesized to prepare the linear peptide constructs **22**, **25**, and **28**. In addition, peptide **20** (cp) was designed with a scrambled amino-acid sequence and synthesized for the preparation of cyclic peptide construct **31** to serve as a negative control, which should not bind to the available mAbs AP33, HC84.1 and V3.2, and DAO5.

2.2.3 Synthesis of the epitope mimics for surface conjugation

Reaction of the thus synthesized precursor peptides with either linker construct **7** or **9** led to cyclic peptide constructs **21**, **23**, **24**, **26**, **27**, **29**, **30**, and **31** and linear peptide constructs **22**, **25**, and **28,** respectively (Scheme 2.2).

Scheme 2.2. Alkylation of precursor peptides with the linker constructs **7** or **9**.

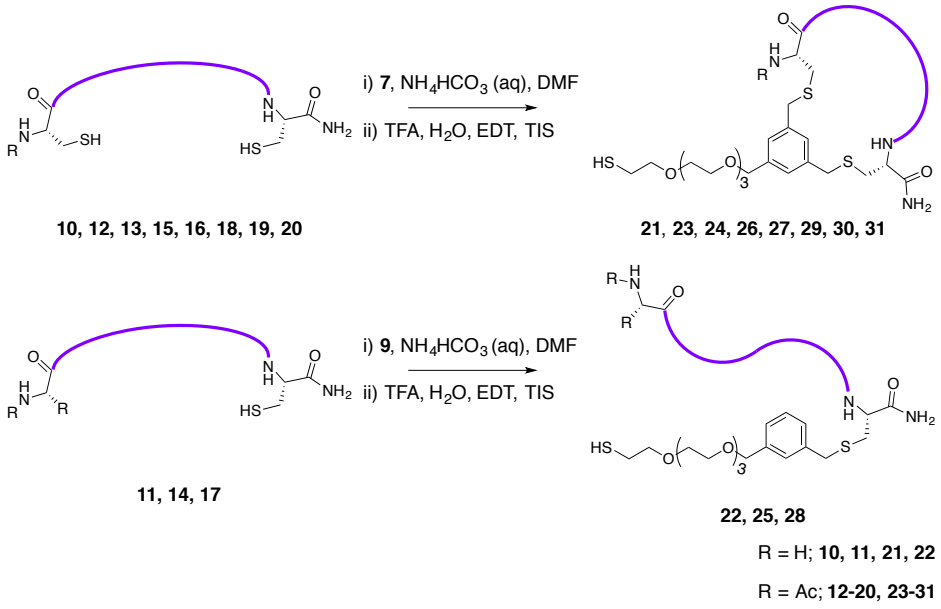

This alkylation procedure is convenient since it can be carried out using the crude, fully deprotected peptides. If the peptides exhibit good water solubility, then normally NH_4HCO_3 in a mixture water/acetonitrile can be used. However, since our peptides were much more hydrophobic, DMF had to be included for dissolving the peptides and the alkylation approach was optimized to dissolve the peptide and the linker in a concentration of 1 mM in aqueous NH_4HCO_3 buffer (20 mM; pH 7.9) in dimethylformamide (DMF) (75%). Immediately after alkylation of the peptide on the linker, the trityl group was removed to liberate the thiol functionality.

Purification of the epitope mimics was achieved by preparative reverse phase HPLC. The TEG spacer improved the aqueous solubility of the cyclic epitope mimics (**21**, **23**, **24**, **26**,

27, **29**, and **30**) and scrambled negative control (**31**), slightly. The linear epitope mimics (**22**, **25**, and **28**) showed a significantly better solubility upon attachment of the TEG containing linker. Nevertheless, all epitope mimics and scrambled control were obtained in reasonable purity and yields (Table 2.2).

Table 2.2. Tabulated yields and purities of epitope mimics **21-31**.

Cyclic epitope mimics	**21**	**23**	**24**	**26**	**27**	**29**	**30**
Yield (%)	2%	16%	15%	2%	5%	7%	14%
Purity (%)	≥95%	≥95%	≥95%	≥90%	≥95%	≥90%	≥90%

Linear epitope mimics	**22**	**25**	**28**
Yield (%)	7%	29%	3%
Purity (%)	≥95%	≥95%	≥90%

Scrambled control	**31**
Yield (%)	9%
Purity (%)	≥95%

After purification the solubility of cyclic epitope mimics **26** and **27** was particularly poor and did not afford proper chromatograms. Instead, the purity of the individual product containing fractions was used to assess the general purity of the final combined products. In our group, Van de Langemheen *et al.*[42] recently developed polar hinges that may be used for future improvement of the general solubility of more hydrophobic peptides in cyclization reactions.

2.2.4 Immobilization by surface conjugation to immobilized maleimide residues

To improve conventional ELISA, the individual epitope mimics were *covalently* ligated onto maleimide-activated plates. To verify antibody recognition of the cyclic epitope mimics (**21**, **23**, **24**, **26**, **27**, **29**, and **30**) coated plate surface, plates were incubated with a three-fold dilution series of mAbs AP33, HC84.1 and V3.2, and DAO5. The scrambled negative control **31** was included to verify specificity of antibody binding.

mAb AP33 showed specific binding towards **21** and showed no binding to the scrambled negative control **31** (Figure 2.3). It was observed that binding of mAb HC84.1 was specific towards **23** (Figure 2.4A) and **24** (Figure 2.4B) and binding of mAb V3.2 was specific towards **27** (Figure 2.5B), but did not show binding to **26** (Figure 2.5A). As expected, the scrambled negative control **31** did not bind either mAb HC84.1 (Figure 2.4) or V3.2 (Figure 2.5). As mentioned before, cyclic epitope IIa mimics **23** and **24**, and cyclic epitope IIb mimics **26** and **27** are both based on the epitope II region. However, the two mAbs HC84.1 and V3.2 bind epitope II via different residues. Therefore, using the different synthetic peptides based on epitope IIa (**13** (cp)) or epitope IIb (**16** (cp)), it is possible to demonstrate selectivity of the mAbs HC84.1 (Figure 2.6A) and V3.2 (Figure 2.6B) towards their respective cyclic epitope mimics **24** or **27** (Figure 2.6). Epitope mimics **29** (Figure 2.7A) and **30** (Figure 2.7B) showed specific binding of mAb DAO5 and showed no binding towards the scrambled negative control (**31**) (Figure 2.7).

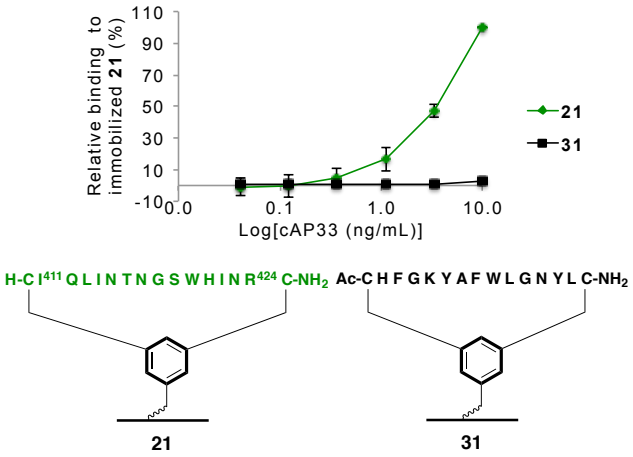

Figure 2.3. ELISA of immobilized cyclic epitope I mimic **21** against epitope I specific mAb AP33 (3-fold dilution over 7 steps at starting concentration: 10 ng/mL). Including immobilized scrambled negative control **31**.

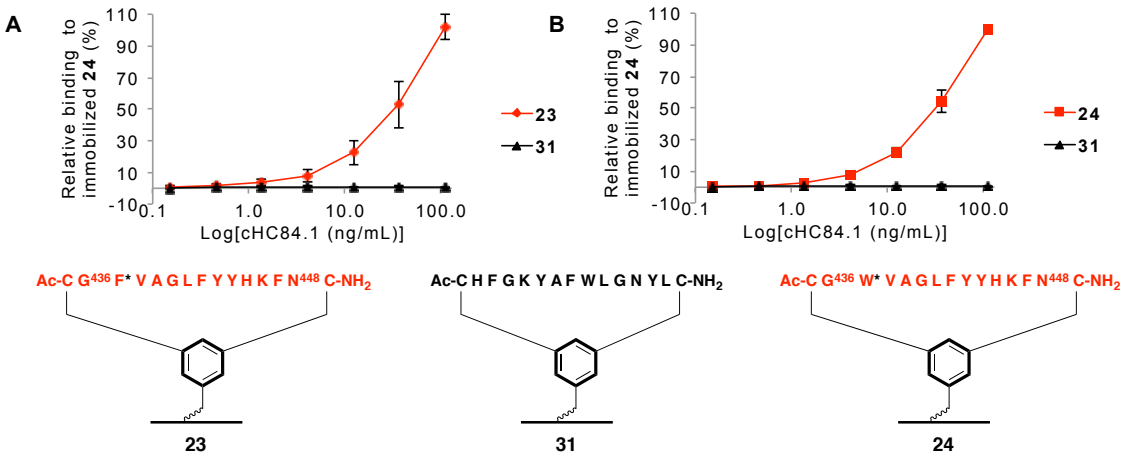

Figure 2.4. ELISA of immobilized cyclic epitope IIa mimics (**A**): **23**; and (**B**): **24**; against epitope IIa specific mAb HC84.1 (3-fold dilution over 7 steps at starting concentration: 111 ng/mL). Including immobilized scrambled negative control **31**.

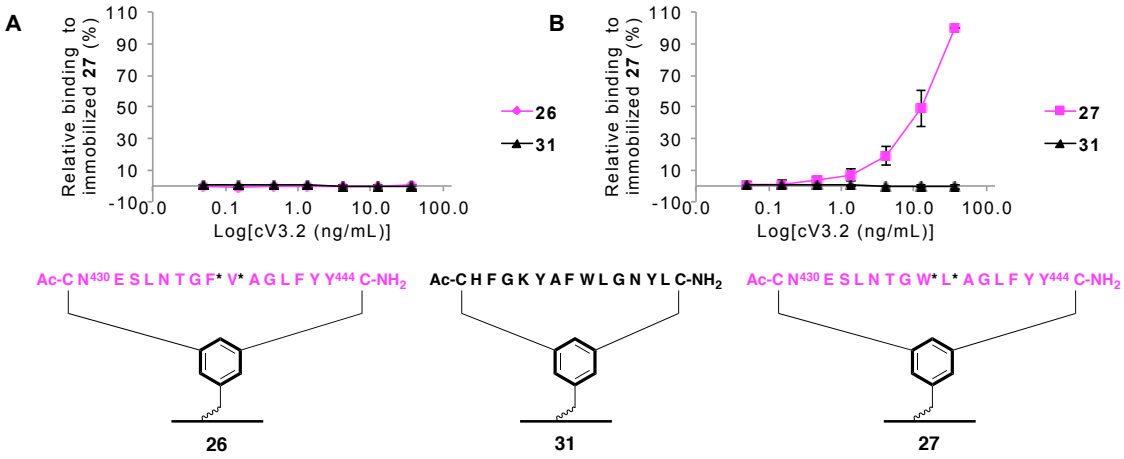

Figure 2.5. ELISA of immobilized cyclic epitope IIb mimics (**A**): **26**; and (**B**): **27**; against epitope IIb specific mAb V3.2 (3-fold dilution over 7 steps at starting concentration: 37 ng/mL). Including immobilized scrambled negative control **31**.

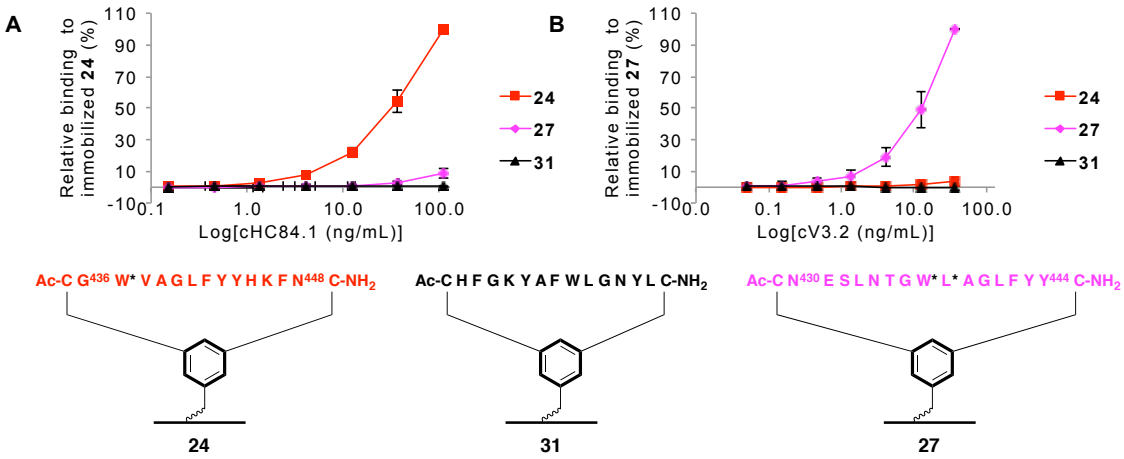

Figure 2.6. ELISA of immobilized cyclic epitope IIa and IIb mimics **24** and **27**, respectively, against (**A**): mAbs HC84.1 (3-fold dilution over 7 steps at starting concentration: 111 ng/mL); (**B**) mAb V3.2 (3-fold dilution over 7 steps at starting concentration: 37 ng/mL). Including immobilized scrambled negative control **31**.

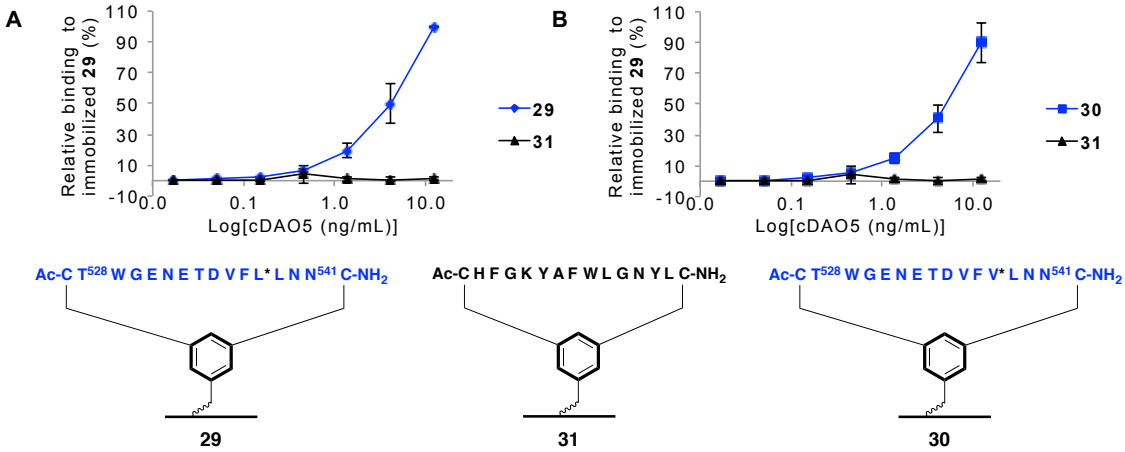

Figure 2.7. ELISA of immobilized cyclic epitope III mimics (**A**): **29**; and (**B**): **30**; against epitope III specific mAb DAO5 (3-fold dilution over 7 steps at starting concentration: 12 ng/mL). Including immobilized scrambled negative control **31**.

2.2.5 Impact of peptide cyclization for adequate mimicry of E2 peptide loops

To understand the impact of cyclization in mimicry of epitopes, we studied the binding of mAbs AP33, HC84.1, and V3.2 to cyclic and linear epitope mimics. To this end, the cyclic (**21**, **24**, and **27**) and linear (**22**, **25**, and **28**) epitopes mimics were ligated separately on maleimide-activated plates. The covalently ligated surfaces were incubated with a three-fold dilution series of mAbs AP33, HC84.1, and V3.2. mAb AP33 bound both cyclic and linear epitope mimics **21** and **22** equally well (Figure 2.8A), which could be due to the

flexible nature of epitope I. In contrast, a significant difference in antibody binding was observed between the immobilized cyclic and linear epitope mimics for mAbs HC84.1 and V3.2 (Figure 2.8B and 2.8C). mAb HC84.1 successfully bound cyclic epitope mimic **24**, but did not show any binding to the corresponding linear epitope mimic **25** (Figure 2.8B). Similarly, mAb V3.2 bound cyclic epitope mimic **27** and showed minor binding to its corresponding linear epitope mimic **28** (Figure. 2.8C). These results strongly underline the importance of peptide cyclization for antibody recognition, which in turn advocates peptide cyclization for accurate mimicry of epitopes. The observed difference in mAb AP33 showing no selectivity towards either a cyclic epitope mimic **21** or linear epitope mimic **22**, HC84.1 not binding linear epitope mimic **25** at all, and mAb V3.2 binding linear epitope mimic **28** to a minor extent suggests that the importance of peptide cyclization could be dependent on the flexibility and sequence associated with the epitope. Perhaps, certain linear peptides readily resemble the conformation of cyclized peptides.

Synthesis of a linear variant of epitope III mimic **29** was attempted to complete the data set, but was unsuccessful. The peptide with a sequence corresponding to epitope III (**18** (cp)) was simply too insoluble. The solubility decreased further when alkylated on linear linker **9** and subsequent purification did not yield enough product.

Cyclization of our peptide sequence resulted in epitope mimics that exhibit a higher affinity towards antibodies. This serves as direct evidence that conformational constraints in peptides resulted in improved mimicry. Nevertheless, the flexibility of linear peptides might allow certain conformations to mould themselves onto binding interfaces; similar to a lock and key model, as observed for mAb AP33 that binds both cyclic and linear conformations of the peptide. Krey *et al.*[10] have successfully co-crystalized human mAb HC84.1 bound to a linear peptide based on the Epitope II region of HCV-E2. The human mAb HC84.1 has been shown to bind the peptide in a α-helical conformation. Perhaps, the linear peptide has adopted partially an α-helix in solution or an α-helix was induced upon binding to HC84.1. In this work, the linear epitope mimic **25** showed a major detrimental effect on binding mAb HC84.1, which could indicate the inability of linear precursor peptide **14** (lp) to form a necessary α-helical structure while alkylated on the linker. However, binding of mAb HC84.1 was achieved by immobilized cyclic epitope mimic **24**, which suggests that the required interacting conformation of the flexible linear peptide might be enforced by cyclization. Since epitope mimicry is based on individual peptide sequences of proteins being grafted on molecular scaffolds, it is inevitable that the intrinsically adopted conformations of linear peptides will be influenced. Therefore,

conformational constraints are necessary to pre-organize the peptides into the required conformations.

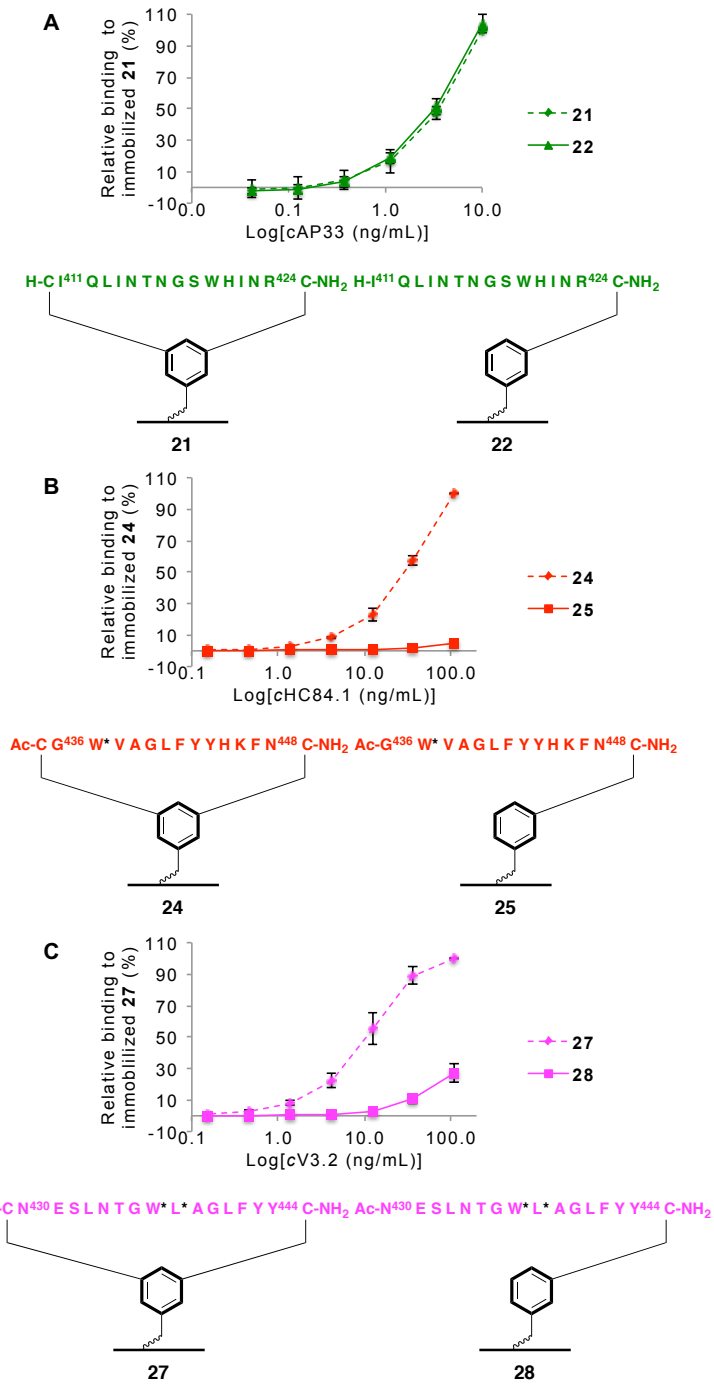

Figure 2.8. ELISA of immobilized cyclic (**21**, **24**, and **27**) versus linear (**22**, **25**, and **28**) epitope mimics against: (**A**) mAb AP33 (3-fold dilution over 7 steps at starting concentration: 10 ng/mL); (**B**): mAb HC84.1 (3-fold dilution over 7 steps at starting concentration: 111 ng/mL); (**C**) mAb V3.2 (3-fold dilution over 7 steps at starting concentration: 111 ng/mL).

2.2.6 Employing epitope mimic coated surfaces for identification of key binding residues

Since peptide cyclic peptide precursor **16** (cp) is shifted towards the N-terminus compared to cyclic peptide precursor **12** (cp) and **13** (cp), some degree of cross-reactivity of mAbs HC84.1 and V3.2 was expected towards both cyclic epitope mimics **23**, **24**, and **27**. However, no such cross-reactivity was observed at the antibody concentrations used (Figure 2.6). Interestingly, residues involved in binding mAb HC84.1 (W^{437}, L^{441}, F^{442}, Y^{443})[9] or mAb V3.2 might differ. Typically, mutagenesis studies are used to identify key binding residues within epitopes involved in antibody recognition. For these, several recombinant mutants of E2 have to be generated that are screened in ELISA to evaluate the altered binding affinity of the antibodies. The process of generating a multitude of different recombinant E2 sequences is a rather laborious and time-consuming process. Instead, epitope mimics could be used as a more high-throughput screening method as collections of synthetic peptides can be easily obtained in a fast and automated fashion. Subsequently, the different synthetic peptides can be conveniently cyclized on linker **7**, conjugated on maleimide-activated plates, and analyzed using ELISA.

In order to evaluate whether cyclic epitope mimics could be used similar to high-throughput mutagenesis studies for identification of key-binding residues, it was decided to try to identify those involved in binding mAb V3.2. The major difference in the overlapping peptide sequence between precursor peptides **12** (cp), **13** (cp), and **16** (cp) is a Phenylalanine-to-Tryptophan change at position 437 and Valine-to-Leucine change at position 438. To this end, mutant precursor peptides **32** (cp) and **33** (cp) were synthesized that contained a Phenylalanine-to-Tryptophan change at position 437 (F437W) or Valine-to-Leucine change on position 438 (V438L) (Table 2.3).

Table 2.3. Overview of synthesized peptidic antigen sequences of epitope **IIa in red**, **IIb in purple**, and **IIab-chimera in black** of HCV-E2 glycoprotein. * Indicates equally represented amino-acid substitutions within the available sequence information of the epitopes.

			Antibodies
Epitope IIa	12 (cp)	Ac – C G^{436} F* V A G L F Y Y H K F N^{448} C – NH_2	HC84.1 [ref.9]
	13 (cp)	Ac – C G^{436} W* V A G L F Y Y H K F N^{448} C – NH_2	
Epitope IIb	16 (cp)	Ac – C N^{430} E S L N T G W* L* A G L F Y Y^{444} C – NH_2	V3.2
Epitope II (a + b)	32 (cp)	Ac – C G^{436} F* L* A G L F Y Y H K F N^{448} C – NH_2	HC84.1 [ref.9]
	33 (lp)	Ac – C G^{436} W* L* A G L F Y Y H K F N^{448} C – NH_2	V3.2

Cyclic precursor peptides **32** (cp) and **33** (cp) were subsequently cyclized to prepare cyclic epitope mimic **34** (purity: ≥95%; yield: 13%) and **35** (purity: ≥95%; yield: 7%), which was then conjugated on maleimide-activated plates, and tested using ELISA. Monoclonal antibodies HC84.1 and V3.2 were tested against plate surfaces containing immobilized cyclic epitope mimics (**23**, **24**, **27**, **34**, or **35**). The cyclic epitope mimics **23** and **24** showed good binding of mAb HC84.1 (Figure 2.9A and 2.9C), but no binding of mAb V3.2 (Figure 2.9B and 2.9D). In contrast, cyclic epitope mimic **27** showed good binding of mAb V3.2 (Figure 2.9B and 2.9D) and no binding of mAb HC84.1 (Figure 2.9A and 2.9C). Mutated cyclic epitope mimics **34** and **35** showed a decrease in binding by mAb HC84.1 (Fig. 2.9A and 2.9C), but only cyclic epitope mimic **35** showed improved binding by mAb V3.2 (Figure 2.9D). This result suggested that the Tryptophan-Leucine sequence at position 437-438 is crucial for binding mAb V3.2.

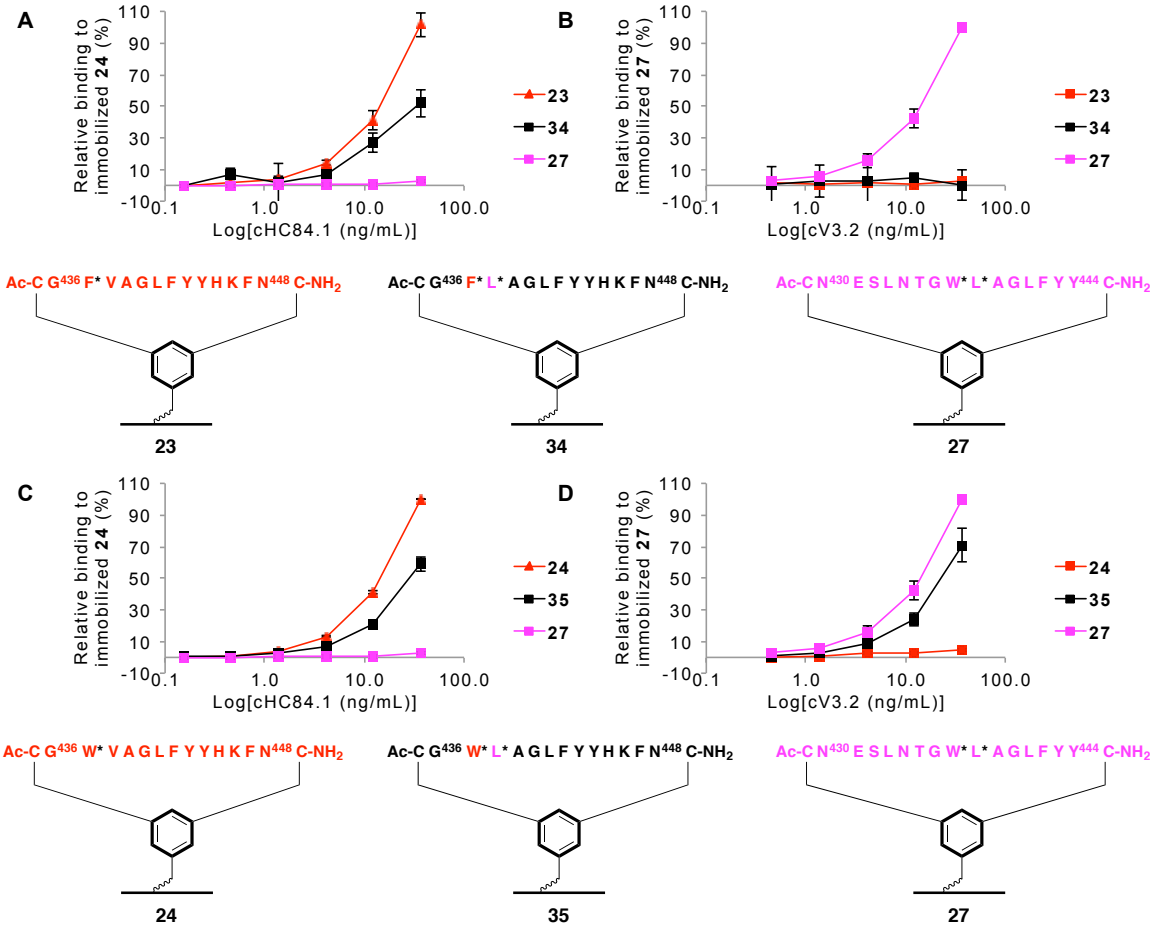

Figure 2.9. ELISA of immobilized cyclic epitope IIa (**23** and **24**), IIb (**27**), and II-chimera (**34** and **35**) mimics, against (**A** and **C**): mAbs HC84.1 (3-fold dilution over 6 steps at starting concentration: 37 ng/mL); (**B** and **D**): mAb V3.2 (3-fold dilution over 5 steps at starting concentration: 37 ng/mL). Including immobilized scrambled negative control **31**.

2.3 Conclusions

In conclusion, we have synthesized epitope mimics containing peptides based on Epitope II of the HCV-E2 glycoprotein using benzyl bis bromide derivatives functionalized with a flexible TEG spacer equipped with a thiol-moiety. The thiol-moiety enabled chemo selective covalent coating of epitope mimics to a maleimide-activated surface. As a result uniform peptide layers were obtained on a solid surface of which we hypothesized that the epitope structure is better preserved than when peptides are non-covalently absorbed onto the ELISA plates. In addition, covalent adsorption prevents a gradual leakage of peptides from the surface. The epitope mimics peptide sequences originated from HCV-E2 and were presented both as cyclic and linear peptides, allowing investigation of the necessity of conformationally constraining of peptide sequences for optimal epitope mimicry.

The broadly neutralizing antibodies AP33, HC84.1 and weakly neutralizing antibody V3.2, and non-neutralizing antibody DAO5 that respectively target epitope I, II, and III of HCV-E2 successfully recognized their corresponding immobilized cyclic epitope mimics. In addition, it has been shown that cyclization significantly improved recognition of epitope mimics. Although it is widely assumed that introducing conformational constraints for example by cyclization in (synthetic) peptides for effective mimicry of epitopes is crucial or at least beneficial for recognition by antibodies, to our knowledge, this is the first time that this has been demonstrated in a convincing molecular experimental approach.

The novel ELISA platform that has been developed here provides an easy, straightforward, and reliable strategy for cyclization of peptides and subsequent conjugation of these cyclic peptides covalently to an ELISA plate. This opens up possibilities for studying antibody-epitope interaction in a high-throughput fashion and might be an attractive tool in vaccine design.

Finally, the use of "mutated"- peptide sequences by this approach instead of using recombinantly mutated protein sequences for studying the relative effectiveness of antibodies is also a particularly promising perspective.

2.4 Experimental section

General procedures. All reagents and solvents were used as received. Fmoc-amino acids were obtained from Activotec (Cambridge, United Kingdom) and *N*,*N*,*N*′,*N*′-Tetramethyl-*O*-(6-chloro-1*H*-benzotriazol-1-yl)uranium hexafluorophosphate (HCTU) was obtained from Matrix Innovation (Quebec, Canada). Tentagel S RAM resin (particle size 90μm, capacity 0.25 $mmol.g^{-1}$) was obtained from IRIS Biotech (Marktredwitz, Germany). Methyl *tert*-butyl ether (MTBE), Hexane (HPLC grade) and TFA were obtained from Aldrich (Milwaukee, USA). DMF (Peptide grade) was obtained from VWR (Lutterworth, United Kingdom). Piperidine, D*i*PEA were obtained from AGTC Bioproducts (Hessle, United Kingdom) and 1,2-ethanedithiol (EDT) was obtained from Merck (Darmstadt, Germany). HPLC grade CH_2Cl_2 and acetonitrile were obtained from Fischer Scientific (Loughborough, United Kingdom). Solid phase peptide synthesis was performed on a PTI Tribute-UV peptide synthesizer. Lyophilizations were performed on a Christ Alpha 2-4 LD*plus* apparatus. Reactions were carried out at ambient temperature unless stated otherwise. Solvents were evaporated under reduced pressure at 40 °C. Reactions in solution were monitored by TLC analysis and R_f-values were determined on Merck pre-coated silica gel 60 F-254 (0.25 mm) plates. Spots were visualized by UV-light and permanganate stain. Column chromatography was performed on Siliaflash P60 (40-63μm) from Silicycle (Canada) or on a Biotage Isolera One purification system using prepacked silica (KP-SIL) Biotage SNAP cartridges. ^1H NMR data was acquired on a Bruker 400 MHz spectrometer in $CDCl_3$ as solvent. Chemical shifts (δ) are reported in parts per million (ppm) relative to trimethylsilane (TMS, 0.00 ppm). Analytical high-pressure liquid chromatography (HPLC) was carried out on a Shimadzu instrument comprising a communication module (CBM-20A), autosampler (SIL-20HT), pump modules (LC-20AT), UV/Vis detector (SPD-20A) and system controller (Labsolutions V5.54 SP), with a Phenomenex Gemini C18 column (110 Å, 5 μm, 250×4.60 mm) or Dr. Maisch Reprosil Gold 200 C18 (5 μm, 250×4.60 mm). UV measurements were recorded at 214 and 254 nm, using a standard protocol: 100% buffer A (acetonitrile/H_2O 5:95 with 0.1% TFA) for 2 minutes followed by a linear gradient of buffer B (acetonitrile/H_2O 95:5 with 0.1% TFA) into buffer A (0-100% or 0-50%) over 30 minutes at a flow rate of 1.0 $mL \cdot min^{-1}$. Liquid chromatography mass spectrometry (LCMS) was carried out on a Thermo Scientific LCQ Fleet quadrupole mass spectrometer with a Dionex Ultimate 3000 LC using a Dr. Maisch Reprosil Gold 120 C18 column (110 Å, 3 μm, 150×4.0 mm) and the same linear gradients of buffer B into buffer A, flowrate and buffers as described for the analytical HPLC.

Purification of the peptidic compounds was performed on an Agilent Technologies 1260 infinity preparative system using both UV and ELSD detectors with a Dr. Maisch Reprosil Gold 200 C18 (10 μm, 250×20 mm). Auto-collection of fractions was used based on the UV measurements at 214 nm, using customized protocols (see below).

Tetraethylene glycol ρ-toluenesulfonate (3). All steps were carried out under N_2 atmosphere. Commercially available TEG **1** (8.6 ml, 50 mmol, 2.0 equiv.) was dissolved in dry CH_2Cl_2 (100 mL). The resulting solution was cooled to 0 °C using an ice bath, followed by addition of TEA (7.0 mL, 50 mmol, 2.0 equiv.). Then ρ-toluenesulfonyl chloride **2** (4.8 g, 25 mmol, 1.0 equiv.) was added, the ice bath was removed, and the resulting reaction mixture was stirred for 16 hours at room temperature. Next, the reaction mixture was washed with 1 M HCl (aq) (2 x 100 mL) and H_2O (100 mL). The obtained aqueous layers were combined and back-extracted with CH_2Cl_2 (100 mL). All CH_2Cl_2 layers were combined and washed with brine (200 mL) and dried over Na_2SO_4, followed by filtration. The filtrate was concentrated *in vacuo*, affording the crude product as a yellowish syrup. Purification by automated flash column chromatography (100% EtOAc) afforded tetraethylene glycol ρ-toluenesulfonate **3** (5.4 g, 16 mmol, 64%) as a clear yellowish syrup. R_f = 0.45 (EtOAc); t_R = 25.0 minutes; ^{1}H-NMR (400 MHz, $CDCl_3$): δ = 7.79 (d, $^3J_{HH}$ = 8.2 Hz, 2H, aryl *o-H*), 7.34 (d, $^3J_{HH}$ = 8.2 Hz, 2H, aryl *m-H*), 4.16 (t, $^3J_{HH}$ = 4.8 Hz, 2H, TsOC*H*$_2$), 3.70 (m, 4H, 1 x TsOCH$_2$C*H*$_2$ & 1 x C*H*$_2$), 3.64 (m, 4H, 2 x C*H*$_2$), 3.60 (m, 6H, 3 x C*H*$_2$), 2.44 (s, 3H, C*H*$_3$), 2.35 (broad m, 1H, O*H*) ppm; ^{13}C-NMR (101 MHz, $CDCl_3$): δ = 144.8 (aryl-*C*), 133.1 (aryl-*C*), 129.8 (aryl *m-C*H), 128.0 (aryl *o-C*H), 72.5 (*C*H$_2$), 70.8 (*C*H$_2$), 70.7 (*C*H$_2$), 70.5 (*C*H$_2$), 70.4 (*C*H$_2$), 69.2 (TsO*C*H$_2$), 68.7 (*C*H$_2$), 61.8 (*C*H$_2$), 21.6 (*C*H$_3$) ppm; HRMS: calculated *m/z* for $C_{15}H_{24}O_7S$: 371.1141 [*M*+Na]$^{1+}$; found 371.1128.

Triphenylmethanethiol (4). All steps were carried out under N_2 atmosphere. Commercially available trityl chloride (14 g, 50 mmol, 1.0 equiv.) was dissolved in acetone (200 mL). The resulting solution was added to a vigorously stirring solution of NaSH•xH_2O (11 g, *ca.* 4.0 equiv.) in acetone/H_2O (1:1, *v/v*) (400 mL). The resulting reaction mixture was stirred at room temperature for 15 minutes. Then, additional H_2O (200 mL) was added to the reaction mixture and stirring was continued for 1 hour. The crude product precipitated as a yellow solid, which was filtered and was washed thoroughly with H_2O. The resulting yellow solid was dried *in vacuo*, affording crude triphenylmethanethiol **4** (11 g, 40 mmol, 80%), which was used without additional purification. R_f = 0.85 (EtOAc/Petroleum Ether 40-60 °C 1:9, *v/v*); t_R = 45.6 minutes; ^{1}H-

NMR (400 MHz, $CDCl_3$): δ = 7.26 (m, 15H, trityl-*H*), 3.08 (s, 1H, S*H*) ppm; ^{13}C-NMR (101 MHz, $CDCl_3$): δ = 147.2 (trityl-*C*), 129.3 (trityl-*C*H), 127.8 (trityl-*C*H), 126.9 (trityl-*C*H), 62.9 (*C*S) ppm. HRMS: calculated *m/z* for $C_{19}H_{16}S$: 275.0895 $[M\text{-H}]^{1-}$; found 275.0892.

Tetraethylene glycol monotrityl thioether (5). All steps were performed under N_2 atmosphere. Crude triphenylmethylthiol **3** (11 g, 40 mmol, 2.6 equiv.) was dissolved in dry THF (100 mL). The resulting solution was cooled to 0 °C using an ice bath, followed by addition of 1.6 g NaH (60% in mineral oil; 40 mmol, 2.6 equiv). The resulting suspension was stirred for 1 hour at 0 °C. A separate solution of tetraethylene glycol ρ-toluenesulfonate **3** (5.4 g, 16 mmol, 1.0 equiv.) was prepared in dry THF (10 mL), which was added to the reaction mixture at 0 °C. After which, the ice bath was removed and the reaction mixture was stirred for another 15-30 minutes at room temperature. Upon completion of the reaction, as was determined by TLC (EtOAc), the reaction mixture was quenched by addition of a sat. NH_4Cl (aq) (100 mL) solution while vigorously stirring for an additional 15 minutes. Then, THF was removed *in vacuo* and EtOAc (100 mL) was added. The aqueous and organic layers were separated. The EtOAc layer was washed with H_2O (2 x 100 mL). The combined aqueous layers were back-extracted with EtOAc (100 mL). The obtained organic layers were combined and washed with brine (200 mL), dried over Na_2SO_4, and filtered. The filtrate was concentrated *in vacuo*, which afforded the crude product as a yellow oil. Purification was immediately performed by automated flash column chromatography (100% EtOAc) afforded tetraethylene glycol monotrityl thioether **5** (6.9 g, 15 mmol, *quant*.) as a yellow oil. R_f = 0.59 (EtOAc); t_R = 39.1 minutes; ^{1}H-NMR (400 MHz, $CDCl_3$): δ = 7.42 (m, 6H, trityl *o*-*H*), 7.28 (m, 6H, trityl *m*-*H*), 7.21 (m, 3H, trityl *p*-*H*), 3.70 (m, 2H, CH_2), 3.64 (m, 4H, 2 x CH_2), 3.58 (m, 4H, 2 x CH_2), 3.45 (m, 2H, CH_2), 3.30 (t, $^3J_{HH}$ = 6.9 Hz, 2H, SCH_2CH_2), 2.44 (t, $^3J_{HH}$ = 6.9 Hz, 2H, SCH_2), 2.34 (s, 1H, O*H*) ppm; ^{13}C-NMR (101 MHz, $CDCl_3$): δ = 144.8 (trityl-*C*), 129.6 (trityl *o*-*C*H), 127.9 (trityl *m*-*C*H), 126.6 (trityl *p*-*C*H), 72.5 (*C*H_2), 70.7(*C*H_2), 70.5 (*C*H_2), 70.4 (*C*H_2), 70.2 (*C*H_2), 69.7 (SCH_2CH_2 (2)), 66.6 (*C*S), 61.8 (*C*H_2), 31.7 (S*C*H_2) ppm; HRMS: calculated *m/z* for $C_{27}H_{32}O_4S$: 475.1919 $[M\text{+Na}]^{1+}$; found 475.1900.

Benzylic bromide linkers. All steps were carried out under N_2 atmosphere. Tetraethylene glycol monotrityl thioether **5** (3.4 g, 7.6 mmol) was dissolved in dry THF (50 mL). The resulting solution was cooled to 0 °C using an ice bath, followed by the addition of 0.50 g NaH (60% in mineral oil; 11 mmol, 1.5 equiv.). After which, the reaction mixture was stirred for 1 hour at 0 °C. Then, tetraethylene glycol monotrityl thioether **5** was added in

portions to a solution of 1, 3, 5-tris(bromomethyl)benzene **6** or α, α'-dibromide-*m*-xylene **8** and stirring continued for 16 hours. Upon completion of the reaction, as determined by TLC (30% EtOAc in petroleum ether 40-60 °C), THF was removed *in vacuo*. Then, the residue was dissolved in EtOAc (100 mL), followed by filtration over Celite to remove NaBr salts. The filtrate was concentrated *in vacuo*, which afforded the crude product. Purification by automated flash column chromatography using a linear gradient (10-30% EtOAc in petroleum ether 40-60 °C over 20 column volumes) afforded pure product.

Cyclization Linker (**7**)*:* 1, 3, 5-tris(bromomethyl)benzene **6** (1.5 g, 4.2 mmol, 1.1 equiv.) was dissolved in dry THF (75 mL), followed by the portionwise addition (5 x 5 mL) of the above described reaction mixture containing tetraethylene glycol monotrityl thioether **5** (1.7 g, 3.8 mmol, 1.0 equiv.) with 15 minute intervals. Purification as described above afforded pure cyclization linker **7** (0.92 g, 1.2 mmol, 32%) as a yellow oil. R_f = 0.31 (petroleum ether 40-60 °C/EtOAc 7:3, *v/v*); t_R = 49.1 minutes; ^{1}H-NMR (400 MHz, $CDCl_3$): δ = 7.41 (m, 6H, trityl *o-H*), 7.32 (m, 1H, aryl *p-H*), 7.29 (m, 2H, aryl *o-H*), 7.26 (m, 6H, trityl *m-H*), 7.20 (m, 3H, trityl *p-H*), 4.53 (s, 2H, OCH_2-aryl), 4.45 (s, 4H, 2 x CH_2Br), 3.65 (m, 8H, 4 x CH_2), 3.57 (m, 2H, CH_2), 3.45 (m, 2H, CH_2), 3.30 (t, $^3J_{HH}$ = 6.9 Hz, 2H, SCH_2CH_2), 2.42 (t, $^3J_{HH}$ = 6.9 Hz, 2H, SCH_2) ppm; ^{13}C-NMR (101 MHz, $CDCl_3$): δ = 144.8 (trityl-*C*), 139.9 (aryl-*C*), 138.5 (aryl-*C*($CH_2Br)_2$), 129.6 (trityl *o-C*H), 128.8 (aryl *p-C*H), 128.1 (aryl *o-C*H), 127.9 (aryl *o-C*H), 127.9 (trityl *m-C*H), 126.6 (trityl *p-C*H), 72.5 (O*C*H_2-aryl), 70.7 (*C*H_2), 70.7 (*C*H_2), 70.6 (*C*H_2), 70.5 (*C*H_2), 70.2 (CH_2), 69.9 (*C*H_2), 69.6 (SCH_2CH_2), 66.6 (C*C*S), 32.8 (2 x *C*H_2Br), 31.7 (S*C*H_2) ppm; HRMS: calculated *m/z* for $C_{36}H_{40}O_4S^{79}Br_2$: 749.0912 $[M+Na]^{1+}$; found 749.0886.

Linear Linker (**9**)*:* α, α'-dibromide-*m*-xylene **8** (1.1 g, 4.2 mmol, 1.1 equiv.) was dissolved in dry THF (75 mL), followed by the portionwise addition (5 x 5 mL) of the above described reaction mixture containing tetraethylene glycol monotrityl thioether **5** (1.7 g, 3.8 mmol, 1.0 eq.) with 15 minute intervals. Purification as described above afforded pure linear linker **9** (1.0 g, 1.6 mmol, 42%) as a yellow oil. R_f = 0.36 (petroleum ether 40-60 °C/EtOAc 7:3, *v/v*); t_R = 48.3 minutes; ^{1}H-NMR (400 MHz, $CDCl_3$): δ = 7.41 (m, 6H, trityl *o-H*), 7.37 (m, 1H, aryl-C*H*), 7.30 (m, 3H, aryl-C*H*), 7.26 (m, 6H, trityl *m-H*), 7.20 (m, 3H, trityl *p-H*), 4.54 (s, 2H, OCH_2-aryl), 4.48 (s, 2H, CH_2Br), 3.64 (m, 8H, 4 x CH_2), 3.57 (m, 2H, CH_2), 3.45 (m, 2H, CH_2), 3.30 (t, $^3J_{HH}$ = 6.9 Hz, 2H, SCH_2CH_2), 2.42 (t, $^3J_{HH}$ = 6.9 Hz, 2H, SCH_2) ppm; ^{13}C-NMR (101 MHz, $CDCl_3$): δ = 144.8 (trityl-*C* (11, 17, 23)), 139.1 (aryl-*C*), 137.9 (aryl-*C*), 129.6 (trityl *o-C*H), 128.8 (aryl-*C*H), 128.2 (aryl-*C*H), 128.2 (aryl-*C*H)**,** 127.9 (trityl *m*-CH), 127.7 (aryl-*C*H), 126.6 (trityl *p-C*H), 72.8 (O*C*H_2-aryl),

70.7 (CH$_2$), 70.5 (CH$_2$), 70.2 (CH_2), 69.7 (CH_2), 69.6 (SCH$_2$$CH_2$), 66.6 (C$C$S), 33.4 ($CH_2$Br), 31.7 (S$CH_2$) ppm; HRMS: calculated *m/z* for $C_{35}H_{39}O_4S^{79}Br$: 657.1650 [M+Na]$^{1+}$; found 657.1629.

General method for automated peptide synthesis. The peptides were synthesized on a PTI Tribute-UV peptide synthesizer. Tentagel S RAM resin (1.0 g, 0.25 mmol, 1.0 equiv. or 0.43 mg, 0.10 mmol, 1.0 equiv.) was allowed to swell in DMF (3 x 10 minutes). De-protection of the Fmoc group was achieved by treatment of the resin with 20% piperidine in DMF using the RV_top_UV_Xtend protocol from the Tribute-UV peptide synthesizer followed by a DMF washing step (5 x 30 seconds). The Fmoc-protected amino acids were coupled using HCTU (with the 0.10 mmol scale 5.0 equiv. was used and with the 0.25 mmol scale 4.0 equiv. was used) and D*i*PEA (with the 0.10 mmol scale 10 equiv. was used and with the 0.25 mmol scale 8.0 equiv. was used) in DMF, as a coupling system, with 2 minutes pre-activation. The coupling time was 10 minutes when the peptide was synthesized on a 0.10 mmol scale and 20 minutes when the 0.25 mmol scale was conducted. After every coupling the resin was washed with DMF (6 x 30 seconds). After coupling of the last amino acid, the Fmoc group was cleaved using the normal de-protection conditions (described above) and the resulting free N-terminus was acetylated by treating the resin bounded peptide with acetic anhydride (250 μL) and D*i*PEA (10 equiv. for the 0.10 mmol scale and 8.0 equiv. for the 0.25 mmol scale) in DMF using the standard coupling times (described above). Acetylation of the N-terminus was omitted for peptides **10** and **11** to improve solubility. In the last step the resin was washed with DMF (5 x 30 seconds), DCM (5 x 30 seconds), dried over a nitrogen flow for 10 minutes, followed by the cleavage of the resin-bounded peptide. Cleavage and de-protection was achieved by treatment of the resin with TFA:H_2O:TIS:EDT (15 mL for the 0.25 mmol scale and 5 mL for the 0.10 mmol scale, 90:5:2.5:2.5, *v*/*v*/*v*/*v*) for 3 hours at room temperature. The peptide was precipitated in MTBE/hexane (1:1, 90 mL for the 0.25 mmol scale and 45 mL for the 0.10 mmol scale), centrifuged (4500 rpm; 5 minutes), the supernatant decanted, and the pellet washed 3 times with MTBE/hexane (1:1, 45 mL). The resulting pellet was re-dissolved in *t*-BuOH/H_2O (1:1, *v*/*v*) and lyophilized.

Cyclic precursor peptide 10 (cp). The peptide was synthesized as described above by solid phase synthesis on a 0.25 mmol scale, which afforded crude peptide (0.30 g). This crude peptide was used in the cyclization by alkylation step. t_R = 16.5 minutes; LRMS: *m/z* calculated for $C_{79}H_{127}N_{27}O_{22}S_2$: 935.96 ½[$M$+2H]$^{2+}$; found: 936.33 (^{13}C [+1]).

Linear precursor peptide 11 (lp). The peptide was synthesized as described above by solid phase synthesis on a 0.25 mmol scale, which afforded crude peptide (0.37 g). This crude peptide was used in the cyclization by alkylation step. t_R = 16.1 minutes; LRMS: *m/z* calculated for $C_{76}H_{122}N_{26}O_{21}S$: 884.46 ½[*M*+2H]$^{2+}$; found: 884.58 (^{13}C [+1]).

Cyclic precursor peptide 12 (cp). The peptide was synthesized as described above by solid phase synthesis on a 0.25 mmol scale, which afforded crude peptide (0.36 g). This crude peptide was used in the cyclization by alkylation step. t_R = 20.7 minutes; LRMS: calculated *m/z* for $C_{87}H_{117}N_{20}O_{19}S_2$: 905.42 ½[*M*+2H]$^{2+}$; found: 905.67.

Cyclic precursor peptide 13 (cp). The peptide was synthesized as described above by solid phase synthesis on a 0.25 mmol scale, which afforded crude peptide (0.40 g). This crude peptide was used in the cyclization by alkylation step. t_R = 19.2 minutes; LRMS: calculated *m/z* for $C_{89}H_{117}N_{21}O_{19}S_2$: 924.92 ½[*M*+2H]$^{2+}$; found: 925.33.

Linear precursor peptide 14 (lp). The peptide was synthesized as described above by solid phase synthesis on a 0.25 mmol scale, which afforded crude peptide (0.43 g). This crude peptide was used in the alkylation step. t_R = 18.9 minutes; LRMS: LRMS: calculated *m/z* for $C_{86}H_{112}N_{20}O_{18}S$: 873.42 ½[*M*+2H]$^{2+}$; found: 873.92.

Cyclic precursor peptide 15 (cp). The peptide was synthesized as described above by solid phase synthesis on a 0.25 mmol scale, which afforded crude peptide (0.30 g). This crude peptide was used in the cyclization by alkylation step. t_R = 20.6 minutes; LRMS: calculated *m/z* for $C_{88}H_{124}N_{20}O_{26}S_2$: 971.43 ½[*M*+2H]$^{2+}$; found: 971.75.

Cyclic precursor peptide 16 (cp). The peptide was synthesized as described above by solid phase synthesis on a 0.25 mmol scale, which afforded crude peptide (0.32 g). This crude peptide was used in the cyclization by alkylation step. t_R = 21.7 minutes; LRMS: calculated *m/z* for $C_{91}H_{127}N_{21}O_{26}S_2$: 997.94 ½[*M*+2H]$^{2+}$; found: 998.08.

Linear precursor peptide 17 (lp). The peptide was synthesized as described above by solid phase synthesis on a 0.25 mmol scale, which afforded crude peptide (0.39 g). This crude peptide was used in the alkylation step. t_R = 21.5 minutes; LRMS: calculated *m/z* for $C_{88}H_{122}N_{20}O_{25}S$: 946.44 ½[*M*+2H]$^{2+}$; found: 946.75.

Cyclic precursor peptide 18 (cp). The peptide was synthesized as described above by solid phase synthesis on a 0.25 mmol scale, which afforded crude peptide (0.40 g). This crude peptide was used in the cyclization by alkylation step. t_R = 18.6 minutes; LRMS: calculated *m/z* for $C_{81}H_{119}N_{21}O_{28}S_2$: 949.91 ½[*M*+2H]$^{2+}$; found: 950.17.

Cyclic precursor peptide 19 (cp). The peptide was synthesized as described above by solid phase synthesis on a 0.25 mmol scale, which afforded crude peptide (0.40 g). This crude peptide was used in the cyclization by alkylation step. t_R = 18.1 minutes; LRMS: calculated *m/z* for $C_{80}H_{117}N_{21}O_{28}S_2$: 942.90 ½[*M*+2H]$^{2+}$; found: 943.00.

Cyclic precursor peptide 20 (cp). The peptide was synthesized as described above by solid phase synthesis on a 0.25 mmol scale, which afforded crude peptide (0.33 g). This crude peptide was used in the cyclization by alkylation step. t_R = 19.1 minutes; LRMS: calculated *m/z* for $C_{90}H_{119}N_{21}O_{19}S_2$: 931.93 ½[*M*+2H]$^{2+}$; found: 932.50.

Cyclic precursor peptide 32 (cp). The peptide was synthesized as described above by solid phase synthesis on a 0.25 mmol scale, which afforded crude peptide (0.35 g). This crude peptide was used in the cyclization by alkylation step. t_R = 19.8 minutes; LRMS: calculated *m/z* for $C_{88}H_{118}N_{20}O_{19}S_2$: 912.42 ½[*M*+2H]$^{2+}$; found: 913.25.

Cyclic precursor peptide 33 (cp). The peptide was synthesized as described above by solid phase synthesis on a 0.25 mmol scale, which afforded crude peptide (0.38 g). This crude peptide was used in the cyclization by alkylation step. t_R = 19.7 minutes; LRMS: calculated *m/z* for $C_{90}H_{119}N_{21}O_{19}S_2$: 931.93 ½[*M*+2H]$^{2+}$; found: 932.33.

General method for peptide alkylation. Crude precursor peptide (25 µmol, 1.0 equiv.) was dissolved in DMF (18 mL). Subsequently, a solution of cyclization (**7**) or linear (**9**) linker (38 µmol, 1.5 equiv.) in DMF (1 mL) was added. Subsequently, an aqueous NH_4HCO_3 buffer solution (pH 7.9, 20 mM; 6 mL) was added dropwise to the reaction mixture, which gave a general peptide concentration of ≤1 mM in DMF/buffer solution (3:1, *v/v*). The reaction mixture was stirred for 2 hours at room temperature, followed by concentration *in vacuo*. The residue was re-dissolved in TFA:H_2O:TIS:EDT (15 mL, 90:5:2.5:2.5, *v/v/v/v)* and the resulting reaction mixture was stirred for 3 hours at room temperature. Then, the crude product was precipitated in 2 x 50 ml MTBE/hexane (1:1, *v/v*). The crude precipitate was obtained by centrifugation (4500 rpm; 5 minutes). The collected precipitate was washed an additional four times using 2 x 50 mL MTBE/hexane

(1:1, *v*/*v*) and centrifugation (4500 rpm; 5 minutes). After this the crude product was dissolved in *t*BuOH/H_2O (1:1, *v*/*v*) and lyophilized.

Cyclic epitope mimic 21. crude cyclic precursor **10** (cp) (47 mg, 25 μmol, 1.0 equiv.) was treated with cyclization linker **7** (24 mg, 34 μmol, 1.4 equiv.) according to the general method for peptide alkylation as described above. The obtained crude product (51 mg) was dissolved in HPLC buffers A and B (1:1, *v*/*v*) in 5 mL and purified by preparative HPLC using a linear gradient of HPLC buffer B in HPLC buffer A (0-40%; 40 minutes). Fractions containing pure product were combined and lyophilized to yield pure cyclic epitope mimic **21** (1.5 mg, 0.68 μmol, 2% overall yield) as a fluffy white powder. t_R = 17.9 minutes; HRMS: calculated *m/z* for $C_{96}H_{151}N_{27}O_{26}S_3$: 1098.0321 ½[*M*+2H]$^{2+}$; found 1098.0355; LRMS: calculated *m/z* for $C_{96}H_{151}N_{27}O_{26}S_3$: 1098.03 ½[*M*+2H]$^{2+}$ / 732.36 [*M*+3H]$^{3+}$; found *m/z* 1098.67 / 732.67.

Linear epitope mimic 22. crude linear precursor **11** (lp) (34 mg, 19 μmol, 1.0 equiv.) was treated with linear linker **9** (13 mg, 21 μmol, 1.1 equiv.) according to the general method for peptide alkylation as described above. The obtained crude product (30 mg) was dissolved in HPLC buffers A and B (1:1, *v*/*v*) in 3 mL and purified by preparative HPLC using a linear gradient of HPLC buffer B in HPLC buffer A (0-40%; 40 minutes). Fractions containing pure product were combined and lyophilized to yield pure linear epitope mimic **22** (4.2 mg, 2.0 μmol, 7% overall yield) as a fluffy white powder. t_R = 18.6 min; HRMS: calculated *m/z* for $C_{92}H_{146}N_{26}O_{25}S_2$: 1040.5275 ½[*M*+2H]$^{2+}$; could not be obtained; LRMS: calculated *m/z* for $C_{92}H_{146}N_{26}O_{25}S_2$: 1040.53 ½[*M*+2H]$^{2+}$ / 694.02 1/3[*M*+3H]$^{3+}$; found *m/z* 1041.00 / 694.42.

Cyclic epitope mimic 23. crude cyclic precursor **12** (cp) (45 mg, 25 μmol, 1.0 equiv.) was treated with cyclization linker **7** (27 mg, 38 μmol, 1.5 equiv.) according to the general method for peptide alkylation as described above. The obtained crude product (51 mg) was dissolved in HPLC buffers A and B (1:1, *v*/*v*) as three batches of 10-20 mg in 1-2 mL. Each batch was purified by preparative HPLC using a linear gradient of HPLC buffer B in HPLC buffer A (0-50%; 60 minutes). Fractions containing pure product were combined and lyophilized to yield pure cyclic epitope mimic **23** (11 mg, 5.1 μmol, 16% overall yield) as a fluffy white powder. t_R = 21.7 minutes; HRMS: calculated *m/z* for $C_{104}H_{140}N_{20}O_{23}S_3$: 1078.4769 ½[*M*+H+Na]$^{2+}$; found 1078.4254; LRMS: calculated *m/z* for $C_{104}H_{140}N_{20}O_{23}S_3$: 1067.49 ½[*M*+2H]$^{2+}$; found 1068.08.

Cyclic epitope mimic 24. crude cyclic precursor **13** (cp) (46 mg, 25 μmol, 1.0 equiv.) was treated with cyclization linker **7** (27 mg, 38 μmol, 1.5 equiv.) according to the general method for peptide alkylation as described above. The obtained crude product (54 mg) was dissolved in HPLC buffers A and B (1:1, *v*/*v*) as three batches of 10-20 mg in 3 mL. Each batch was purified by preparative HPLC using a linear gradient of HPLC buffer B in HPLC buffer A (0-50%; 60 minutes). Fractions containing pure product were combined and lyophilized to yield pure cyclic epitope mimic **24** (9.7 mg, 4.5 μmol, 15% overall yield) as a fluffy white powder. t_R = 21.6 minutes; HRMS: calculated *m/z* for $C_{106}H_{141}N_{21}O_{23}S_3$: 1086.9914 ½[*M*+2H]$^{2+}$; found 1086.9400; LRMS: calculated *m/z* for $C_{106}H_{141}N_{21}O_{23}S_3$: 1086.99 ½[*M*+2H]$^{2+}$; found 1087.58.

Linear epitope mimic 25. crude linear precursor **14** (lp) (66 mg, 38 μmol, 1.0 equiv.) was treated with linear linker **9** (36 mg, 56.5 μmol, 1.5 equiv.) according to the general method for peptide alkylation as described above. The obtained crude product (68 mg) was dissolved in HPLC buffers A and B (1:1, *v*/*v*) as two batches of 20-40 mg in 2-5 mL. Each batch was purified by preparative HPLC using a linear gradient of HPLC buffer B in HPLC buffer A (0-50%; 60 minutes). Fractions containing pure product were combined and lyophilized to yield pure linear epitope mimic **25** (23 mg, 11 μmol, 29% overall yield) as a fluffy white powder. t_R = 22.1 minutes; HRMS: calculated *m/z* for $C_{102}H_{136}N_{20}O_{22}S_2$: 1029.4868 ½[*M*+2H]$^{2+}$; found 1029.4826; LRMS: calculated *m/z* for $C_{102}H_{136}N_{20}O_{22}S_2$: 1029.49 ½[*M*+2H]$^{2+}$; found 1030.00.

Cyclic epitope mimic 26. crude cyclic precursor **15** (cp) (49 mg, 25 μmol, 1.0 equiv.) was treated with cyclization linker **7** (27 mg, 38 μmol, 1.5 equiv.) according to the general method for peptide alkylation as described above. The obtained crude product (57 mg) was dissolved in 10% TFA supplemented with MeCN as three batches of 10-20 mg in 3 mL. Each batch was purified by preparative HPLC using a linear gradient of HPLC buffer B in HPLC buffer A (20-60%; 60 minutes). Fractions containing pure product were combined and lyophilized to yield pure cyclic epitope mimic **26** (2.3 mg, 1.0 μmol, 2% overall yield) as a fluffy white powder. t_R = 21.5 minutes; HRMS: calculated *m/z* for $C_{105}H_{148}N_{20}O_{30}S_3$: 1133.4994 ½[*M*+2H]$^{2+}$; found 1133.4959; LRMS: calculated *m/z* for $C_{105}H_{148}N_{20}O_{30}S_3$: 1133.50 ½[*M*+2H]$^{2+}$; found 1133.67.

Cyclic epitope mimic 27. crude cyclic precursor **16** (cp) (51 mg, 25 μmol, 1.0 equiv.) was treated with cyclization linker **7** (28 mg, 38 μmol, 1.5 equiv.) according to the general method for peptide alkylation as described above. The obtained crude product (61 mg) was

dissolved in 10% TFA supplemented with MeCN as three batches of respectively 15-25 mg in 3 mL. Each batch was purified by preparative HPLC using a linear gradient of HPLC buffer B in HPLC buffer A (20-60%; 60 minutes). Fractions containing pure product were combined and lyophilized to yield pure cyclic epitope mimic **27** (4.3 mg, 1.9 μmol, 5% overall yield) as a fluffy white powder. t_R = 22.6 minutes; HRMS: calculated *m/z* for $C_{108}H_{151}N_{21}O_{30}S_3$: 1160.0127 ½[*M*+2H]$^{2+}$; could not be obtained; LRMS: calculated *m/z* for $C_{108}H_{151}N_{21}O_{30}S_3$: 1160.01 ½[*M*+2H]$^{2+}$; found 1160.33.

Linear epitope mimic 28. crude linear precursor **17** (lp) (73 mg, 38 μmol, 1.0 equiv.) was treated with linear linker **9** (36 mg, 57 μmol, 1.5 equiv.) according to the general method for peptide alkylation as described above. The obtained crude product (78 mg) was dissolved in HPLC buffers A and B (1:1, *v*/*v*) as two batches of 20-30 mg in 2-3 mL. Each batch was purified by preparative HPLC using a linear gradient of HPLC buffer B in HPLC buffer A (20-60%; 60 minutes). Fractions containing pure product were combined and lyophilized to yield pure linear epitope mimic **28** (3.5 mg, 1.6 μmol, 3% overall yield) as a fluffy white powder. t_R = 23.6 minutes; HRMS: calculated *m/z* for $C_{104}H_{146}N_{20}O_{29}S_2$: 1102.5081 ½[*M*+2H]$^{2+}$; could not be obtained; LRMS: calculated *m/z* for $C_{104}H_{146}N_{20}O_{29}S_2$: 1102.51 ½[*M*+2H]$^{2+}$; found 1102.75.

Cyclic epitope mimic 29. crude cyclic precursor **18** (cp) (48 mg, 25 μmol, 1.0 equiv.) was treated with cyclization linker **7** (27 mg, 38 μmol, 1.5 equiv.) according to the general method for peptide alkylation as described above. The obtained crude product (61 mg) was dissolved in MeCN/*t*BuOH/H_2O (1:1:1, *v*/*v*/*v*) as three batches of 10-20 mg in 3 mL. Each batch was purified by preparative HPLC using a linear gradient of HPLC buffer B in HPLC buffer A (0-50%; 60 minutes). Fractions containing pure product were combined and lyophilized to yield pure cyclic epitope mimic **29** (4.8 mg, 2.2 μmol, 7% overall yield) as a fluffy white powder. t_R = 19.9 minutes; HRMS: calculated *m/z* for $C_{98}H_{143}N_{21}O_{32}S_3$: 1109.9607 ½[*M*-2H]$^{2-}$; found 1109.9435; LRMS: calculated *m/z* for $C_{98}H_{143}N_{21}O_{32}S_3$: 1111.98 ½[*M*+2H]$^{2+}$; found 1112.83.

Cyclic epitope mimic 30. crude cyclic precursor **19** (cp) (47 mg, 25 μmol, 1.0 equiv.) was treated with cyclization linker **7** (27 mg, 38 μmol, 1.5 equiv.) according to the general method for peptide alkylation as described above. The obtained crude product (53 mg) was dissolved in MeCN/*t*BuOH/H_2O (1:1:1, *v*/*v*/*v*) as three batches of 10-20 mg in 3 mL. Each batch was purified by preparative HPLC using a linear gradient of HPLC buffer B in HPLC buffer A (0-50%; 60 minutes). Fractions containing pure product were combined

and lyophilized to yield pure cyclic epitope mimic **30** (8.9 mg, 4.0 μmol, 14% overall yield) as a fluffy white powder. t_R = 19.4 minutes; HRMS: calculated *m/z* $C_{97}H_{141}N_{21}O_{32}S_3$: 1102.9529 ½[*M*-2H]$^{2-}$; found 1102.9654; LRMS: calculated *m/z* for $C_{97}H_{141}N_{21}O_{32}S_3$: 1104.97 ½[*M*+2H]$^{2+}$; found 1105.50.

Scrambled negative control 31. crude cyclic precursor **20** (cp) (46 mg, 25 μmol, 1.0 equiv.) was treated with cyclization linker **7** (27 mg, 38 μmol, 1.5 equiv.) according to the general method for peptide alkylation as described above. The obtained crude product (50 mg) was dissolved in HPLC buffers A and B (1:1, *v*/*v*) as three batches of 10-20 mg in 2-3 mL. Each batch was purified by preparative HPLC using a linear gradient of HPLC buffer B in HPLC buffer A (0-50%; 60 minutes). Fractions containing pure product were combined and lyophilized to yield pure cyclic epitope mimic **31** (6.7 mg, 3.1 μmol, 9% overall yield) as a fluffy white powder. t_R = 21.8 minutes; HRMS: calculated *m/z* for $C_{107}H_{143}N_{21}O_{23}S_3$: 1093.9992 ½[*M*+2H]$^{2+}$; found 1093.9936; LRMS: calculated *m/z* for $C_{107}H_{143}N_{21}O_{23}S_3$: 1094.00 ½[*M*+2H]$^{2+}$; found 1094.58.

Cyclic epitope mimic 34. crude cyclic precursor **32** (cp) (46 mg, 25 μmol, 1.0 equiv.) was treated with cyclization linker **7** (27 mg, 38 μmol, 1.5 equiv.) according to the general method for peptide alkylation as described above. The obtained crude product (53 mg) was dissolved in HPLC buffers A and B (1:1, *v*/*v*) as three batches of 10-20 mg in 3 mL. Each batch was purified by preparative HPLC using a linear gradient of HPLC buffer B in HPLC buffer A (0-50%; 60 minutes). Fractions containing pure product were combined and lyophilized to yield pure cyclic epitope mimic **34** (9.0 mg, 4.2 μmol, 13% overall yield) as a fluffy white powder. t_R = 22.5 minutes; HRMS: calculated *m/z* for $C_{105}H_{142}N_{20}O_{23}S_3$: 1074.4938 ½[*M*+2H]$^{2+}$; found 1074.4909; LRMS: calculated *m/z* for $C_{105}H_{142}N_{20}O_{23}S_3$: 1074.49 ½[*M*+2H]$^{2+}$; found 1075.08.

Cyclic epitope mimic 35. crude cyclic precursor **33** (cp) (46 mg, 25 μmol, 1.0 equiv.) was treated with cyclization linker **7** (27 mg, 38 μmol, 1.5 equiv.) according to the general method for peptide alkylation as described above. The obtained crude product (51 mg) was dissolved in HPLC buffers A and B (1:1, *v*/*v*) as three batches of 10-20 mg in 2-3 mL. Each batch was purified by preparative HPLC using a linear gradient of HPLC buffer B in HPLC buffer A (0-50%; 60 minutes). Fractions containing pure product were combined and lyophilized to yield pure cyclic epitope mimic **35** (4.9 mg, 2.2 μmol, 7% overall yield) as a fluffy white powder. t_R = 22.3 minutes; HRMS: calculated *m/z* for $C_{107}H_{143}N_{21}O_{23}S_3$:

1093.9993 ½[*M*+2H]$^{2+}$; found 1093.9941; LRMS: calculated *m/z* for $C_{107}H_{143}N_{21}O_{23}S_3$: 1094.00 ½[*M*+2H]$^{2+}$; found 1094.50.

Monoclonal antibodies. The mAbs AP33[40], HC84.1[9], and DAO5[30] were kindly provided by Prof. A. H. Patel and his research group.

General method for ELISA. Pierce® maleimide activated 96-well plates were purchased from Thermo Scientific. The wells were washed three times with 200 µL wash buffer (0.10 M Na_3PO_4, 0.15 M NaCl, 0.05% Tween®-20 detergent; pH 7.2). Then, the desired epitope mimic (100 – 500 µg) was suspended in 1 mL binding buffer (0.10 M Na_3PO_4, 0.15 M NaCl, 10 mM EDTA; pH 7.2) and further diluted (10 – 50 fold) to a concentration of 10 µg/mL. To each well, 200 µL of the epitope mimic solution was added and incubated overnight at 4 °C. After this, the wells were washed three times with 200 µL wash buffer. For capping unreacted maleimide groups, immediately before use, a solution of 10 µg/mL *N*-acetylated cysteine was prepared and 200 µL was added to each of the wells, followed by incubation of 1-2 hours at room temperature. Then, the wells were washed three times with 200 µL wash buffer. A three-fold dilution series of primary mAb was prepared and 100 µL was transferred to each well, followed by incubation for 1-2 hours at room temperature. After this, the wells were washed three times with PBST, before supplying 100 µL 1:2000 horse radish peroxidase (HRP) conjugated secondary α-mouse A4416 (Sigma) to each well. Incubation continued for 1-2 hours at room temperature, followed by washing the wells three times with PBST. The plates were developed using 100 µL 3, 3', 5, 5' tetramethylbenzidine (TMB) solution per well, obtained from Life Technologies, and incubating for 25 minutes at room temperature, after which, further development was stopped using 50 µL 0.50 M H_2SO_4 per well. Absorbance at 450 nm was measured on a Varioskan (Thermoscientific) or PHERAstar FS (BMG Labtech) instrument. Background signal (no mAb) was subtracted. The data are represented as a percentage relative to immobilized epitope mimic **21**, **24**, **27** and **29** for antibodies AP33, HC84.1, V3.2, and DAO5, respectively, with the absorbance of the highest antibody concentration being set to 100% per individual experiment. Data was collected from at least 3 independent experiments. All experiments were performed in duplicate. Error bars represent the standard deviation.

2.5 References

1. Hajarizadeh, B., Grebely, J., Dore, G. J. (2013) Epidemiology and natural history of HCV infection. *Nat. Rev. Gastroenterol. Hepatol. 10*(9):553-562. DOI: 10.1038/nrgastro.2013.107
2. Chung, R. T., Baumert T. F. (2014) Curing chronic hepatitis C--the arc of a medical triumph. *N. Engl. J. Med. 370*(17):1576-1578. DOI: 10.1056/NEJMP1400986
3. Callaway E. (2014) Hepatitis C drugs not reaching poor. *Nature. 508*(7496):295-296. DOI: 10.1038/508295a
4. Midgard, H., Bjøro, B., Maeland, A., *et al*. (2016) Hepatitis C reinfection after sustained virological response. *J. Hepatol. 64*(5):1020-1026. DOI: 10.1016/j.jhep.2016.01.001
5. Kong, L., Jackson, K. N., Wilson, I. A., *et al.* (2015) Capitalizing on knowledge of hepatitis C virus neutralizing epitopes for rational vaccine design. *Curr. Opin. Virol*. *11*:148-157. DOI: 10.1016/j.coviro.2015.04.001
6. Tarr, A. W., Khera, T., Hueging, K., *et al.* (2015) Genetic diversity underlying the envelope glycoproteins of hepatitis C virus: Structural and functional consequences and the implications for vaccine design. *Viruses. 7*(7):3995-4046. DOI: 10.3390/v7072809
7. Helle, F., Goffard, A., Morel, V., *et al.* (2007) The neutralizing activity of anti-hepatitis C virus antibodies is modulated by specific glycans on the E2 envelope glycoprotein. *J. Virol. 81*(15):8101-8111. DOI: 10.1128/jvi.00127-07
8. Sautto, G., Tarr, A. W., Mancini, N., *et al.* (2013) Structural and antigenic definition of hepatitis C virus E2 glycoprotein epitopes targeted by monoclonal antibodies. *Clin. Dev. Immunol. 2013*:450963. DOI: 10.1155/2013/450963
9. Keck, Z. Y., Xia, J., Wang, Y., *et al*. (2012) Human monoclonal antibodies to a novel cluster of conformational epitopes on HCV E2 with resistance to neutralization escape in a genotype 2a Isolate. *PLoS Pathog. 8*(4):e1002653. DOI: 10.1371/journal.ppat.1002653
10. Krey, T., Meola, A., Keck, Z. Y., *et al.* (2013) Structural basis of HCV neutralization by human monoclonal antibodies resistant to viral neutralization escape. *PLOS Pathog. 9*(5):e1003364. DOI: 10.1371/journal.ppat.1003364

11. Ball, J. K., Tarr, A. W., McKeating, J. A. (2014) The past, present and future of neutralizing antibodies for hepatitis C virus. *Antiviral Res. 105*:100–111. DOI: 10.1016/j.antiviral.2014.02.013
12. Kong, L., Giang, E., Nieusma, T., *et al*. (2013) Hepatitis C virus E2 envelope glycoprotein core structure. *Science*. *342*(6162):1090-1094. DOI: 10.1126/science.1243876
13. Kong, L., Lee, D. E., Kadam, R. U., *et al*. (2016) Structural flexibility at a major conserved antibody target on hepatitis c virus E2 antigen. *Proc. Natl. Acad. Sci. USA. 113*(45):12768–12773. DOI: 10.1073/pnas.1609780113
14. Hijnen, M., Van Zoelen, D. J., Chamorro, C., *et al.* (2007) A novel strategy to mimic discontinuous protective epitopes using a synthetic scaffold. *Vaccine. 25*(37-38):6807-6817. DOI: 10.1016/vaccine.2007.06.027
15. Werkhoven, P. R., Van de Langemheen, H., Van der Wal, S., *et al.* (2014) Versatile convergent synthesis of a three peptide loop containing protein mimic of whooping cough pertactin by successive Cu(I)-catalyzed azide alkyne cycloaddition on an orhtogonal alkyne functionalized TAC-scaffold. *J. Pept. Sci. 20*(4):235-239. DOI: 10.1002/psc.2624
16. Werkhoven, P. R., Liskamp, R. M. J. (2013) Chemical approaches for localization, characterization and mimicry of peptide loops. *RSC Drug Discovery Series No. 36. Biotherapeutics: Recent Developments using Chemical and Molecular Biology* (Jones, L. H. and McKnight, A. J., Eds.) pp. 263–284, Chapter 10, The Royal Society of Chemistry, Cambride. DOI: unavailable
17. Mulder, G. E., Quarles van Ufford, H. C. Van Ameijde, J., *et al.* (2013) Scaffold optimization in discontinuous epitope containing protein mimics of gp120 using smart libraries. *Org. Biomol. Chem. 11*(16):2676-2684. DOI: 10.1039/c3ob27470e
18. Werkhoven, P. R., Elwakiel, M., Meuleman, T. J., *et al.* (2016) Molecular construction of HIV-gp120 discontinuous epitope mimics by assembly of cyclic peptides on an orthogonal alkyne functionalized TAC-scaffold. *Org. Biolmol. Chem. 14*,(2):701-710. DOI: 10.1039/c5ob02014j
19. Skwarczynski, M., Toth, I. (2016) Peptide-based synthetic vaccines. *Chem. Sci. 7*(2):842-854. DOI: 10.1039/c5sc03892h
20. Robinson, J. A. (2013) Max Bergmann lecture: Protein epitope mimetics in the age of structural vaccinology. *J. Pept. Sci. 19*(3):127-140. DOI: 10.1002/psc.2482
21. Udugamasooriya, D. G., Spaller, M. R. (2008) Conformational constraints in protein ligand design and the inconsistency of binding entropy. *Biopolymers. 89*(8):653-667. DOI: 10.1002/bip.20983

22. Hill, T. A., Shepherd, N. E., Diness, F., *et al.* (2014) Constraining cyclic peptides to mimic protein structure motifs. *Angew. Chem. Int. Ed. Engl. 53*(48):13020-13041. DOI: 10.1002/anie.201401058
23. Cardote, T. A., Cuilli, A. (2016) Cyclic and macrocyclic peptides as chemical tools to recognize protein surfaces and probe protein-protein interactions. *ChemMedChem. 11*(8):787-794. DOI: 10.1002/cmdc201500450
24. Nevola, L., Giralt, E. (2015) Modulating protein-protein interactions: The potential of peptides. *Chem. Commun. (Camb).* 51(16):3302-3315. DOI: 10.1039/c4cc08565e
25. Fujiwara, D., Kitada, H., Oguri, M., *et al.* (2016) A cyclized helix-loop-helix peptide as a molecular scaffold for the design of inhibitors of intracellular protein-protein interactions by epitope and arginine grafting. *Angew. Chem. Int. Ed. Engl. 55*(36):10612-10615. DOI: 10.1002/anie.201603230
26. Sable, R., Durek, T., Taneja, V., *et al.* (2016) Constrained cyclic peptides as immunomodulatory inhibitors of the CD2:CD58 protein-protein interaction. *ACS Chem. Biol. 11*(8):2366-2374. DOI: 10.1021/acschembio.6b00486
27. Clayton, R. F., Owsianka, A., Aitken, J., *et al.* (2002) Analysis of antigenicity and topology of E2 glycoprotein present on recombinant hepatitis C virus-like particles. *J. Virol. 76*(15), 7672-7682. DOI: 10.1128/jvi.76.15.7672-7692.2002
28. Logan, M., Law, J., Wong, J. A. J, *et al.* (2016) Native folding of a recombinant gpE1/gpE2 heterodimer vaccine antigen from a precursor protein fused with Fc IgG. *J. Virol. 91*(1):e01552-16. DOI: 10.1128/jvi.01552-16
29. Abdelhafez, T. H., Bader El Din, N. G., Tabll, A. A., *et al.* (2017) Mice antibody response to conserved nonadjuvanted multiple antigenic peptides derived from E1/E2 regions of hepatitic C virus. *Viral Immunol. 30*(5)**:**359-365. DOI: 10.1089/vim.2016.0123
30. Vasiliauskaite I, Owsianka A, England P, *et al.* (2017) Conformational flexibility in the immunoglobulin-like domain of the hepatitis C virus glycoprotein E2. *MBio. 8*(3):e00382-17. DOI: 10.1128/mbio.00382-17
31. Tarr, A. W., Owsianka, A. M., Timms, J. M., *et al.* (2006) Characterization of the hepatitis C virus epitope defined by the broadly neutralizing monoclonal antibody AP33. *Hepatology. 43*(3):592-601. DOI: 10.1002/hep21088
32. Pierce, B. G., Keck, Z. Y., Lau, P., *et al.* (2016) Global mapping of antibody recognition of the hepatitis C virus E2 glycoprotein: Implications for vaccine design. *Proc. Natl. Acad. Sci. USA. 113*(45):E6946–E6954. DOI: 10.1073/pnas.1614942113

33. Owsianka, A. M., Timms, J. M., Tarr, A. W., *et al.* (2006) Identification of conserved residues in the E2 envelope glycoprotein of the hepatitis C virus that are critical for CD81 binding. *J. Virol. 80*(17):8695-8704. DOI: 10.1128/jvi.00271-06
34. Nieto, A., Gayá, A., Moreno, C., *et al.* (1985) Adsorption-desorption of antigen to polystyrene plates used in ELISA. *Ann. Inst. Pasteur Immunol. 137C*(2):161-172. DOI: unavailable
35. Gori, A., Sola, L., Gagni, P., *et al.* (2016) Screening complex biological samples with peptide microarrays: The favorable impact of probe orientation via chemoselective immobilization strategies on clickable polymeric coatings. *Bioconjug. Chem. 27*(11):2669-2677. DOI: 10.1021/acs.bioconjchem.6b00426
36. Trzcinska, R., Balin, K., Kubacki, J., *et al.* (2014) Relevance of the poly(ethylene glycol) linkers in peptide surfaces for proteases assays. *Langmuir*. *30*(17):5015-5025. DOI: 10.1021/la500457q
37. Merriflied, R. B. (1963) Solid phase peptide synthesis. I. The synthesis of a tetrapeptide. *J. Am. Chem. Soc. 85*(14):2149-2154. DOI: 10.1021/ja00897a025
38. Merrifield, B. (1986) Solid phase Synthesis. *Science. 232*(4748):341-347. DOI: 10.1126/science.3961484
39. Drummer, H. E., Boo, I., Maerz, A. L., *et al.* (2006) A conserved Gly(436)- Trp-Leu-Ala-Gly-Leu-Phe-Tyr motif in hepatitis C virus glycoprotein E2 is a determinant of CD81 binding and viral entry. *J. Virol. 80*(16):7844-7853. DOI: 10.1128/jvi.00029-06
40. Owsianka, A., Tarr, A. W., Juttla, V. S., *et al.* (2005) Monoclonal antibody AP33 defines a broadly neutralizing epitope on the hepatitis C virus E2 envelope protein. *J. Virol. 79*(17):11095-11104. DOI: 10.1128/jvi.79.17.11095-11104.2005
41. Meola, A., Tarr, A. W., England, P., *et al.* (2015) Structural flexibility of a conserved antigenic region in hepatitis C virus glycoprotein E2 recognized by broadly neutralizing antibodies. *J. Virol. 89*(4):2170-2181. DOI: 10.1128/jvi.02190-14
42. Van de Langemheen, H., Korotkovs, V., Bijl, J., *et al.* (2017) Polar hinges as functionalized conformational constraints in (bi)cyclic peptides. *ChemBioChem. 18*(4):387-395. DOI: 10.1002/cbic.201600612

CHAPTER 3

Improving the aqueous solubility of HCV-E2 glycoprotein epitope mimics by cyclization using polar hinges

Parts of the work presented here will be published in:

Meuleman, T. J., Cowton, V. M., Patel, A. H., Liskamp, R. M. J. (*in press*) Improving the aqueous solubility of HCV-E2 glycoprotein epitope mimics by cyclization using polar hinges. *J. Pep. Sci. X*(X):XXX-XXX

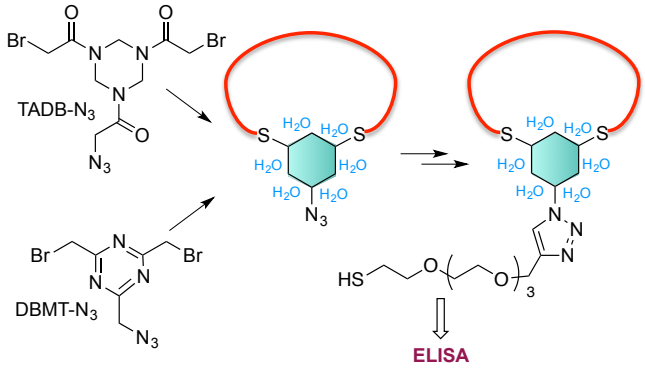

Abstract

In this research we describe the improvement of the water-solubility of cyclic epitope mimics based on the HCV-E2 glycoprotein by incorporation of suitable polar hinges. The poor solubility of epitope mimics based on peptide sequences in the envelope (E2) protein hampered their synthesis and purification, and made it very difficult to prepare the molecular constructs for evaluation of their bioactivity. Since changes in the amino acid composition are hardly possible in these epitope mimics to increase water-solubility, a polar cyclization hinge may offer a remedy leading to a significant increase of polarity and therefore water solubility. These polar hinges were applied in the synthesis of better water-soluble HCV-E2 epitopes. An azide functionality in the polar hinges allowed attachment of a tetraethylene glycol linker by Cu-catalyzed azide-alkyne cyclo-addition (CuAAC) for a convenient conjugation to ELISA plates in order to evaluate the bio-activity of the epitope mimics. Immunoassays indicated that the use of more polar cyclization hinges still supported anti-HCV antibody recognition and did not negatively influence their bioactivity. This significantly increased solubility induced by polar hinges should therefore allow for the molecular construction and ultimate evaluation of synthetic vaccine molecules.

3.1 Introduction

The rapidly increasing therapeutic potential of cyclic peptides is due to multiple favourable molecular attributes.[1] These attributes include the ability to access large and often flat surface areas within protein binding sites, thereby achieving high-selectivity and binding-affinity. Furthermore, peptide cyclization improves its proteolytic stability compared to the linear peptide. Earlier, we have shown that cyclic peptides therefore might be especially attractive in the molecular construction of epitope mimics.[2,3] Moreover, it was recently found that cyclic peptides were better epitope mimics than the linear, non-cyclized compounds.[2,3] As part of our efforts directed towards synthetic vaccines we have been especially interested in HIV-gp120 and the HCV-E2.[2,4] Presently the focus is on HCV, which is a rapidly mutating and highly diverse virus. The natural immune response to this virus often falls short due to various immune evasive strategies and hypervariable immunogenic decoy domains of the virus that do not impede its viral efficiency.[5-8] In essence, the immune system of the host is exhausting itself by targeting ineffective viral epitopes. Despite enormous efforts, no vaccine is available as yet against HCV.[9] An approach to remedy this might be selection of effective and conserved epitopes, which could be mimicked by cyclic peptides and thereby, circumvent problems with immunogenic decoys and inefficient epitopes.[10]

Multiple cyclic peptides were considered based on promising neutralizing epitopes located within the CD81 binding site of the HCV-E2 glycoprotein. This binding site consists of 4 epitope domains (epitopes I, II, III, and IV) to which various antibodies have been generated and isolated that bind these epitopes individually (continuous) or as parts of a larger domain (discontinuous).[11] Their therapeutic potential is based on these antibodies being capable of neutralizing HCV infection by blocking the CD81 binding site of the E2 glycoprotein.[12-14] Epitopes II and IV were found to bind the same class of HC84 antibodies.[11,14] Recently, we have shown that antibody HC84.1 binds our previously developed epitope II mimic without parts of epitope IV.[3] Therefore, in this study we have focused on epitopes I, II, and III.

One of the most attractive cyclization methods, presently available is based on thioether-formation with cysteine-containing peptides. Electrophilic bromide (for example benzylic-bromide) derivatives and Michael acceptors (Figure 3.1), among others, have been applied in the synthesis of many diverse (bi)cyclic peptides also towards synthetic vaccines.[2,3,15-24] However, depending on the sequence, the solubility of cyclized peptides onto a benzylic

core (*i.e.* TBMB) or derivatives thereof can be very poor. Poor water-solubility may hamper purification of cyclized peptides using reverse phase chromatography, resulting in very low yields, thereby also limiting their therapeutic potential. In general, poor water-solubility of peptides is often responsible for a large attrition rate similar to that observed in the small molecule drug discovery process.[25]

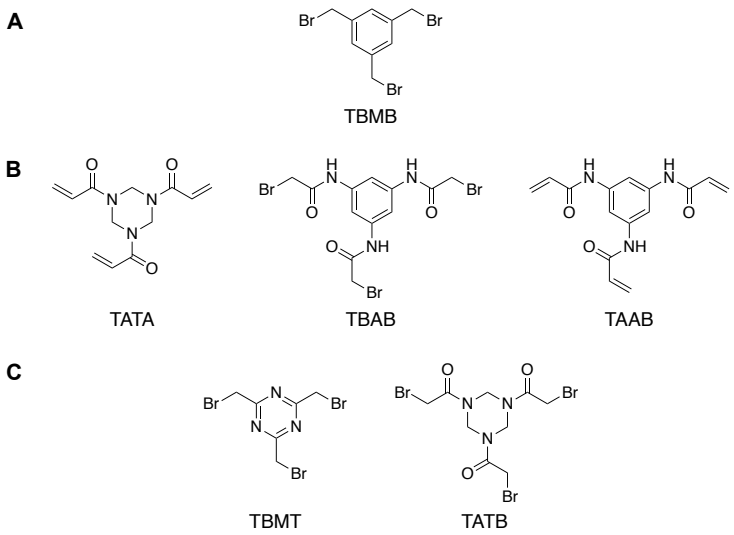

Figure 3.1. Chemical structures of cyclization hinges for preparation of bicyclic peptides 1,3,5-tris(bromomethyl)benzene (TBMB) (**A**); 1,3,5-triacryloyl-1,3,5-triazinane (TATA), *N,N',N''*-(benzene-1,3,5-triyl)-tris(2-bromoacetamide) (TBAB) and *N,N',N''*-benzene-1,3,5-triyltrisprop-2-enamide (TAAB) described by Chen *et al.*[16] and Rim *et al.*[26] (**B**); and 2,4,6-tris(bromomethyl)-s-triazine (TBMT) and 1,1',1''-(1,3,5-triazinane-1,3,5-triyl)tris(2-bromoethanone) (TATB) described by Van de Langemheen *et al.*[27] (**C**).

Several hinges with increasing polarity for cyclization of peptides have been described in the literature to improve the water solubility of resulting molecular constructs.[16-23,26,27] Examples of such polar hinges are shown in Figure 3.1 and include the 2,4,6-1,3,5-triacryloyl-1,3,5-triazinane (TATA), *N,N',N''*-(benzene-1,3,5-triyl)-tris(2-bromoacetamide) (TBAB) and *N,N',N''*-benzene-1,3,5-triyltrisprop-2-enamide (TAAB) tris(bromomethyl)-s-triazine (TBMT) and 1,1',1''-(1,3,5-triazinane-1,3,5-triyl)tris(2-bromoethanone) (TATB) cyclization hinges.[16,26,27] Especially, the latter two, recently developed by Van de Langemheen *et al.* (Figure 3.1C),[27] have shown to be beneficial for the aqueous solubility of cyclic peptides.

Recently, Heinis *et al.* have described a phage display protocol with respect to high-throughput screening of bicyclic peptides, thereby opening up a wide range of potential therapeutics.[19] Interestingly, they found that different hinge structures (*i.e.* TBMT, TATA,

TBAB, and TAAB) incorporated into bicyclic peptides resulted in different conformations of the bicyclized peptide.[16] Moreover, changing the cyclization hinge on a promising isolated sequence from the phage display library could reduce or even completely abolish (binding) activity.[16-18] In addition, depending on the used cyclization hinge, different peptide consensus sequences were isolated from the phage display library.[18] Taken together, this suggested that the core structure of the cyclization hinges does have a significant impact on the overall structure of the cyclized peptide.

The main goal of the work reported here focussed on the improvement of the water-solubility of cyclic epitope mimics based on the HCV-E2 glycoprotein by incorporation of suitable polar hinges. The poor solubility of the peptide sequences corresponding with these epitopes hampered the synthesis and purification of the epitope mimics, and made it very difficult to prepare the molecular construct for evaluation of their bioactivity. Evidently, possibilities to change amino acids in these epitope mimics in order to increase water-solubility are very limited, as their peptide sequences have to resemble the mimicked peptide segments of the epitopes as closely as possible. Recently, we have addressed the issue of poor solubility of peptide loops for attachment to our molecular (TAC) scaffolds by development of polar hinges, which upon incorporation led to a significant increase of polarity and therefore their water solubility. Therefore, we wished to apply these polar hinges in the synthesis of better water-soluble HCV-E2 epitopes. Here, we describe the preparation of cyclized synthetic peptide sequences onto various cyclization (polar) hinges, equipped with a functional azide handle.[27] In addition, an alkyne-functionalized linker equipped with a trityl-protected thiol moiety is described that allowed for conjugation of cyclic peptides with different core structures via by Cu-catalyzed azide-alkyne cyclo-addition (CuAAC). Upon deprotection of the thiol-moiety, the resulting epitope mimics were readily conjugated to a maleimide-activated surface and their bio-activity was evaluated by ELISA (Figure 3.2).

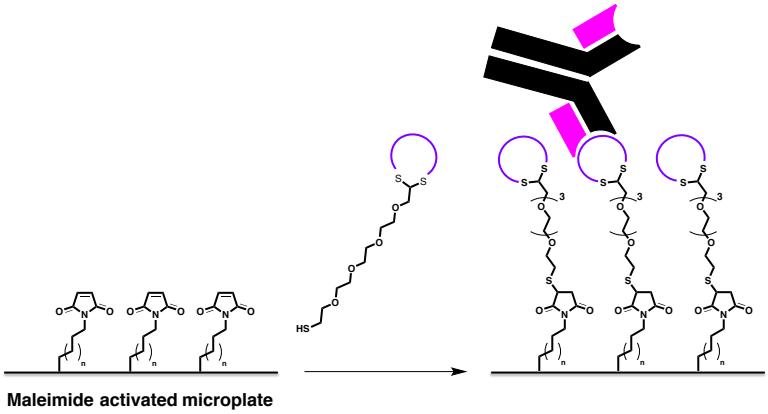

Figure 3.2. Thiol-maleimide conjugation of epitope mimics forming a plate-surface with uniformly oriented peptides used for ELISA to evaluate epitope mimicry.

3.2 Results and discussion

3.2.1 Synthesis of the polar triazine (TBMT) and triazinane (TATB) cyclization hinges and subsequent azide functionalization

Van de Langemheen *et al.*[27] opened up the availability of more polar cyclization hinges for the formation of bicyclic peptides. According to the literature procedure[27], bromoacetonitrile **1** was treated with triflic acid **2** to afford TBMT **3** (5%) (Scheme 3.1A). The obtained yield (5%) was lower compared to the reported yield (22%)[27] in literature. The lower yield could be attributed to the increased formation of 2-bromo-*N*-(2-bromoacetyl)acetamide **4** as a side product. The hydroscopic nature of triflic acid made it difficult to keep the reaction free of water, which promoted formation of 2-bromo-*N*-(2-bromoacetyl)acetamide **4**. TATB **6** was synthesized and kindly provided by Dr. Helmus van de Langemheen and Joachim Bijl, Msc. according to their literature procedure[27], by treating bromoacetonitrile **1** with 1,3,5-trioxane **5** and a catalytic amount of sulfuric acid (Scheme 3.1B)

Scheme 3.1. Synthesis of (**A**) TBMT **3** was synthesized according to the literature procedure[27]; (**B**) TATB **6** was synthesized and kindly provided by Dr. Helmus van de Langemheen and Joachim Bijl, Msc. according to their literature procedure.[27]

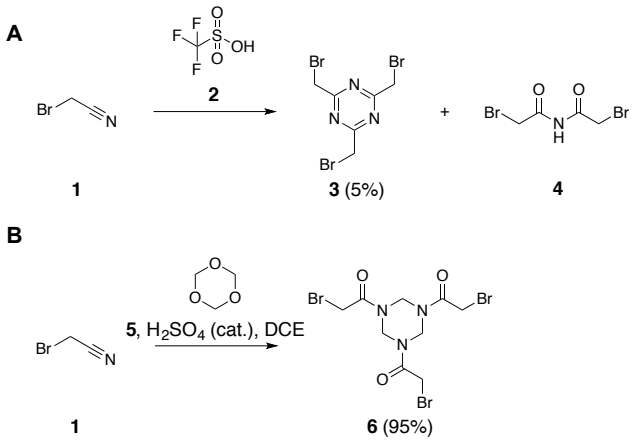

Next, installation of the azide-moiety was achieved by reacting TBMT **3**, TATB **6**, and commercially available TBMB **7** with sodium azide, which afforded a set of three cyclization hinges 1-(azidomethyl)-3,5-bis(bromomethyl)-s-triazine (DBMT-N_3) **8** (Scheme 3.2A), azido triazinane-tris(2-bromoethanone) (TADB-N_3) **9** (Scheme 3.2B), and 1-(azidomethyl)-3,5-bis(bromomethyl)benzene (DBMB-N_3) **10** (Scheme 3.2C),

respectively. Inevitably, di- and tri-substituted side products were formed that resulted in a difficult purification, which accounts for the low to moderate obtained yields.

Scheme 3.2. Synthesis of azide-functionalized cyclization hinges (**A**) DBMT-N_3 **8**; (**B**) TADB-N_3 **9**; (**C**) DBMB-N_3 **10**.

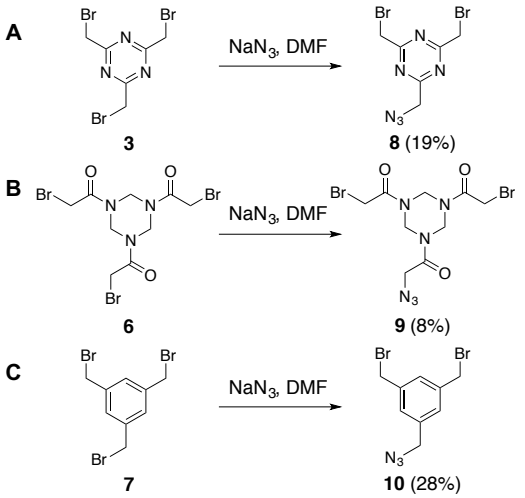

3.2.2 Synthesis of an alkyne-functionalized tetraethylene glycol monotrityl thioether

In order to improve the water-solubility of the recently developed cyclic and linear epitope HCV-E2 mimics equipped with a TEG spacer for binding to a surface using maleimide-thiol conjugation[3], we have incorporated more polar cyclization hinges **8** and **9** in addition to benzyl-derivatives **10** and **11** (see Chapter 2)[3] (Figure 3.3).

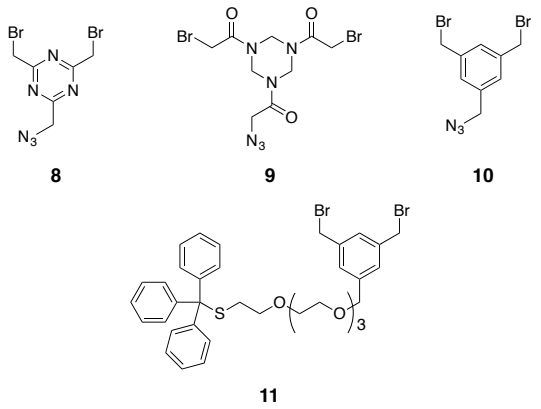

Figure 3.3. 1-(azidomethyl)-3,5-bis(bromomethyl)-s-triazine (DBMT-N_3) **8**, azido triazinane-tris(2-bromoethanone) (TADB-N_3) **9**, 1-(azidomethyl)-3,5-bis(bromomethyl)benzene (DBMB-N_3) **10**, and cyclization linker **11**.[3,27]

Instead of installing the different cyclization hinges on the previously developed TEG spacer directly, as was earlier described for the bis-benzyl bromide linker **11** (see Chapter 2)[3], it was decided to opt for a more modular approach. The peptides were cyclized onto the hinges first, followed by CuAAC to install the S-trityl-TEG linker used for conjugation to a maleimide plate. The required propargyl S-trityl-TEG linker **14** was easily accessible from the earlier synthesized S-trityl-TEG **12** (see Chapter 2)[3] by alkylation with propargyl bromide **13** (Scheme 3.3).

Scheme 3.3. Synthesis of the propargyl moiety containing PEG-based thiol linker for Cu-catalyzed azide-alkyne cyclo-addition of cyclic peptides.

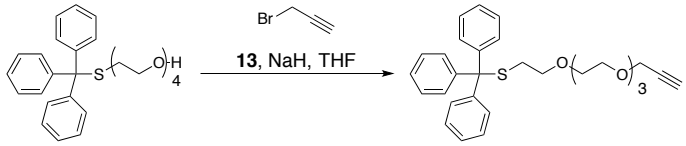

12 **14** (58%)

3.2.3 Synthesis of cysteine containing peptides and subsequent cyclization

The required containing peptides containing two cysteines were obtained by solid phase peptide synthesis (SPPS)[31,32] (Table 3.1). These peptide sequences originated from promising antigenic regions located within the HCV-E2 glycoprotein denoted as epitopes I (I^{411}QLINTNGSWHINR^{424}, **15**), II (G^{436} WVAGLFYYHKFN^{448}, **16**), and III (T^{528}WGENETDVFLLNN^{541}, **17**). Epitope I is a flexible broadly neutralizing immunogenic domain recognized by neutralizing antibody (nAb) AP33 (Table 3.1).[28-30] Epitope II is a broadly neutralizing immunogenic domain recognized by nAb HC84.1 (Table 3.1).[14] Particularly, broadly neutralizing antibodies AP33[28] and HC84.1[14] are of special interest as they have been found to neutralize HCV pseudo-particles (HCVpp) carrying E2 glycoprotein of various genotypes, indicating that these are highly conserved epitopes in an otherwise rapidly mutating virus. Epitope III is an immunogenic domain of interest, as together with epitopes I and II it is located in the CD81 binding site of the viral E2 glycoprotein.[33] A sequence within epitope III is recognized by non-neutralizing antibody DAO5 (Table 3.1)[33], which despite being non-neutralizing could still validate the conformation of the epitope mimics. In addition, a scrambled peptide sequence **18** was synthesized based on the epitope II region as a negative control.

Table 3.1. Overview of synthetic peptide sequences corresponding to epitope **I in green** (**15**), **II in red** (**16**), and **III in blue** (**17**) of HCV-E2 glycoprotein. Including a **scrambled negative control in black** (**18**).

			anti-HCV E2 antibodies
Epitope I	15	H – C I^{411} Q L I N T N G S W H I N R^{424} C – NH_2	AP33 [ref.38]
Epitope II	16	Ac – C G^{436} W V A G L F Y Y H K F N^{448} C – NH_2	HC84.1 [ref.9]
Epitope III	17	Ac – C T^{528} W G E N E T D V F L L N N^{541} C – NH_2	DAO5 [ref.30]
Scrambled	18	Ac – C H F G K Y A F W L G N Y L C – NH_2	None

Cyclization of dicysteine peptides with different hinges DBMT-N_3 **8**, TADB-N_3 **9**, and DBMB-N_3 **10** (Figure 3.3) was carried out as described by Van de Langemheen *et al.* (Scheme 3.4).[27] Precursor peptide and the chosen cyclization hinge were dissolved in DMF, followed by dropwise addition of an aqueous NH_4HCO_3 buffer (20 mM; pH 7.2<7.4) or H_2O.

Generally, an aqueous NH_4HCO_3 buffer (20 mM; pH 7.9) is used for peptide cyclization, however a lower pH was used to improve selectivity towards thioether formation and avoid alkylation of potential free lysine-amines and/or free N-terminal amines. The solubility of peptide **15** was poor when aqueous NH_4HCO_3 buffer was used and resulted in a suspension, which was suggested to increase polymerization of the peptide onto the cyclization hinges. Therefore, cyclization of peptide **15** onto DBMT-N_3 **8** and TADB-N_3 **9** was performed using H_2O to try and avoid a suspension. However, cyclization of peptide **15** on DBMB-N_3 **10** using H_2O did not yield the desired product and required addition of aqueous NH_4HCO_3 (pH 7.2<7.4) instead.

Scheme 3.4. Cyclization of precursor peptides **15-18** with azido cyclization hinges DBMT-N_3 **8**, TADB-N_3 **9**, and DBMB-N_3 **10**. Including: epitopes **I in green** (**15**), **II in red** (**16**), **III in blue** (**17**), and **scrambled in black** (**18**). The reported yields are of purified products, after preparative reverse phase HPLC.

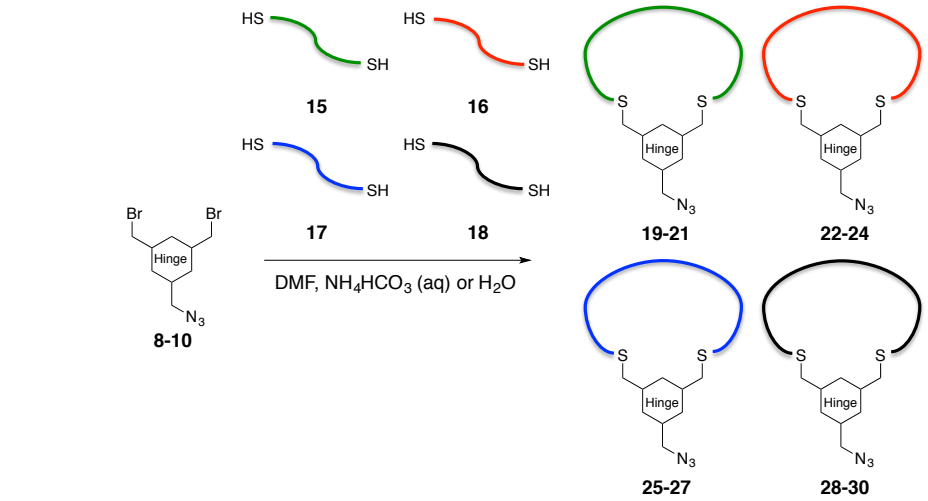

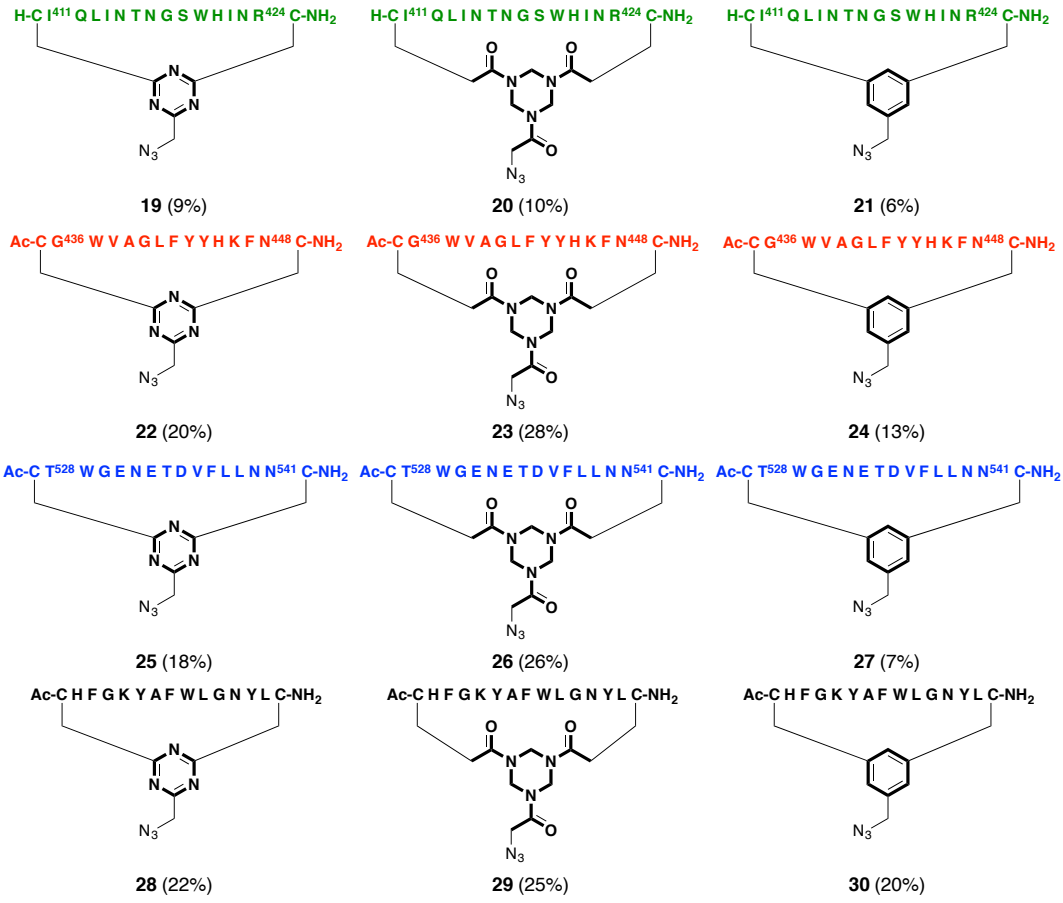

The purification of peptides cyclized on polar hinges DBMT-N_3 **8** and TADB-N_3 **9** hinges was significantly improved, which resulted in higher yields compared to the peptides cyclized with the DBMB-N_3 **10** hinge (Scheme 3.4). Furthermore, HPLC-traces showed shorter retention times for peptides cyclized with the DBMT-N_3 **8** and TADB-N_3 **9** polar hinges, indicating a higher polarity compared to peptides cyclized with benzylic hinge **10** (Figure 3.4). Thus, the water solubility was indeed improved using the polar DBMT-N_3 **8** and TADB-N_3 **9** cyclization hinges. The effect of the latter was the most prominent.

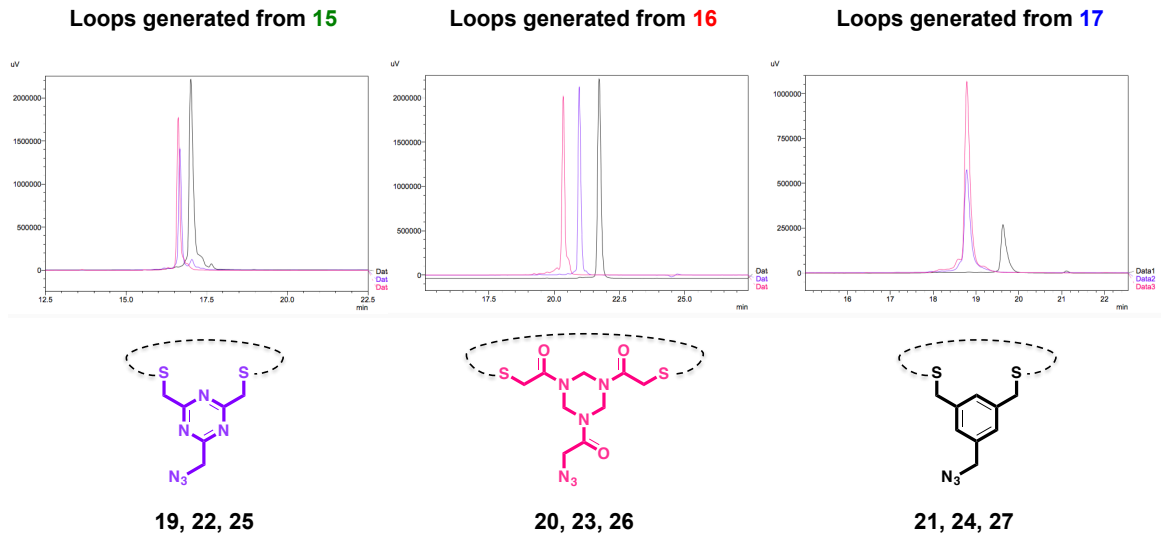

Figure 3.4. Analytical HPLC traces overlay of peptides **15-17** cyclized on DBMT-N_3 (**8**; **purple**), TADB-N_3 (**9**; **pink**), and DBMB-N_3 (**10**; **black**), cyclization hinges. Column: Dr. Maisch Reprosil gold 200 C18, 5 µm 250 x 4.6 mm; Gradient: 0 to 100% buffer B in 30 minutes.

Ideally, a more accurate representation of the improved aqueous solubility could be presented by assessing the concentration of a synthetic peptide from the same batch cyclized on the different DBMT-N_3 **8**, TADB-N_3 **9**, and DBMB-N_3 **10**. This could be demonstrated for cyclic peptides **25**, **26**, and **27** based on peptide **17**. Purification of these compounds resulted in a suspension that was clarified by centrifugation. The afforded pellet was resuspended and lyophilized to assess the amount of crude product that was present in the supernatant and subsequently purified. Crude cyclic peptide **26** based on TADB-N_3 **9** afforded the highest concentration (16 mg/mL) in the supernatant, followed by the concentration (9.3 mg/mL) of crude cyclic peptide **25** based on DBMT-N_3 **8**. As expected, crude cyclic peptide **27** based on DBMB-N_3 **10** resulted in the lowest concentration (5.6 mg/mL) in the supernatant. This provided a clear trend that the aqueous solubility improved in the order of DBMB-N_3 **10**, DBMT-N_3 **8**, and TADB-N_3 **9**,

respectively. Purification of crude cyclic peptides **19-21** was not investigated in this way, since the resulting suspension was too fine and could not be clarified by centrifugation or filtration. In addition, crude cyclic peptides **22-24** and **28-30** were readily soluble in the concentrations used for purification and yielded none to negligible insoluble pellets after centrifugation. Considering the low to modest yields obtained for the purified cyclic peptides, we did not pursue a similar concentration study for the purified products.

It is important to note that the amino-acid sequence does remain the more dominant factor with respect to overall aqueous solubility of the cyclic peptides. In addition, the therapeutic potential of the (cyclic) peptides is highly dependent on their amino-acid composition and does not allow for a lot of changes. For example, peptide **15** exhibits very poor water solubility despite leaving the N-terminus non-acetylated, as well as incorporation of an extra arginine-residue. This extra arginine-residue was only possible because it is present in roughly 50% of the known available sequences of the HCV-E2 glycoprotein and was not part of the epitope sequence.[11]

3.2.4 Assembling the cyclic epitope mimics

CuAAC is a widely used and highly versatile conjugation method of an azide and alkyne moiety.[34] Typically, the reaction can be conducted using moderate quantities of reagents being $CuSO_4 \bullet 5H_2O$ (0.30 equiv.), sodium-L-ascorbate (0.90 equiv.) and TBTA (0.15 equiv.) in a mixture of DMF and H_2O (3:2, *v/v*).[2] However, these conditions were found to be slow and unsuitable for using our newly developed alkyne linker **14**. Possibly, this could be ascribed to an interaction of the thioether moieties with the formed Cu(I)-catalyst. Optimization of the reaction conditions afforded our desired 'clicked' products **31**, **32**, **34**, **35**, **38**, **39**, and **40** within 15 minutes at room temperature using more equivalents of the reagents $CuSO_4 \bullet 5H_2O$ (1.8 equiv.), sodium-L-ascorbate (10 equiv.) and TBTA (0.5 equiv.) still in a mixture of DMF and H_2O (3:2, *v/v*) (Scheme 3.5).

Arginine-dehydroascorbate adduct formation has been reported as a side-reaction for CuAAC in the presence of arginine-residues.[35] Dehydroascorbate is a by-product formed from ascorbate after reduction of Cu(II) to the catalytically active Cu(I)-species. Similar dehydroascorbate adducts were formed here after prolonged reaction times with the DBMT-N_3 **8** polar hinge structure. As was reported, formation of dehydroascorbate adducts could be prevented/decreased by addition of aminoguanidine•HCl (11 equiv.) to the CuAAC reaction mixture.

Scheme 3.5. Cyclic epitope mimics with different hinges DBMT-N_3 (**19**, **22**, **25**, **28**), TADB-N_3 (**20**, **23**, **26**, **29**), and DBMB-N_3 (**21**, **24**, **30**) based on cyclized epitopes **I in green** (**19-21**), **II in red** (**22-24**), **III in blue** (**25-26**), and **scrambled in black** (**28-30**). The red crosses indicate the mimics, which were only obtained in trace amounts. The green tick marks indicate the mimics, which were obtained in satisfactory amounts.

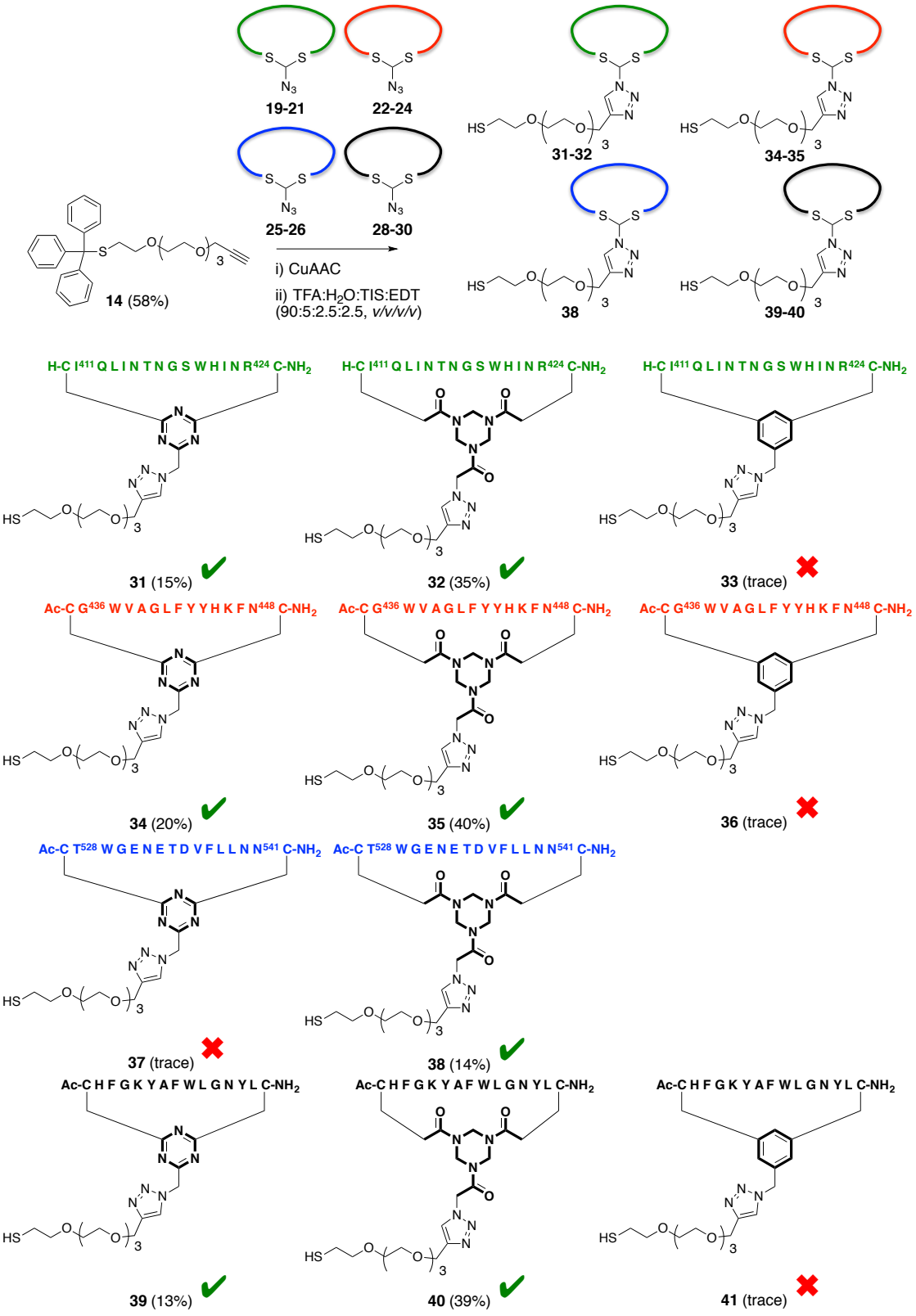

After CuAAC, epitope mimics containing the trityl-group protecting the thiol functionality, had to be purified. However, the presence of this trityl-group decreased the water-solubility of these epitope mimics considerably, resulting in benzylic-hinge based mimics **33**, **36**, and **41** which were obtained only in trace amounts (indicated with red crosses in Scheme 3.5). Furthermore, the water-solubility of peptide **17** was not sufficiently improved by the DBMT-N_3 **8** polar hinge and also only a trace amount of the corresponding epitope mimic **37** was obtained (indicated with a red cross in Scheme 3.5). Because of this, it was expected that cyclic peptide **19** based on the apolar cyclization hinge DBMB-N_3 **3** would not afford its respective epitope mimic and was omitted from this study.

3.2.5 Validating the biological activity of cyclic epitopes based on different cyclization hinges

Recently Kale *et al.* reported on the influence of variation of the incorporated hinge on the structural diversity of macrocyclic peptides during screening.[20] As a consequence we were interested in verifying the use of alternative azide-functionalized cyclization hinges and study their impact on antibody binding. To investigate whether different cyclization hinges support the desired conformation of synthetic peptides based on promising HCV-E2 epitopes for antibody binding we decided to employ our previously described ELISA screen.[3] In order to compare the obtained results we wanted to include epitope mimics **42-45** (Figure 3.5) based on our previously reported cyclization linker **11** (see Chapter 2)[3] (Figure 3.3). Since these previously studied epitope mimics had not been obtained by CuAAC and therefore did not contain a triazole moiety, we had wished to include the corresponding epitope mimics **33** and **36**, and scrambled negative control **41** containing a triazole moiety for comparison of their bio-activity monitored by ELISA. Nevertheless, we did not expect a significant influence of the triazole moiety, because of its distance from the epitope sequence. Unfortunately, any effect of the triazole moiety could not be studied because epitope mimics **33** and **36**, and scrambled negative control **41** were not obtained in sufficient yields (Scheme 3.5). The inability of obtaining these epitopes containing the hydrophobic DBMB-N_3 **10** hinge underlines the importance of having a hinge with improved solubility properties thereby providing better access to the said epitopes.

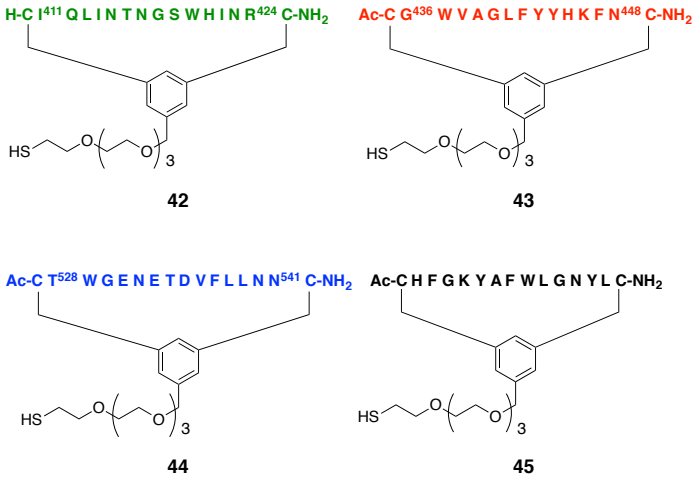

Figure 3.5. Mimics of epitopes **I in green** (**42**), **II in red** (**43**), **III in blue** (**44**), and **scrambled in black** (**45**) as described in Chapter 2.[3]

Epitope mimics **31**, **32**, **34**, **35**, **38**, **42, 43**, and **44**, as well as the scrambled negative controls **39**, **40**, and **45** (Scheme 3.5 and Figure 3.5) were covalently immobilized on Pierce® maleimide activated 96-well plates by maleimide-thiol conjugation. Subsequently, the resulting immobilized epitope mimics and scrambled negative controls were evaluated for antibody binding by ELISA.[3]

The immobilized epitope I mimics **31**, **32**, and **42** were evaluated in the ELISA against nAb AP33 (Figure 3.6). Immobilized epitope mimic **32** compared excellently to epitope mimic **40** towards binding of antibody nAb AP33 (Figure 3.6B). In addition, immobilized epitope mimic **31** showed excellent binding of nab AP33 (Figure 3.6A). However, the immobilized scrambled loop **39**, serving as a negative control, showed some unexpected binding of nAb AP33 that was not observed for immobilized scrambled negative controls **40** and **45** (Figure 3.6). This suggests that the DBMT-N_3 **8** polar hinge causes indirect binding to nAb AP33 and would be unsuitable for developing an epitope I mimic.

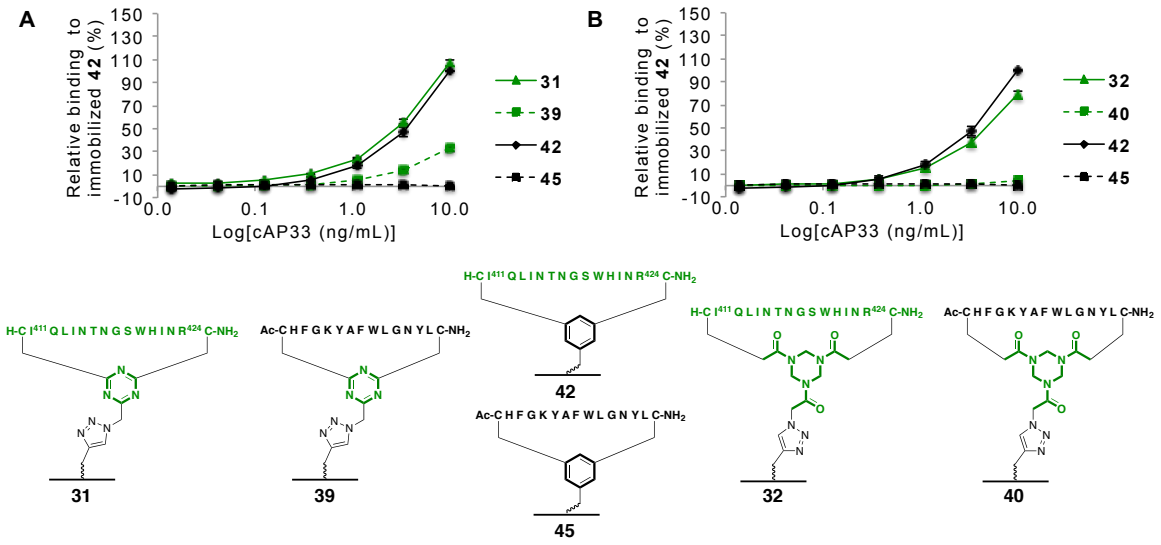

Figure 3.6. ELISA comparing immobilized epitope I mimics having **(A)**: DBMT **31** and **(B)**: TADB **32** hinges and immobilized scrambled negative controls **(A)**: DBMT **39** and **(B)**: TADB **40**. Including immobilized epitope I mimic **42** and immobilized scrambled negative control **45** based on the previously published benzylic-based linker **11**.[3]

Immobilized loop II mimics **34**, **35**, and **43** were evaluated for binding of nAb HC84.1 (Figure 3.7). Both immobilized epitope mimics **34** (Figure 3.7A) and **35** (Figure 3.7B) showed similar if not slightly better binding towards nAb HC84.1 compared to immobilized epitope mimic **43**. None of the immobilized scrambled negative controls **39**, **40**, and **45** showed binding of this antibody (Figure 3.7).

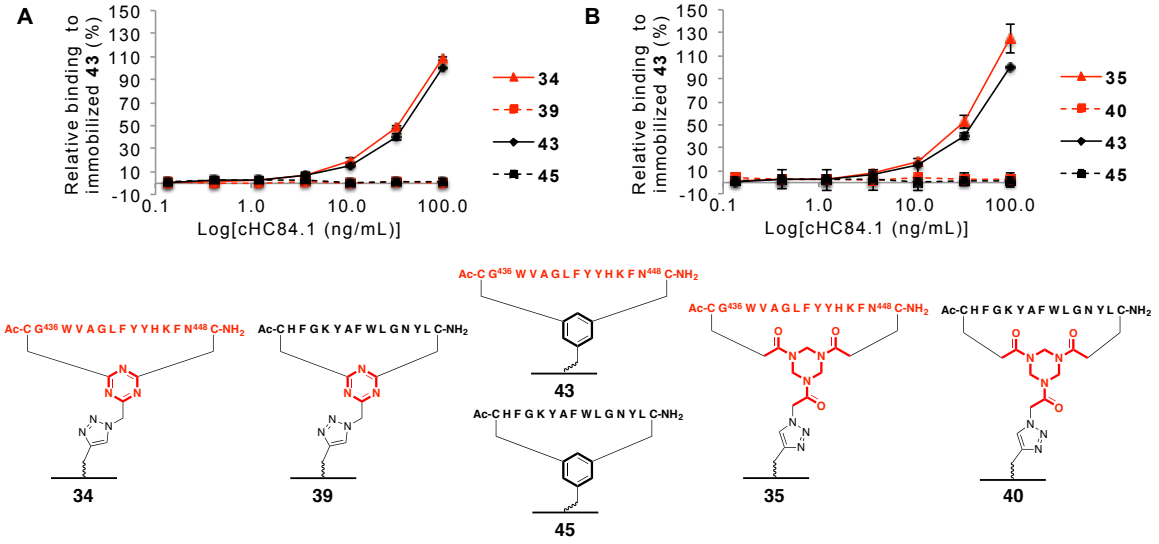

Figure 3.7. ELISA comparing immobilized epitope II mimics having **(A)**: DBMT **34** and **(B)**: TADB **35** hinges and immobilized scrambled negative controls **(A)**: DBMT **39** and **(B)**: TADB **40**. Including immobilized epitope II mimic **43** and immobilized scrambled negative control **45** based on the previously published benzylic-based linker **11**.[3]

Finally, loop III immobilized mimics **38** and **44** were subjected to an ELISA against Ab DAO5 (Figure 3.8). No difference in binding of Ab DAO5 was observed between immobilized epitope mimics **38** and **44**, and no binding of immobilized scrambled negative controls **40** and **45** was observed of this antibody (Figure 3.8).

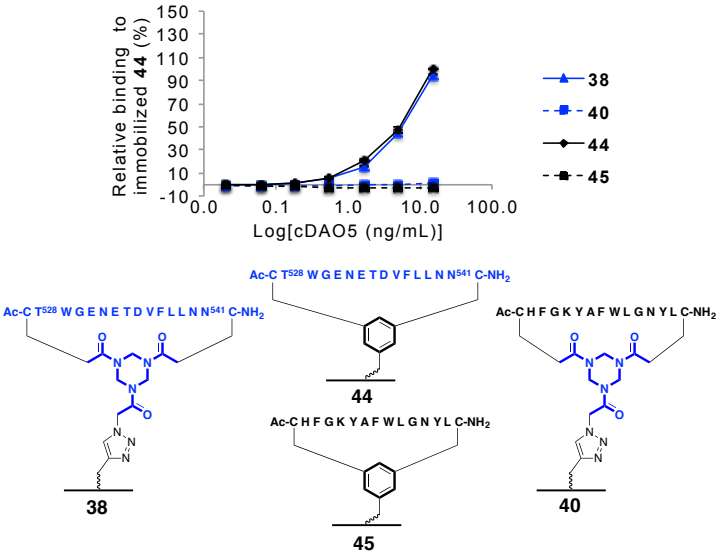

Figure 3.8. ELISA comparing immobilized epitope III mimics having TADB **38** hinge and immobilized scrambled negative controls **40**. Including immobilized epitope III mimic **44** and immobilized scrambled negative control **45** based on the previously published benzylic-based linker **11**.[3]

3.3 Conclusions

In conclusion, utilizing more polar cyclization hinges did improve the water-solubility of cyclic peptides. Higher yields were obtained for peptides cyclized on DBMT-N_3 **8** and TADB-N_3 **9** cyclization hinges compared to both DBMB-N_3 **10** and our previously reported linker **11** (see Chapter 2)[3] without the presence of a triazole ring. As a consequence higher concentrations of compound could be dissolved in the buffer system for purification by preparative HPLC. In addition, analytical HPLC showed shorter retention times for DBMT-N_3 **8** and TADB-N_3 **9**, indicating an increased polarity and likely an improved water-solubility of the resulting cyclic peptides. Heinis *et al.* showed that using different cyclization hinges have a significant influence on the conformation of the resulting (bi)cyclic peptides.[16-20] However, the epitope mimics reported here did not show any difference with respect to antibody binding as indicated by ELISA for the different cyclization hinges used. This does not in anyway indicate that the different cyclization hinges do not induce conformational changes, but in view of the size of rings of the cyclic peptides, this may not be 'detected' by the antibody. It is known that the HCV-E2 glycoprotein is a flexible protein, adopting multiple different conformations, and this may be reflected in the individual peptide epitopes. This dynamic nature of the viral protein may be one of the major hurdles that hinder the development of a therapeutic vaccine against HCV.[29.30.36] Nevertheless, our epitope mimics significantly benefit from the use of more polar cyclization hinges, with respect to water-solubility, facilitating their purification and evaluation without compromising their ability for antibody binding.

3.4 Experimental section

General procedure. All reagents and solvents were used as received. Fmoc-amino acids were obtained from Activotec (Cambridge, United Kingdom) and *N*,*N*,*N*′,*N*′-Tetramethyl-*O*-(6-chloro-1*H*-benzotriazol-1-yl)uranium hexafluorophosphate (HCTU) was obtained from Matrix Innovation (Quebec, Canada). Tentagel S RAM resin (particle size 90μm, capacity 0.25 $mmol.g^{-1}$) was obtained from IRIS Biotech (Marktredwitz, Germany). Methyl *tert*-butyl ether (MTBE), Hexane (HPLC grade) and TFA were obtained from Aldrich (Milwaukee, USA). DMF (Peptide grade) was obtained from VWR (Lutterworth, United Kingdom). Piperidine, D*i*PEA were obtained from AGTC Bioproducts (Hessle, United Kingdom) and 1,2-ethanedithiol (EDT) was obtained from Merck (Darmstadt, Germany). HPLC grade CH_2Cl_2 and acetonitrile were obtained from Fischer Scientific (Loughborough, United Kingdom). Solid phase peptide synthesis was performed on a PTI Tribute-UV peptide synthesizer. Lyophilizations were performed on a Christ Alpha 2-4 LD*plus* apparatus. Reactions were carried out at ambient temperature unless stated otherwise. Solvents were evaporated under reduced pressure at 40 °C. Reactions in solution were monitored by TLC analysis and R_f-values were determined on Merck pre-coated silica gel 60 F-254 (0.25 mm) plates. Spots were visualized by UV-light and permanganate stain. Column chromatography was performed on Siliaflash P60 (40-63μm) from Silicycle (Canada) or on a Biotage Isolera One purification system using prepacked silica (KP-SIL) Biotage SNAP cartridges. ^1H NMR data was acquired on a Bruker 400 MHz spectrometer in $CDCl_3$ as solvent. Chemical shifts (δ) are reported in parts per million (ppm) relative to trimethylsilane (TMS, 0.00 ppm). Analytical high-pressure liquid chromatography (HPLC) was carried out on a Shimadzu instrument comprising a communication module (CBM-20A), autosampler (SIL-20HT), pump modules (LC-20AT), UV/Vis detector (SPD-20A) and system controller (Labsolutions V5.54 SP), with a Phenomenex Gemini C18 column (110 Å, 5 μm, 250×4.60 mm) or Dr. Maisch Reprosil Gold 200 C18 (5 μm, 250×4.60 mm). UV measurements were recorded at 214 and 254 nm, using a standard protocol: 100% buffer A (acetonitrile/H_2O 5:95 with 0.1% TFA) for 2 minutes followed by a linear gradient of buffer B (acetonitrile/H_2O 95:5 with 0.1% TFA) into buffer A (0-100% or 0-50%) over 30 minutes at a flow rate of 1.0 $mL \cdot min^{-1}$. Liquid chromatography mass spectrometry (LCMS) was carried out on a Thermo Scientific LCQ Fleet quadrupole mass spectrometer with a Dionex Ultimate 3000 LC using a Dr. Maisch Reprosil Gold 120 C18 column (110 Å, 3 μm, 150×4.0 mm) and the same linear gradients of buffer B into buffer A, flowrate and buffers as described for the analytical HPLC.

Purification of the peptidic compounds was performed on an Agilent Technologies 1260 infinity preparative system using both UV and ELSD detectors with a Dr. Maisch Reprosil Gold 200 C18 (10 μm, 250×20 mm). Auto-collection of fractions was used based on the UV measurements at 214 nm, using customized protocols using the same buffers as described for the analytical HPLC.

2,4,6-tris(bromomethyl)-s-triazine (3). This synthesis was carried out as described by van de Langemheen *et al.*[27]

Bromoacetonitrile **1** (10 mL, 0.14 mol, 1.0 equiv.) was added to a stirring solution of triflic acid **2** (38 ml, 0.43 mol, 3.0 equiv.) under N_2. The resulting reaction mixture was stirred overnight at room temperature and developed a deep red colour over time. After which, the reaction mixture was added to a vigorously stirring solution of CH_2Cl_2 (500 mL) and saturated sodium bicarbonate (aq.) (500 mL) resulting in formation of a white precipitate. Next, the mixture was filtered and the precipitated washed with water and CH_2Cl_2. The aqueous phase of the filtrate was separated and back-extracted with CH_2Cl_2 (200 mL). After which, the combined organic layers were washed with brine (200 mL), dried over Na_2SO_4 and filtered. The filtrate was concentrated *in vacuo* and purified via automated flash column chromatography using a linear gradient of EtOAc in petroleum ether 40-60 °C (0-20% over 20 column volumes). Affording pure 2,4,6-tris(bromomethyl)-s-triazine **3** (2.7 g, 7.5 mmol, 5%). R_f = 0.72 (EtOAc/Petroleum Ether 40–60 °C 1:1, *v/v*); t_R = 28.9 minutes; ^{1}H-NMR (400 MHz, $CDCl_3$): δ = 4.48 (s, 6H, 3 x CH_2Br); ^{13}C-NMR (101 MHz, $CDCl_3$): δ = 176.2 (3 x *C*$CH_2Br)_3$), 31.2 (3 x *C*H_2Br); HRMS: *m/z* calc. for $C_6H_6N_3{}^{79}Br_3$: 355.8034 $[M–H]^{1–}$; found: 355.8037.

1,1',1''-(1,3,5-triazinane-1,3,5-triyl)tris(2-bromoethanone) (6). Was kindly provided by Joachim Bijl, Msc. and Dr. Helmus van de Langemheen synthesized according to their literature procedure.[27] t_R = 21.6 minutes; ^{1}H-NMR (400 MHz, $CDCl_3$): δ = 5.33 (s, 6H, 3 x NCH_2N), 4.10 (s, 6H, 3 x CH_2CO) ppm; ^{13}C-NMR (101 MHz, $CDCl_3$): δ = 167.2 (*C*O), 57.8 (N*C*H_2N), 25.4 (*C*H_2CO) ppm; HRMS: *m/z* calc. for $C_9H_{12}N_3O_3{}^{79}Br_3$: 469.8327 $[M+Na]^{1+}$; found: 469.8327.

1-(azidomethyl)-3,5-bis(bromomethyl)-s-triazine (8). This synthesis was carried out as described by van de Langemheen *et al.*[27]

2,4,6-tris(bromomethyl)-s-triazine **3** (2.7 g, 7.5 mmol, 1.2 equiv.) was dissolved in DMF (100 ml). To the resulting solution, NaN_3 (0.41 g, 6.2 mmol, 1.0 equiv.) was added. The reaction was stirred for 3 hours at room temperature, followed by removal of solvent *in vacuo*. The residue was taken up in CH_2Cl_2 (50 mL) and the NaBr salt was filtered off, followed by concentrating the filtrate *in vacuo*. Purification by automated flash column chromatography using a linear gradient of EtOAc in petroleum ether 40-60 °C (0-15% over 15 column volumes) afforded 1-(azidomethyl)-3,5-bis(bromomethyl)-s-triazine **8** (0.36 g, 1.2 mmol, 19%) as an orange/red oil. R_f = 0.69 (EtOAc/Petroleum Ether 40–60 °C 1:1, *v/v*); t_R = 28.1 minutes; ^{1}H-NMR (400 MHz, $CDCl_3$): δ = 4.51 (s, 2H, CH_2N$_3$), 4.48 (s, 4H, (2 x CH_2Br); ^{13}C-NMR (101 MHz, $CDCl_3$): δ = 175.9 (*C*CH$_2$N$_3$), 175.9 (2 x *C*CH$_2$Br), 54.2 (*C*H$_2$N$_3$), 31.2 (2 x *C*H$_2$Br); HRMS: *m/z* calc. for $C_6H_6N_6{}^{79}Br_2$: 318.8943 [*M*-H]$^{1-}$; found: 318.8955.

azido triazinane-tris(2-bromoethanone) (9). This synthesis was carried out as described by van de Langemheen *et al.*[27]

1,1',1''-(1,3,5-triazinane-1,3,5-triyl)tris(2-bromoethanone) **6** (6.3 g, 14 mmol, 1.1 equiv.) was dissolved in DMF (200 ml). To the resulting solution, sodium azide (0.75 g, 12 mmol, 1.0 equiv.) was added. The reaction was stirred for 3 hours at room temperature, followed by removal of solvent *in vacuo*. The residue was taken up in CH_2Cl_2 (100 mL) and the NaBr salt was filtered off, followed by concentrating the filtrate *in vacuo*. Purification by automated flash column chromatography using a linear gradient of EtOAc in petroleum ether 40-60 °C (0-40% over 10 column volumes), followed by an isocratic gradient of EtOAc in petroleum ether 40-60 °C (40% over an additional 15 column volumes) afforded azido triazinane-tris(2-bromoethanone) **9** (0.43 g, 1.0 mmol, 8%) as a white solid. R_f = 0.23 (EtOAc/Petroleum Ether 40–60 °C 1:1, *v/v*); t_R = 21.4 minutes; ^{1}H-NMR (400 MHz, $CDCl_3$): δ = 5.35 (s, 2H, NCH_2N), 5.34 (s, 2H, NCH_2N), 5.23 (s, 2H, NCH_2N), 4.20 (s, 2H, CH_2CO) 4.14 (s, 2H, CH_2CO), 4.10 (s, 2H, CH_2CO); ^{13}C-NMR (101 MHz, $CDCl_3$): δ = 167.9 (*C*O), 167.2 (*C*O), 167.1 (*C*O), 57.7 (N*C*H$_2$N), 57.6 (N*C*H$_2$N), 56.4 (N*C*H$_2$N), 50.6 (*C*H$_2$CO), 25.3 (*C*H$_2$CO), 25.2 (*C*H$_2$CO); HRMS: *m/z* calc. for $C_9H_{12}N_6O_3{}^{79}Br_2$: 432.9236 [*M*+Na]$^{1+}$; found: 432.9222.

1-(azidomethyl)-3,5-bis(bromomethyl)benzene (10). This synthesis was carried out as described by van de Langemheen *et al.*[27]

Commercially available 1,3,5-tris(bromomethyl)benzene **7** (2.0 g, 5.6 mmol, 1.2 equiv.) was dissolved in DMF (100 mL), followed by the addition of sodium azide (0.33 g, 4.6 mmol, 1.0 equiv.). The resulting reaction mixture was stirred for 3 hours at room temperature, followed by removal of solvent *in vacuo*. The residue was taken up in CH_2Cl_2 (100 mL) and the NaBr salt was filtered off, followed by concentrating the filtrate *in vacuo*. Crude product was dry-loaded and purified by automated flash column chromatography using a linear gradient of EtOAc in petroleum ether 40-60 °C (0-1.5% over 10 column volumes). Pure 1-(azidomethyl)-3,5-bis(bromomethyl)benzene **10** (0.43 g, 1.3 mmol, 28%) was obtained as a yellow oil. R_f = 0.53 (EtOAc/Petroleum Ether 40–60 °C 1:10, *v/v*); t_R = 37.3 minutes; ^{1}H-NMR (400 MHz, $CDCl_3$): δ = 7.39 (s, 1H, aryl-*H*), 7.28 (s, 2H, aryl-*H*), 4.47 (s, 4H, 2 x C*H*$_2$Br), 4.37 (s, 2H, C*H*$_2$N$_3$); ^{13}C-NMR (101 MHz, $CDCl_3$): δ = 139.1 (aryl-*C*), 137.0 (aryl-*C*), 129.4 (aryl-*C*H), 128.6 (aryl-*C*H), 54.2 (*C*H$_2$N$_3$), 32.4 (2 x *C*H$_2$Br); HRMS: *m/z* calc. for $C_9H_9N_3{}^{79}Br_2$: 315.9085 [*M*-H]$^{1-}$; could not obtained.

Cyclization linker (11). Obtained as described in Chapter 2: Cyclization linker **7**.[3]

Tetraethylene glycol mono-trityl thioether (12). Obtained as described in Chapter 2: Tetraethylene glycol mono-trityl thioether **5**.[3]

Alkyne functionalized tetraethylene glycol monotrityl thioether (14). All steps were performed under N_2 atmosphere. Tetraethylene glycol monotrityl thioether **12** (2.4 g, 5.3 mmol, 1.0 equiv.) was dissolved in dry THF (150 mL). The resulting solution was cooled to 0 °C using an ice bath, followed by addition of 0.32 g NaH (60% dispersion in mineral oil; 7.5 mmol, 1.4 equiv.). The resulting reaction mixture was stirred for 1 hour at 0 °C. After which, 770 µL propargyl bromide **13** (80wt.% in toluene; 6.9 mmol, 1.3 equiv.) was added to the reaction mixture. The ice bath was removed and the reaction mixture was stirred for 1 day at room temperature, after which the reaction had not achieved complete conversion according to TLC (EtOAc). Nevertheless, solvent was removed *in vacuo* and the residue was taken up in CH_2Cl_2 (100 mL). The resulting NaBr precipitate was filtered off over Celite and the filtrate was concentrated *in vacuo*. Purification by automated flash column chromatography using a linear gradient of EtOAc in petroleum ether 40-60 °C (0-50% over 20 column volumes) afforded pure alkyne modified tetraethylene glycol monotrityl thioether **14** (1.5 g, 3.1 mmol, 59%). R_f = 0.86 (100% EtOAc); t_R = 32.7 minutes; ^{1}H-NMR (400 MHz, $CDCl_3$): δ = 7.41 (m, 6H, trityl *o*-*H*), 7.27 (m, 6H, trityl *m*-*H*), 7.21 (m, 3H, *p*-*H*), 4.19 (d, $^3J_{HH}$ = 2.3 Hz, 2H, C*H*$_2$CCH), 3.67 (m, 4H, C*H*$_2$), 3.62 (m,

4H, CH_2), 3.56 (m, 2H, CH_2CH_2O-alkyne), 3.45 (m, 2H, CH_2CH_2O-alkyne), 3.30 (t, $^3J_{HH}$ = 6.9 Hz, 2H, SCH$_2$CH_2), 2.43 (t, $^3J_{HH}$ = 6.9 Hz, 2H, SCH_2), 2.40 (t, $^3J_{HH}$ = 2.3 Hz, 1H, CC*H*); ^{13}C-NMR (101 MHz, $CDCl_3$): δ = 144.8 (trityl-*C*), 129.6 (trityl *o*-*C*), 127.9 (trityl *m*-*C*), 126.6 (trityl *p*-*C*), 79.7 (*C*CH), 74.5 (C*C*H), 70.6 (*C*H$_2$), 70.5 (*C*H$_2$), 70.4 (*C*H$_2$*C*H$_2$O-alkyne), 70.2 (*C*H$_2$*C*H$_2$O-alkyne), 69.6 (SCH$_2$*C*H$_2$), 69.1 (*C*H$_2$), 66.6 (*C*S), 58.4 (*C*H$_2$CCH), 31.7 (S*C*H$_2$) ppm; HRMS: *m/z* calc. for $C_{30}H_{34}O_4S$: 513.2076 [*M*+Na]$^{1+}$; found: 513.2062.

General method for automated peptide synthesis. Peptides were synthesized on a PTI Tribute-UV peptide synthesizer. Tentagel S RAM resin (1.0 g, 0.25 mmol, 1.0 equiv. or 0.43 g, 0.10 mmol, 1.0 equiv.) was allowed to swell in DMF (3 x 10 minutes). De-protection of the Fmoc group was achieved by treatment of the resin with 20% piperidine in DMF using the RV_top_UV_Xtend protocol from the Tribute-UV peptide synthesizer followed by a DMF washing step (5 x 30 seconds). Fmoc-protected amino acids were coupled using HCTU (on the 0.10 mmol scale 5.0 equiv. were used and on the 0.25 mmol scale 4.0 equiv. were used) and D*i*PEA (on the 0.10 mmol scale 10 equiv. were used and on the 0.25 mmol scale 8.0 equiv. were used) in DMF, as a coupling reagent, with 2 minutes pre-activation. The coupling time was 10 minutes when the peptide was synthesized on a 0.10 mmol scale and 20 minutes when the 0.25 mmol scale was conducted. After every coupling the resin was washed with DMF (6 x 30 seconds), followed by a capping step for 10 minutes using capping solution (24 mL acetic anhydride and 11 mL D*i*PEA in 500 mL DMF; using 3 mL for the 0.10 mmol scale and 6 mL for the 0.25 mmol scale). After coupling of the last amino acid, the Fmoc group was deprotected using the standard de-protection conditions (described above) and the resulting free N-terminus was maintained (peptide **15**) or acetylated (peptides **16-18**) by treating the resin bound peptide with capping solution (24 mL acetic anhydride and 11 mL D*i*PEA in 500 mL DMF; using 3 mL for the 0.10 mmol scale and 6 mL for the 0.25 mmol scale) for 10 minutes. After the last step the resin was washed with DMF (5 x 30 seconds) and dried over a nitrogen flow for 10 minutes. Cleavage and de-protection was achieved by treatment of the resin with TFA:H_2O:TIS:EDT (15 mL for the 0.25 mmol scale and 5 mL for the 0.10 mmol scale, 90:5:2.5:2.5, *v*/*v*/*v*/*v*) for 3 hours at room temperature. The peptide was then precipitated in Et_2O (90 mL for the 0.25 mmol scale and 45 mL for the 0.10 mmol scale), centrifuged (4500 rpm; 5 min), the supernatant decanted and the pellet washed 3 times with Et_2O (90 mL for the 0.25 mmol scale and 45 mL for the 0.10 mmol scale). The resulting pellet was re-dissolved in *t*BuOH/H_2O (1:1, *v*/*v*) and lyophilized.

Peptide 15. This peptide was synthesized as described above by solid phase synthesis on a 0.25 mmol scale, which afforded crude peptide (0.38 g). This crude peptide was used in the cyclization by alkylation step. t_R = 16.5 min; LRMS: *m/z* calculated for $C_{79}H_{127}N_{27}O_{22}S_2$: 935.96 ½[*M*+2H]$^{2+}$; found: 936.50.

Peptide 16. This peptide was synthesized as described above by solid phase synthesis on a 0.25 mmol scale, which afforded crude peptide (0.40 g). This crude peptide was used in the cyclization by alkylation step. t_R = 20.8 minutes; LRMS: *m/z* calculated for $C_{89}H_{117}N_{21}O_{19}S_2$: 924.92 ½[*M*+2H]$^{2+}$; found: 925.42 (^{13}C [+1]).

Peptide 17. This peptide was synthesized as described above by solid phase synthesis on a 0.25 mmol scale, which afforded crude peptide (0.35 g). This crude peptide was used in the cyclization by alkylation step. t_R = 18.8 minutes; LRMS: *m/z* calculated for $C_{81}H_{119}N_{21}O_{28}S_2$: 949.91 ½[*M*+2H]$^{2+}$; found: 950.17 (^{13}C [+1]).

Peptide 18. This peptide was synthesized as described above by solid phase synthesis on a 0.25 mmol scale, which afforded crude peptide (0.40 g). This crude peptide was used in the cyclization by alkylation step. t_R = 19.1 minutes; LRMS: *m/z* calculated for $C_{90}H_{119}N_{21}O_{19}S_2$: 931.93 ½[*M*+2H]$^{2+}$; found: 932.33 (^{13}C [+1]).

General method for peptide cyclization. Crude peptide (1.0 equiv.) was dissolved in DMF (30 ml), followed by addition of cyclization hinge (1.1-1.5 equiv.) in DMF (1 mL). Subsequently, an aqueous solution of NH_4HCO_3 (20 mM, pH 7.2<7.4; 10 mL) or H_2O (10 mL) was added dropwise to the reaction mixture. The resulting reaction mixture consisted of a peptide concentration of <1 mM and was stirred for 15 minutes (NH_4HCO_3 (aq)) or 1 hour (H_2O) at room temperature, followed by removal of the solvents *in vacuo* (60 °C). The residue was dissolved in *t*BuOH/H_2O (1:1, *v/v*) aided by sonication. Lyophilization afforded the crude cyclized peptides.

Epitope mimics **42-45**. Removal of the trityl group was performed using TFA:H_2O:TIS:EDT (90:5:2.5:2.5, *v/v/v/v*) (1 ml) for 15 minutes at room temperature, affording the free-thiol moiety. Then, the product was precipitated in Et_2O (15 ml) and collected by centrifugation (4500 rpm; 5 minutes). The collected precipitate was washed twice using Et_2O (15 ml), followed by centrifugation (4500 rpm; 5 minutes). After which, the precipitate was dissolved in *t*BuOH/H_2O (1:1, *v/v*) and lyophylized, which afforded crude epitope mimics.

Crude product was dissolved in HPLC buffer and the resulting solutions were clarified by centrifugation (4500 rpm; 5 min). After which, the compound in the supernatant was purified by preparative HPLC.

Cyclic peptide 19. Peptide **15** (47 mg, 25 μmol, 1.0 equiv.) was treated with 1-(azidomethyl)-3,5-bis(bromomethyl)-s-triazine **8** (12 mg, 38 μmol, 1.5 equiv.) in DMF/H_2O as described above. The obtained crude product (55 mg) was dissolved in 6 mL buffer A and purified as two batches of 3 mL: 100% buffer A for 5 min followed by a linear gradient of buffer B into buffer A (0-40%) over 40 min at a flow rate of 12.5 mL·min^{-1}. Affording cyclic peptide **19** (5.3 mg, 2.6 μmol, 9% overall yield). t_R = 16.7 minutes; HRMS: calculated *m/z* for $C_{85}H_{131}N_{33}O_{22}S_2$: 1015.9872 ½[*M*+2H]$^{2+}$; found 1015.9878; LRMS: calculated *m/z* for $C_{85}H_{131}N_{33}O_{22}S_2$: 1015.99 ½[*M*+2H]$^{2+}$; found 1016.58.

Cyclic peptide 20. Peptide **15** (47 mg, 25 μmol, 1.0 equiv.) was treated with azido triazinane-tris(2-bromoethanone) **9** (16 mg, 38 μmol, 1.5 equiv.) in DMF/H_2O as described above. The obtained crude product (67 mg) was dissolved in 6 mL buffer A and purified as two batches of 3 mL: 100% buffer A for 5 min followed by a linear gradient of buffer B into buffer A (0-40%) over 40 min at a flow rate of 12.5 mL·min^{-1}. Affording cyclic peptide **20** (6.3 mg, 3.0 μmol, 10% overall yield). t_R = 16.6 minutes; HRMS: calculated *m/z* for $C_{88}H_{137}N_{33}O_{25}S_2$: 1061.0031 ½[*M*+2H]$^{2+}$; found 1061.0027; LRMS: calculated *m/z* for $C_{88}H_{137}N_{33}O_{25}S_2$: 1061.00 ½[*M*2+H]$^{2+}$; found 1061.50.

Cyclic peptide 21. Peptide **15** (47 mg, 25 μmol, 1.0 equiv.) was treated with azido di(bromomethyl)benzene **10** (12 mg, 37 μmol, 1.5 equiv.) in DMF/NH_4HCO_3 (pH 7.2<7.4) as described above. The obtained crude product (61 mg) was dissolved in 6 mL buffer A and purified as two batches of 3 mL: 100% buffer A for 5 min followed by a linear gradient of buffer B into buffer A (0-40%) over 40 min at a flow rate of 12.5 mL·min^{-1}. Affording cyclic peptide **21** (3.7 mg, 1.8 μmol, 6% overall yield). t_R = 17.0 minutes; HRMS: calculated *m/z* for $C_{88}H_{134}N_{30}O_{22}S_2$: 1014.4943 ½[*M*+2H]$^{2+}$; found 1014.4966; LRMS: calculated *m/z* for $C_{88}H_{134}N_{30}O_{22}S_2$: 1014.49 ½[*M*+2H]$^{2+}$; found 1015.08.

Cyclic peptide 22. Peptide **16** (47 mg, 25 μmol, 1.0 equiv.) was treated with 1-(azidomethyl)-3,5-bis(bromomethyl)-s-triazine **8** (9.9 mg, 31 μmol, 1.2 equiv.) in DMF/NH_4HCO_3 (pH 7.2<7.4) as described above. The obtained crude product (59 mg) was dissolved as batches of 10-15 mg in 1 mL buffer A:B (1:1, *v/v*) and purified: 100%

buffer A for 5 min followed by a linear gradient of buffer B into buffer A (30-70%) over 40 min at a flow rate of 12.5 mL·min^{-1}. Affording cyclic peptide **22** (12 mg, 5.8 μmol, 20% overall yield). t_R = 21.0 minutes; HRMS: calculated *m/z* for $C_{95}H_{121}N_{27}O_{19}S_2$: 1004.9465 ½[*M*+2H]$^{2+}$; found 1004.9470; LRMS: calculated *m/z* for $C_{95}H_{121}N_{27}O_{19}S_2$: 1004.95 ½[*M*+2H]$^{2+}$; found 1005.50.

Cyclic peptide 23. Peptide **16** (47 mg, 25 μmol, 1.0 equiv.) was treated with azido triazinane-tris(2-bromoethanone) **9** (11 mg, 28 μmol, 1.1 equiv.) in DMF/NH_4HCO_3 (pH 7.2<7.4) as described above. The obtained crude product (63 mg) was dissolved in 3 mL buffer A:B (1:1, *v/v*) and purified: 20% buffer B in buffer A for 5 min followed by a linear gradient of buffer B into buffer A (20-60%) over 40 min at a flow rate of 12.5 mL·min^{-1}. Affording cyclic peptide **23** (17 mg, 2.0 μmol, 28% overall yield). t_R = 20.3 minutes; HRMS: calculated *m/z* for $C_{98}H_{127}N_{27}O_{22}S_2$: 1049.9623 ½[*M*+2H]$^{2+}$; found 1049.9598; LRMS: calculated *m/z* for $C_{98}H_{127}N_{27}O_{22}S_2$: 1049.96 ½[*M*+2H]$^{2+}$; found 1050.58.

Cyclic peptide 24. Peptide **16** (46 mg, 25 μmol, 1.0 equiv.) was treated with azido di(bromomethyl)benzene **10** (9.0 mg, 28 μmol, 1.1 equiv.) in DMF/NH_4HCO_3 (pH 7.2<7.4) as described above. The obtained crude product (58 mg) was dissolved as batches of 10-15 mg in 1 mL buffer A:B (1:1, *v/v*) and purified: 30% buffer B in buffer A for 5 min followed by a linear gradient of buffer B into buffer A (30-70%) over 80 min at a flow rate of 12.5 mL·min^{-1}. Affording cyclic peptide **24** (7.7 mg, 3.8 μmol, 13% overall yield). t_R = 21.7 minutes; HRMS: calculated *m/z* for $C_{98}H_{124}N_{24}O_{19}S_2$: 1003.4536 ½[*M*+2H]$^{2+}$; found 1003.4567; LRMS: calculated *m/z* for $C_{98}H_{124}N_{24}O_{19}S_2$: 1003.45 ½[*M*+2H]$^{2+}$; found 1004.08.

Cyclic peptide 25. Peptide **17** (48 mg, 25 μmol, 1.0 equiv.) was treated with 1-(azidomethyl)-3,5-bis(bromomethyl)-s-triazine **8** (11 mg, 33 μmol, 1.3 equiv.) in DMF/NH_4HCO_3 (pH 7.2<7.4) as described above. The obtained crude product (58 mg) was suspended in 3 mL buffer A:B (1:1, *v/v*) and centrifuged (4500 rpm; 5 minutes), which resulted in a pellet of un-dissolved crude (30 mg; after lyophilization). The supernatant was purified: 20% buffer B in buffer A for 5 min followed by a linear gradient of buffer B into buffer A (20-60%) over 40 min at a flow rate of 12.5 mL·min^{-1}. Affording cyclic peptide **25** (6.3 mg, 3.1 μmol, 18% overall yield). t_R = 18.8 minutes; HRMS: calculated *m/z* for $C_{87}H_{123}N_{27}O_{28}S_2$: 1029.9314 ½[*M*+2H]$^{2+}$; found 1029.9345; LRMS: calculated *m/z* for $C_{87}H_{123}N_{27}O_{28}S_2$: 1029.93 ½[*M*+2H]$^{2+}$; found 1030.25.

Cyclic peptide 26. Peptide **17** (48 mg, 25 μmol, 1.0 equiv.) was treated with azido triazinane-tris(2-bromoethanone) **9** (11 mg, 28 μmol, 1.1 equiv.) in DMF/NH_4HCO_3 (pH 7.2<7.4) as described above. The obtained crude product (65 mg) was suspended in 3 mL buffer A:B (1:1, *v/v*) and centrifuged (4500 rpm; 5 minutes), which resulted in a pellet of un-dissolved crude (17 mg; after lyophilization). The supernatant was purified: 20% buffer B in buffer A for 5 min followed by a linear gradient of buffer B into buffer A (20-60%) over 40 min at a flow rate of 12.5 mL·min^{-1}. Affording cyclic peptide **26** (14 mg, 6.6 μmol, 26% overall yield). t_R = 18.8 minutes; HRMS: calculated *m/z* for $C_{90}H_{129}N_{27}O_{31}S_2$: 1074.9473 ½[*M*+2H]$^{2+}$; found 1074.9444; LRMS: calculated *m/z* for $C_{90}H_{129}N_{27}O_{31}S_2$: 1074.95 ½[*M*+2H]$^{2+}$; found 1075.42.

Cyclic peptide 27. Peptide **17** (48 mg, 25 μmol, 1.0 equiv.) was treated with azido di(bromomethyl)benzene **10** (8.9 mg, 28 μmol, 1.1 equiv.) in DMF/NH_4HCO_3 (pH 7.2<7.4) as described above. The obtained crude product (56 mg) was suspended in 3 mL buffer A:B (1:1, *v/v*) and centrifuged (4500 rpm; 5 minutes), which resulted in a pellet of un-dissolved crude (40 mg; after lyophilization). The supernatant was purified: 20% buffer B in buffer A for 5 min followed by a linear gradient of buffer B into buffer A (20-60%) over 40 min at a flow rate of 12.5 mL·min^{-1}. Affording cyclic peptide **27** (1.4 mg, 0.68 μmol, 7% overall yield). t_R = 19.6 minutes; HRMS: calculated *m/z* for $C_{90}H_{126}N_{24}O_{28}S_2$: 1028.4386 ½[*M*+2H]$^{2+}$; found 1028.4374; LRMS: calculated *m/z* for $C_{90}H_{126}N_{24}O_{28}S_2$: 1028.44 ½[*M*+2H]$^{2+}$; found 1028.92.

Cyclic peptide 28. Peptide **18** (47 mg, 25 μmol, 1.0 equiv.) was treated with 1-(azidomethyl)-3,5-bis(bromomethyl)-s-triazine **8** (8.9 mg, 28 μmol, 1.1 equiv.) in DMF/NH_4HCO_3 (pH 7.2<7.4) as described above. The obtained crude product (60 mg) was dissolved in 3 mL buffer A:B (1:1, *v/v*) and purified: 20% buffer B in buffer A for 5 min followed by a linear gradient of buffer B into buffer A (20-60%) over 40 min at a flow rate of 12.5 mL·min^{-1}. Affording cyclic peptide **28** (13 mg, 6.3 μmol, 22% overall yield). t_R = 20.9 minutes; HRMS: calculated *m/z* for $C_{96}H_{123}N_{27}O_{19}S_2$: 1011.9543 ½[*M*+2H]$^{2+}$; found 1011.9544; LRMS: calculated *m/z* for $C_{96}H_{123}N_{27}O_{19}S_2$: 1011.95 ½[*M*+2H]$^{2+}$; found 1012.58.

Cyclic peptide 29. Peptide **18** (46 mg, 25 μmol, 1.0 equiv.) was treated with azido triazinane-tris(2-bromoethanone) **9** (12 mg, 28 μmol, 1.1 equiv.) in DMF/NH_4HCO_3 (pH 7.2<7.4) as described above. The obtained crude product (61 mg) was dissolved in 3 mL buffer A:B (1:1, *v/v*) and purified: 20% buffer B in buffer A for 5 min followed by a linear

gradient of buffer B into buffer A (20-60%) over 40 min at a flow rate of 12.5 mL·min^{-1}. Affording cyclic peptide **29** (15 mg, 7.1 μmol, 25% overall yield). t_R = 20.5 minutes; HRMS: calculated *m/z* for $C_{99}H_{129}N_{27}O_{22}S_2$: 1056.9702 ½[*M*+2H]$^{2+}$; found 1056.9688; LRMS: calculated *m/z* for $C_{99}H_{129}N_{27}O_{22}S_2$: 1056.97 ½[*M*+2H]$^{2+}$; found 1057.58.

Cyclic peptide 30. Peptide **18** (47 mg, 25 μmol, 1.0 equiv.) was treated with azido di(bromomethyl)benzene **10** (8.8 mg, 28 μmol, 1.1 equiv.) in DMF/NH_4HCO_3 (pH 7.2<7.4) as described above. The obtained crude product (59 mg) was dissolved in 3 mL buffer A:B (1:1, *v/v*) and purified: 20% buffer B in buffer A for 5 min followed by a linear gradient of buffer B into buffer A (20-60%) over 40 min at a flow rate of 12.5 mL·min^{-1}. Affording cyclic peptide **30** (12 mg, 5.8 μmol, 20% overall yield). t_R = 21.8 minutes; HRMS: calculated *m/z* for $C_{99}H_{126}N_{24}O_{19}S_2$: 1010.4614 ½[*M*+2H]$^{2+}$; found 1010.4581; LRMS: calculated *m/z* for $C_{99}H_{126}N_{24}O_{19}S_2$: 1010.46 ½[*M*+2H]$^{2+}$; found 1011.08.

General method for CuAAC of cyclized peptides to propargyl linker 14. Hinge cyclized peptide (1.0 equiv.), linker **14** (1.1 equiv.), and TBTA (0.45 equiv.) were dissolved separately in DMF (100 μl). The separate reagents were then combined. After which, $CuSO_4$•$5H_2O$ (1.8 equiv.) was dissolved in H_2O (100 μL), and sodium L-ascorbate (10 equiv.) and aminoguanidine•HCl (11 equiv., addition of this was omitted in the preparation of epitope mimics **34-36**, as no arginine residues are present in their peptide sequence) were each dissolved separately in H_2O (50 μL). A premix was prepared by adding the sodium L-ascorbate (50 μl) solution to the $CuSO_4$•$5H_2O$ (100 μL) solution, followed by immediate addition of the aminoguanidine•HCl (50 μL) solution. Then, the premix (200 μL) was added to the reaction mixture, which was stirred for 15 minutes at room temperature under constant N_2 flow. Analysis by analytical HPLC indicated completion of the reaction after 15 minutes, followed by addition of HPLC buffers A:B (1:1, *v/v*) (500 μL). The solution was centrifuged (12,000 rpm; 5 minutes) and the compound in the supernatant was purified by preparative HPLC: 50% buffer A for 5 min followed by a linear gradient of buffer B into buffer A (50-100%) over 10 min at a flow rate of 12.5 mL·min^{-1} using the same buffers as described for the analytical HPLC. Fractions containing pure product were identified by analytical HPLC and were pooled and lyophilized, affording pure trityl-protected product as a fluffy white powder. Removal of the trityl group was performed using TFA:H_2O:TIS:EDT (90:5:2.5:2.5, *v/v/v/v*) (1 ml) for 15 minutes at room temperature, affording the free-thiol moiety. Then, the product was precipitated in Et_2O (15 ml) and collected by centrifugation (4500 rpm; 5 minutes). The collected precipitate was washed twice using Et_2O (15 ml), followed by centrifugation

(4500 rpm; 5 minutes). After which, the precipitate was dissolved in *t*BuOH/H_2O (1:1, *v/v*) and lyophylized, affording the pure product.

Epitope mimic 31. Cyclic peptide **19** (5.3 mg, 2.6 μmol) and linker **14** (5.0 mg, 10 μmol; dissolved in 355 μl DMF of which 100 μl was used) was subjected to the above described CuAAC with $CuSO_4$•$5H_2O$ (1.9 mg, 7.6 μmol; dissolved in 162 μl H_2O of which 100 μl was used), L-ascorbate (16 mg, 81 μmol; dissolved in 162 μl H_2O of which 50 μl was used), TBTA (1.1 mg, 2.1 μmol; dissolved in 179 μl DMF of which 100 μl was used), aminoguanidine•HCl (5.5 mg, 50 μmol; dissolved in 87 μl of which 50 μl was used). Purification and subsequent deprotection, afforded epitope mimic **31** (0.90 mg, 0.39 μmol, 15%). t_R = 17.4 minutes; HRMS: calculated *m/z* for $C_{96}H_{151}N_{33}O_{26}S_3$: 760.3635 1/3[*M*+3H]$^{3+}$; found 760.3664; LRMS: calculated *m/z* for $C_{96}H_{151}N_{33}O_{26}S_3$: 1140.04 ½[*M*+2H]$^{2+}$ / 760.36 1/3[*M*+3H]$^{3+}$; found 1140.50 / 760.67 (^{13}C [+1]).

Epitope mimic 32. Cyclic peptide **20** (3.7 mg, 1.7 μmol) and linker **14** (4.1 mg, 8.4 μmol; dissolved in 440 μl DMF of which 100 μl was used) was subjected to the above described CuAAC with $CuSO_4$•$5H_2O$ (4.7 mg, 19 μmol; dissolved in 605 μl H_2O of which 100 μl was used), sodium L-ascorbate (13 mg, 64 μmol; dissolved in 188 μl H_2O of which 50 μl was used), TBTA (1.7 mg, 3.2 μmol; dissolved in 400 μl DMF of which 100 μl was used), aminoguanidine•HCl (6.5 mg, 59 μmol; dissolved in 157 μl of which 50 μl was used). Purification and subsequent deprotection, afforded epitope mimic **32** (1.3 mg, 0.55 μmol, 35%). t_R = 17.3 minutes; HRMS: calculated *m/z* for $C_{99}H_{157}N_{33}O_{29}S_3$: 790.3740 1/3[*M*+3H]$^{3+}$; found 790.3769; LRMS: calculated *m/z* for $C_{99}H_{157}N_{33}O_{29}S_3$: 1185.06 ½[*M*+2H]$^{2+}$ / 790.37 1/3[*M*+3H]$^{3+}$; found 1185.50 / 790.67 (^{13}C [+1]).

Epitope mimic 33. Cyclic peptide **21** (3.7 mg, 1.8 μmol) and linker **14** (4.6 mg, 9.4 μmol; dissolved in 475 μl DMF of which 100 μl was used) was subjected to the above described CuAAC with $CuSO_4$•$5H_2O$ (3.3 mg, 13 μmol; dissolved in 405 μl H_2O of which 100 μl was used), sodium L-ascorbate (9.9 mg, 50 μmol; dissolved in 139 μl H_2O of which 50 μl was used), TBTA (0.90 mg, 1.7 μmol; dissolved in 210 μl DMF of which 100 μl was used), and aminoguanidine•HCl (6.8 mg, 62 μmol; dissolved in 155 μl of which 50 μl was used). Purification and subsequent deprotection, afforded only a trace of epitope mimic **25**. t_R = 17.5 minutes; HRMS: calculated *m/z* for $C_{99}H_{154}N_{30}O_{26}S_3$: 759.3682 1/3[*M*+3H]$^{3+}$; found 759.3712; LRMS: calculated *m/z* for $C_{99}H_{154}N_{30}O_{26}S_3$: 1138.55 ½[*M*+2H]$^{2+}$ / 759.37 1/3[*M*+3H]$^{3+}$; found 1139.08 / 759.67 (^{13}C [+1]).

Epitope mimic 34. Cyclic peptide **22** (2.0 mg, 1.0 μmol) was dissolved in 200 μl of a linker **14** (11 mg, 22 μmol; dissolved in 4.0 ml DMF) solution. Next, 100 μl of a TBTA (0.30 mg, 0.56 μmol; dissolved in 125 μl DMF) solution was added. Then, 100 μl of a $CuSO_4 \bullet 5H_2O$ (1.6 mg, 6.4 μmol; dissolved in 355 μl H_2O) solution and 100 μl of a sodium L-ascorbate (3.2 mg, 16 μmol; dissolved in 160 μl H_2O) solution were premixed, of which 200 μl was added to the reaction mixture. After 15 minutes, the reaction was complete as gauged by analytical HPLC. Purification and subsequent deprotection, afforded epitope mimic **34** (0.40 mg, 0.18 μmol, 20%). t_R = 21.2 minutes; HRMS: calculated *m/z* for $C_{106}H_{141}N_{27}O_{23}S_3$: 1129.0006 ½[*M*+2H]$^{2+}$; found 1129.0049; LRMS: calculated *m/z* for $C_{106}H_{141}N_{27}O_{23}S_3$: 1129.00 ½[*M*+2H]$^{2+}$ / 753.00 1/3[M+3H]$^{3+}$; found 1129.33 / 753.17 (^{13}C [+1]).

Epitope mimic 35. Cyclic peptide **23** (2.0 mg, 1.0 μmol) was dissolved in 200 μl DMF, followed by addition of 200 μl of a linker **14** (5.2 mg, 10.5 μmol; dissolved in 2.1 ml DMF) solution. Next, 200 μl of a TBTA (0.30 mg, 0.57 μmol; dissolved in 200 μl DMF) solution was added. Then, 400 μl of a $CuSO_4 \bullet 5H_2O$ (2.9 mg, 12 μmol; dissolved in 1.3 ml H_2O) solution and 400 μl of a sodium L-ascorbate (6.8 mg, 34 μmol; dissolved in 690 μl H_2O) solution were premixed, of which 400 μl was added to the reaction mixture. After 15 minutes, the reaction was complete as gauged by analytical HPLC. Purification and subsequent deprotection, afforded epitope mimic **35** (0.90 mg, 0.38 μmol, 40%). t_R = 20.9 minutes; HRMS: calculated *m/z* for $C_{109}H_{147}N_{27}O_{26}S_3$: 1174.0165 ½[*M*+2H]$^{2+}$; found 1174.0163; LRMS: calculated *m/z* for $C_{109}H_{147}N_{27}O_{26}S_3$: 11174.02 ½[*M*+2H]$^{2+}$ / 783.01 1/3[M+3H]$^{3+}$; found 1174.42 / 783.03 (^{13}C [+1]).

Epitope mimic 36. Cyclic peptide **24** (2.0 mg, 1.0 μmol) was dissolved in 200 μl of a linker **14** (11 mg, 22 μmol; dissolved in 4.0 ml DMF) solution. Next, 100 μl of a TBTA (0.90 mg, 1.7 μmol; dissolved in 375 μl DMF) solution was added. Then, 400 μl of a $CuSO_4 \bullet 5H_2O$ (4.0 mg, 16 μmol; dissolved in 890 μl H_2O) solution and 400 μl of a sodium L-ascorbate (12 mg, 59 μmol; dissolved in 590 μl H_2O) solution were premixed, of which 200 μl was added to the reaction mixture. After 15 minutes, the reaction was complete by analytical HPLC. Purification and subsequent deprotection, afforded only a trace of epitope mimic **36**. t_R = 21.5 minutes; HRMS: calculated *m/z* for $C_{109}H_{144}N_{24}O_{23}S_3$: 1127.5077 ½[*M*+2H]$^{2+}$; found 1127.5071; LRMS: calculated *m/z* for $C_{109}H_{144}N_{24}O_{23}S_3$: 1127.51 ½[*M*+2H]$^{2+}$ / 752.01 1/3[M+3H]$^{3+}$; found 1127.92 / 751.92 (^{13}C [+1]).

Epitope mimic 37. Pure cyclic peptide **25** (3.3 mg, 1.6 µmol) and linker **14** (3.1 mg, 6.3 µmol; dissolved in 262 µl DMF of which 100 µl was used) was subjected to the above described CuAAC with $CuSO_4$•$5H_2O$ (2.3 mg, 9.2 µmol; dissolved in 320 µl H_2O of which 100 µl was used), L-ascorbate (12 mg, 59 µmol; dissolved in 185 µl H_2O of which 50 µl was used), TBTA (1.7 mg, 3.2 µmol; dissolved in 440 µl DMF of which 100 µl was used), aminoguanidine•HCl (9.0 mg, 81 µmol; dissolved in 230 µl of which 50 µl was used). Purification, afforded only a trace of trityl-protected epitope mimic **37**. t_R = 25.0 minutes; HRMS: calculated *m/z* for $C_{117}H_{157}N_{27}O_{32}S_3$: 1275.0403 ½[*M*+2H]$^{2+}$; could not be obtained; LRMS: calculated *m/z* for $C_{117}H_{157}N_{27}O_{32}S_3$: 1275.04 ½[*M*+2H]$^{2+}$; found: 1275.08.

Epitope mimic 38. Cyclic peptide **26** (11 mg, 5.0 µmol) and linker **14** (4.1 mg, 8.4 µmol; dissolved in 112 µl DMF of which 100 µl was used) was subjected to the above described CuAAC with $CuSO_4$•$5H_2O$ (10 mg, 41 µmol; dissolved in 455 µl H_2O of which 100 µl was used), sodium L-ascorbate (20 mg, 89 µmol; dissolved in 89 µl H_2O of which 50 µl was used), TBTA (4.9 mg, 9.2 µmol; dissolved in 405 µl DMF of which 100 µl was used), aminoguanidine•HCl (16 mg, 0.14 mmol; dissolved in 130 µl of which 50 µl was used). Purification and subsequent deprotection, afforded epitope mimic **38** (1.7 mg, 0.71 µmol, 14%). t_R = 19.2 minutes; HRMS: calculated *m/z* for $C_{101}H_{149}N_{27}O_{35}S_3$: 1220.9834 ½[*M*+2Na]$^{2+}$; found 1220.9838 LRMS: calculated *m/z* for $C_{101}H_{149}N_{27}O_{35}S_3$: 1199.00 ½[*M*+2H]$^{2+}$; found 1199.42 (^{13}C [+1]).

Scrambled negative control 39. Cyclic peptide **28** (6.0 mg, 3.0 µmol) and linker **14 (**8.0 mg, 16 µmol; dissolved in 490 µl DMF of which 100 µl was used) was subjected to the above described CuAAC with $CuSO_4$•$5H_2O$ (5.8 mg, 23 µmol; dissolved in 430 µl H_2O of which 100 µl was used), sodium L-ascorbate (15 mg, 76 µmol; dissolved in 127 µl H_2O of which 50 µl was used), TBTA (1.8 mg, 3.4 µmol; dissolved in 245 µl DMF of which 100 µl was used), aminoguanidine•HCl (7.4 mg, 67 µmol; dissolved in 101 µl of which 50 µl was used). Purification and subsequent deprotection, afforded epitope mimic **39** (1.0 mg, 0.44 µmol, 13%). t_R = 21.0 minutes; HRMS: calculated *m/z* for $C_{107}H_{143}N_{27}O_{23}S_3$: 1136.0084 ½[*M*+2H]$^{2+}$; found 1136.0112; LRMS: calculated *m/z* for $C_{107}H_{143}N_{27}O_{23}S_3$: 1136.01 ½[*M*+2H]$^{2+}$ / 757.67 1/3[*M*+3H]$^{3+}$; found 1136.50 / 758.00 (^{13}C [+1]).

Scrambled negative control 40. Cyclic peptide **29** (7.0 mg, 3.3 µmol; dissolved in 200 µl) and linker **14** (7.8 mg, 16 µmol; dissolved in 640 µl DMF of which 200 µl was used) was subjected to the above described CuAAC with $CuSO_4$•$5H_2O$ (7.1 mg, 28 µmol; dissolved

in 955 µl H_2O of which 200 µl was used), sodium L-ascorbate (18 mg, 89 µmol; dissolved in 270 µl H_2O of which 100 µl was used), TBTA (1.8 mg, 3.4 µmol; dissolved in 410 µl DMF of which 200 µl was used), aminoguanidine•HCl (11 mg, 99 µmol; dissolved in 150 µl of which 100 µl was used). Purification and subsequent deprotection, afforded epitope mimic **40** (3.1 mg, 1.3 µmol, 39%). t_R = 20.9 minutes; HRMS: calculated *m/z* for $C_{110}H_{149}N_{27}O_{26}S_3$: 1181.0243 ½[*M*+2H]$^{2+}$; found 1181.0253; LRMS: calculated *m/z* for $C_{110}H_{149}N_{27}O_{26}S_3$: 1181.02 ½[*M*+2H]$^{2+}$ / 787.69 1/3[*M*+3H]$^{3+}$; found 1181.58 / 788.17 (^{13}C [+1]).

Scrambled negative control 41. Cyclic peptide **30** (4.1 mg, 2.0 µmol) and linker **14** (7.4 mg, 15 µmol; dissolved in 685 µl DMF of which 100 µl was used) was subjected to the above described CuAAC with $CuSO_4$•$5H_2O$ (3.3 mg, 13 µmol; dissolved in 365 µl H_2O of which 100 µl was used), sodium L-ascorbate (12 mg, 59 µmol; dissolved in 147 µl H_2O of which 50 µl was used), TBTA (1.3 mg, 2.4 µmol; dissolved in 265 µl DMF of which 100 µl was used), aminoguanidine•HCl (8.2 mg, 74 µmol; dissolved in 168 µl of which 50 µl was used). Purification and subsequent deprotection, afforded only a trace of epitope mimic **41**. t_R = 21.3 minutes; HRMS: calculated *m/z* for $C_{110}H_{146}N_{24}O_{23}S_3$: 1134.5156 ½[*M*+2H]$^{2+}$; found 1134.5160; LRMS: calculated *m/z* for $C_{110}H_{146}N_{24}O_{23}S_3$: 1134.52 ½[*M*+2H]$^{2+}$ / 756.68 1/3[*M*+3H]$^{3+}$; found 1135.00 / 756.92 (^{13}C [+1]).

Epitope mimic 42. Obtained as described in Chapter 2: Cyclic epitope mimic **21**.

Crude peptide **15** (38 mg, 20 µmol, 1.1 equiv.) was treated with our previously developed cyclization linker **11**[3] (22 mg, 31 µmol, 1.5 equiv.) as described above in the *general method for peptide cyclization*. The obtained crude product (34 mg) was suspended in 4 mL buffer A and centrifuged (4500 rpm; 5 minutes), which resulted in a pellet of un-dissolved crude (9.5 mg; after lyophilization). The supernatant was purified in two batches of 2 mL: 0% buffer A for 5 min followed by a linear gradient of buffer B into buffer A (0-40%) over 40 min at a flow rate of 12.5 mL·min^{-1}. Affording epitope mimic **42** (1.7 mg, 0.77 µmol, 4% overall yield). t_R = 17.9 minutes; HRMS: see Chapter 2: Cyclic epitope mimic **21**; LRMS: calculated *m/z* for $C_{96}H_{151}N_{27}O_{26}S_3$: 1098.03 ½[*M*+2H]$^{2+}$ / 732.36 1/3[*M*+3H]$^{3+}$; found 1098.50 / 732.50.

Epitope mimic 43. Obtained as described in Chapter 2: Cyclic epitope mimic **24**.[3]

Crude peptide **16** (46 mg, 25 μmol, 1.0 equiv.) was treated with our previously developed cyclization linker **11**[3] (27 mg, 38 μmol, 1.5 equiv.) as described above in the *general method for peptide cyclization*. The obtained crude product (54 mg) was dissolved as three batches of 10-20 mg in 3 mL buffer A:B (1:1, *v/v*) and purified: 100% buffer A for 5 min followed by a linear gradient of buffer B into buffer A (0-50%) over 60 min at a flow rate of 12.5 mL·min^{-1}. Affording epitope mimic **43** (9.7 mg, 4.5 μmol, 15% overall yield). t_R = 22.3 minutes; HRMS: calculated *m/z* for $C_{106}H_{141}N_{21}O_{23}S_3$: 1086.9914 ½[*M*+2H]$^{2+}$; found 1086.9949; LRMS: calculated *m/z* for $C_{106}H_{141}N_{21}O_{23}S_3$: 1086.99 ½[*M*+2H]$^{2+}$; found 1087.25.

Epitope mimic 44. Obtained as described in Chapter 2: Cyclic epitope Mimic **29**.

Crude peptide **17** (49 mg, 26 μmol, 1.0 equiv.) was treated with our previously developed cyclization linker **11**[3] (28 mg, 38 μmol, 1.5 equiv.) as described above in the *general method for peptide cyclization*. The obtained crude product (57 mg) was suspended in 6 mL buffer A:B (1:1, *v/v*) and clarified by centrifugation (4500 rpm; 5 minutes), which resulted in a pellet of un-dissolved crude (19 mg; after lyophilization). The supernatant was purified: 20% buffer B in buffer A for 5 min followed by a linear gradient of buffer B into buffer A (20-60%) over 40 min at a flow rate of 12.5 mL·min^{-1}. Affording epitope mimic **44** (0.40 mg, 0.18 μmol, 1% overall yield). t_R = 20.1 minutes; HRMS: see Chapter 2: Cyclic epitope mimic **29**; LRMS: calculated *m/z* for $C_{98}H_{143}N_{21}O_{32}S_3$: 1111.98 ½[*M*+2H]$^{2+}$; found 1112.33.

Scrambled negative control 45. Obtained as described in Chapter 2: Scrambled negative control **31**.[3]

Crude cyclic precursor **18** (48 mg, 26 μmol, 1.0 equiv.) was treated with our previously developed cyclization linker **11**[3] (21 mg, 29 μmol, 1.1 equiv.) as described above in the *general method for peptide cyclization*. The obtained crude product (52 mg) was dissolved in 3 mL buffer A:B (1:1, *v/v*) and purified: 20% buffer B in buffer A for 5 min followed by a linear gradient of buffer B into buffer A (20-60%) over 40 min at a flow rate of 12.5 mL·min^{-1}. Affording scrambled negative control **45** (10 mg, 4.6 μmol, 16% overall yield). t_R = 22.0 minutes; HRMS: calculated *m/z* for $C_{107}H_{143}N_{21}O_{23}S_3$: 1093.9992 ½[*M*+2H]$^{2+}$; found 1093.9997; LRMS: calculated *m/z* for $C_{107}H_{143}N_{21}O_{23}S_3$: 1094.00 ½[*M*+2H]$^{2+}$; found 1094.58.

Monoclonal antibodies. The mAbs AP33[28], HC84.1[14], and DAO5[33] used in this work were kindly provided by Prof. Arvind Patel and co-workers.

Immobilisation method and ELISA. *Immobilisation:* Pierce® maleimide activated 96-well plates were purchased from Thermo Scientific. The wells were washed three times with 200 µL wash buffer (0.10 M Na_3PO_4, 0.15 M NaCl, 0.05% Tween®-20 detergent; pH 7.2). Then, the desired epitope mimic (100 – 500 µg) was suspended in 1 mL binding buffer (0.10 M Na_3PO_4, 0.15 M NaCl, 10 mM EDTA; pH 7.2) and further diluted (10 – 50 fold) to a concentration of 10 µg/mL. To each well, 200 µL of the epitope mimic solution was added and incubated overnight at 4 °C. After this, the wells were washed three times with 200 µL wash buffer. For capping unreacted maleimide groups, immediately before use, a solution of 10 µg/mL *N*-acetylated cysteine was prepared and 200 µL was added to each of the wells, followed by incubation of 1-2 hours at room temperature. The wells were washed three times with 200 µL wash buffer and used immediately or stored dry at -20°C until use.

ELISA: The wells were washed three times with 200 µL wash buffer. A three-fold dilution series of primary anti-HCV E2 antibodies (AP33 [10 – 0.014 ng/ml]; HC84.1 [100 – 0.14 ng/ml]; DAO5 [15 – 0.021 ng/ml]) was prepared over 7 steps and 100 µL was transferred to each well, followed by incubation for 1-2 hours at room temperature. After this, the wells were washed three times with PBST, before supplying 100 µL 1:2000 secondary α-mouse A4416 (Sigma) to each well. Incubation continued for 1-2 hours at room temperature, followed by washing the wells three times with PBST. The plates were developed using 100 µL 3, 3', 5, 5' tetramethylbenzidine (TMB) solution per well, obtained from Life Technologies, and incubating for 25 minutes at room temperature. After which, development was stopped using 50 µL 0.50 M H_2SO_4 per well. Absorbance at 450 nm was measured on a Varioskan (Thermoscientific) or PHERAstar FS (BMG Labtech) instrument. Background signal (no mAb) was subtracted. The data are represented as a percentage relative to immobilized epitope mimic **42**, **43** and **44** for antibodies AP33, HC84.1, and DAO5, respectively, with the absorbance of the highest mAb concentration being set to 100% per individual experiment. Data was collected from at least 3 independent experiments. All experiments were performed in duplicate. Error bars represent the standard deviation.

3.5 References

1. Zorzi, A., Deyle, K., Heinis, C. (2017) Cyclic peptide therapeutics: past, present and future. *Curr. Opin. Chem. Biol. 38*:24-29. DOI: 10.1016/j.cbpa.2017.02.006
2. Werkhoven, P. R., Elwakiel, M., Meuleman, T. J., *et al.* (2016) Molecular construction of HIV-gp120 discontinuous epitope mimics by assembly of cyclic peptides on an orthogonal alkyne functionalized TAC-scaffold. *Org. Biomol. Chem. 14*(2):701-710. DOI: 10.1039/c5ob02014j
3. Meuleman, T. J., Dunlop, J. I., Owsianka, A. M., *et al.* (2018) Immobilization by surface conjugation of cyclic peptides for effective mimicry of the HCV-envelope E2 protein as a strategy toward synthetic vaccines. *Bioconjug. Chem. 29*(4):1091-1101. DOI: 10.1021/acs.bioconjchem.7b00755
4. Mulder, G. E., Quarles van Ufford, H. C., Van Ameijde, J., *et al.* (2013) Scaffold optimization in discontinuous epitope containing protein mimics of gp120 using smart libraries. *Org. Biomol. Chem. 11*(16):2676-2684. DOI: 10.1039/c3ob27470e
5. Dustin, L. B., Cashman, S. B., Laidlaw, S. M. (2014) Immune control and failure in HCV infection—tipping the balance. *J. Leukoc. Biol. 96*(4):535-548. DOI: 10.1189/jlb.4RI0214-126R
6. Lavie, M., Hanoulle, X., Dubuisson, J. (2018) Glycan shielding and modulation of hepatitis C virus neutralizing antibodies. *Front. Immunol. 9*(910):1-9. DOI: 10.3389/fimmu.2018.00910
7. Ray, R. B., Ray, R. (2019) Hepatitis C virus manipulates humans as its favourite host for a long-term relationship. *Hepatology. 69*(2):889-900. DOI: 10.1002/hep.30214
8. Kwon, Y. C., Ray, R. (2019) Complement Regulation and Immune Evasion by Hepatitis C Virus. In: Law M. (eds) Hepatitis C Virus Protocols. *Methods in Molecular Biology*, 1*911*. Humana Press, New York, NY. DOI: 10.1007/978-1-4939-8976-8_23
9. Walker, C. M. (2017) Designing an HCV vaccine: a unique convergence of prevention and therapy? *Curr. Opin. Virol. 23*:113-119. DOI: 10.1016/j.coviro.2017.03.014
10. Tarr, A. W., Owsianka, A. M., Javaraj, D.,*et al.* (2007) Determination of the human antibody response to the epitope defined by the hepatitis C virus-neutralizing monoclonal antibody AP33. *J. Gen. Virol. 88*:2991-3001. DOI: 10.1099/vir.0.83065-0

11. Cowton, V. M., Singer, J. B., Gifford, R. J., *et al.* (2018) Predicting the effectiveness of hepatitis C virus neutralizing antibodies by bioinformatics analysis of conserved epitope residues using public sequence data. *Front Immunol. 9*:1470. DOI: 10.3389/fimmu.2018.01470
12. Sautto, G., Tarr, A. W., Mancini, N., *et al.* (2013) Structural and antigenic definition of hepatitis C virus E2 glycoprotein epitopes targeted by monoclonal antibodies. *Clin. Dev. Immunol. 2013*:450963. DOI: 10.1155/2013/450963
13. Owsianka, A., Clayton, R. F., Loomis-Price, L. D., *et al.* (2001) Functional analysis of hepatitis C virus E2 glycoproteins and virus-like particles reveals structural dissimilarities between different forms of E2. *J. Gen. Virol. 82*:1877-1883. DOI: 10.1099/0022-1317-82-8-1877
14. Keck, Z. Y., Xia, J., Wang, Y., *et al.* (2012) Human monoclonal antibodies to a novel cluster of conformational epitopes on HCV E2 with resistance to neutralization escape in a genotype 2a isolate. *PLoS Pathog. 8*(4):e1002653. DOI: 10.1371/journal.ppat.1002653
15. Werkhoven, P. R., Van de Langemheen, H., Van der Wal, S., *et al.* (2014) Versatile convergent synthesis of a three peptide loop containing protein mimic of whooping cough pertactin by successive Cu(I)-catalyzed azide alkyne cycloaddition on an orthogonal alkyne functionalized TAC-scaffold. *J. Pept. Sci*. *20*(4):235-239. DOI: 10.1002/psc.2624
16. Chen, S., Morales-Sanfrutos, J., Angelini, *et al.* (2012) Structurally diverse cyclisation linkers impose different backbone conformations in bicyclic peptides. *ChemBioChem. 13*(7):1032-1038. DOI: 10.1002/cbic.201200049
17. Angelini, A., Cendron, L., Chen, S., *et al.* (2012) Bicyclic peptide inhibitors reveals large contact interface with a protease target. *ACS Chem. Biol. 7*(5):817-821. DOI: 10.1021/cb200478t
18. Chen, S., Bertoldo, D., Angelini, A., *et al.* (2014) Peptide ligands stabilized by small molecules. *Angew. Chem. Int. Ed. Engl. 53*(6):1602-1606. DOI: 10.1002/anie.201309459
19. Deyle, K., Kong, X. D., Heinis C. (2017) Phage selection of cyclic peptides for application in research and drug development. *Acc. Chem. Res. 50*(8):1866-1874. DOI: 10.1021/acs.accounts.7b00184
20. Kale, S. S., Villequey, C., Kong, X. D., *et al.* (2018) Cyclization of peptides with two chemical bridges affords large scaffold diversities. *Nat. Chem. 10*(7):715-723. DOI: 10.1038/s41557-018-0042-7

21. Richelle, G. J. J., Ori, S., Hiemstra, H., *et al.* (2018) General and facile route to isomerically pure tricyclic peptides based on template tandem CLIPS/CuAAC cyclizations. *Angew. Chem. Int. Ed. Engl. 57*(2):501-505. DOI: 10.1002/anie.201709127
22. Richelle, G. J. J., Schmidt, M., Ippel, H., *et al.* (2018) A one pot ‘’triple-C’’ multicyclization methodology for the synthesis of highly constrained isomerically pure tetracyclic peptides. *ChemBioChem. 19*(18):1934-1938. DOI: 10.1002/cbic.201800346
23. Streefkerk, D. E., Schmidt, M., Ippel, J. H., *et al.* (2019) Synthesis of constrained tetracyclic peptides by consecutive CEPS, CLIPS, and oxime ligation. *Org. Lett. 21*(7):2095-2100. DOI: 10.1021/acs.orglett.9b00378
24. Longin, O., Hezwani, M., Van de Langemheen, H., *et al.* (2018) Synthetic antibody protein mimics of infliximab by molecular scaffolding on novel CycloTriVeratrilene (CTV) derivatives. *Org. Biomol. Chem. 16*(29):5254-5274. DOI: 10.1039/c8ob01104d
25. Kalepu, V., Nekkanti, V. (2015) Insoluble drug delivery strategies: review of recent advances and business prospects. *Acta Pharm. Sin. B. 5*(5):442-453. DOI: 10.1016/j.apsb.2015.07.003
26. Rim, C., Lahey, L. J., Patel, V. G., *et al.* (2009) Thiolene reactions of 1,3,5,triacryloylhexahydro-1,3,5-triazine (TAT): facile access to functional tripodal thioethers. *Tetrahedron Lett. 50*(7):745-747. DOI: 10.1016/j.tetlet.2008.11.094
27. Van de Langemheen, H., Korotkovs, V., Bijl, J., *et al.* (2017) Polar hinges as functionalized conformational constraints in (bi)cyclic peptides. *ChemBioChem. 18*(4):387-395. DOI: 10.1002/cbic.201600612
28. Owsianka, A., Tarr, A. W., Juttla, V. S., *et al.* (2005) Monoclonal antibody AP33 defines a broadly neutralizing epitope on the hepatitis C virus E2 envelope glycoprotein. *J. Virol. 79*(11):11095-11104. DOI: 10.1128/JVI.79.17.11095-11104.2005
29. Meola, A., Tarr, A. W., England, P., *et al.* (2015) Structural flexibility of a conserved antigenic region in hepatitis C virus glycoprotein E2 recognized by broadly neutralizing antibodies. *J. Virol. 89*(4): 2170-2181. DOI: 10.1128/JVI.02190-14
30. Kong, L., Lee, D. E., Kadam, R. U., *et al.* (2016) Structural flexibility at a major conserved antibody target on hepatitis C virus E2 antigen. *Proc. Natl. Acad. Sci. U. S. A. 113*(45):12768-12773. DOI: 10.1073/pnas.1609780113

31. Merriflied, R. B. (1963) Solid phase peptide synthesis. I. The synthesis of a tetrapeptide. *J. Am. Chem. Soc. 85*(14):2149-2154. DOI: 10.1021/ja00897a025
32. Merrifield, B. (1986) Solid phase Synthesis. *Science. 232*(4748):341-347. DOI: 10.1126/science.3961484
33. Vasiliauskaite, I., Owsianka, A., England, P., *et al.* (2017) Conformational flexibility in the immunoglobulin-like domain of the hepatitis C virus glycoprotein E2. *MBio. 8*(3):e00382-17. DOI: 10.1128/mBio.00382-17
34. Liang, L., Astruc, D. (2011) The copper(I)-catalyzed alkyne-azide cycloaddition (CuAAC) ‘’click’’ reaction and its applications. An Overview. *Coordination Chemistry Reviews. 255*:2933-2945. DOI: 10.1016/j.ccr.2011.06.028
35. Conibear, A. C., Farbiarz, K., Mayer, R. L., *et al.* (2016) Arginine side-chain modification that occurs during copper-catalysed azide-alkyne click reactions resembles an advanced glycation end product. *Org. Biomol. Chem. 14*(16):6205-6211. DOI: 10.1039/c6ob00932h
36. Yost, S. A., Wang, Y., Marcotrigiano, J. (2018) Hepatitis C virus envelope glycoproteins: a balancing act of order and disorder. *Front. Immunol. 9*:1917. DOI: 10.3389/fimmu.2018.01917

CHAPTER 4

Construction of HCV-E2 glycoprotein continuous and discontinuous epitope mimics and investigating their potential as synthetic vaccines to elicit an anti-HCV E2 glycoprotein antibody response

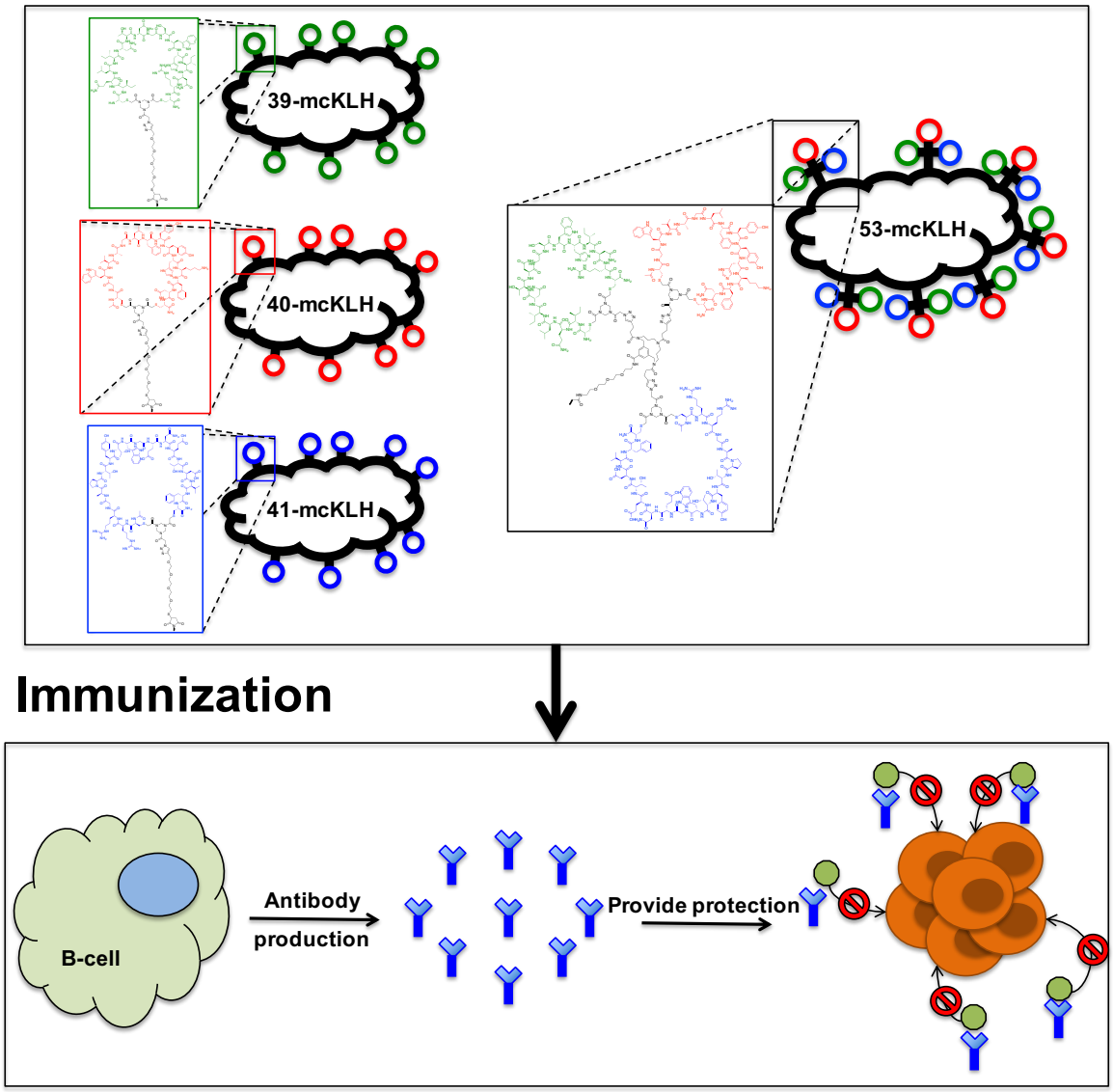

Abstract

Hepatitis C virus remains a global threat, despite the availability of highly effective direct-acting antiviral (DAA) drugs. With thousands of new infections annually, the need for a prophylactic vaccine is evident. However, traditional vaccine design has been unable to provide an effective vaccine so far. Therefore, alternative strategies need to be investigated. In this work a chemistry-based approach is explored towards fully synthetic peptide-based vaccines using epitope mimicry, by focussing on highly effective and conserved amino acid sequences known to inhibit HCV upon antibody binding. Here the importance of peptide cyclization for proper epitope mimicry has been shown. In addition, the need for sufficiently aqueous soluble cyclization hinges and their effect on antibody binding has been explored. Now, the time has come to combine past efforts into synthesizing continuous and discontinuous epitope mimics based on the HCV-E2 glycoprotein using fully synthetic cyclic peptides. These scaffolded epitope mimics have been submitted to a single immunization experiment to assess the elicitation of anti-HCV E2 glycoprotein antibodies representing a first step in employing epitope mimicry as a novel strategy towards vaccine design.

4.1 Introduction

Vaccination has been an essential tool in controlling a wide variety of virus infections throughout history.[1,2] However, the emergence of more complex viruses, like the human immunodeficiency virus (HIV)[3,4] and hepatitis C virus (HCV)[5-7], has not experienced similar success. Traditional approaches for vaccine design, including inactivated, attenuated, subunit, and recombinant vaccine strategies, appeared to be unable to cope with the new level of complexity associated with these viruses. The major obstacles for effective vaccine design against, for example HCV, can be attributed to its high mutation rate that results in viral escape.[8,9] The immune system struggles to adapt to these ever-changing viruses and is therefore unable to resolve the infection naturally in most of the cases.[10] Furthermore, the complexity of these viruses can be found in their adopted strategies to negatively influence the immune system to maintain infection. For HCV this includes the manipulation of communication within the immune system[10,11], as well as providing a wide variety of shielding and decoy factors (*i.e.* glycan shielding[12], association with host lipoprotein[13], and immunodominant epitopes[14]) that hinder or occupy the immune system without reducing the efficiency of the virus.

Instead of looking towards previously developed strategies to target these new threats, it is necessary to adopt alternative strategies to develop effective vaccines. One such strategy could be found in protein mimicry.[15,16] Conceptually protein mimicry is based on capitalizing on known peptide sequences (antibody epitopes) within the viral proteins that reduce virus efficiency when targeted by the immune system. These epitopes can be synthesized by solid phase peptide synthesis (SPPS)[17,18] and presented as a vaccine to induce a more targeted immune response absent of any immunomodulatory effects natural to the virus (Figure 4.1).[19,20] In addition, these epitopes can be identified to be highly conserved and resistant to escape mutations that result in decreased efficiency.[21-27] Even though it is unlikely to have absolute conservation of the epitope or to fully rule out the possibility of escape mutations, the synthetic approach allows for a rapid modular approach that can quickly adopt to viral variation by simply exchanging the synthetic peptides. Thereby providing a tool to rapidly adjust to the dynamic and exchangeable nature of viruses like HIV and HCV.

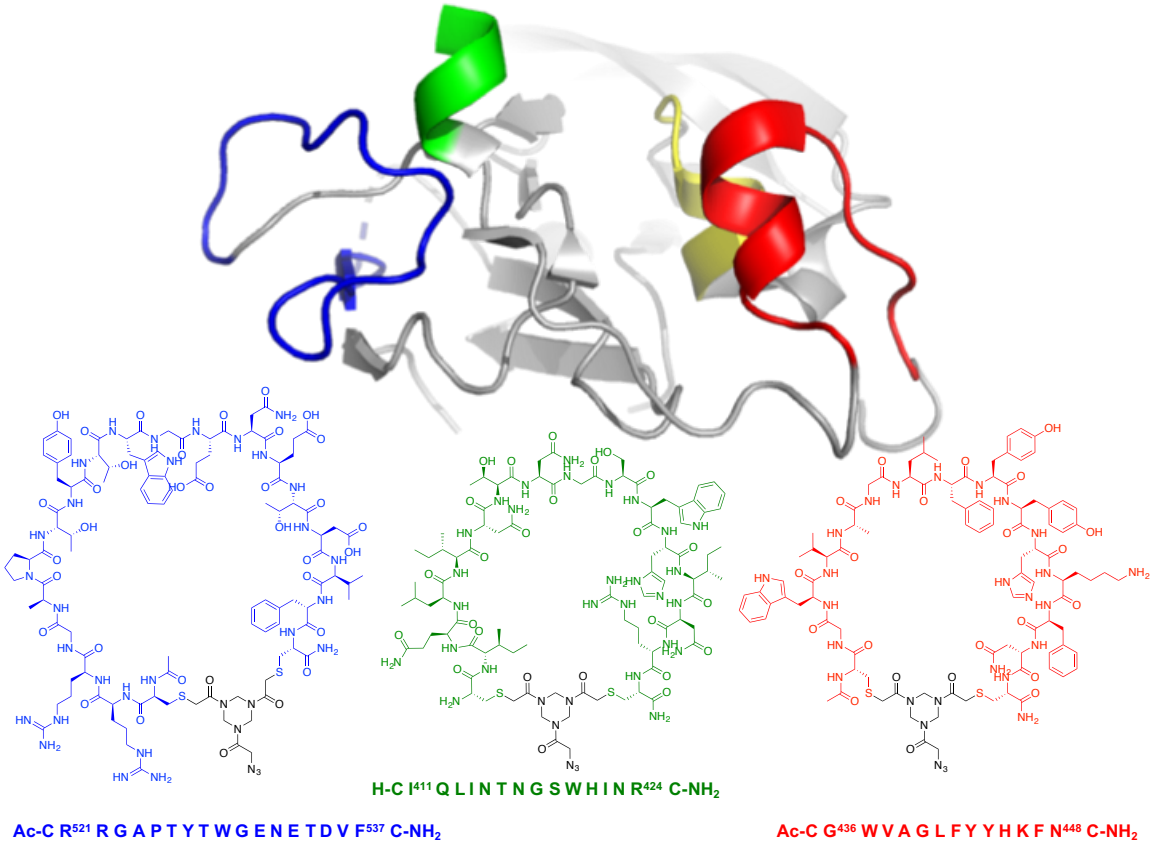

Figure 4.1. Illustration of synthetic continuous epitope mimics based on cyclized synthetic peptide based on epitope I (411-424) denoted in **green**; epitope II (436-448) denoted in **red**; epitope III (521-537) denoted in **blue**. Epitope IV (611-617) denoted in **yellow** was not considered for mimicry, as it is not recognized as a continuous epitope. The crystal structure of E2 core was obtained by Kong *et al.* [PDB 4MWF][28]

Successful mimicry, however, does not only rely on synthetic peptides with the appropriate amino acid sequence. Instead, these epitopes have complex structural conformations when presented within the viral protein that need to be included.[15,16] Such conformations can include loops, α-helices, and β-sheet like structures. Epitopes can be targeted as one single continuous row of amino acids, referred to as a continuous epitope (Figure 4.1). Alternatively, epitopes can consist of multiple peptide segments within the viral protein that form a recognition site by the overall folding of the protein. Mimicry of a discontinuous epitope is significantly more challenging. Whereas a continuous epitope might be successfully mimicked by a single synthetic peptide, a discontinuous epitope requires incorporation of multiple synthetic peptides within the same vaccine. Ideally, these multiple synthetic peptides must be incorporated into a single molecular structure that is capable of preserving their spatial orientation with respect to each other, as they are found within the viral protein (Figure 4.2). Such single molecular structures carrying

multiple (cyclic) peptide segments are referred to as molecular scaffolds. Despite consisting of a single peptide segment, continuous epitope mimics must generally be constrained, for by example cyclization, to induce (a) similar conformation(s) otherwise induced by the protein structure (Figure 4.1).

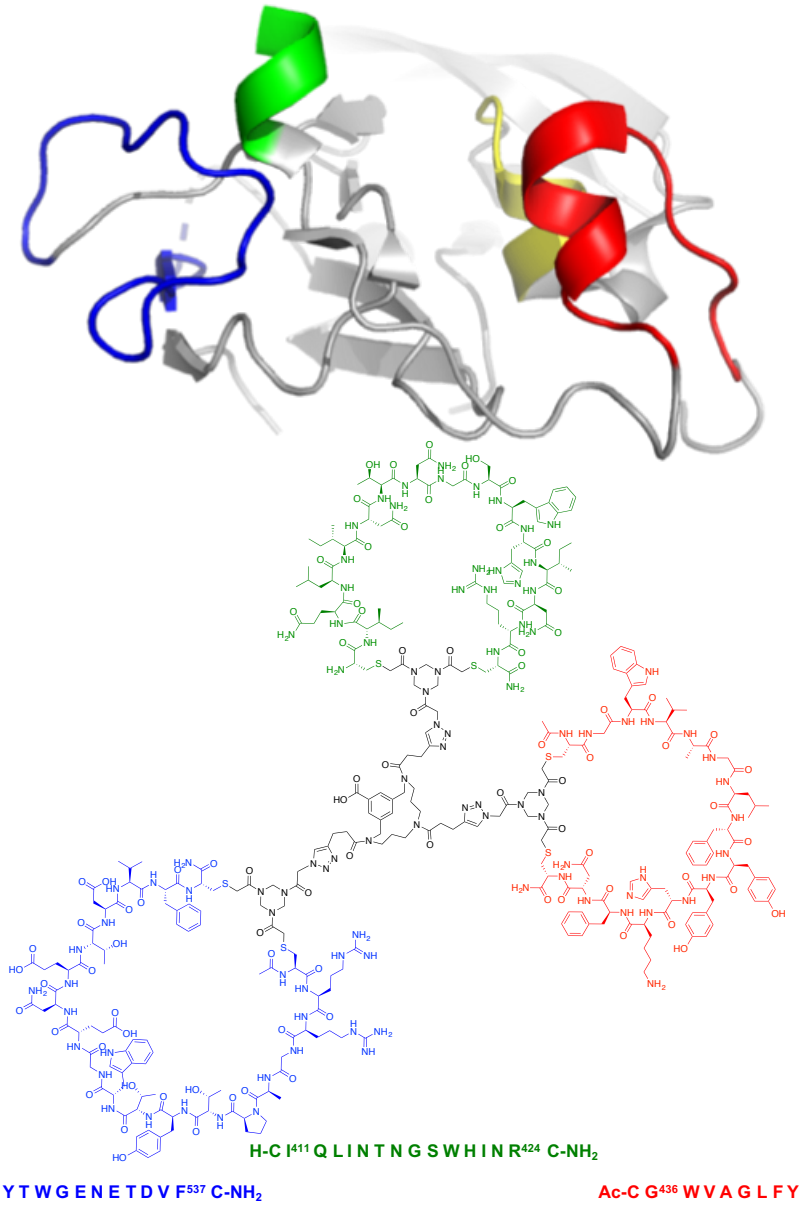

Figure 4.2. Illustration of a synthetic discontinuous epitope mimic based on the TAC-scaffold containing epitope I (411-424) denoted in **green**; epitope II (436-448) denoted in **red**; epitope III (521-537) denoted in **blue**. Epitope IV (611-617) denoted in **yellow** was not considered for mimicry, as it is not recognized as a continuous epitope. Therefore, it was not previously included as a mimic and thus omitted in the discontinuous epitope mimic. The crystal structure of E2 core was obtained by Kong *et al.* [PDB 4MWF][28]

Liskamp *et al.* have extensively researched approaches to assemble multiple synthetic peptides into one individual molecule towards development of synthetic receptors[29], antibodies[30,31], and vaccines[19,20,32]. Werkhoven *et al.* has developed an orthogonally protected trialkyne triazacyclophane (TAC) scaffold that can incorporate synthetic peptides by copper(I) catalyzed alkyne-azide cycloaddition (CuAAC) and has been used towards the development of synthetic vaccines.[20,32]

So far, our work has been focussed on highly conserved and neutralizing continuous epitopes within the HCV-E2 glycoprotein. We started by investigating the effect of peptide cyclization on epitope mimicry by verifying antibody binding (see Chapter 2).[33] Next, we have improved upon the low aqueous solubility associated with the previously used benzylic-derivatives by exchanging the cyclization hinge to more polar structures designed by Van de Langemheen *et al.*[34] (see Chapter 3).[35] In turn, we validated that these novel structures did not negatively influence epitope mimicry and biological activity by ELISA (see Chapter 3).[35]

Our findings so far have allowed us to synthesize continuous epitope mimics based on the HCV-E2 glycoprotein. Here, we have improved upon the TAC-scaffold developed by Werkhoven *et al.*[32] by introducing a suitably protected linker for attachment to a carrier protein that was compatible with CuAAC. The individual cyclic peptides were selectively attached to the TAC-scaffold to obtain a discontinuous epitope. Upon deprotection, the introduced linker was used to conjugate the discontinuous epitope mimic to a mariculture keyhole limpet hemocyanin (mcKLH) carrier protein. Both the previously developed continuous epitope mimics, as well as the currently developed discontinuous epitope mimics, were used in an immunization experiment to elicit anti-HCV E2 glycoprotein antibodies and validate their potential as synthetic vaccines.

4.2 Results and discussion

4.2.1 Synthesis of the triazacyclophane (TAC) scaffold

To assemble a discontinuous epitope mimic based on the HCV-E2 glycoprotein, a suitable scaffold molecule was required. Werkhoven *et al.*[32] has developed an orthogonally protected trialkyne scaffold to selectively incorporate three cyclic azido-peptides via CuAAC.

First, the pentynoic acid amidated TAC-scaffold **11** was constructed and provided by Dr. Anna Mickowska, according to the literature procedure of Werkhoven *et al.*[32] (Scheme 4.1). Commercially available 3-bromopropylamine hydrobromide **1** was protected with *ortho*-nitrobenzenesulfonyl chloride **2** (*o*NBS) to obtain *o*NBS-protected bromopropylamine **3**. Then, bromopropylamine **3** was further alkylated with 1,3-diaminopropane **4** to afford triamine **5**. Next, the primary amine of triamine **5** was protected using ethyl trifluoroacetate **6** to obtain doubly protected triamine **7**. The remaining secondary amine was coupled to pentynoic acid **8** by amide bond formation using (benzotriazol-1-yloxy)tris(dimethylamino)phosphonium hexafluorophosphate (BOP) to afford alkyne containing triamine **9**. Subsequent cyclization of alkyne containing triamine **9** on dibromide **10** resulted in alkyne containing TAC-scaffold **11**. Both the methyl ester and the trifluoroacetyl protection groups were removed by treatment with base to afford alkyne containing TAC-scaffold **12**. The resulting free amine was protected using 9-fluorenylmethyloxycarbonyl *N*-hydroxysuccinimide ester (Fmoc-OSu) **13** to afford alkyne containing TAC-scaffold **14**.

Scheme 4.1. Synthesis of the alkyne containing TAC-scaffold **14** precursor as performed by Dr. Anna Mickowska, according to the literature procedure of Werkhoven *et al.*[32]

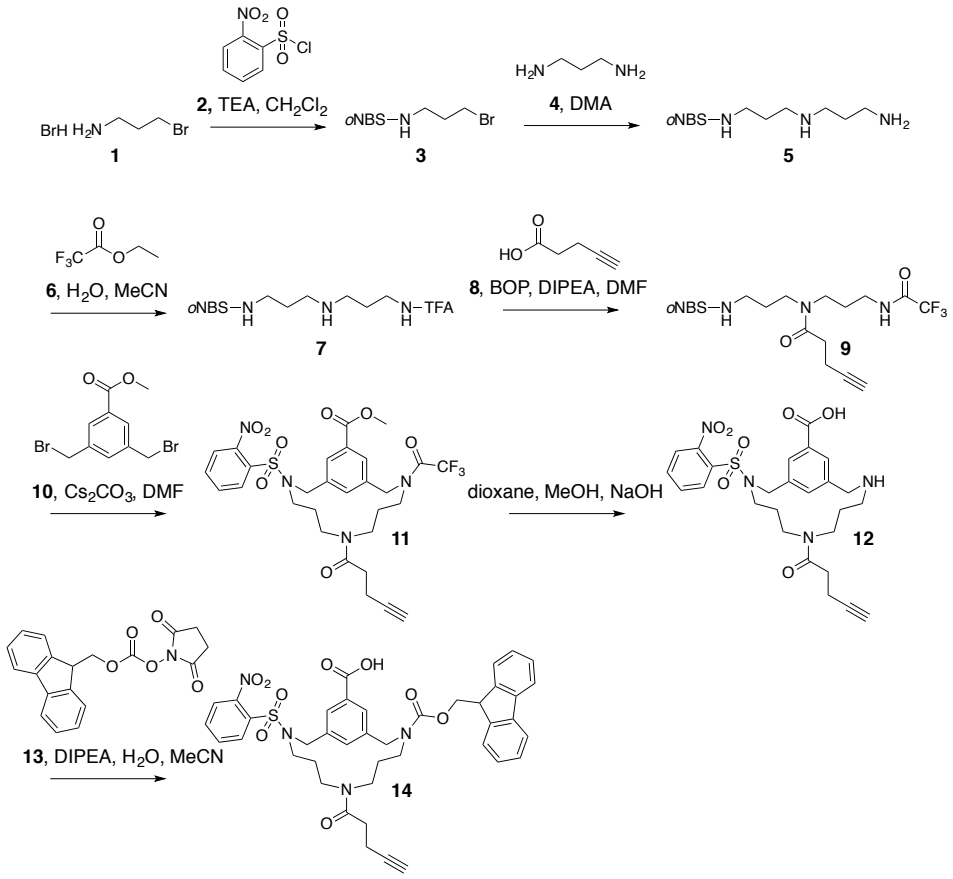

Orthogonally protected pentynoic acids were synthesized to obtain the orthogonally protected trialkyne TAC-scaffold (Scheme 4.2). To this end, commercially available pentynoic acid **8** was first reacted with *tert*-butyl 2,2,2-trichloro acetamide **15** to obtain protected *tert*-butyl ester **16** in good yield (81%). Acetamide **17** precipitated out of the reaction mixture and could be easily removed by filtration. Next, orthogonal silyl protection groups were introduced on the alkynes of *tert*-butyl ester **16** using triisopropylsilyl (TIPS) chloride **18** and triethylsilyl (TES) chloride **20** to afford protected alkynes **19** (54%) and **21** (52%), respectively. Lastly, *tert*-butyl esters **19** and **21** were hydrolysed to give the TIPS- and TES- protected pentynoic acids **22** (34%) and **23** (29%), respectively. The obtained *tert*-butyl esters **16**, **19**, and **21** were surprisingly volatile, which made concentrating the compounds *in vacuo* exceptionally challenging and decreased their yield considerably. Introducing the silyl-protection groups only marginally reduced their volatility. Installing the silyl-protection groups onto the alkyne (pKa 25) required the use of very strong bases (*i.e.* n-BuLi or LDA; pKa 50 and 35 of their conjugated acid, respectively) that also resulted in enolate formation (pKa 21), which in turn resulted in the

formation of several side products. The subsequent purifications were therefore challenging, however, acceptable yields were obtained.

Scheme 4.2. Synthesis of orthogonally protected pentynoic acid **22** and **23**, adapted from the literature procedure of Werkhoven *et al.*[32]

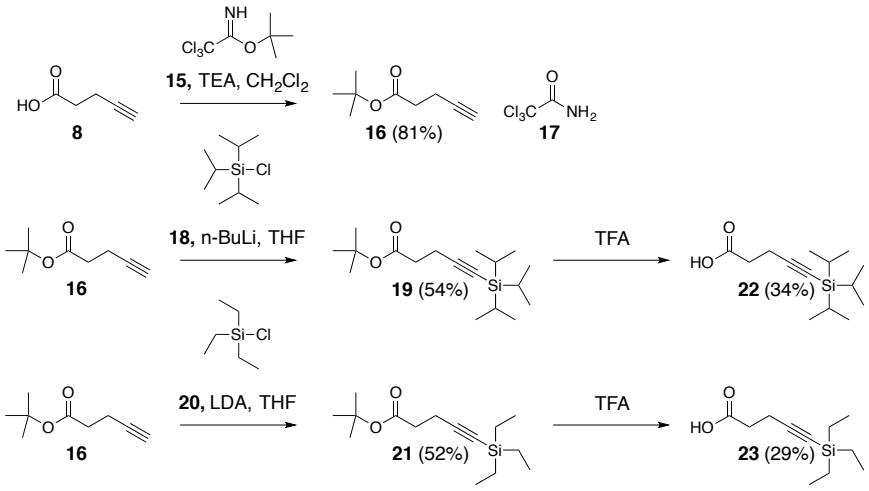

Instalment of the orthogonally protected alkynes **22** and **23** on alkyne containing TAC-scaffold **14** were performed on a solid phase support (Scheme 4.3). To this end, alkyne TAC-scaffold **14** was loaded onto 2-chlorotrityl chloride resin **24** and the Fmoc-group was removed by treatment with piperidine. Then, TIPS-alkyne **22** was coupled to the liberated amine using BOP. Next, the *o*NBS group was removed using 1,8-diazabicyclo[5.4.0]undec-7-ene (DBU) and 2-mercaptoethanol, followed by coupling of TES-alkyne **23** to the free amine using BOP. Lastly, the complete orthogonally protected trialkyne TAC-scaffold **25** was obtained in good yield (*quant.*) by cleavage from the resin using hexafluoro-2-propanol (HFIP).

Scheme 4.3. Synthesis of orthogonally protected trialkyne TAC-scaffold **25**, according to the literature procedure of Werkhoven *et al.*[32]

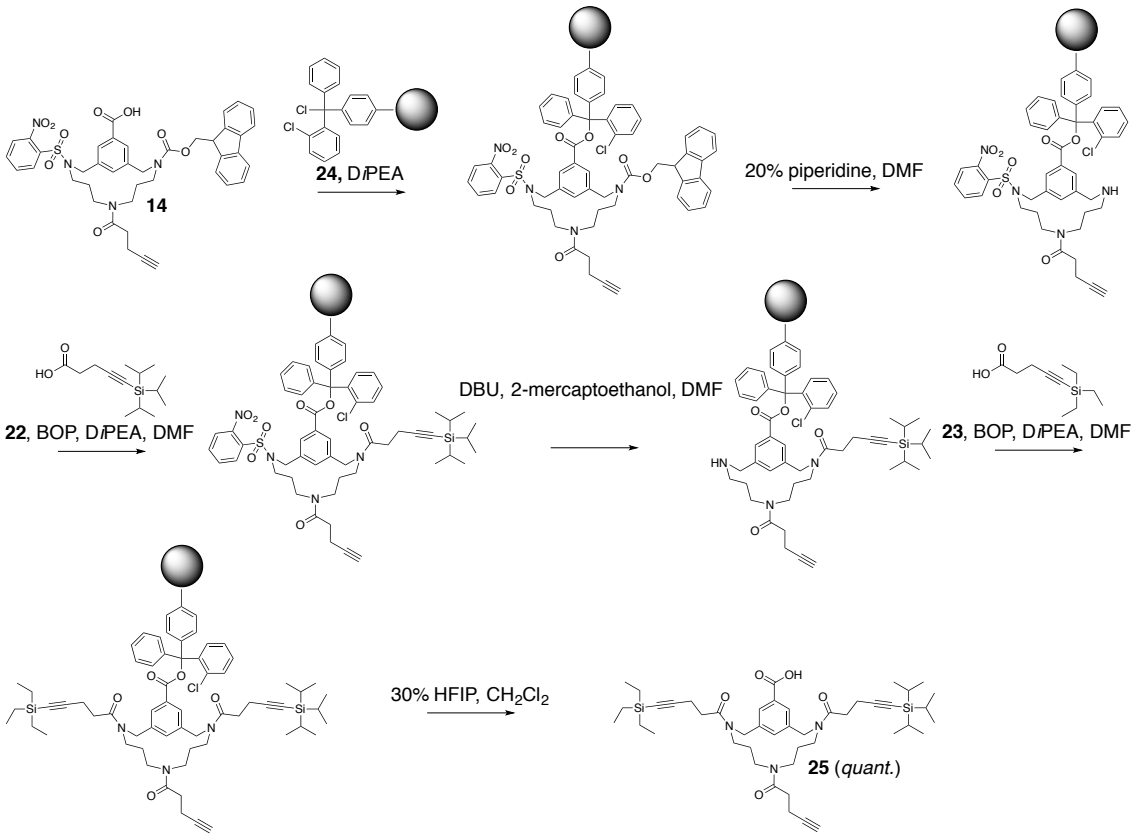

4.2.2 Synthesis and subsequent instalment of a triethylene glycol monotrityl thioether ethylamine linker on the TAC-scaffold

The earlier described synthesis of monocyclic peptide constructs with a flexible linker and a free thiol-moiety (see Chapter 2 and Chapter 3)[33,35] that allowed for thiol-maleimide conjugation on ELISA plate surfaces provided inspiration for a similar approach applied to TAC-scaffold **25** (Scheme 4.4). To this end, tetraethylene glycol monotrityl thioether **26** (see Chapter 2)[33] was reacted with ρ-toluenesulfonyl chloride **27** to obtain tosylate **28** in good yield (74%). Next, the tosylate **28** was reacted to amine **29** by treatment with aqueous ammonia. Despite that aqueous ammonia was not efficient in substituting the tosylate, as demonstrated by the low yield of amine **29** (14%), it does have a practical advantage in providing a simple one-step reaction. In contrast to exchanging the tosylate by an azide, followed by sequential reduction of the azide to form an amine. Triethylene glycol monotrityl thioether ethylamine **29** was coupled to TAC-scaffold **25** via amide bond formation using BOP, affording an orthogonally protected trialkyne TAC-scaffold **30** that

upon liberation of the thiol-moiety could be further conjugated to a maleimide-activated mcKLH carrier protein.

Scheme 4.4. Synthesis of triethylene glycol monotrityl thioether ethylamine **29** and subsequent instalment on TAC-scaffold **25**.

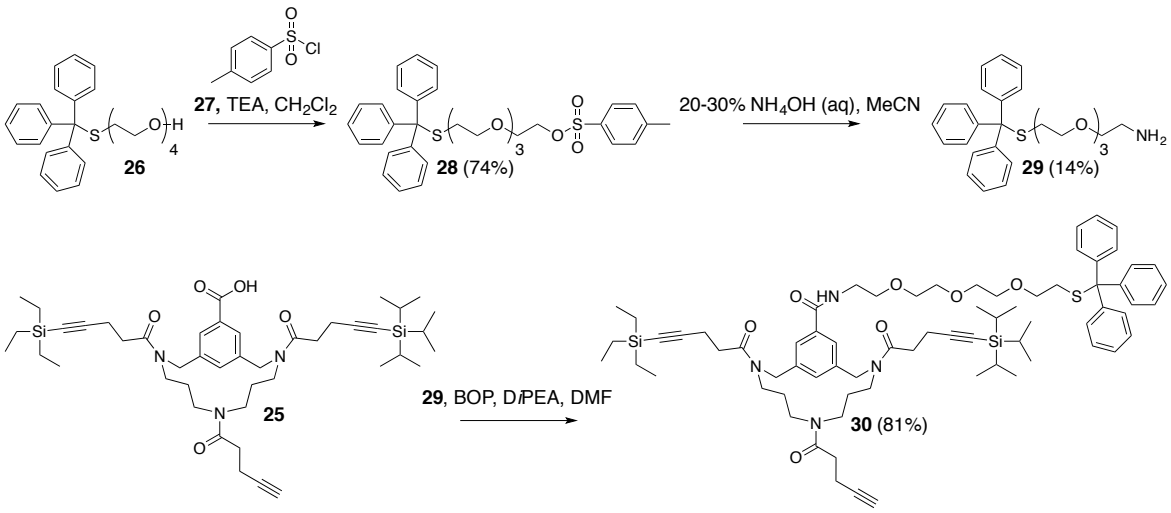

4.2.3 Synthesis of cysteine containing peptides based on HCV-E2 glycoprotein epitopes and subsequent cyclization

A highly conserved discontinuous epitope is located within the CD81 binding site of HCV-E2 glycoprotein that consists of four peptide segments.[26] Individually, these peptide segments are referred to as epitopes I, II, III, and IV. So far, we have shown the antigenic potential of monocyclic peptides based on epitopes I, II, and III, which were conjugated onto a maleimide-activated surface, using ELISA plates (see Chapter 2 and Chapter 3).[33,35] Epitope IV has not been considered as a continuous epitope as it combines with epitopes I, II, and III to form a discontinuous epitope.[26] Because only epitopes I, II, and III were previously included as epitope mimics, we decided to omit epitope IV. Epitope I includes residues 411-424 and is considered a highly conserved but flexible immunogenic region.[21-23] Epitope II comprises a highly conserved immunogenic region that includes residues 436-448.[24,25] Epitope III consists of a promising immunogenic region between residues 521-541.[26,27] For epitope III, we previously focussed on a peptide segment spanning residues 528-541 that was successfully recognized by non-neutralizing antibody DAO5 (see Chapter 2 and Chapter 3).[33,35] However, recent work done by Cowton *et al.*[26] showed key binding amino acid residues within epitope III that were involved in antibody binding of the combined I-II-III discontinuous epitope. Therefore, the peptide sequence of epitope III

was changed to residues 521-537. Peptides **31**, **32**, and **33** based on epitopes I, II, and III, respectively, and containing two cysteines were synthesized by SPPS[17,18] to construct both continuous epitope mimics as well as a combined discontinuous epitope mimic (Table 4.1).

Table 4.1. Synthetic peptide sequences containing two cysteines based on epitopes **I in green** (**31**), **II in red** (**32**), and **III in blue** (**33**) of the HCV-E2 glycoprotein. Together these epitopes form the discontinuous epitopes.

Epitope I	**31**	**H –**	**C**	**I^{411}**	**Q**	**L**	**I**	**N**	**T**	**N**	**G**	**S**	**W**	**H**	**I**	**N**	**R^{424}**				**C**	**– NH$_2$**
Epitope II	**32**	**Ac –**	**C**	**G^{436}**	**W**	**V**	**A**	**G**	**L**	**F**	**Y**	**Y**	**H**	**K**	**F**	**N^{448}**					**C**	**– NH$_2$**
Epitope III	**33**	**Ac –**	**C**	**R^{521}**	**R**	**G**	**A**	**P**	**T**	**Y**	**T**	**W**	**G**	**E**	**N**	**E**	**T**	**D**	**V**	**F^{537}**	**C**	**– NH$_2$**

The synthetic peptides were cyclized on the more water-soluble azido triazinane-tris(2-bromoethanone) (TADB-N_3) **34** (Scheme 4.5), developed by Van de Langemheen *et al.*[34] The reaction was scaled up to obtain sufficient amounts of the cyclic peptides and to facilitate this, the purification by preparative HPLC was optimized using custom focussed gradients for high-throughput.

Scheme 4.5. Cyclization of two cysteine containing peptides **31-33** with TADB-N_3 **34**.[35] Including: epitopes **I in green** (**35**), **II in red** (**36**), and **III in blue** (**37**). The reported yields are of purified products, after preparative reverse phase HPLC.

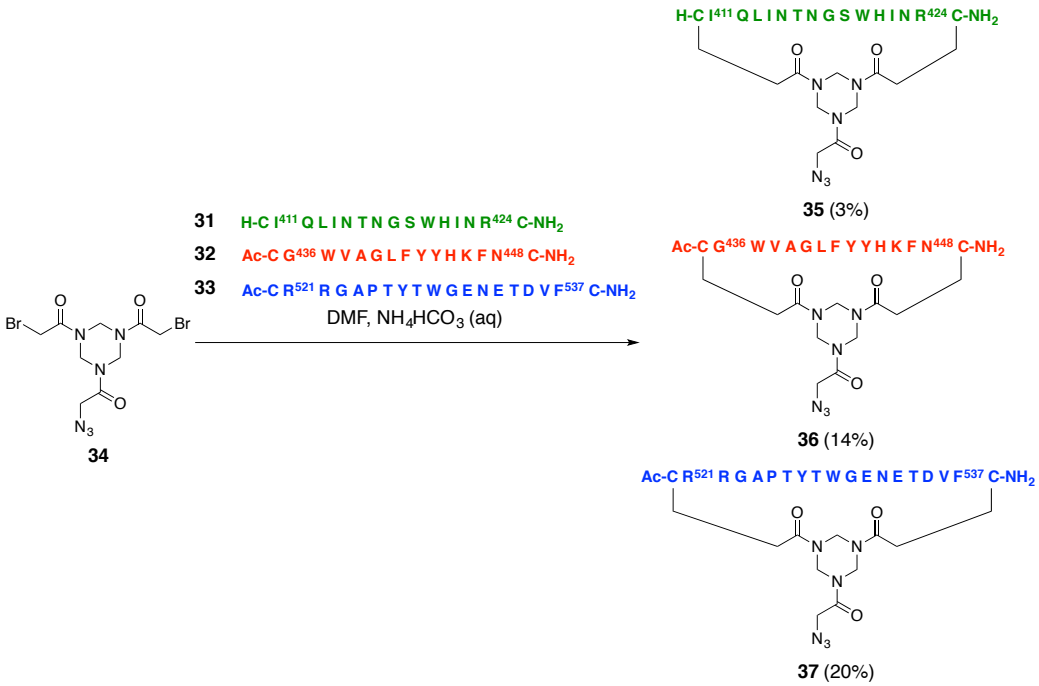

4.2.4 Assembling continuous epitope mimics via CuAAC on the developed alkyne linker

Cyclization of peptides **31-33** onto TADB-N_3 **34** resulted in the instalment of an azide-handle for attachment of cyclic peptides **35**, **36**, and **37** to our previously developed alkyne-linker **38** via CuAAC (see Chapter 3)[35] (Scheme 4.6). Subsequent deprotection resulted in a free thiol-group that could be used to conjugate continuous epitope mimics **39-41** to maleimide-activated mcKLH carrier protein for immunization experiments and elicitation of anti-HCV E2 glycoprotein antibodies.

Scheme 4.6. Synthesis of continuous epitope mimics **39**, **40**, and **41** by CuAAC as developed in Chapter 3.[35]

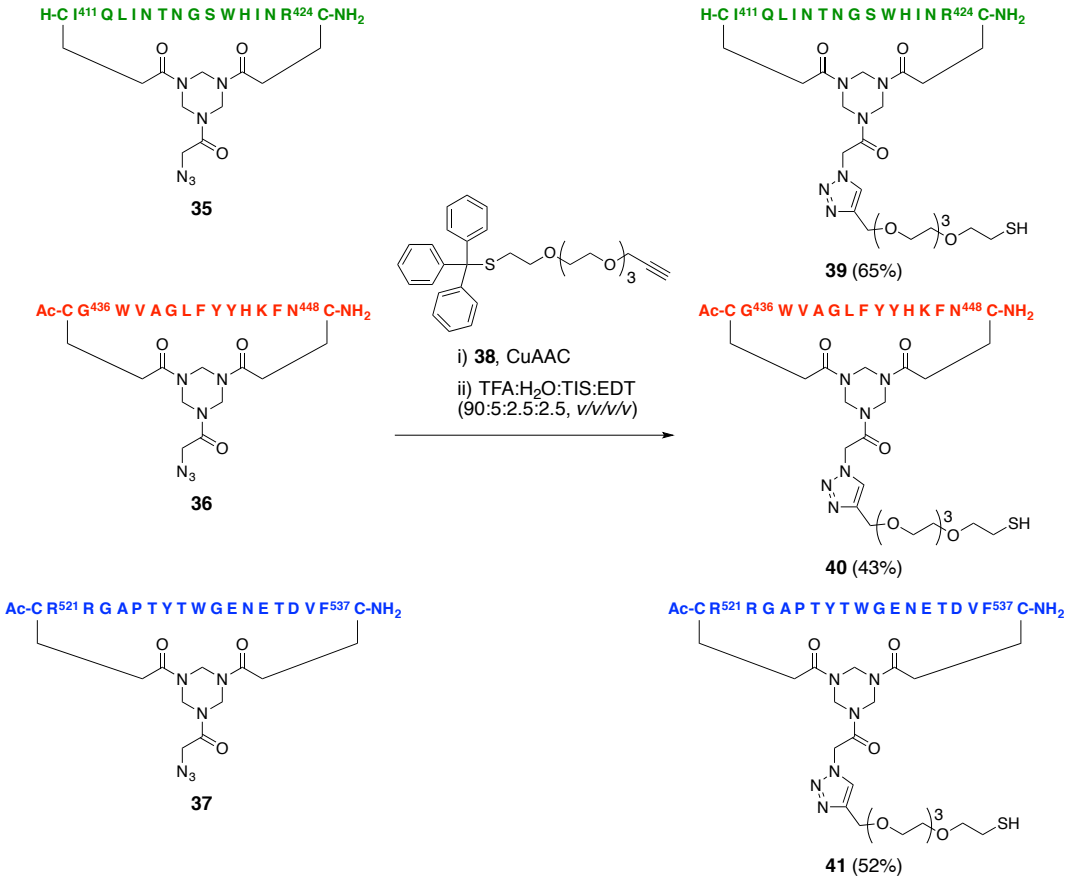

4.2.5 Assembling a discontinuous epitope mimic by combining cyclic peptides on the monotrityl thioether modified TAC-scaffold

The previously developed CuAAC procedure (see Chapter 3)[35] was used in attempts to selectively conjugate cyclic peptides **39**, **40**, and **41** to the monotrityl thioether modified TAC-scaffold **30**. However, the trityl-protection group on the linker was very unstable when conjugated to the TAC-scaffold causing premature deprotection of the thiol-moiety. The liberated thiol-moiety might bind the required Cu(I)-catalyst, thereby preventing catalysis of the cycloaddition of the azide and alkyne moieties. Analysis of TAC-scaffold **30** did not indicate significant deprotection of the trityl-group, however, even small amounts might have been sufficient to fully deactivate the reactive Cu(I)-species. In contrast, the trityl-protective group on our previously developed alkyne linker **38**[35] (Scheme 4.6) was stable and no problems were encountered during the synthesis of continuous epitope mimics **39-41**.

4.2.6 Synthesis and subsequent instalment of a triethylene glycol Boc-amide ethylamine linker on the TAC-scaffold

To circumvent the problem observed with the unstable trityl-group on TAC-scaffold **30**, we decided to switch to a Boc-group containing amide linker **47** (Scheme 4.7). Removal of the Boc-group will lead to a primary amine that could be used to conjugate the TAC-scaffold onto a carrier protein. Tosylate **42** (see Chapter 2)[33] was reacted with aqueous ammonia to install a free amine **43** that was immediately protected with a Boc-group using di-*tert*-butyl dicarbonate **44**, affording tetraethylene glycol Boc-amide **45** (52%). Then, amide **45** was tosylated using ρ-toluenesulfonyl chloride **27** to obtain tosylate **46** (43%). Next, a free amine was installed by treating tosylate **46** with aqueous ammonia to obtain triethylene glycol Boc-amide ethylamine linker **47** (36%). TAC-scaffold **25** was equipped with triethylene glycol Boc-amide ethylamine linker **47** via amide bond formation using BOP coupling that afforded orthogonally protected trialkyne TAC-scaffold **48** (86%). After removal of the Boc-group, the linker containing scaffold can be conjugated to a carrier protein such as mcKLH via amide bond formation.

Scheme 4.7. Synthesis of triethylene glycol Boc-amide ethylamine **47** and subsequent instalment onto TAC-scaffold **25**.

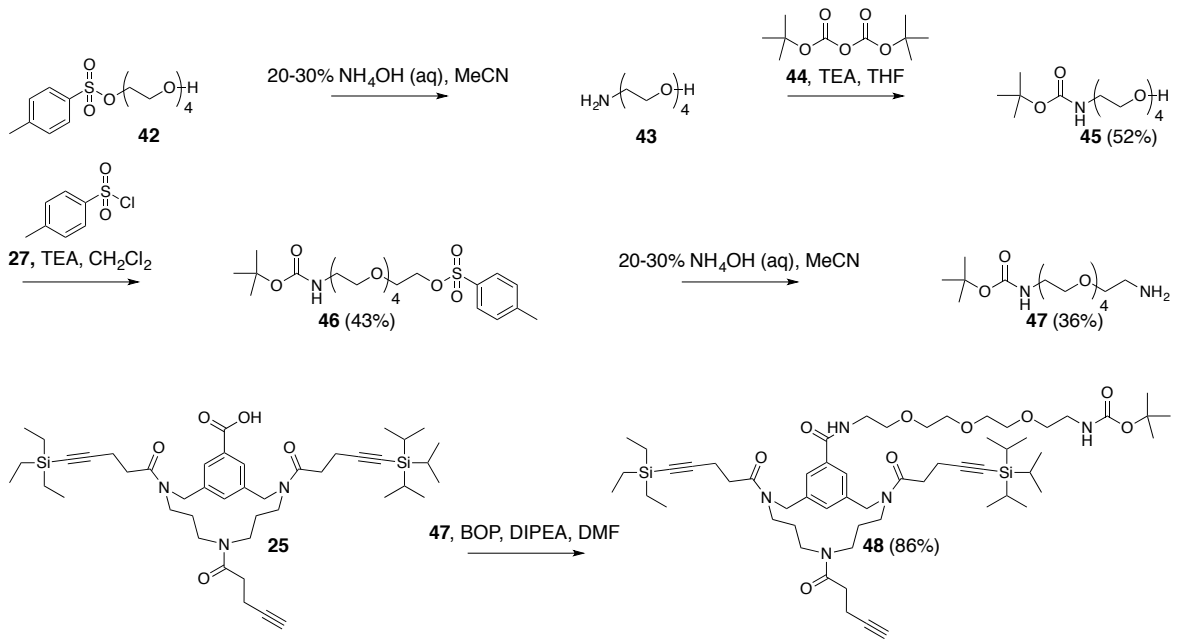

4.2.7 Assembling a discontinuous epitope mimic by combining cyclic peptides on the Boc-amide modified TAC-scaffold

The Boc-protected amide linker installed TAC-scaffold **48** was used to selectively incorporate three cyclic peptides **35-37** with our previously developed CuAAC conditions (see Chapter 3)[35] (Scheme 4.8 to 4.10). Cyclic peptide **36** was coupled to the first free alkyne, followed by removal of the TES-protection group in a one-pot reaction by adding silver nitrate to liberate the next alkyne and afford scaffold **49** (26%) (Scheme 4.8). Incorporation of the second cyclic peptide **37** afforded scaffold **50** (23%). After purification by preparative HPLC the procedure was continued by removal of the TIPS-protection group using tetrabutylammonium fluoride trihydrate (TBAF•$3H_2O$) to obtain scaffold **51** (40%). The resulting deprotected alkyne was used to incorporate cyclic peptide **35**, which afforded discontinuous epitope mimic **52** (24%) (Scheme 4.9). Treatment with trifluoro acetic acid removed the Boc-protection group and afforded discontinuous epitope mimic **53** (*quant.*) (Scheme 4.10), which could be conjugated by amide bond formation to carrier protein mcKLH for immunization experiments and development of anti-HCV E2 glycoprotein antibodies.

The orthogonality between the TES- and TIPS- protection groups made it possible to selectively synthesize different combinations of cyclic peptides onto the TAC-scaffold.

The available crystal structure of HCV-E2 glycoprotein suggested that cyclic peptide **35** should be incorporated first, followed by cyclic peptide **36**, and lastly cyclic peptide **37**. However, cyclic peptide **35** was only obtained in very low yield (3%) due to a low solubility and challenging purification. In contrast, cyclic peptides **36** and **37** were obtained in reasonable yields (14% and 20%, respectively) and were considered for incorporation at the first and second positions, respectively. Generally less product was obtained for every step in the reaction (Schemes 4.8, 4.9, and 4.10, respectively), which made it important to perform the first step on a sufficiently high scale. Cyclic peptide **35** was incorporated last, based on the lower yield associated with cyclic peptide **35** (3%).

Scheme 4.8. Installing the first cyclic peptide **36** on TAC-scaffold **48**, followed by removal of the TES-group.

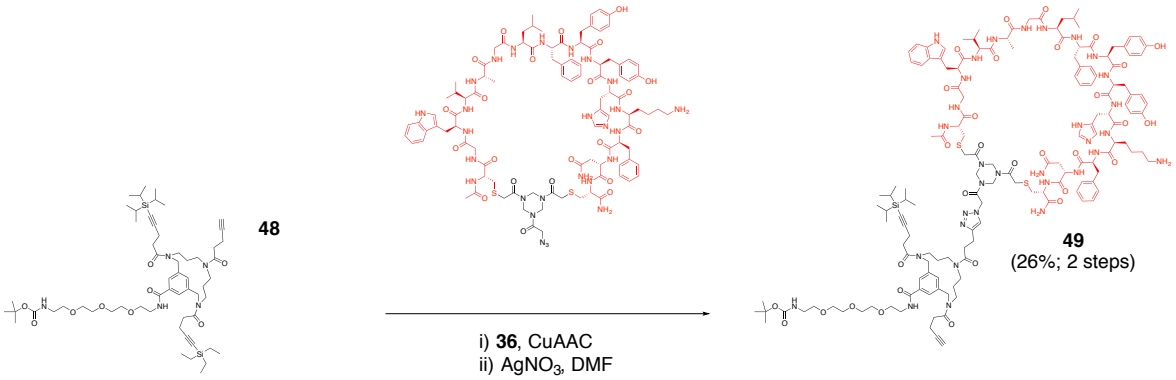

Scheme 4.9. Installing the second cyclic peptide **37** on TAC-scaffold **49**, followed by removal of the TIPS-group.

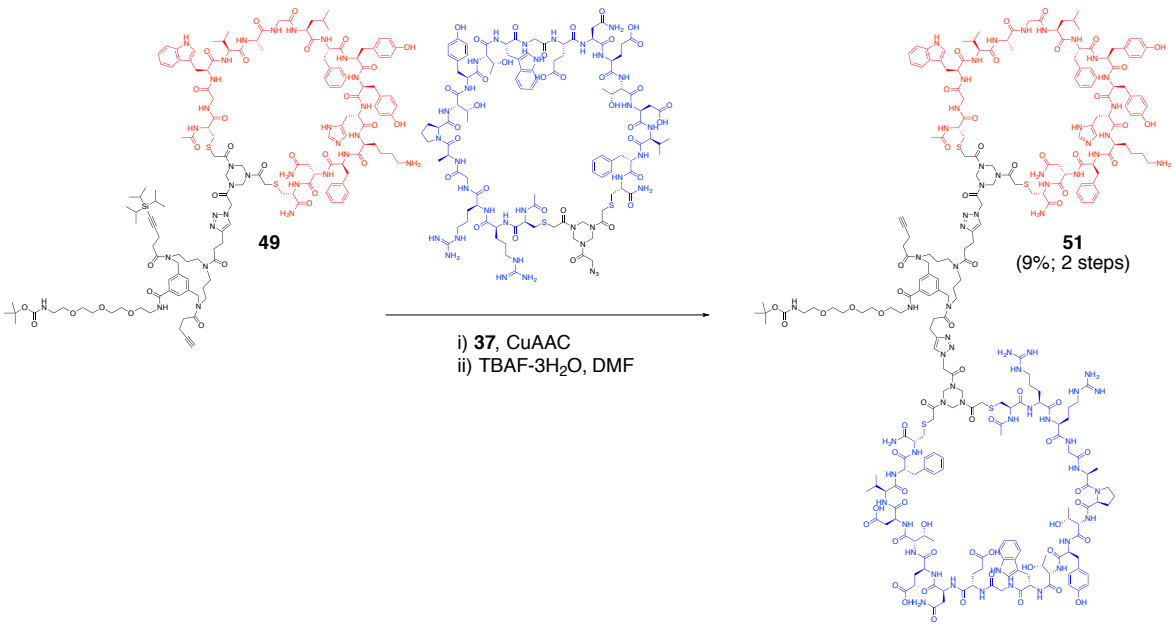

Scheme 4.10. Installing the third cyclic peptide **35** on TAC-scaffold **51**, followed by removal of the Boc-group.

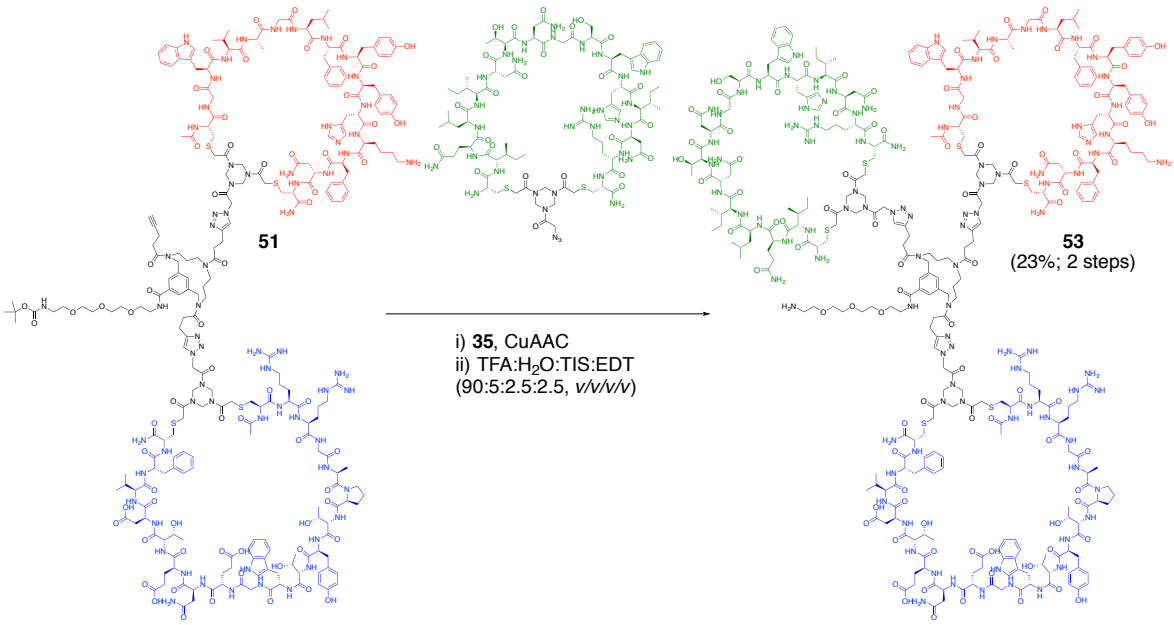

4.2.8 Elicitation of anti-HCV E2 glycoprotein antibodies

The biological relevance of our continuous **39-41** and discontinuous **53** epitope mimics as synthetic vaccines was investigated by performing an immunization experiment. The first question we wanted to address was if our synthetic vaccines could elicit an anti-HCV E2 glycoprotein antibody response *in vivo*. To do this the epitope mimics had to be conjugated to a suitable carrier protein, which could be done through the incorporated thiol- and amine- linkers on the epitope mimics. mcKLH is a stable and efficient carrier protein that is known to produce a strong immune response.[36]

Continuous epitope mimics **39**, **40**, and **41** were conjugated on maleimide-activated mcKLH protein through thiol-maleimide conjugation using an Imject® maleimide activated carrier protein spin kit (Figure 4.3). Discontinuous epitope mimic **53** could not be obtained with a similar thiol linker and was prepared with a free amine instead, which was conjugated on mcKLH via amide bond formation using an Imject® 1-ethyl-3-[3-dimethylaminopropyl]carbodiimide hydrochloride (EDC) carrier protein spin kit (Figure 4.4). Thiol-maleimide conjugation does not result in cross-linking of the constructs and carrier-protein, instead each maleimide reacts selectively and exclusively with one copy of epitope mimic. In contrast to conjugation via amide bond formation, extensive cross-linking through carrier-protein and discontinuous epitope mimic **53** is possible due to the

numerous available carboxylic acids and free-amines on mcKLH. In addition to the installed amine linker, discontinuous epitope mimic **53** contains a free N-terminus in cyclic peptide **35** and a Lysine at position 446 in cyclic peptide **36** that are also susceptible to amide bond formation by EDC. This prevents selective conjugation of discontinuous epitope mimic **53** to mcKLH via the amine linker alone. Instead, it is probable that conjugation to mcKLH occurs unselectively via one, two, or all three of the available free amines.

Sera were obtained from a single immunization experiment of four groups of animals (n = number of animals per group) treated with epitope mimics **39**-mcKLH (group O; n =3), **40**-mcKLH (group P; n =3), **41**-mcKLH (group Q; n = 3), and **53**-mcKLH (group R; n =3 however one animal expired due to causes unrelated to the immunization). Sera were evaluated by ELISA against surfaces coated with HCV soluble E2 (sE2) glycoprotein for the presence of anti-HCV E2 glycoprotein antibodies (Figure 4.5). Broadly neutralizing monoclonal antibody AP33[21] was included within the ELISA as a positive control.

These results have been obtained from a single immunization experiment, including a relatively small number of animals. As a consequence, the results just allowed for a very preliminary view of the potential of the synthesized epitope mimics. Evidently, more immunization experiments are required on a larger scale to properly validate the potential of the epitope mimics presented here.

The signal observed for binding of monoclonal antibody (mAb) AP33 has to be considered carefully when comparing to the signal observed for binding of antibodies in the obtained sera. Since mAb AP33 is available in a stock solution of known concentration it was possible to generate a distinct serial dilution of set concentration ranges. In contrast, the antibody concentration in the obtained sera was unknown and should not be compared directly to mAb AP33.

Nevertheless, group Q – epitope III (**41**-mcKLH) has elicited a strong anti-HCV E2 glycoprotein antibody response in all three animals that is comparable with broadly neutralizing mAb AP33. Group O – epitope I (**39**-mcKLH) would suggest an anti-HCV E2 glycoprotein antibody response in two of the three animals, but did not appear significantly different compared to the pre-immunization test bleed (PB). In contrast, group P – epitope II (**40**-mcKLH) and group R – scaffold (**53**-mcKLH) did not appear to have elicited an anti-HCV E2 glycoprotein antibody response.

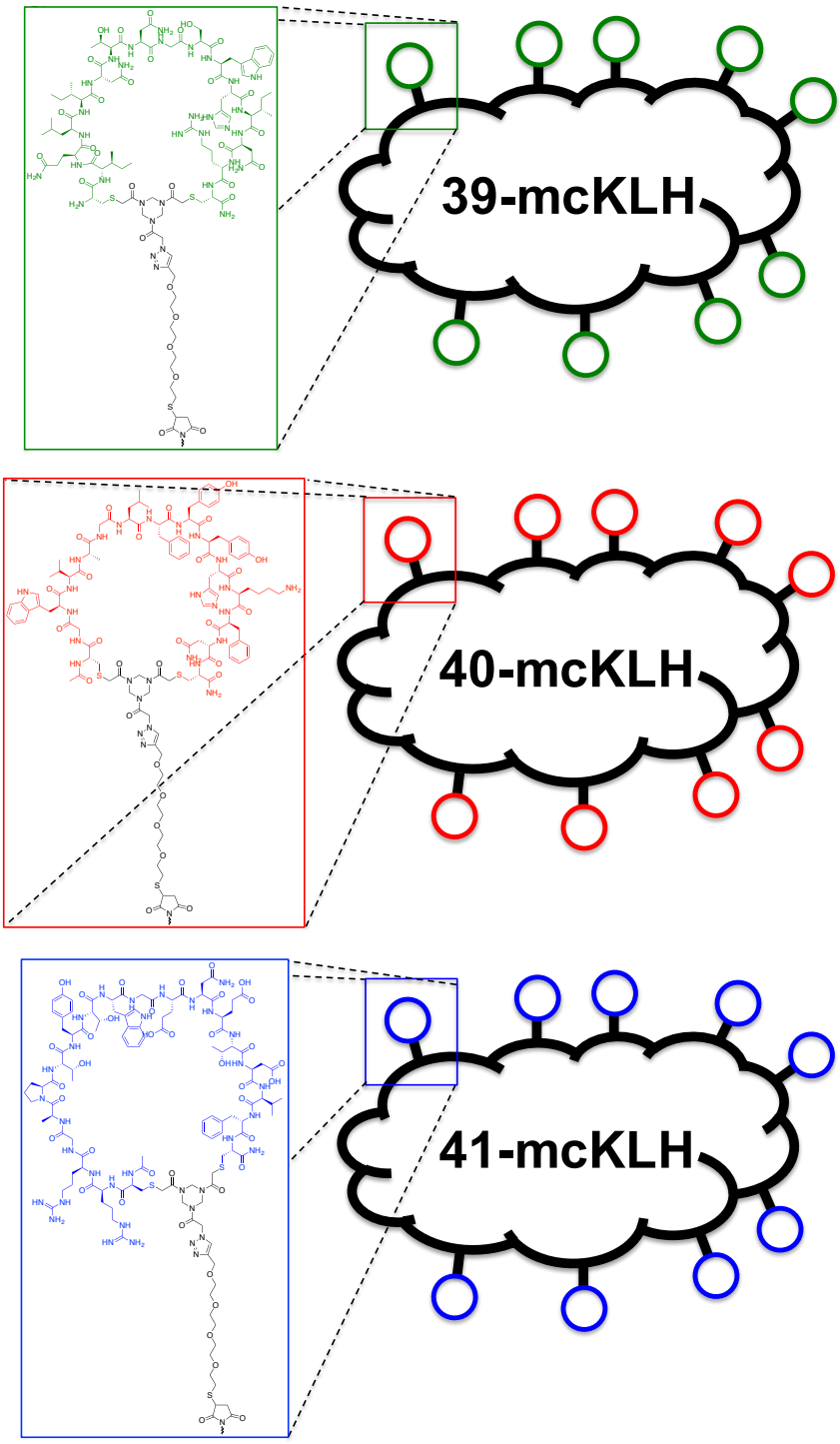

Figure 4.3. Continuous epitope mimics **39**, **40**, and **41** are presented separately on mcKLH using thiol-maleimide conjugation.

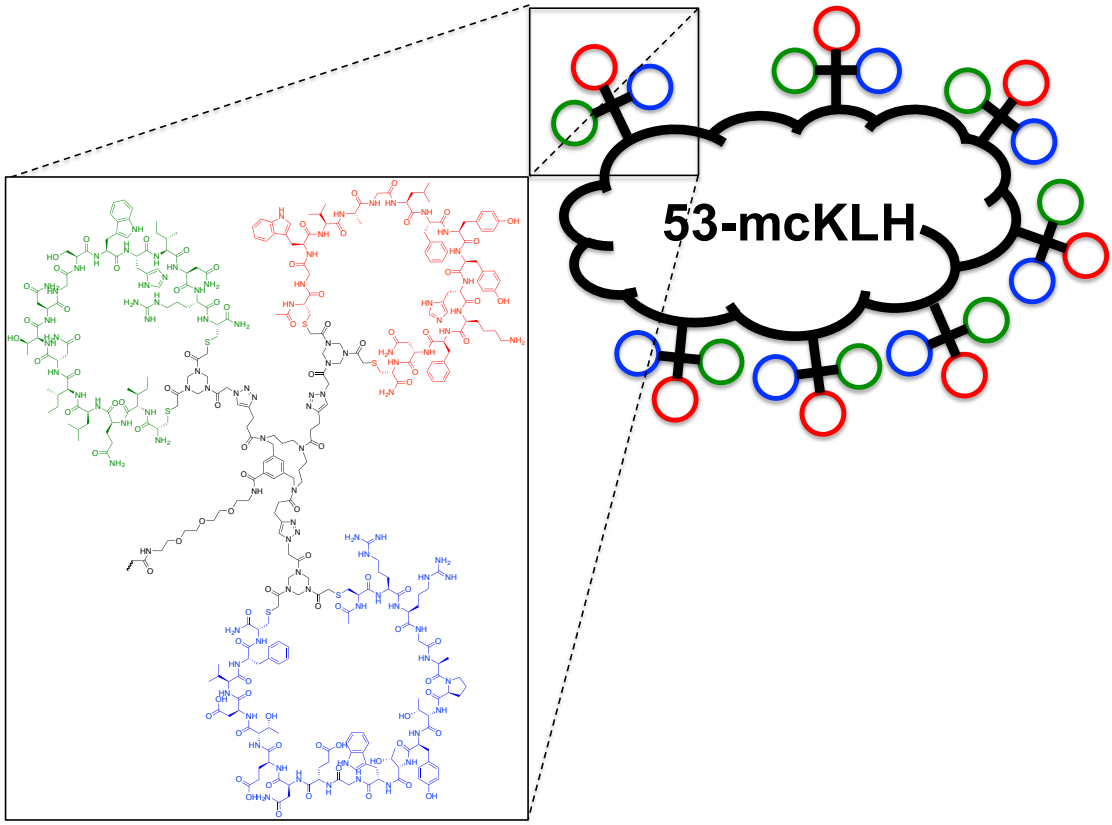

Figure 4.4. Discontinuous epitope mimic **53** is presented on mcKLH using EDC amide bond formation.

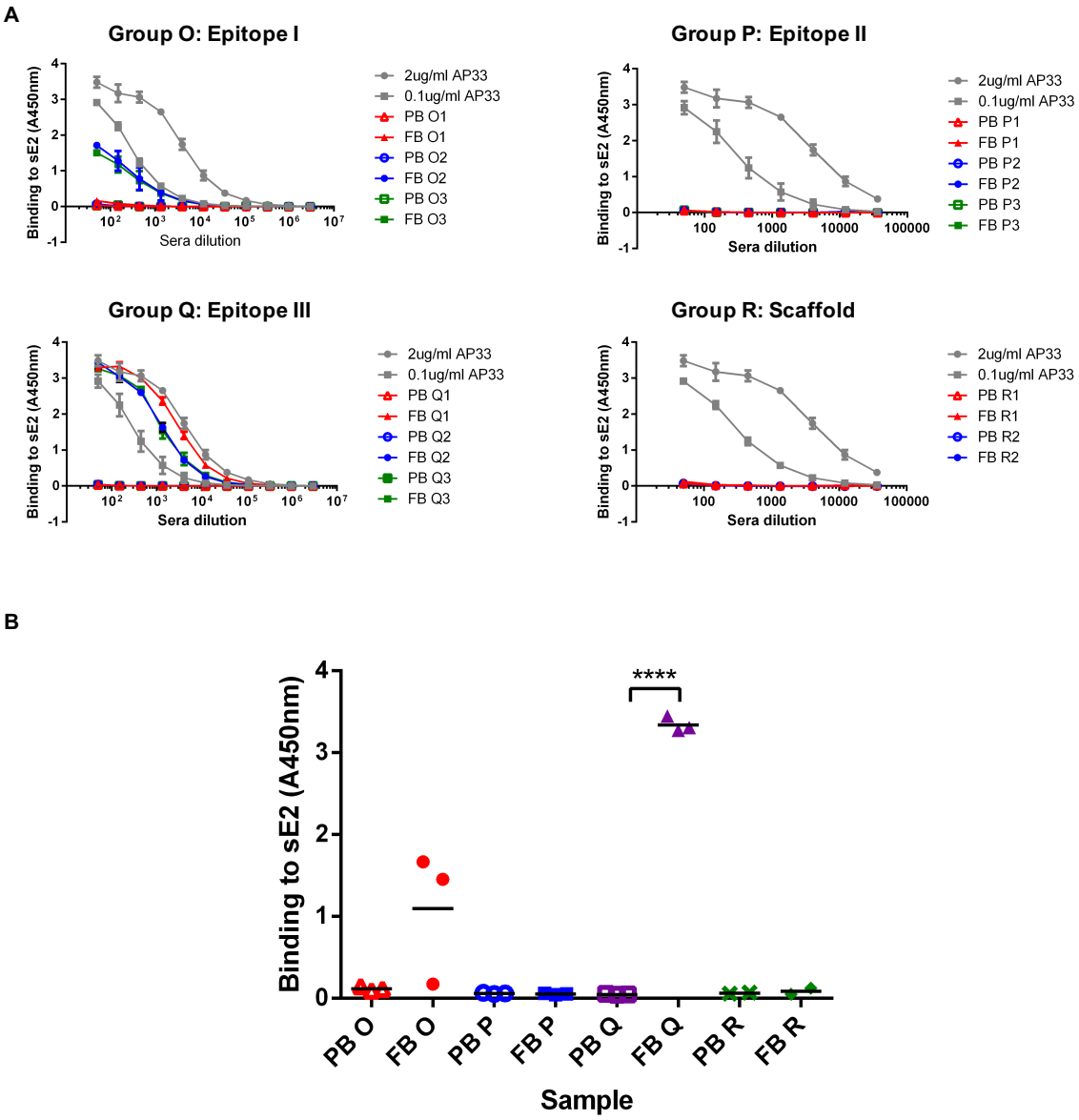

Figure 4.5. ELISA of immobilized sE2 against sera obtained from the final bleed (FB). Including: group O – epitope I (**39**-mcKLH); group P – epitope II (**40**-mcKLH); group Q – epitope III (**41**-mcKLH); group R – scaffold (**53**-mcKLH). Sera obtained from the pre-immunization bleed (PB) were included as a negative control. Monoclonal antibody AP33 was included as positive control. (**A)** Three-fold dilutions, including: FB (starting dilution of 1:50); PB (starting dilution of 1:50); AP33 (starting concentrations of 2.0 µg/mL and 0.1 µg/mL). O1, P1, Q1, R1, etc. refer to an individual animal in the corresponding group. (**B**) Absorbance of FB and PB at a 1:50 dilution, each dot indicates serum per animal. The ELISA was performed in triplicate, with the exception of group O – epitope I (**39**-mcKLH) that was done in duplicate. Background signal (no mAb) was subtracted. Error bars represent the standard error of the mean. The data was obtained and the Figure provided by collaborators of the MRC-University of Glasgow Centre for Virus Research.

In the field of epitope mimicry there is much to be considered with respect to epitope design. Optimization of the synthetic peptide sequence, length, loop size, and location of the non-native cysteines for cyclization can translate to better mimicry. For example, group Q – epitope III (**41**-mcKLH) did result in a strong *in vivo* anti-HCV E2 antibody response. The peptide sequence corresponds to an elongated version based on epitope III that was shifted more towards the N-terminus of the HCV-E2 glycoprotein and included more key-binding residues associated with neutralizing antibodies.[26] The epitope design presented here was rationalized based on previous *in vitro* studies (see Chapter 2 and Chapter 3)[33,35] that indicated accurate mimicry, with the non-native cysteines incorporated at the N-terminus and C-terminus as to preserve the native continuous amino acid sequence. The question remains as to why this design did not translate to a strong elicitation of an *in vivo* anti-HCV E2 antibody response for group group O – epitope I (**39**-mcKLH) and group P – epitope II (**40**-mcKLH).

One aspect could be that HCV-E2 contains 11 *N*-linked glycans, of which two are located in epitope I (Asn-417, Asn-423), one is located in epitope II (Asn-448), and two are located in epitope III (Asn-532, Asn-540). However, since these glycosylation sites are known to shift and modulate virus neutralization, it was decided not to consider these in the epitope design.[37] The rationale being that by keeping the design as simple as possible, there would be a higher likelihood of inducing a neutralizing antibody response that would be resistant to escape. Although, Pierce *et al.*[38] successfully elicited a neutralizing anti-HCV E2 antibody response using a mono-glycosylated cyclic peptide based on epitope I. In contrast, Sandomenico *et al.*[39] used a non-glycosylated cyclic peptide based on epitope I that did not result in a neutralizing anti-HCV E2 antibody response. Introducing *N*-linked glycans could be required for a more accurate design of epitope mimics. However, group Q – epitope III (**41**-mcKLH) did elicit a strong anti-HCV E2 antibody response without incorporation of *N*-linked glycans. In turn, this suggests that there is a degree of ambiguity between the importance of various *N*-linked glycans.

The design of discontinuous epitope mimic **53** was considerably more ambitious, with respect to a mimic that presents all the different substructures of a larger immunogenic region of HCV-E2. Multiple neutralizing antibodies have been found to bind residues spread across epitopes I, II, and III.[26] Despite discontinuous epitope mimic **53** being considerably more complex in design, its mimicry was not validated *in vitro* as was done for continuous epitope mimics **39** and **40** by ELISA (see Chapter 2 and Chapter 3)[33,35]. The reason for this was that discontinuous epitope mimic **53** could only be obtained with an

amine handle for conjugation, which was incompatible with the previously used maleimide-activated plates for ELISA (Chapter 2 and Chapter 3) [33,35]. In addition, discontinuous epitope mimic **53** contains three free amines that prevents selective conjugation in a single orientation and would most likely result in cross-linking. In the absence of any prior validation of the mimicry of discontinuous epitope mimic **53**, it could be considered unlikely to elicit an anti-HCV E2 antibody response. Indeed, no anti-HCV E2 antibody response was observed for group R – scaffold (**53**-mcKLH). At the very least, conventional ELISA studies, in which discontinuous epitope mimic **53** would be adsorbed to polystyrene plates, should have been performed using mAbs AP33[21] and/or HC84.1[24] known to bind epitopes I and II, respectively. This would have provided some validation of its mimicry, because discontinuous epitope mimic **53** contains peptide sequences based on epitope I and epitope II, it should bind mAbs AP33 and/or HC84.1. Additional experiments could be suggested to highlight the importance of the TAC scaffold for inducing the proper spatial orientation of epitopes I, II, and III. These include a comparison between a mixture of continuous epitope mimics **39**, **40**, and **41** versus discontinuous epitope mimic **53** by ELISA and elicitation of anti-HCV E2 glycoprotein by immunization.

Another aspect that could be considered is that the conjugation of continuous epitope mimics **39** and **40**, and discontinuous epitope mimic **53** to mcKLH was unsuccessful. This could have been analysed by conventional ELISA studies, in which the conjugated mcKLH would be adsorbed to polystyrene plates, using mAbs AP33 and/or HC84.1 known to bind epitopes I and II, respectively. Since discontinuous epitope mimic **53** contains peptide sequences based on epitope I and epitope II, it should bind mAbs AP33 and/or HC84.1 when properly presented on mcKLH.

Despite the very preliminary nature of the obtained results, there is definitely promise for use of peptide-based synthetic vaccines. In the current study, a single cyclic peptide construct (**41**-mcKLH; group O) was capable of eliciting antibodies that recognize the HCV-E2 glycoprotein. However, it remains unknown whether these antibodies are functional in the sense that they can neutralize HCV.

4.3 Conclusions

In conclusion, we have been able to obtain a complex fully synthetic discontinuous epitope mimic based on the HCV-E2 glycoprotein using a modified orthogonally protected trialkyne TAC-scaffold. The modification included a flexible linker that was used to conjugate the discontinuous epitope mimic onto mcKLH through amide bond formation. In addition, we have re-synthesized our previously developed continuous epitope mimics and attached these to mcKLH through thiol-maleimide conjugation. Both continuous and discontinuous epitope mimics were subjected to an immunization experiment to try and obtain anti-HCV E2 glycoprotein antibodies. In this way we have investigated the validity our epitope mimics as potential synthetic vaccines.

We have attempted to modify the TAC-scaffold with a similar trityl-protected thioether linker, which was previously found to be successful for our continuous epitope mimics. This would then be used to attach our discontinuous epitope mimic to mcKLH through thiol-maleimide conjugation as was done for the continuous epitopes. However, we found that the trityl-protected thioether was not compatible with CuAAC in the case of the TAC-scaffold due to instability of the trityl-group.

The singular and small-scale immunization experiment indicated that a single cyclic peptide construct (**41**-mcKLH) elicited a strong anti-HCV E2 glycoprotein antibody response. Thereby, preliminarily validating epitope mimicry as a potentially promising strategy towards vaccine design. However, to fully validate this and the potential of the other epitope mimics, more immunization studies will have to be carried out on a larger scale. In addition, further research is needed to show whether the observed antibody response can neutralize HCV and prevent infection.

4.4 Future work

Despite the considerable progress made within this work, there is still a lot of future work to be considered. First and foremost, the designed discontinuous epitope mimic should be properly studied *in vitro* before progressing to *in vivo* studies as suggested above. In addition, optimization of the designed continuous epitope mimics by varying the peptide sequence, length, loop size, and location of the non-native cysteines for cyclization could be explored.

Never the less, we have been able to obtain anti-HCV E2 glycoprotein antibodies by immunization. However, the results obtained so far are from a single small-scale immunization experiment that needs to be repeated numerous times on a larger scale to provide significant results. Also, we do not know where the elicited antibodies bind the HCV-E2 glycoprotein or if these antibodies are capable of reducing HCV infectivity. To address these questions additional experiments will be needed in the form of additional immunization studies and binding studies including our epitope mimics and multiple recombinant E2 glycoproteins. Neutralization experiments using HCV pseudo-particles (HCVpp), in which the infectivity of HCV-type particles treated with sera are compared to untreated, will be needed to indicate the level of neutralization of the obtained antibodies.

The key-feature of a vaccine is to not only elicit an antibody response *in vivo*, but this response must also result in protection against HCV infection *in vivo*. The lack of small animal models for HCV makes this very challenging. Instead, the elicited antibody response *in vivo* is generally further researched *in vitro* using cell culture models and HCVpp. Infectious HCVpp can be generated by assembling E1 and E2 glycoproteins onto retroviral core proteins, including a green fluorescent protein (GFP) as a marker to monitor infection.[40] For example, by transfection of human 293T cells with three separate expression vectors encoding HCV E1 and E2, murine leukemia virus (MLV) Gag-Pol core proteins, and a packaging competent MLV-derived genome encoding GFP.[40] Retroviruses are excellent platforms for assembly of HCVpp because their core proteins support incorporation of various different cellular and viral glycoproteins, as well as package and integrate genetic markers like GFP.[41-44] Future work would involve the generation of infectious HCVpp to investigate whether the obtained antibodies are capable to prevent infection *in vitro*.

From a chemistry point of view, future work could include the use of different scaffold molecules like the cyclotriveraltrylene (CTV)[30] scaffold in synthesizing discontinuous epitope mimics. Various different discontinuous epitope mimics could be synthesized and tested by varying the order in which the cyclized azido-peptides are incorporated onto the scaffold. As mentioned before, the EDC conjugation of our designed epitope mimic **53** possibly resulted in crosslinking that could have hindered its immunogenicity. Perhaps an alternative and selective conjugation strategy could be used, similar to the selectivity of the maleimide-thiol conjugation, to improve its immunogenicity. The influence of the linker length of the epitope mimics could be further investigated. Alternative sequences, for example epitope IV could be readily investigated using the approaches provided within this thesis.

4.5 Experimental section

General procedure. All reagents and solvents were used as received. Fmoc-amino acids were obtained from Activotec (Cambridge, United Kingdom) and *N*,*N*,*N*′,*N*′-Tetramethyl-*O*-(6-chloro-1*H*-benzotriazol-1-yl)uranium hexafluorophosphate (HCTU) was obtained from Matrix Innovation (Quebec, Canada). Tentagel S RAM resin (particle size 90μm, capacity 0.25 $mmol.g^{-1}$) was obtained from IRIS Biotech (Marktredwitz, Germany). Methyl *tert*-butyl ether (MTBE), Hexane (HPLC grade) and TFA were obtained from Aldrich (Milwaukee, USA). DMF (Peptide grade) was obtained from VWR (Lutterworth, United Kingdom). Piperidine, D*i*PEA were obtained from AGTC Bioproducts (Hessle, United Kingdom) and 1,2-ethanedithiol (EDT) was obtained from Merck (Darmstadt, Germany). HPLC grade CH_2Cl_2 and acetonitrile were obtained from Fischer Scientific (Loughborough, United Kingdom). Solid phase peptide synthesis was performed on a PTI Tribute-UV peptide synthesizer. Lyophilizations were performed on a Christ Alpha 2-4 LD*plus* apparatus. Reactions were carried out at ambient temperature unless stated otherwise. Solvents were evaporated under reduced pressure at 40°C. Reactions in solution were monitored by TLC analysis and R_f-values were determined on Merck pre-coated silica gel 60 F-254 (0.25 mm) plates. Spots were visualized by UV-light and permanganate stain. Column chromatography was performed on Siliaflash P60 (40-63μm) from Silicycle (Canada) or on a Biotage Isolera One purification system using prepacked silica (KP-SIL) Biotage SNAP cartridges. ^{1}H NMR data was acquired on a Bruker 400 MHz spectrometer in $CDCl_3$ as solvent. Chemical shifts (δ) are reported in parts per million (ppm) relative to trimethylsilane (TMS, 0.00 ppm). Analytical high-pressure liquid chromatography (HPLC) was carried out on a Shimadzu instrument comprising a communication module (CBM-20A), autosampler (SIL-20HT), pump modules (LC-20AT), UV/Vis detector (SPD-20A) and system controller (Labsolutions V5.54 SP), with a Phenomenex Gemini C18 column (110 Å, 5 μm, 250×4.60 mm) or Dr. Maisch Reprosil Gold 200 C18 (5 μm, 250×4.60 mm). UV measurements were recorded at 214 and 254 nm, using a standard protocol: 100% buffer A (acetonitrile/H_2O 5:95 with 0.1% TFA) for 2 minutes followed by a linear gradient of buffer B (acetonitrile/H_2O 95:5 with 0.1% TFA) into buffer A (0-100% or 0-50%) over 30 minutes at a flow rate of 1.0 $mL{\cdot}min^{-1}$. Liquid chromatography mass spectrometry (LCMS) was carried out on a Thermo Scientific LCQ Fleet quadrupole mass spectrometer with a Dionex Ultimate 3000 LC using a Dr. Maisch Reprosil Gold 120 C18 column (110 Å, 3 μm, 150×4.0 mm) and the same linear gradients of buffer B into buffer A, flowrate and buffers as described for the analytical HPLC. Purification of the peptidic

compounds was performed on an Agilent Technologies 1260 infinity preparative system using both UV and ELSD detectors with a Dr. Maisch Reprosil Gold 200 C18 (10 µm, 250×20 mm). Auto-collection of fractions was used based on the UV measurements at 214 nm, using customized protocols using the same buffers as described for the analytical HPLC.

Pentynoic acid amidated TAC-scaffold (14). Was synthesized and kindly provided by Dr. Anna Mickowska according to the literature procedure of Werkhoven *et al.*[32] t_R = 26.7 min; HRMS: calculated *m/z* for $C_{41}H_{40}N_4O_9S$: 787.2414 $[M+Na]^{1+}$; found 787.2378. LRMS: calculated *m/z* for $C_{41}H_{40}N_4O_9S$: 765.26 $[M+H]^{1+}$; found 765.17.

***tert*-butyl pent-4-yonate (16).** All steps were performed under N_2 atmosphere. 4-pentynoic acid **8** (3.1 g, 32 mmol, 1.0 equiv.) was dissolved in anhydrous CH_2Cl_2 (100 mL), followed by the addition of *tert*-butyl 2,2,2-trichloro acetamide **15** (8.5 mL, 48 mmol, 1.5 equiv.). The resulting reaction was stirred overnight at room temperature. The next morning, the trichloroacetamide precipitate **17** was filtered off over Celite®. The filtrate was concentrated *in vacuo*, followed by purification via automated flash gel chromatography (CH_2Cl_2) and visualized with a potassium permanganate stain. Pure *tert*-butyl pent-4-yonate **16** (4.0 g, 26 mmol, 81%) was obtained as a clear yellowish oil. R_f = 0.79 (CH_2Cl_2); ^{1}H-NMR (400 MHz, $CDCl_3$): δ = 2.41 (m, 4H, C*H*$_2$C*H*$_2$), 1.93 (m, 1H, C*H*), 1.42 (s, 9H, C(C*H*$_3$)$_3$) ppm; ^{13}C-NMR (101 MHz, $CDCl_3$): δ = 171.0 (*t*BuOO*C*), 82.7 (*C*CH), 80.7 (*C*(CH$_3$)$_3$), 68.7 (*C*H), 34.5 (*t*BuOO*C*H$_2$), 28.0 (C(*C*H$_3$)$_3$), 14.4 (*t*BuOOCH$_2$*C*H$_2$) ppm; HRMS: calculated *m/z* for $C_9H_{14}O_2$: 177.0892 $[M+Na]^{1+}$; found 177.0881.

***tert*-butyl 5-(triisopropylsilyl)-pent-4-yonate (19).** This synthesis was carried out as described by Werkhoven *et al.*[32]

All steps were performed under N_2 atmosphere. *tert*-butyl pent-4-yonate **16** (1.0 g, 6.5 mmol, 1.0 equiv.) was dissolved in anhydrous THF (20 ml) and the resulting solution was cooled to -78°C using a dry ice and acetone bath. After which, n-BuLi (2.6 mL, 2.5 M in hexane, 6.5 mmol, 1.0 equiv.) was added in dropwise fashion. The reaction was allowed to stir for 10 minutes, followed by replacing the dry ice and acetone bath by an ice bath (0°C). Then, TIPS-Cl **18** (1.7 mL, 7.9 mmol, 1.2 equiv.) was added dropwise to the reaction mixture. The reaction was stirred for 3 hours at room temperature, while being monitored by TLC (5% EtOAc in petroleum ether 40-60°C) and visualized with a

potassium permanganate stain. After which, despite not being fully completed, a saturated aqueous solution of NH_4Cl (40 mL) was added to quench the reaction. Next, THF was removed *in vacuo* and the resulting aqueous residue was diluted with H_2O (50 mL). The aqueous residue was extracted with EtOAc (3 x 30 mL) and the combined EtOAc-layers were dried over $MgSO_4$ and filtered. The filtrate was concentrated *in vacuo* and purified by automated flash column chromatography using a linear gradient (0-10% Et_2O in hexane over 10 column volumes) and visualized with a potassium permanganate stain. Pure *tert*-butyl 5-(triisopropylsilyl)-pent-4-yonate **19** (1.1 g, 3.5 mmol, 54%) was obtained as an orange oil. R_f = 0.47 (5% EtOAc in petroleum ether 40-60°C); ^{1}H-NMR (400 MHz, $CDCl_3$): δ = 2.48 (m, 4H, CH_2CH_2), 1.44 (s, 9H, C(CH_3))$_3$, 1.04 (m, 21H, Si(CH(CH_3)$_2$)$_3$) ppm; ^{13}C-NMR (101 MHz, $CDCl_3$): δ = 171.1 (*t*BuOO*C*), 107.1 (*C*CSi), 80.8 (*C*(CH$_3$)$_3$ or CCSi), 80.6 (*C*(CH$_3$)$_3$ or CCSi), 35.2 (*t*BuOOC*C*H$_2$), 28.1 (C(*C*H$_3$)$_3$), 18.6 (Si(CH(*C*H$_3$)$_2$)$_3$), 15.9 (*t*BuOOCCH$_2$*C*H$_2$), 11.2 (Si(*C*H(CH$_3$)$_2$)$_3$) ppm; HRMS: calculated *m/z* for $C_{18}H_{34}O_2Si$: 333.2226 [*M*+Na]$^{1+}$; found 333.2208.

***tert*-butyl 5-(triethylsilyl)-pent-4-yonate (21).** All steps were performed under N_2 atmosphere. *tert*-butyl- pent-4-yonate **16** (3.9 g, 25 mmol, 1.0 equiv.) was dissolved in anhydrous Et_2O (50 mL) and the resulting solution was cooled to -78°C using a dry ice and acetone bath. After which, LDA (13 mL, 2 M in hexane, 26 mmol, 1.0 equiv.) was added in dropwise fashion. The reaction was allowed to stir for 10 minutes, followed by replacing the dry ice and acetone bath by an ice bath (0°C). Then, TES-Cl **20** (6.4 mL, 38 mmol) was added dropwise to the reaction mixture. The reaction was stirred for 3 hours at room temperature, followed by addition of a saturated aqueous solution of NH_4Cl (100 mL) to quench the reaction. After which, the aqueous and organic layers were separated. The aqueous layer was extracted with Et_2O (3 x 50 mL) and the combined Et_2O-layers were dried over $MgSO_4$ and filtered. The filtrate was concentrated *in vacuo* and manual purified by silica gel column chromatography using a linear gradient (0-1% Et_2O in pentane) and visualized with a potassium permanganate stain. Pure *tert*-butyl 5-(triisopropylsilyl)-pent-4-yonate **21** (3.4 g, 13 mmol, 52%) was obtained as an orange oil. R_f = 0.43 (5% EtOAc in petroleum ether 40-60°C); ^{1}H-NMR (400 MHz, $CDCl_3$): δ = 2.47 (m, 4H, CH_2CH_2), 1.44 (s, 9H, C(CH_3)$_3$, 0.96 (t, $^3J_{HH}$ = 7.9 Hz, 9H, Si(CH$_2$CH_3)$_3$), 0.55 (q, $^3J_{HH}$ = 7.9 Hz, 6H, Si(CH_2CH$_3$)$_3$) ppm; ^{13}C-NMR (101 MHz, $CDCl_3$): δ = 171.1 (*t*BuOO*C*), 106.5 (*C*CSi), 82.2 (*C*(CH$_3$)$_3$ or CCSi), 80.6 (*C*(CH$_3$)$_3$ or CCSi), 35.0 (*t*BuOOC*C*H$_2$), 28.1 (C(*C*H$_3$)$_3$), 16.0 (*t*BuOOCCH$_2$*C*H$_2$), 7.4 (Si(CH$_2$*C*H$_3$)$_3$), 4.5 (Si(*C*H$_2$CH$_3$)$_3$) ppm; HRMS: calculated *m/z* for $C_{15}H_{28}O_2Si$: 291.1757 [*M*+Na]$^{1+}$; found 291.1749.

5-(triisopropylsilyl)-4-pentynoic acid (22). This synthesis was carried out as described by Werkhoven *et al.*[32]

tert-butyl 5-(triisopropylsilyl)-pent-4-yonate **19** (1.1 g, 3.5 mmol, 1.0 equiv.) was dissolved in 15% TFA in SPS grade CH_2Cl_2 (50 mL) and the resulting reaction mixture was stirred for 2.5 hours at room temperature. After which, the reaction mixture was quenched using aqueous solution of 1.0 M NH_4OAc (100 mL). Next, the organic and aqueous layers were separated, followed by the extraction of the aqueous layer using CH_2Cl_2 (2 x 100 mL). Then, the combined organic layers were washed with brine (150 mL) and dried over $MgSO_4$. The resulting suspension was filtered and the filtrate was concentrated *in vacuo*, followed by purification using automated flash column chromatography with a linear gradient (0-10% Et_2O in hexane with 1% AcOH over 10 column volumes) and visualized with a potassium permanganate stain. Pure fractions containing product were combined and concentrated *in vacuo*. Residual AcOH was removed by dissolving purified 5-(triisopropylsilyl)-4-pentynoic acid **22** in CH_2Cl_2 (30 mL) and washing the resulting solution with a aqueous solution of 1.0 M $KHSO_4$ (50 mL), H_2O (50 mL), and brine (50 mL). After which, the organic layer was dried over MgSO4 and filtered. The filtrate was concentrated *in vacuo* to afford pure 5-(triisopropylsilyl)-4-pentynoic acid **22** (0.31 g, 1.2 mmol, 34%). R_f = 0.58 (30% EtOAc in petroleum ether 40-60°C supplemented with acetic acid); ^{1}H-NMR (400 MHz, $CDCl_3$): δ = 2.59 (m, 4H, CH_2CH_2), 1.05 (m, 21H, Si(CH(CH_3)$_2$)$_3$) ppm; ^{13}C-NMR (101 MHz, $CDCl_3$): δ = 177.6 (HOO*C*), 106.2 (*C*CSi), 81.7 (C*C*Si), 33.7 (HOOC*C*H$_2$), 18.6 (Si(CH(*C*H$_3$)$_2$)$_3$,, 15.7 (HOOCCH$_2$*C*H$_2$), 11.2 (Si(*C*H(CH$_3$)$_2$)$_3$) ppm; HRMS: calculated *m/z* for $C_{14}H_{26}O_2Si$: 277.1600 [*M*+Na]$^{1+}$; found 277.1600.

5-(triethylsilyl)-4-pentynoic acid (23). This synthesis was carried out as described by Werkhoven *et al.*[32]

tert-butyl 5-(triethylsilyl)-pent-4-yonate **21** (3.4 g, 13 mmol, 1.0 equiv.) was dissolved in 15% TFA in SPS grade CH_2Cl_2 (100 mlL and the resulting reaction mixture was stirred for 1.5 hours at room temperature. Upon completion of the reaction, determined by TLC (5% EtOAc in petroleum ether 40-60°C) and visualization with a potassium permanganate stain, the mixture was quenched using 1M aqueous solution of NH_4OAc (200 mL) for 1 hour. Next, the organic and aqueous layers were separated, followed by the extraction of the aqueous layer using CH_2Cl_2 (2 x 100 mL). Then, the combined organic layers were washed with brine (150 mL) and dried over $MgSO_4$. The resulting suspension was filtered

and the filtrate was concentrated *in vacuo*, followed by manual purification using silica gel column chromatography with a linear gradient (0-10% Et_2O in hexane with 1% AcOH) and visualized with a potassium permanganate stain. Pure fractions containing product were combined and residual AcOH was removed by washing with H_2O (2 x 50 mL). The aqueous layer was back-extracted using CH_2Cl_2 (2 x 100 mL). Next, the combined organic layers were dried over $MgSO_4$ and filtered. The filtrate was concentrated *in vacuo*, which afforded pure 5-(triethylsilyl)-4-pentynoic acid **23** (0.80 g, 3.8 mmol, 29%). R_f = 0.58 (30% EtOAc in petroleum ether 40-60°C supplemented with acetic acid); R_f = 0.50 (30% EtOAc in petroleum ether 40-60°C supplemented with acetic acid) ^{1}H-NMR (400 MHz, $CDCl_3$): δ = 2.58 (m, 4H, C*H*$_2$C*H*$_2$), 0.96 (t, $^3J_{HH}$ = 7.9 Hz, 9H, Si(CH$_2$C*H*$_3$)$_3$), 0.56 (q, $^3J_{HH}$ = 7.9 Hz, 6H, Si(C*H*$_2$CH$_3$)$_3$) ppm; ^{13}C-NMR (101 MHz, $CDCl_3$): δ = 178.0 (HOO*C*), 105.6 (*C*CSi), 82.9 (C*C*Si), 33.6 (HOOC*C*H$_2$), 15.6 (HOOCCH$_2$*C*H$_2$), 7.4 (Si(CH$_2$*C*H$_3$)$_3$), 4.4 (Si(*C*H$_2$CH$_3$)$_3$) ppm; HRMS: calculated *m/z* for $C_{11}H_{20}O_2Si$: 235.1131 [*M*+Na]$^{1+}$; found 235.1115.

Orthogonally protected trialkyne TAC-scaffold (25). This synthesis was carried out as described by Werkhoven *et al.*[32]

Pentynoic acid amidated TAC-scaffold **14** (0.42 g, 0.55 mmol, 0.60 equiv.) was dissolved in anhydrous CH_2Cl_2 (20 mL), followed by the addition of D*i*PEA (382 µL, 2.2 mmol, 2.4 equiv.). Next, 2-Cl-trityl chloride resin **24** (1.1 g, 0.91 mmol loading capacity, 1.0 equiv) was added to the reaction mixture. The resulting suspension was stirred overnight at room temperature. The following morning, D*i*PEA (1.0 mL, 5.7 mmol, 6.3 equiv.) and MeOH (4 mL) were added and the mixture was stirred for 30 minutes at room temperature. The resin was transferred to solid phase synthesis glassware and washed with MeOH (3 x 20 mL), Et_2O (3 x 20 mL), and dried under N_2.

Fmoc loading test: Three aliquots of resin were collected (±10 mg) to each of which 2% DBU in DMF (2.0 mL) was added. After 30 minutes, each resin was further diluted by addition of MeCN (10 mL). Of the resulting dilution 2.0 mL was taken and further diluted to a total volume of 25 mL by addition of MeCN. Next, the UV-absorption of 3.0 mL of the final dilution versus a blank reference solution was performed at 304 nm. Affording an average loading of 0.34 mmol/g (n = 3), which equalled to 0.36 mmol pentynoic acid amidated TAC-scaffold **14** that has been successfully loaded onto the resin.

First coupling: The resin was washed using CH_2Cl_2 (3 x 20 mL) and subsequently with DMF (3 x 20 mL). Next, 20% piperidine in DMF (20 mL) was added and the mixture was bubbled through with N_2 for 30 minutes at room temperature. After which, the resin was washed with DMF (3 x 20 mL) and CH_2Cl_2 (3 x 20 mL). Upon successful deprotection of the Fmoc, as determined by a positive bromophenol blue-test, the resin was washed with DMF (3 x 20 mL). Then, BOP (0.32 g, 0.72 mmol, 2.0 equiv.) and 5-(triisopropylsilyl)-4-pentynoic acid **22** (0.18 g, 0.71 mmol, 2.0 equiv.) were added to the resin, followed by DMF (20 mL). Lastly, D*i*PEA (290 µL, 1.7 mmol, 4.3 equiv.) was added to the reaction mixture, which was then stirred for 2 hours at room temperature. After which, the resin was washed with DMF (3 x 20 mL) and CH_2Cl_2 (3 x 20 mL). A negative bromophenol-blue test indicated successful instalment of 5-(triisopropylsilyl)-4-pentynoic acid **22**.

Second coupling: The resin was washed using DMF (3 x 20 mL). Next, 2-mercaptoethanol (255 µL, 3.6 mmol, 10 equiv.) and DBU (270 µL, 1.8 mmol, 5.0 equiv.) in DMF (20 mL) was added and the mixture was bubbled through with N_2 for 15 minutes (2x). After which, the resin was washed with DMF (3 x 20 mL) and CH_2Cl_2 (3 x 20 mL). Upon successful *o*NBS-deprotection, as determined by a positive bromophenol blue-test, the resin was washed with DMF (3 x 20 mL). Then, BOP (0.32 g, 0.72 mmol, 2.0 equiv.) and 5-(triisopropylsilyl)-4-pentynoic acid **23** (015 g, 0.71 mmol, 2.0 equiv.) were added to the resin, followed by DMF (20 ml). Lastly, D*i*PEA (250 µl, 1.4 mmol, 3.8 equiv.) was added to the reaction mixture, which was then stirred for 2 hours at room temperature. After which, the resin was washed with DMF (3 x 20 mL) and CH_2Cl_2 (3 x 20 mL). A negative bromophenol-blue test indicated successful instalment of 5-(triethylsilyl)-4-pentynoic acid **23**.

Cleavaging off the 2-Cl-trityl resin: The resin was transferred to a round bottom flask and 30% HFIP in CH_2Cl_2 (20 mL) was added. After stirring the mixture for 45 minutes at room temperature, the resin was filtered off and washed with CH_2Cl_2. The filtrate was collected and EtOAc (50 mL) was added, followed by removing the solvents *in vacuo*. Purification by automated flash column chromatography using a linear gradient (0-6% MeOH in CH_2Cl_2 over 12 column volumes), afforded pure orthogonally protected trialkyne TAC-scaffold **25** (0.26 g, 0.33 mmol, *quant.*). R_f = 0.39 (6% MeOH in CH_2Cl_2 supplemented with acetic acid); t_R = 35.6 min; ^{1}H-NMR (400 MHz, $CDCl_3$): δ = 8.00 (m, 2H, aryl-*H*), 7.44 (m, 1H, aryl-*H*), 4.66 (m, 4H, 2 x NC*H*$_2$-aryl), 3.45 (m, 4H, NC*H*$_2$CH$_2$C*H*$_2$N), 2.93 (m, 4H, NC*H*$_2$CH$_2$C*H*$_2$N), 2.70 (m, 8H, 2 x C*H*$_2$C*H*$_2$CCSi), 2.46 (m, 4H, C*H*$_2$C*H*$_2$CCH), 1.94 (m, 1H, CC*H*), 1.47 (m, 4H, 2 x NCH$_2$C*H*$_2$CH$_2$N), 1.06 (m, 21H, Si(C*H*(C*H*$_3$)$_2$)$_3$),

0.98 (t, $^{3}J_{HH}$ = 7.9 Hz, 9H, Si(CH$_2$C*H*$_3$)$_3$), 0.58 (q, $^{3}J_{HH}$ = 7.9 Hz, 6H, Si(C*H*$_2$CH$_3$)$_3$) ppm; ^{13}C-NMR (101 MHz, $CDCl_3$): δ = 131.7 (aryl-*C*H), 130.4 (aryl-*C*H), 128.9 (aryl-*C*H), 54.0 (N*C*H$_2$-aryl), 51.5 (N*C*H$_2$-aryl), 47.9 (N*C*H$_2$CH$_2$*C*H$_2$N), 46.0 (N*C*H$_2$CH$_2$*C*H$_2$N), 45.7 (N*C*H$_2$CH$_2$*C*H$_2$N), 43.5 (N*C*H$_2$CH$_2$*C*H$_2$N), 33.1 (C*H*$_2$C*H*$_2$CCSi), 33.0 (C*H*$_2$C*H*$_2$CCSi), 32.0 (*C*H$_2$*C*H$_2$CCH), 28.2 (NCH$_2$*C*H$_2$CH$_2$N), 28.2 (NCH$_2$*C*H$_2$CH$_2$N), 18.7 (Si(*C*H(*C*H$_3$)$_2$)$_3$), 16.3 (C*H*$_2$C*H*$_2$CCSi), 14.5 (*C*H$_2$*C*H$_2$CCH), 11.3 (Si(*C*H(*C*H$_3$)$_2$)$_3$), 7.5 (Si(CH$_2$*C*H$_3$)$_3$), 4.5 (Si(*C*H$_2$CH$_3$)$_3$) ppm; HRMS: calculated *m/z* for $C_{45}H_{69}N_3O_5Si_2$: 810.4674 [*M*+Na]$^{1+}$; found 810.4634. LRMS: calculated *m/z* for $C_{45}H_{69}N_3O_5Si_2$: 788.49 [*M*+H]$^{1+}$; found 788.58.

Tetraethylene glycol monotrityl thioether (26). Obtained as described in Chapter 2: Tetraethylene glycol monotrityl thioether **5**.[33]

Tetraethylene glycol monotrityl thioether p-toluenesulfonate (27). Tetraethylene glycol monotrityl thioether **26** (2.6 g, 5.8 mmol, 1.0 equiv.) was dissolved in anhydrous CH_2Cl_2 (50 mL). The resulting solution was cooled to 0°C using an ice bath, followed by addition of TEA (1.6 mL, 12 mmol, 2.1 equiv.). After 1 hour, ρ-toluenesulfonyl chloride **27** (2.3 g, 12 mmol, 2.1 equiv.) was added. The resulting reaction mixture was stirred overnight at room temperature. Upon completion of the reaction, as determined by TLC (50% EtOAc in petroleum ether 40-60°C), the mixture was washed with H_2O (100 mL). Next, the aqueous layer was back-extracted with CH_2Cl_2 (2 x 100 mL). Then, the combined organic layers were washed using brine (1 x 100 mL), dried over $MgSO_4$, and filtered. The filtrate was concentrated *in vacuo* and purified by automated flash column chromatography using a linear gradient (30-50% EtOAc in petroleum ether 40-60°C over 10 column volumes). Pure fractions were combined and concentrated *in vacuo*, affording pure tetraethylene glycol monotrityl thioether ρ-toluenesulfonate **28** (2.6 g, 4.3 mmol, 74%) as a yellowish oil. R_f = 0.52 (50% EtOAc in petroleum ether 40-60°C); t_R = 46.6 min; ^{1}H-NMR (400 MHz, $CDCl_3$): δ = 7.79 (d, $^{3}J_{HH}$ = 8.2 Hz, 2H, aryl *o*-*H*), 7.41 (m, 6H, trityl *o*-*H*), 7.32 (d, $^{3}J_{HH}$ = 8.2 Hz, 2H, aryl *m*-*H*), 7.28 (m, 6H, trityl *m*-*H*), 7.21 (m, 3H, trityl *p*-*H*), 4.14 (t, $^{3}J_{HH}$ = 4.8 Hz, 2H, TsOC*H*$_2$), 3.66 (t, $^{3}J_{HH}$ = 4.8 Hz, 2H, TsOCH$_2$C*H*$_2$), 3.53 (m, 6H, 3xC*H*$_2$), 3.43 (m, 2H, C*H*$_2$), 3.30 (t, $^{3}J_{HH}$ = 6.9 Hz, 2H, SCH$_2$C*H*$_2$), 2.43 (t, $^{3}J_{HH}$ = 6.9 Hz, 2H, SC*H*$_2$), 2.43 (s, 3H, C*H*$_3$) ppm; ^{13}C-NMR (101 MHz, $CDCl_3$): δ = 144.8 (aryl-*C*), 144.7 (aryl-*C*), 133.1 (aryl-*C*), 130.1 (aryl-*C*), 129.8 (aryl *m*-*C*H), 129.6 (trityl *o*-*C*H), 128.0 (aryl *o*-*C*H), 127.9 (trityl *m*-*C*H), 126.6 (trityl *p*-*C*H), 70.7 (*C*H$_2$), 70.5 (*C*H$_2$), 70.5 (*C*H$_2$), 70.2 (*C*H$_2$), 69.6 (SCH$_2$*C*H$_2$), 69.2 (TsO*C*H$_2$), 68.7 (TsOCH$_2$*C*H$_2$), 66.6 (*C*S), 31.7

(S*C*H$_2$), 21.6 (*C*H$_3$) ppm; HRMS: calculated *m/z* for $C_{34}H_{38}O_6S_2$: 629.2008 [*M*+Na]$^{1+}$; found 629.1996.

Triethylene glycol monotrityl thioether ethylamine (29). ρ-toluenesulfonate tetraethylene glycol monotrityl thioether **28** (2.6 g, 4.3 mmol, 1.0 equiv.) was dissolved in MeCN (100 mL), followed by the addition of aqueous 25% ammonia (50 mL). The resulting reaction mixture was stirred overnight at room temperature. The next morning the reaction did not achieve full conversion, as determined by TLC (20% MeOH in CH_2Cl_2). Nevertheless, MeCN was removed *in vacuo* and the aqueous layer was extracted using CH_2Cl_2 supplemented with 1% TEA (3 x 50 mL). The combined CH_2Cl_2 layer were washed with brine (100 mL), dried over $NaSO_4$, and filtered. The filtrate was concentrated *in vacuo*, followed by purification using automated flash column chromatography using a linear gradient (0-10% MeOH in CH_2Cl_2 supplemented with 1% TEA over 10 column volumes). Pure triethylene glycol monotrityl thioether ethylamine **29** (0.26 g, 0.58 mmol, 14%) was obtained as a yellowish oil. R_f = 0.27 (10% MeOH in CH_2Cl_2 supplemented with TEA); t_R = 34.4 min; ^{1}H-NMR (400 MHz, $CDCl_3$): δ = 7.41 (m, 6H, trityl *o-H*), 7.27 (m, 6H, trityl *m-H*), 7.21 (m, 3H, trityl *p-H*), 3.61 (m, 4H, 2 x C*H*$_2$), 3.57 (m, 2H, C*H*$_2$), 3.50 (t, $^3J_{HH}$ = 5.2 Hz, 2H, C*H*$_2$CH$_2$NH$_3^+$), 3.45 (m, 2H, C*H*$_2$), 3.31 (t, $^3J_{HH}$ = 6.9 Hz, 2H, SCH$_2$C*H*$_2$), 2.85 (t, $^3J_{HH}$ = 5.2 Hz, 2H, C*H*$_2$NH$_3^+$), 2.43 (t, $^3J_{HH}$ = 6.9 Hz, 2H, SC*H*$_2$), 1.91 (broad s, 3H, NH_3^+) ppm; ^{13}C-NMR (101 MHz, $CDCl_3$): δ = 144.8 (trityl-*C*), 129.6 (trityl *o-C*H), 127.9 (trityl *m-C*H), 126.7 (trityl *p-C*H), 73.1 (*C*H$_2$CH$_2$NH$_3^+$), 70.6 (*C*H$_2$), 70.5 (*C*H$_2$), 70.3 (*C*H$_2$), 70.2 (*C*H$_2$), 69.6 (SCH$_2$*C*H$_2$), 66.6 (*C*S), 41.7 (*C*H$_2$NH$_3^+$), 31.7 (S*C*H$_2$) ppm; HRMS: calculated *m/z* for $C_{27}H_{33}NO_3S$: 452.2259 [*M*+H]$^{1+}$; found 452.2244.

Triethylene glycol monotrityl thioether ethylamine equipped TAC-scaffold (30). TAC-scaffold **25** (42 mg, 53 μmol, 1.0 equiv.) was dissolved in DMF (8 mL). Next BOP (30 mg, 68 μmol, 1.3 equiv.) was dissolved in DMF (3 x 2 mL) and subsequently added to the solution containing TAC-scaffold **25**. Then, triethylene glycol monotrityl thioether ethylamine **29** (51 mg, 0.11 mmol,) was dissolved in DMF (3 x 2 mL) and added. Lastly, D*i*PEA (37 μL, 0.21 mmol, 4.0 equiv.) was added and the reaction mixture was stirred for 1 hour at room temperature. Upon completion of the reaction, as determined by LCMS, solvent was removed *in vacuo*. The residue was taken up in *t*BuOH/H_2O (1:1, *v/v*) and lyophilized. The crude yellowish oil was dissolved in CH_2Cl_2 and, purified manually using silica gel chromatography (2% MeOH in CH_2Cl_2) and visualized with UV and potassium permanganate stain. Pure fractions were combined and concentrated *in vacuo*, the residue taken up in *t*BuOH/H_2O (1:1, *v/v*) and lyophilized, affording pure triethylene glycol

monotrityl thioether ethylamine equipped TAC-scaffold **30** (52 mg, 43 μmol, 81%) as a white powder. R_f = 0.52 (5% MeOH in CH_2Cl_2); t_R = 49.6 min; ^{1}H-NMR (400 MHz, $CDCl_3$): δ = 7.69 (m, 2H, aryl-*H*), 7.39 (m, 6H, trityl *o*-*H*), 7.34 (m, 1H, aryl-*H*), 7.27 (m, 6H, trityl *m*-*H*), 7.20 (m, 3H, trityl *p*-*H*), 6.84 (m, 1H, OCH_2CH_2NH), 4.61 (m, 4H, 2 x NCH_2-aryl), 3.64 (m, 8H, 4 x CH_2), 3.58 (m, 2H, OCH_2CH_2NH), 3.43 (m, 6H, $NCH_2CH_2CH_2N$ and OCH_2CH_2NH), 3.27 (t, $^3J_{HH}$ = 6.8 Hz, 2H, SCH_2CH_2), 2.96 (m, 4H, $NCH_2CH_2CH_2N$), 2.64 (m, 8H, 2 x CH_2CH_2CCSi), 2.44 (m, 4H, CH_2CH_2CCH), 2.39 (t, $^3J_{HH}$ = 6.8 Hz, 2H, SCH_2CH_2), 1.95 (m, 1H, CCH), 1.45 (m, 4H, 2 x $NCH_2CH_2CH_2N$), 1.05 (m, 21H, $Si(CH(CH_3)_2)_3$), 0.97 (t, $^3J_{HH}$ = 7.9 Hz, 9H, $Si(CH_2CH_3)_3$), 0.58 (q, $^3J_{HH}$ = 7.9 Hz, 6H, $Si(CH_2CH_3)_3$) ppm; ^{13}C-NMR (101 MHz, $CDCl_3$): δ = 144.7 (trityl-*C*), 129.6 (trityl *o*-*C*H), 127.9 (trityl *m*-*C*H), 126.8 (aryl-*C*H) 126.6 (trityl *p*-*C*H), 126.2 (aryl-*C*H), 70.6 (CH_2), 70.4 (OCH_2CH_2NH), 70.3 (CH_2), 70.1 (OCH_2CH_2NH), 69.7 (CH_2), 69.6 (SCH_2CH_2), 68.6 (*C*CH), 53.9 (NCH_2-aryl), 51.9 (NCH_2-aryl), 47.8 ($NCH_2CH_2CH_2N$), 45.8 ($NCH_2CH_2CH_2N$), 45.6 ($NCH_2CH_2CH_2N$), 43.5 ($NCH_2CH_2CH_2N$), 40.0 (CH_2), 33.0 (CH_2CH_2CCSi), 32.9 (CH_2CH_2CCSi), 31.9 (CH_2CH_2CCH), 31.7 (SCH_2CH_2), 28.5 ($NCH_2CH_2CH_2N$), 27.5 ($NCH_2CH_2CH_2N$), 18.7 ($Si(CH(CH_3)_2)_3$), 18.4 (C*C*H), 16.4 (CH_2CH_2CCSi), 16.4 (CH_2CH_2CCSi), 14.5 (CH_2CH_2CCH), 11.3 ($Si(CH(CH_3)_2)_3$), 7.5 ($Si(CH_2CH_3)_3$), 4.4 ($Si(CH_2CH_3)_3$) ppm; HRMS: calculated *m/z* for $C_{72}H_{100}N_4O_7SSi_2$: 1221.6929 $[M+H]^{1+}$; found 1221.6870; LRMS: calculated *m/z* for $C_{72}H_{100}N_4O_7SSi_2$: 1221.69 $[M+H]^{1+}$ / 1243.67 $[M+Na]^{1+}$; found 1222.92 / 1244.17.

General method for automated peptide synthesis. Peptides were synthesized on a PTI Tribute-UV peptide synthesizer. Tentagel S RAM resin (1.0 g, 0.25 mmol, 1.0 equiv. or 0.43 g, 0.10 mmol, 1.0 equiv.) was allowed to swell in DMF (3 x 10 minutes). De-protection of the Fmoc group was achieved by treatment of the resin with 20% piperidine in DMF using the RV_top_UV_Xtend protocol from the Tribute-UV peptide synthesizer followed by a DMF washing step (5 x 30 seconds). Fmoc-protected amino acids were coupled using HCTU (on the 0.10 mmol scale 5.0 equiv. were used and on the 0.25 mmol scale 4.0 equiv. were used) and D*i*PEA (on the 0.10 mmol scale 10 equiv. were used and on the 0.25 mmol scale 8.0 equiv. were used) in DMF, as a coupling reagent, with 2 minutes pre-activation. The coupling time was 10 minutes when the peptide was synthesized on a 0.10 mmol scale and 20 minutes when the 0.25 mmol scale was conducted. After every coupling the resin was washed with DMF (6 x 30 seconds), followed by a capping step for 10 minutes using capping solution (24 mL acetic anhydride and 11 mL D*i*PEA in 500 mL DMF; using 3 mL for the 0.10 mmol scale and 6 mL for the 0.25 mmol scale). After coupling of the last amino acid, the Fmoc group was deprotected

using the standard de-protection conditions (described above) and the resulting free N-terminus was maintained (peptide **31**) or acetylated (peptides **32** and **33**) by treating the resin bound peptide with capping solution (24 mL acetic anhydride and 11 mL D*i*PEA in 500 mL DMF; using 3 mL for the 0.10 mmol scale and 6 mL for the 0.25 mmol scale) for 10 minutes. After the last step the resin was washed with DMF (5 x 30 seconds) and dried over a nitrogen flow for 10 minutes. Cleavage and de-protection was achieved by treatment of the resin with TFA:H_2O:TIS:EDT (15 mL for the 0.25 mmol scale and 5 mL for the 0.10 mmol scale, 90:5:2.5:2.5, *v*/*v*/*v*/*v*) for 3 hours at room temperature. The peptide was then precipitated in Et_2O (90 mL for the 0.25 mmol scale and 45 mL for the 0.10 mmol scale), centrifuged (4500 rpm; 5 min), the supernatant decanted and the pellet washed 3 times with Et_2O (90 mL for the 0.25 mmol scale and 45 mL for the 0.10 mmol scale). The resulting pellet was re-dissolved in *t*BuOH/H_2O (1:1, *v*/*v*) and lyophilized.

Peptide 31. This peptide was synthesized as described above by solid phase synthesis on a 0.25 mmol scale, which afforded crude peptide (0.28 g). This crude peptide was used in the cyclization by alkylation step. t_R = 16.5 min; LRMS: *m/z* calculated for $C_{79}H_{127}N_{27}O_{22}S_2$: 935.96 ½[*M*+2H]$^{2+}$; found: 936.75.

Peptide 32. This peptide was synthesized as described above by solid phase synthesis on a 0.25 mmol scale, which afforded crude peptide (0.35 mg). This crude peptide was used in the cyclization by alkylation step. t_R = 19.2 min; LRMS: *m/z* calculated for $C_{89}H_{117}N_{21}O_{19}S_2$: 924.92 ½[*M*+2H]$^{2+}$; found: 925.67.

Peptide 33. This peptide was synthesized as described above by solid phase synthesis on a 0.25 mmol scale, which afforded crude peptide (0.35 g). This crude peptide was used in the cyclization by alkylation step. t_R = 16.7 min; LRMS: *m/z* calculated for $C_{96}H_{140}N_{28}O_{31}S_2$: 1123.49 ½[*M*+2H]$^{2+}$; found: 1124.17.

azido triazinane-tris(2-bromoethanone) (TADB-N_3) (34). This synthesis has been described in Chapter 3: azido triazinane-tris(2-bromoethanone) (TADB-N_3) **9**.[35]

General method for peptide cyclization. Crude peptide (0.25 mmol, 1.0 equiv.) was dissolved in DMF (225 mL), followed by addition of TADB-N_3 **34** (1.1-1.5 equiv.) in DMF (1 mL). Subsequently, an aqueous solution of NH_4HCO_3 (20 mM, pH 7.2<7.4; 75 mL) was added to the reaction mixture. The resulting reaction mixture consisted of a peptide concentration of <1 mM and was stirred for 15 minutes at room temperature,

followed by removal of the solvents *in vacuo* (60 °C). The residue was dissolved in *t*BuOH/H_2O/MeCN (1:1:1, *v/v/v*) aided by sonication. Lyophilization afforded the crude cyclized peptide, which was suspended/dissolved and clarified by centrifugation (4500 rpm; 5 minutes). The resulting compound in the supernatant was purified by reverse phase preparative HPLC. Fractions containing pure product were identified by analytical HPLC and were pooled and lyophilized.

Cyclic peptide 35. Crude peptide **31** (0.28 g, 0.25 mmol, 1.0 equiv.) was treated with TADB-N_3 **34** (0.11g, 0.28 mmol, 1.1 equiv.). Purification was done in batches of 10-15 mg crude suspended in 4 mL buffer A:B (75:25, *v/v*) using a custom protocol: 25% buffer B in buffer A for 2 minutes, followed by a linear gradient of 28-38% buffer B in buffer A for 10 minutes, which affording cyclic peptide **35** (16 mg, 7.6 μmol, 3%). t_R = 16.9 min; HRMS: calculated *m/z* for $C_{88}H_{137}N_{33}O_{25}S_2$: 1061.0031 ½[*M*+2H]$^{2+}$; found 1061.0002; LRMS: calculated *m/z* for $C_{88}H_{137}N_{33}O_{25}S_2$: 1061.00 ½[*M*+2H]$^{2+}$ / 707.67 1/3[*M*+3H]$^{3+}$; found 1061.58 / 708.25.

Cyclic peptide 36. Crude peptide **32** (0.35 mg, 0.25 mmol, 1.0 equiv.) was treated with TADB-N_3 **34** (0.12 g, 0.30 mmol, 1.2 equiv.). Purification was done in batches of 30-40 mg crude dissolved in 3 mL buffer A:B (62:38, *v/v*) using a custom protocol: 38% buffer B in buffer A for 2 minutes, followed by a linear gradient of 38-48% buffer B in buffer A for 10 minutes, which afforded cyclic peptide **36** (71 mg, 34 μmol, 14%). t_R = 20.6 min; HRMS: calculated *m/z* for $C_{98}H_{127}N_{27}O_{22}S_2$: 1049.9623 ½[*M*+2H]$^{2+}$; found 1049.9608; LRMS: calculated *m/z* for $C_{98}H_{127}N_{27}O_{22}S_2$: 1049.96 ½[*M*+2H]$^{2+}$; found 1050.58.

Cyclic peptide 37. Crude peptide **33** (0.35 g, 0.25 μmol, 1.0 equiv.) was treated with TADB-N_3 **34** (0.12 g, 0.30 mmol, 1.2 equiv.). Purification was done in batches of 30-40 mg crude dissolved in 3 mL buffer A:B (75:25, *v/v*) using a custom protocol: 27% buffer B in buffer A for 2 minutes, followed by a linear gradient of 27-38% buffer B in buffer A for 10 minutes, which afforded cyclic peptide **37** (0.12 g, 49 μmol, 20%). t_R = 17.4 min; HRMS: calculated *m/z* for $C_{105}H_{150}N_{34}O_{34}S_2$: 1248.5326 ½[*M*+2H]$^{2+}$; found 1248.5361; LRMS: calculated *m/z* for $C_{105}H_{150}N_{34}O_{34}S_2$: 1248.53 ½[*M*+2H]$^{2+}$; found 1249.58.

Alkyne functionalized tetraethylene glycol monotrityl thioether (38). This synthesis has been described in Chapter 3: alkyne modified tetraethylene glycol monotrityl thioether **14**.[35]

General method for CuAAC of cyclized peptides to propargyl linker 38. Hinge cyclized peptide (1.0 equiv.) was dissolved in DMF (400 µL). Then, linker **38** (1.1 equiv.) and TBTA (0.50 equiv.) were dissolved separately in DMF (100 µL). The separate reagents were then combined. After which, $CuSO_4$•$5H_2O$ (1.8 equiv.), sodium L-ascorbate (10 equiv.), and aminoguanidine•HCl (11 equiv,) were each dissolved seperately in H_2O (100 µL). A premix was prepared by adding the sodium L-ascorbate (100 µL) solution to the $CuSO_4$•$5H_2O$ (100 µL) solution, followed by immediate addition of the aminoguanidine•HCl (100 µL) solution. Then, the premix (300 µL) was added to the reaction mixture, which was stirred for 15 minutes at room temperature under constant N_2 flow. Analysis by analytical HPLC indicated completion of the reaction after 15 minutes, followed by addition of HPLC buffers A:B (1:1, *v/v*) (1 mL). The solution was centrifuged (12.000 rpm; 5 minutes) and the compound in the supernatant was purified by preparative HPLC using a custom protocol: 50% buffer B in buffer A for 5 minutes, followed by a linear gradient of 50-100% buffer B in buffer A for 10 minutes. Fractions containing pure product were identified by analytical HPLC and were pooled and lyophilized, affording pure trityl-protected product as a fluffy white powder. Removal of the trityl group was performed using TFA:H_2O:TIS:EDT (90:5:2.5:2.5, *v/v/v/v*) (1 mL) for 15 minutes at room temperature, affording the free-thiol moiety. Then, the product was precipitated in Et_2O (50 mL) and collected by centrifugation (4500 rpm, 5 minutes). The collected precipitate was washed twice using Et_2O (50 mL), followed by centrifugation (4500 rpm; 5 minutes). After which, the precipitate was dissolved in *t*BuOH/H_2O/MeCN (1:1:1, *v/v/v*) and lyophylized, affording the pure product.

Continuous epitope mimic 39. Cyclic peptide **35** (12 mg, 5.7 µmol) and linker **38 (**5.7 mg, 12 µmol; dissolved in 140 µL DMF of which 100 µL was used) was subjected to the above described CuAAC with $CuSO_4$•$5H_2O$ (6.0 mg, 24 µmol; dissolved in 240 µL H_2O of which 100 µL was used), sodium L-ascorbate (11 mg, 55 µmol; dissolved in 100 µL H_2O of which 100 µL was used), TBTA (1.6 mg, 3.0 µmol; dissolved in 109 µL DMF of which 100 µL was used), aminoguanidine•HCl (15 mg, 0.13 mmol; dissolved in 220 µL of which 100 µL was used). Purification and subsequent deprotection, afforded continuous epitope mimic **39** (8.8 mg, 3.7 µmol, 65%). t_R = 17.4 min; HRMS: calculated *m/z* for $C_{99}H_{157}N_{33}O_{29}S_3$: 790.3740 1/3[*M*+3H]$^{3+}$ / 797.7014 1/3[*M*+2H+Na]$^{3+}$; found *m/z* 790.3764 / 797.7046; LRMS: calculated *m/z* for $C_{99}H_{157}N_{33}O_{29}S_3$: 1185.06 ½[*M*+2H]$^{2+}$ / 790.37 1/3[*M*+3H]$^{3+}$; found 1186.08 / 791.42.

Continuous epitope mimic 40. Cyclic peptide **36** (25 mg, 12 μmol) and linker **38 (**11 mg, 22 μmol; dissolved in 124 μL DMF of which 100 μL was used) was subjected to the above described CuAAC with $CuSO_4$•$5H_2O$ (7.5 mg, 30 μmol; dissolved in 141 μL H_2O of which 100 μL was used), sodium L-ascorbate (28 mg, 0.14 mmol; dissolved in 120 μL H_2O of which 100 μL was used), TBTA (3.8 mg, 7.2 μmol; dissolved in 122 μL DMF of which 100 μL was used), aminoguanidine•HCl (16 mg, 0.15 mmol; dissolved in 112 μL of which 100 μL was used). Purification and subsequent deprotection, afforded continuous epitope mimic **40** (12 mg, 5.1 μmol, 43%). t_R = 20.6 min; HRMS: calculated *m/z* for $C_{109}H_{147}N_{27}O_{26}S_3$: 1174.0165 ½[*M*+2H]$^{2+}$; found 1174.0163; LRMS: calculated *m/z* for $C_{109}H_{147}N_{27}O_{26}S_3$: 1174.02 ½[*M*+2H]$^{2+}$ / 783.01 1/3[*M*+3H]$^{3+}$; found 1175.00 / 784.08.

Continuous epitope mimic 41. Cyclic peptide **37** (29 mg, 12 μmol) and linker **38 (**16 mg, 33 μmol; dissolved in 190 μL DMF of which 100 μL was used) was subjected to the above described CuAAC with $CuSO_4$•$5H_2O$ (8.3 mg, 33 μmol; dissolved in 160 μL H_2O of which 100 μL was used), sodium L-ascorbate (28 mg, 0.14 mmol; dissolved in 122 μL H_2O of which 100 μL was used), TBTA (5.2 mg, 9.8 μmol; dissolved in 170 μL DMF of which 100 μL was used), aminoguanidine•HCl (17 mg, 0.15 mmol; dissolved in 122 μL of which 100 μL was used). Purification and subsequent deprotection, afforded continuous epitope mimic **41** (17 mg, 6.2 μmol, 52%). t_R = 17.8 min; HRMS: calculated *m/z* for $C_{116}H_{170}N_{34}O_{38}S_3$: 1372.5867 ½[*M*+2H]$^{2+}$; found 1372.5808; LRMS: calculated *m/z* for $C_{116}H_{170}N_{34}O_{38}S_3$: 1372.59 ½[*M*+2H]$^{2+}$ / 915.39 1/3[*M*+3H]$^{3+}$; found 1373.75 / 916.58.

Tetraethylene glycol ρ-toluenesulfonate (42). Obtained as described in Chapter 2: Tetraethylene glycol mono-trityl thioether **3**.[33]

Tetraethylene glycol Boc-amide (45). Tetraethylene glycol ρ-toluenesulfonate **42** (7.2 g, 21 mmol, 1.0 equiv.) was taken up in aqueous 25% ammonia (50 mL) and the reaction was stirred overnight at room temperature. The next morning the reaction was not fully completed, as determined by TLC (100% EtOAc) and visualized with a ninhydrin stain. Therefore, the solvents were removed *in vacuo* and the residue dissolved in MeCN (50 mL) and fresh aqueous 25% ammonia (50 mL) was added. After an additional 8 hours, the reaction still didn't reach completion. Again, solvents were removed *in vacuo* and the residue was taken up in aqueous 25% ammonia (50 mL) and stirred overnight at room temperature. The next morning, the reaction was complete as determined by TLC (100% EtOAc) and visualized with a ninhydrin stain. The solvent was removed *in vacuo* and the residue was co-evaporated with toluene (2x). Next, the crude amine **43** was dissolved in

anhydrous THF (50 mL), followed by addition of di-*tert*-butyl dicarbonate **44** (8.2 g, 38 mmol, 1.8 equiv.). The resulting reaction mixture was cooled to 0 °C using an ice bath, followed by addition of TEA (5.5 mL, 40 mmol, 1.9 equiv.). The reaction was stirred overnight while slowly allowed to reach room temperature. The next morning THF was removed *in vacuo*. The residue was taken up in CH_2Cl_2 (50 mL) and washed with H_2O (3 x 100 mL). The aqueous layers were combined and back-extracted with CH_2Cl_2 (3 x 100 mL). The resulting CH_2Cl_2 layers were combined and washed with brine (300 mL), dried over $MgSO_4$, and filtered. The filtrate was concentrated *in vacuo*, purified by automated flash column chromatography (100% EtOAc) and visualized with a ninhydrin stain. Pure tetraethylene glycol Boc-amide **45** (3.1 g, 11 mmol, 52%) was obtained as a colourless oil. R_f = 0.70 (5% MeOH in CH_2Cl_2); ^{1}H-NMR (400 MHz, $CDCl_3$): δ = 5.62 (broad s, 1H, boc-N*H*), 3.69 (m, 4H, 2 x CH_2), 3.62 (m, 8H, 4 x CH_2), 3.52 (t, $^3J_{HH}$ = 5.3 Hz, 2H, boc-NHCH$_2$CH_2), 3.30 (q, $^3J_{HH}$ = 5.3 Hz, 2H, boc-NHCH_2), 3.05 (broad s, 1H, O*H*), 1.42 (s, 9H, C(CH_3)$_3$) ppm; ^{13}C-NMR (101 MHz, $CDCl_3$): δ = 156.2 (*t*BuOO*C*), 78.9 (*C*(CH$_3$)$_3$), 72.6 (*C*H$_2$), 70.6 (*C*H$_2$), 70.5 (*C*H$_2$), 70.3 (boc-NHCH$_2$*C*H$_2$), 70.1 (*C*H$_2$), 61.7 (*C*H$_2$), 40.4 (boc-NH*C*H$_2$), 28.4 (C(*C*H$_3$)$_3$) ppm; HRMS: calculated *m/z* for $C_{13}H_{27}NO_6$: 316.1736 [*M*+Na]$^{1+}$; found 316.1725.

Tetraethylene glycol Boc-amide p-toluenesulfonate (46). All steps were performed under N_2 atmosphere. Boc-protected amino-tetraethylene glycol **45** (3.1 g, 11 mmol, 1.0 equiv.) and ρ-toluenesulfonyl chloride **27** (3.2 g, 17 mmol, 1.5 equiv.) was dissolved in anhydrous CH_2Cl_2 (50 mL). The resulting mixture was cooled to 0 °C using an ice bath, followed by addition of TEA (2.3 mL, 17 mmol, 1.5 equiv.). The reaction was stirred overnight at room temperature. The next morning the reaction was not fully completed, as determined by TLC (100% EtOAc) and visualized with UV and ninhydrin stain. Nevertheless, the reaction mixture was washed with H_2O (3 x 50 mL). Then, the combined aqueous layers were back-extracted with CH_2Cl_2 (2 x 100 mL). The combined CH_2Cl_2 layers were washed with brine (250 mL), dried over $MgSO_4$, and filtered. Next, the filtrate was concentrated *in vacuo*, purified by automated flash column chromatography using a linear gradient (50-60% EtOAc in petroleum ether 40-60 °C over 10 column volumes) and visualized with UV and ninhydrin stain. Fractions containing pure product were combined and concentrated *in vacuo*, affording tetraethylene glycol Boc-amide p-toluenesulfonate **46** (2.1 g, 4.7 mmol, 43%) as a colourless oil. R_f = 0.55 (EtOAc); t_R = 33.0 min; ^{1}H-NMR (400 MHz, $CDCl_3$): δ = 7.79 (d, $^3J_{HH}$ = 8.2 Hz, 2H, aryl *o*-*H*), 7.33 (d, $^3J_{HH}$ = 8.2 Hz, 2H, aryl *m*-*H*), 4.98 (broad s, 1H, boc-N*H*), 4.15 (t, $^3J_{HH}$ = 4.8 Hz, 2H, TsOCH_2), 3.69 (t, $^3J_{HH}$ = 4.8 Hz, 2H, TsOCH$_2$CH_2), 3.59 (m, 8H, 4 x CH_2), 3.52 (t, $^3J_{HH}$ = 5.3 Hz, 2H, boc-

NHCH$_2$C*H*$_2$), 3.29 (q, $^3J_{HH}$ = 5.3 Hz, 2H, boc-NHC*H*$_2$), 2.44 (s, 3H, C*H*$_3$), 1.43 (s, 9H, C(C*H*$_3$)$_3$) ppm; ^{13}C-NMR (101 MHz, $CDCl_3$): δ = 156.0 (*t*BuOO*C*), 144.8 (aryl-*C*), 133.1 (aryl-*C*), 129.8 (aryl *m*-*C*H), 128.0 (aryl *o*-*C*H), 79.2 (*C*(*C*H$_3$)$_3$), 70.8 (*C*H$_2$), 70.6 (*C*H$_2$), 70.5 (*C*H$_2$), 70.2 (*C*H$_2$), 70.2 (boc-NHCH$_2$*C*H$_2$), 69.2 (TsO*C*H$_2$), 68.7 (TsOCH$_2$C*H*$_2$ (7)), 40.4 (boc-NH*C*H$_2$), 28.4 (C(*C*H$_3$)$_3$), 21.6 (*C*H$_3$) ppm; HRMS: calculated *m/z* for $C_{20}H_{33}NO_8S$: 470.1825 [*M*+Na]$^{1+}$; found 470.1814.

Triethylene glycol Boc-amide ethylamine (47). ρ-toluenesulfonate tetraethylene glycol with a Boc-protected amine **46** (2.1 g, 4.7 mmol, 1.0 equiv.) was dissolved in MeCN (50 mL), followed by the addition of aqueous 28-30% ammonia (50 mL). The reaction was stirred overnight at room temperature. The next morning, the reaction did not reach completion and the solvents were removed *in vacuo*. After which, the residue was re-dissolved in MeCN (50 mL) and fresh aqueous 28-30% ammonia (50 mL) was added. Despite the reaction being refreshed a total of two additional times, the reaction did not reach full completion as determined by TLC (5% MeOH in CH_2Cl_2 supplemented with TEA) and visualized with ninhydrin stain. Nevertheless, solvent was removed *in vacuo* and the residue was dissolved in CH_2Cl_2 (100 mL). The resulting solution was washed with aqueous 1.0 M NaOH (3 x 100 mL) and the resulting aqueous layer was back-extracted with CH_2Cl_2 (3 x 100 mL). The CH_2Cl_2 layers were combined and washed with brine (200 mL), dried over $MgSO_4$, and filtered. Next, the filtrate was concentrated *in vacuo*, purified by automated flash column chromatography using a linear gradient (0-5% MeOH in CH_2Cl_2 over 10 column volumes) and visualized with UV and ninhydrin stain. Pure fractions were combined and concentrated *in vacuo*, affording pure triethylene glycol Boc-amide ethylamine **47** (0.49 g, 1.7 mmol, 36%) as an colourless oil. R_f = 0.41 (5% MeOH in CH_2Cl_2 supplemented with TEA); ^{1}H-NMR (400 MHz, $CDCl_3$): δ = 5.26 (broad s, 1H, boc-N*H*), 3.62 (m, 8H, 4 x C*H*$_2$), 3.53 (m, 4H, boc-NHCH$_2$C*H*$_2$ and C*H*$_2$CH$_2$NH$_2$), 3.29 (m, 2H, boc-NHC*H*$_2$), 2.88 (m, 2H, C*H*$_2$NH$_2$), 2.43 (m, 2H, N*H*$_2$), 1.43 (s, 9H, C(C*H*$_3$)$_3$) ppm; ^{13}C-NMR (101 MHz, $CDCl_3$): δ = 156.1 (*t*BuOO*C*), 79.1 (*C*(*C*H$_3$)$_3$), 72.7 (boc-NHCH$_2$*C*H$_2$ or *C*H$_2$CH$_2$NH$_2$), 70.5 (*C*H$_2$), 70.5 (*C*H$_2$), 70.2 (boc-NHCH$_2$*C*H$_2$ or *C*H$_2$CH$_2$NH$_2$), 41.5 (*C*H$_2$NH$_2$), 40.4 (boc-NH*C*H$_2$), 28.4 (C(*C*H$_3$)$_3$) ppm; HRMS: calculated *m/z* for $C_{13}H_{28}N_2O_5$: 315.1896 [*M*+Na]$^{1+}$; found 315.1883.

Triethylene glycol Boc-amide ethylamine equipped TAC-scaffold (48). TAC-scaffold **25** (39 mg, 50 μmol, 1.0 equiv.) was dissolved in DMF (8 mL). Next, BOP (26 mg, 59 μmol, 1.2 equiv.) was dissolved in DMF (3 x 2 mL) and subsequently added to the solution containing TAC-scaffold **25**. Then, triethylene glycol Boc-amide ethylamine **47** (29 mg,

100 μmol, 2.0 equiv.) was dissolved in DMF (3 x 2 mL) and added. Lastly, D*i*PEA (35 μl, 0.20 mmol) was added and the reaction mixture was stirred for 1 hour at room temperature. Upon completion of the reaction, as determined by LCMS, solvent was removed *in vacuo* (60 °C). The residue was taken up in *t*BuOH/H_2O (1:1, *v/v*) and lyophilized. The crude yellowish oil was dissolved in CH_2Cl_2 and purified using automated flash column chromatography with a linear gradient (0-5% MeOH in CH_2Cl_2 over 10 column volumes) and visualized with UV and ninhydrin stain. Pure fractions were combined and concentrated *in vacuo* (60 °C), the residue was taken up in *t*BuOH/H_2O (1:1, *v/v*) and lyophilized, affording triethylene glycol Boc-amide ethylamine equipped TAC-scaffold **48** (46 mg, 43 μmol, 86%) as a white powder. R_f = 0.43 (5% MeOH in CH_2Cl_2); t_R = 54.2 min; ^{1}H-NMR (400 MHz, $CDCl_3$): δ = 7.73 (m, 2H, aryl-*H*), 7.28 (m, 1H, aryl-*H*), 6.90 (broad s, 1H, OCH_2CH_2NH), 5.11 (broad s, 1H, boc-N*H*), 4.64 (m, 4H, 2 x NCH_2-aryl), 3.65 (m, 10H, 4 x CH_2 and OCH_2CH_2NH), 3.52 (t, $^3J_{HH}$ = 5.2 Hz, 2H, boc-$NHCH_2CH_2$), 3.43 (m, 4H, $NCH_2CH_2CH_2N$), 3.27 (q, $^3J_{HH}$ = 5.2 Hz, 2H, boc-$NHCH_2$), 2.95 (m, 6H, $NCH_2CH_2CH_2N$ and OCH_2CH_2NH), 2.64 (m, 8H, 2 x CH_2CH_2CCSi), 2.45 (m, 4H, CH_2CH_2CCH), 1.95 (m, 1H, CC*H*), 1.58 (m, 4H, 2 x $NCH_2CH_2CH_2N$), 1.43 (s, 9H, $C(CH_3)_3$), 1.06 (m, 21H, $Si(CH(CH_3)_2)_3$), 0.98 (t, $^3J_{HH}$ = 7.9 Hz, 9H, $Si(CH_2CH_3)_3$), 0.58 (q, $^3J_{HH}$ = 7.9 Hz, 6H, $Si(CH_2CH_3)_3$) ppm; ^{13}C-NMR (101 MHz, $CDCl_3$): δ = 156.0 (*t*BuOO*C*)), 129.2 (aryl-*C*H), 126.8 (aryl-*C*H), 70.5 (CH_2), 70.5 (CH_2), 70.3 (CH_2), 70.2 (boc-$NHCH_2CH_2$ or OCH_2CH_2NH), 70.2 (boc-$NHCH_2CH_2$ or OCH_2CH_2NH), 70.1 (CH_2), 53.9 (NCH_2-aryl), 51.9 (NCH_2-aryl), 48.0 ($NCH_2CH_2CH_2N$ or OCH_2CH_2NH), 45.9 ($NCH_2CH_2CH_2N$ or OCH_2CH_2NH), 45.7 ($NCH_2CH_2CH_2N$ or OCH_2CH_2NH), 45.3 ($NCH_2CH_2CH_2N$ or OCH_2CH_2NH), 43.7 ($NCH_2CH_2CH_2N$ or OCH_2CH_2NH), 40.3 (boc-$NHCH_2$), 39.8 (CH_2), 33.0 (CH_2CH_2CCSi), 33.0 (CH_2CH_2CCSi), 32.0 (CH_2CH_2CCH), 28.4 ($C(CH_3)_3$), 28.0 ($NCH_2CH_2CH_2N$), 28.0 ($NCH_2CH_2CH_2N$), 18.6 ($Si(CH(CH_3)_2)_3$), 16.3 (CH_2CH_2CCSi), 16.3 (CH_2CH_2CCSi), 14.5 (CH_2CH_2CCH), 11.3 ($Si(CH(CH_3)_2)_3$), 7.5 ($Si(CH_2CH_3)_3$), 4.5 ($Si(CH_2CH_3)_3$) ppm; HRMS: calculated *m/z* for $C_{58}H_{95}N_5O_9Si_2$: 1084.6566 $[M+Na]^{1+}$; found 1084.6559; LRMS: calculated *m/z* for $C_{58}H_{95}N_5O_9Si_2$:1062.67 $[M+H]^{1+}$ / 1084.66 $[M+Na]^{1+}$; Found *m/z* 1062.83 / 1084.75.

Assembling discontinuous epitope: Cycloaddition of the first cyclic peptide and subsequent TES deprotection. Triethylene glycol Boc-amide ethylamine equipped TAC-scaffold **48** (66 mg, 62 μmol, 1.8 equiv.) was dissolved in DMF (600 μL) and added to cyclic peptide **36** (71 mg, 34 μmol, 1.0 equiv.). The flask-containing scaffold **48** was rinsed with additional DMF (500 μL), which was added to the reaction mixture to ensure all was transferred. Next, TBTA (15 mg, 28 μmol) was dissolved in DMF (161 μL), of

which 100 µL (17 µmol, 0.50 equiv.) was added to the reaction mixture. Then, aqueous solutions of $CuSO_4$•$5H_2O$ (24 mg, 97 µmol; dissolved in 158 µL H_2O), sodium L-ascorbate (68 mg, 0.34 mmol; dissolved in 202 µL H_2O), and aminoguanidine•HCl (59 mg, 0.53 mmol; dissolved in 142 µL H_2O) were prepared. The resulting aqueous solutions were mixed ($CuSO_4$•$5H_2O$ (100 µL, 61 µmol, 1.8 equiv.), sodium L-ascorbate (200 µL, 0.34 mmol, 10 equiv.), and aminoguanidine•HCl (100 µL, 0.38 mmol, 11 equiv.)) and the resulting mix (400 µL) was added dropwise to the stirring reaction mixture. The reaction was kept under N_2-atmosphere and monitored by LCMS. After 3 hours the reaction was completed, followed by addition of Cuprisorb resin to capture the Cu-species. The reaction mixture was filtered and, the reaction vessel and filter were washed with extra DMF (5 x 2 mL). Next, DMF was removed *in vacuo* (60 °C) and the residue was dissolved in *t*BuOH/H_2O/MeCN (1:1:1, *v/v/v*), and lyophilized.

The resulting crude was dissolved in DMF (1 mL) and an aqueous solution of $AgNO_3$ (0.25 g, 1.5 mmol; dissolved in 235 µL H_2O) was prepared, of which 100 µL (0.62 mmol, 18 equiv.) was added. The reaction was stirred under N_2-atmosphere for 1 hour at room temperature and monitored by LCMS. After 1 hour, the reaction did not reach completion and an additional 100 µL (0.62 mmol, 18 equiv.) was added. The reaction was complete the following hour as verified by LCMS. After which, additional DMF (900 µL) was added to the reaction mixture and an aqueous solution of NaCl (0.12 g, 2.1 mmol; dissolved in 510 µL H_2O) was prepared, of which 300 µL (1.2 mmol, 35 equiv.) was added to the reaction mixture. After 15 minutes, the reaction mixture was collected and the reaction vessel rinsed with DMF (3 x 2 mL). The resulting AgCl precipitate was removed by centrifugation (4500 rpm; 5 minutes), the resulting precipitate was washed with DMF (5 mL) and centrifuged again. The supernatants were collected and pooled, followed by removing DMF *in vacuo* (60°C). The residue was taken up in *t*BuOH/H_2O/MeCN (1:1:1, *v/v/v*) and lyophilized.

The obtained crude product was dissolved in buffer 4 mL A:B (1:1, *v/v*), clarified by centrifugation (4500 rpm; 5 minutes), and purified by preparative HPLC using a custom protocol: 50% buffer B in buffer A for 5 minutes, followed by a linear gradient of 50-100% buffer B in buffer A for 50 minutes. Fractions containing pure product were identified by analytical HPLC, pooled, and lyophilized, which afforded pure scaffold **49** (27 mg, 8.9 µmol, 26%). t_R = 27.5 min; HRMS: calculated *m/z* for $C_{150}H_{208}N_{32}O_{31}S_2Si$: 1523.7525 ½[*M*+2H]$^{2+}$; found 1523.7543; LRMS: calculated *m/z* for $C_{150}H_{208}N_{32}O_{31}S_2Si$: 1523.75 ½[*M*+2H]$^{2+}$ / 1016.17 1/3[*M*+3H]$^{3+}$; found 1524.83 / 1016.92.

Assembling the discontinuous epitope: Cycloaddition of the second cyclic peptide. Cyclic peptide **37** (50 mg, 20 μmol, 1.5 equiv.) was dissolved in DMF (500 μL) and added to scaffold **49** (40 mg, 13 μmol, 1.0 equiv.). The flask-containing cyclic peptide **37** was rinsed with additional DMF (500 μL), which was added to the reaction mixture to ensure all was transferred. Next, TBTA (9.3 mg, 18 μmol) was dissolved in DMF (265 μL), of which 100 μL (6.6 μmol, 0.51 equiv.) was added to the reaction mixture. Then, aqueous solutions of $CuSO_4$•$5H_2O$ (12 mg, 48 μmol; dissolved in 198 μL H_2O), sodium L-ascorbate (52 mg, 0.26 mmol; dissolved in 200 μL H_2O), and aminoguanidine•HCl (32 mg, 0.29 mmol; dissolved in 200 μL H_2O) were prepared. The resulting aqueous solutions were mixed (($CuSO_4$•$5H_2O$ (100 μL, 24 μmol, 1.8 equiv.), sodium L-ascorbate (100 μL, 0.13 mmol, 10.0 equiv.), and aminoguanidine•HCl (100 μL, 0.15 mmol, 11 equiv.)) and the resulting mix (300 μL) was added dropwise to the stirring reaction mixture. The reaction was kept under N_2-atmosphere and monitored by LCMS. After 6 hours the reaction was completed, followed by addition of Cuprisorb resin to capture the Cu-species. The reaction mixture was filtered and, the reaction vessel and filter were washed with extra DMF (5 x 2 mL). Next, DMF was removed *in vacuo* (60°C), the residue was dissolved in *t*BuOH/H_2O/MeCN (1:1:1, *v/v/v*), and lyophilized.

The obtained crude product was dissolved in buffer 5 mL A:B (1:1, *v/v*), clarified by centrifugation (4500 rpm; 5 minutes), and the resulting compound in the supernatant was purified by preparative HPLC using a custom protocol: 40% buffer B in buffer A for 5 minutes, followed by a linear gradient of 40-70% buffer B in buffer A for 60 minutes. Fractions containing pure product were identified by analytical HPLC, pooled, and lyophilized, which afforded pure scaffold **50** (17 mg, 3.0 μmol, 23%). t_R = 23.7 min; HRMS: calculated *m/z* for $C_{255}H_{358}N_{66}O_{65}S_4Si$: 1386.1425 1/4[*M*+4H]$^{4+}$; found 1386.1481; LRMS: calculated *m/z* for $C_{255}H_{358}N_{66}O_{65}S_4Si$: 1847.85 1/3[*M*+3H]$^{3+}$ / 1386.14 1/4[*M*+4H]$^{4+}$; found 1849.00 / 1387.17.

Assembling the discontinuous epitope: TIPS deprotection. TBAF•$3H_2O$ (13 mg, 41 μmol) was dissolved in DMF (133 μL), of which 100 μL (31 μmol, 10 equiv.) was used to dissolve scaffold **50** (17 mg, 3.0 μmol, 1.0 equiv.). The reaction was stirred under N_2-atmosphere and closely monitored by LCMS. After 5 hours no conversion was observed and fresh TBAF•$3H_2O$ (14 mg, 44 μmol; dissolved in 152 μL DMF, of which 100 μL (29 μmol, 10 equiv.)) was added. The next day the reaction progressed, but was not completed. Therefore, fresh TBAF•$3H_2O$ (24 mg, 76 μmol; dissolved in 255 μL DMF, of which 100 μL (29.8 μmol, 9.9 equiv.)) was added. The next morning, the reaction was complete as

verified by LCMS. The reaction mixture was collected and the reaction vessel was rinsed with 5 mL buffer A:B (1:1, *v/v*). Next, the reaction mixture was clarified by centrifugation (4500 rpm; 5 minutes) and purified by preparative HPLC using a custom protocol: 20% buffer B in buffer A for 5 minutes, followed by a linear gradient of 20-50% buffer B in buffer A for 40 minutes. Fractions containing pure product were identified by analytical HPLC, pooled, and lyophilized, which afforded pure discontinuous epitope mimic **51** (6.6 mg, 1.2 μmol, 40%). t_R = 20.4 min; HRMS: calculated *m/z* for $C_{246}H_{338}N_{66}O_{65}S_4$: 1347.1092 1/4[*M*+4H]$^{4+}$; found 1347.1139; LRMS: calculated *m/z* for $C_{246}H_{338}N_{66}O_{65}S_4$: 1795.81 1/3[*M*+3H]$^{3+}$ / 1347.11 1/4[*M*+4H]$^{4+}$; found 1797.17 / 1348.42.

Assembling the discontinuous epitope: Cycloaddition of the third cyclic peptide. Cyclic peptide **35** (4.4 mg, 2.1 μmol, 1.8 equiv.) was dissolved in DMF (500 μL) and added to scaffold **51** (6.6 mg, 1.2 μmol, 1.0 equiv.). The flask-containing cyclic peptide **35** was rinsed with additional DMF (500 μL), which was added to the reaction mixture to ensure all was transferred. Next, TBTA (1.1 mg, 2.0 μmol) was dissolved in DMF (330 μL), of which 100 μL (0.60 μmol, 0.50 equiv.) was added to the reaction mixture. Then, aqueous solutions of $CuSO_4$•$5H_2O$ (3.0 mg, 12 μmol; dissolved in 555 μL H_2O), sodium L-ascorbate (15 mg, 76 μmol; dissolved in 635 μL H_2O), and aminoguanidine•HCl (14 mg, 0.13 mmol; dissolved in 950 μL H_2O) were prepared. The resulting aqueous solutions were mixed (($CuSO_4$•$5H_2O$ (100 μL, 2.2 μmol, 1.8 equiv.), sodium L-ascorbate (100 μL, 12 μmol, 10 equiv.), and aminoguanidine•HCl (100 μL, 14 μmol, 12 equiv.)) and the resulting mix (300 μL) was added dropwise to the stirring reaction mixture. The reaction was kept under N_2-atmosphere and monitored by LCMS. After 3 hours no more cyclic peptide **35** was observed in the reaction mixture, but scaffold **51** was still present. Therefore, additional cyclic peptide **35** (2.7 mg, 1.3 μmol, 1.1 equiv.) was dissolved in DMF (100 μL) and added. After 1 hour no improvement was observed by LCMS and fresh reagents were prepared. TBTA (1.1 mg, 2.0 μmol) was dissolved in DMF (330 μL), of which 100 μL (0.6 μmol, 0.5 equiv.) was added to the reaction mixture. Then, solutions of $CuSO_4$•$5H_2O$ (6.0 mg, 24 μmol; dissolved in 555 μL H_2O), sodium L-ascorbate (7.9 mg, 40 μmol; dissolved in 166 μL H_2O), and aminoguanidine•HCl (11 mg, 99 μmol; dissolved in 370 μL H_2O) were prepared. The resulting solutions were mixed (($CuSO_4$•$5H_2O$ (50 μL, 2.2 μmol, 1.8 equiv.), sodium L-ascorbate (50 μL, 12 μmol, 10 equiv.), and aminoguanidine•HCl (100 μL, 13 μmol, 11.0 equiv.)) and the resulting mix (150 μL) was added dropwise to the stirring reaction mixture. The reaction was continued to stir under N_2-atmosphere and monitored by LCMS. After 2 hours some additional product was formed, but the reaction was not fully complete. Regardless, Cuprisorb resin was added to

capture the Cu-species. The reaction mixture was filtered and, the reaction vessel and filter were washed with extra DMF (5 x 2 mL). Next, DMF was removed *in vacuo* (60°C), the residue was dissolved in *t*BuOH/H_2O/MeCN (1:1:1, *v/v/v*), and lyophilized.

The obtained crude product was suspended in buffer 3 mL A:B (1:1, *v/v*), clarified by centrifugation (4500 rpm; 5 minutes), and the resulting compound in the supernatant was purified by preparative HPLC using a custom protocol: 0% buffer B in buffer A for 5 minutes, followed by a linear gradient of 0-50% buffer B in buffer A for 50 minutes. Fractions containing pure product were identified by analytical HPLC, pooled, and lyophilized, which afforded pure discontinuous epitope mimic **52** (2.2 mg, 0.29 μmol, 24%). t_R = 19.6 min; HRMS: calculated *m/z* for $C_{334}H_{475}N_{99}O_{90}S_6$: 1501.8870 1/5[*M*+5H]$^{5+}$; found 1501.8881; LRMS: calculated *m/z* for $C_{334}H_{475}N_{99}O_{90}S_6$: 1877.11 1/4[*M*+4H]$^{4+}$ / 1501.89 1/5[*M*+5H]$^{5+}$ / 1251.74 1/6[*M*+6H]$^{6+}$; found 1878.42 / 1503.00 / 1252.58.

Assembling the discontinuous epitope: Boc deprotection. Discontinuous epitope mimic **52** (2.2 mg, 0.29 μmol, 1.0 equiv.) was dissolved in 250 μL TFA:H_2O:TIS:EDT (90:5:2.5:2.5, *v/v/v/v*) and the reaction mixture was stirred for 30 minutes at room temperature. After which, the reaction mixture was added to Et_2O (15 mL) to precipitate the product. The reaction vessel was rinsed (x3) with an additional 250 μL TFA:H_2O:TIS:EDT (90:5:2.5:2.5, *v/v/v/v*), which was added to separate Et_2O (15 mL) to collect all product. Precipitated product was obtained by centrifugation (4500 rpm; 5 minutes), which was washed twice using Et_2O (15 mL), followed by centrifugation (4500 rpm; 5 minutes). The obtained precipitated pellets were dissolved in *t*BuOH/H_2O/MeCN (1:1:1, *v/v/v*), pooled, and lyophilized, which afforded pure discontinuous epitope mimic **53** (2.0 mg, 0.27 μmol, *quant.*). t_R = 18.9 min; HRMS: calculated *m/z* for $C_{329}H_{467}N_{99}O_{88}S_6$: 1481.8765 1/5[*M*+5H]$^{5+}$; found 1481.8699; LRMS: calculated *m/z* for $C_{329}H_{467}N_{99}O_{88}S_6$: 1852.09 1/4[*M*+4H]$^{4+}$ / 1481.88 1/5[*M*+5H]$^{5+}$ / 1235.07 1/6[*M*+6H]$^{6+}$; found 1853.42 / 1483.00 / 1236.17.

Conjugation of free thiol containing continuous epitope mimics (39, 40, and 41) on maleimide activated macriculture keyhole limpet hemocyanin (mcKLH). This procedure was performed as instructed by the Imject® Maleimide Activated Carrier Protein Spin Kits purchased from Therno Scientific.

One vial of the activated mcKLH was reconstituted per conjugation by adding 200 µL ultrapure H_2O to obtain a 10 mg/mL translucent to whitish blue solution. Next, 2.0 mg of continuous epitope mimic (**39**, **40**, and **41**) were dissolved separately in 500 µL conjugation buffer (83 mM sodium phosphate, 0.10 M EDTA, 0.90 M sodium chloride, 0.10 M sorbitol, and 0.02% sodium azide; pH 7.2). Immediately, each solution of continuous epitope mimic was mixed with one vial of activated mcKLH were mixed and incubated for 2 hours at room temperature.

After the conjugation, 10 mL of ultrapure H_2O was added to one bottle of Imject purification buffer salts (83 mM sodium phosphate, 0.90 M sodium chloride, 0.10 M sorbitol; pH 7.2) per conjugation sample. One desalting column was drained by centrifugation (1000 x g; 2 minutes) per conjugation sample. The desalting columns were prepared by slowly adding 1 mL of purification buffer and draining by centrifugation (1000 x g; 2 minutes) for a total of four times. Each conjugation sample was collected and centrifuged (1000 x g; 2 minutes), the pellets were kept and the resulting supernatants (700 µL) were carefully loaded on separate desalting columns. Each desalting column was placed in a clean collection tube and centrifuged (1000 x g; 2 minutes) to collect the conjugation samples. The collected conjugation samples were used to resuspend their corresponding pellets. The obtained continuous epitope-mcKLH conjugates (**39**-mcKLH, **40**-mcKLH, and **41**-mcKLH) were stored at -20 °C until immunization.

Conjugation of free amine containing discontinuous epitope mimic (53) on mcKLH by EDC coupling. This procedure was performed as instructed by the Imject® EDC Carrier Protein Spin Kits purchased from Therno Scientific.

One vial of mcKLH was reconstituted by adding 200 µL ultrapure H_2O to obtain a 10 mg/mL translucent to whitish blue solution. Next, 2.0 mg of discontinuous epitope mimic **53** was dissolved in 450 µL Imject® EDC conjugation buffer (0.10 M MES, 0.90 M sodium chloride, 0.02% sodium azide; pH 4.7) and was added to the mcKLH solution. After which, one vial of EDC (10 mg) was dissolved in 1 mL ultrapure H_2O, of which 50 µL was immediately added to the epitope-mcKLH mixture. Then, the mixture was incubated for 2 hours at room temperature.

After the conjugation, 10 mL of ultrapure H_2O was added to one bottle of Imject purification buffer salts (83 mM sodium phosphate, 0.90 M sodium chloride, 0.10 M sorbitol; pH 7.2). One desalting column was drained by centrifugation (1000 x g; 2

minutes) and was prepared by slowly adding 1 mL of purification buffer and draining by centrifugation (1000 x g; 2 minutes) for a total of four times. The conjugation sample was collected and centrifuged (1000 x g; 2 minutes), the pellet was kept and the resulting supernatant (650 μL) was carefully loaded on the desalting column. The desalting column was placed in a clean collection tube and centrifuged (1000 x g; 2 minutes) to collect the conjugation sample. The collected conjugation sample was used to resuspend the obtained pellet and the resulting discontinuous epitope-mcKLH conjugate (**53-mcKLH**) was stored at -20 °C until immunization.

Immunization experiment. The immunization experiment was kindly carried out by collaborators at the MRC-University of Glasgow Centre for Virus Research. The mouse immunization experiments were approved by the University of Glasgow Animal Welfare and Ethical Board and were carried out under the Home Office Project License P9722FD8E held by Prof. Arvind H. Patel at the MRC-University of Glasgow Centre for Virus Research.

Four groups containing three mice each were injected subcutaneously with epitope-mcKLH conjugate (**39**-mcKLH, **40**-mcKLH, **41**-mcKLH, or **53**-mcKLH) mixed with Addavax (Invivogen) adjuvant (350 μL). Prime immunization was performed with 50 μg (131 μL) epitope-mcKLH conjugate (**39**-mcKLH, **40**-mcKLH, **39**-mcKLH, or **53**-mcKLH). After two weeks, the prime immunization was followed up by one boost immunization of 10 μg (26 μL) epitope-mcKLH conjugate (**39**-mcKLH, **40**-mcKLH, **41**-mcKLH, or **53**-mcKLH) every week for four weeks. The animals were sacrificed 8 days after the last boost immunization and sera were collected for binding assays.

Monoclonal antibodies. The mAb AP33[21] used in this work were kindly provided by Prof. Arvind Patel and co-workers.

General method for ELISA. The ELISA experiments were kindly carried out by collaborators at the MRC-University of Glasgow Centre for Virus Research.

Plate preparation: Immulon 2HB 96-well plates were coated with 1 μg/mL sE2 Gt1a H77 (purified from mammalian HEK-F cells) overnight at room temperature. After which, the wells were blocked overnight at room temperature with 200 μL 2% skimmed milk in PBST (phosphate buffered saline supplemented with 0.05% Tween®-20). Next, the wells were washed three times with PBST and used immediately or stored at -20°C until use.

Sera preparation: The blood was incubated for 1 hour at 37 °C and the tubes were flicked to dislodge the blood clot. Then, the tubes were incubated at 4 °C for 2 hours or overnight to enhance blood clotting. After which, the blood clots were centrifuged (10,000 g; 10 minutes) at 4 °C. Sera was collected from the blot clots and transferred to a fresh tube. The centrifugation/transfer step was repeated if necessary.

ELISA: Three-fold dilution series of sera were prepared starting from a 1:50 dilution (3 µL sera and 147 µL PBST) and added to the plates (100 µL/well). Monoclonal antibody AP33 was included as a positive control (3-fold dilution at starting concentrations: 2.0 µg/mL and 0.1 µg/mL). The plates were incubated for 1-2 hours at room temperature. After which, the plates were washed three times with PBST, before supplying 100 µL 1:3000 secondary α-mouse A4416 (Sigma) to each well. The plates were incubated for 1 hour at room temperature and washed six times with PBST. The plates were developed using 100 µL 3, 3', 5, 5' tetramethylbenzidine (TMB) solution per well, obtained from Life Technologies, and incubating for 10 minutes at room temperature. After which, development was stopped using 50 µL 0.5 M H_2SO_4 per well. Absorbance at 450 nm was measured on a Varioskan (Thermoscientific) instrument.

4.6 References

1. Bandyopadhyay, A. S., Garon, J., Seib, K., *et al.* (2015) Polio vaccination: past, present, and future. *Future Microbiol. 10*(5):791-808. DOI: 10.2217/fmb.15.19
2. Goodson, J. L., Seward, J. F. (2015) Measles 50 years after use of measles vaccine. *Infect. Dis. Clin. North. Am. 29*(4):725-743. DOI: 10.1016/j.idc.2015.08.001
3. Rios, A. (2018) Fundamental challenges to the development of a preventive HIV vaccine. *Curr. Opin. Virol. 29*:26-32. DOI: 10.1016/j.coviro.2018.02.004
4. Stephenson, K. E. (2018) Therapeutic vaccination for HIV: hopes and challenges. *Curr. Opin. HIV. AIDS. 13*(5):408-415. DOI: 10.1097/COH.0000000000000491
5. Honegger, J. R., Zhou, Y., Walker, C. M. (2014) Will there be a vaccine to prevent HCV infection? *Semin. Liver Dis. 34*(1):79-88. DOI: 10.1055/s-0034-1371081
6. Shoukry, N. H. (2018) Hepatitis C vaccines, antibodies, and T cells. *Front. Immunol. 9*:1480. DOI: 10.3389/fimmu.2018.01480
7. Baily, J. R., Barnes, E., Cox, A. L. (2019) Approaches, progress, and challenges to hepatitis C vaccine development. *Gastroenterology. 156*(2):418-430. DOI: 10.1053/j.gastro.2018.08.060
8. Neumann, A. U., Lam, N. P., Dahari, H., *et al.* (1998) Hepatitis C viral dynamics in vivo and the antiviral efficacy of interferon-alpha therapy. *Science. 282*(5386):103-107. DOI: 10.1126/science.282.5386.103
9. Rong, L., Dahari, H., Ribeiro, R. M., *et al.* (2010) Rapid emergence of protease inhibitor resistance in hepatitis C virus. *Sci. Transl. Med. 2*(30):30ra32. DOI: 10.1126/scitranslmed.3000544
10. Dustin, L. B. (2017) Innate and adaptive immune responses in chronic HCV infection. *Curr. Drug Targets. 18*(7):826-843. DOI: 10.2174/1389450116666150825110532
11. Horner, S. M., Gale, M. Jr. (2013) Regulation of hepatic innate immunity by hepatitis C virus. *Nat. Med. 19*(7):879–888. DOI: 10.1038/nm.3253
12. Helle, F., Duverlie, G., Dubuisson, J. (2011) The hepatitis C virus glycan shield and evasion of the humoral response. *Viruses. 3*(10):1909-1932. DOI: 10.3390/v3101909
13. Catanese, M. T., Uryu, K., Kopp, M., *et al.* (2013) Ultra-structural analysis of hepatitis C virus particles. *Proc. Natl. Acad. Sci. USA. 110*(23):9505-9510. DOI:10.1073/pnas.1307527110

14. Mondelli, M. U., Cerino, A., Segagni, L., *et al.* (2001) Hypervariable region 1 of hepatitis C virus: Immunological decoy or biologically relevant domain? *Antiviral Res. 52*(2):153-159. DOI: 10.1016/SO166-3542(01)00180-2
15. Werkhoven, P. R., Liskamp, R. M. J. (2013) Chemical approaches for localization, characterization and mimicry of peptide loops. *RSC Drug Discovery Series No. 36. Biotherapeutics: Recent Developments using Chemical and Molecular Biology* (Jones, L. H. and McKnight, A. J., Eds.) pp. 263–284, Chapter 10, The Royal Society of Chemistry, Cambride
16. Gross, A., Hashimoto, C., Sticht, H., *et al.* (2015) Synthetic peptide as protein mimics. *Front. Bioeng. Biotechnol. 3*:211. DOI: 10.3389/fbioe.2015.00211
17. Merriflied, R. B. (1963) Solid phase peptide synthesis. I. The synthesis of a tetrapeptide. *J. Am. Chem. Soc. 85*(14):2149-2154. DOI: 10.1021/ja00897a025
18. Merrifield, B. (1986) Solid phase Synthesis. *Science. 232*(4748):341-347. DOI: 10.1126/science.3961484
19. Hijnen, M., Van Zoelen, D. J., Chamorro, C., *et al.* (2007) A novel strategy to mimic discontinuous protective epitopes using a synthetic scaffold. *Vaccine. 25*(37-38):6807-6817. DOI: 10.1016/vaccine.2007.06.027
20. Werkhoven, P. R., Van de Langemheen, H., Van der Wal, S., Kruijtzer, J. A. W, Liskamp, R. M. J. (2014) Versatile convergent synthesis of a three peptide loop containing protein mimic of whooping cough pertactin by successive Cu(I)-catalyzed azide alkyne cycloaddition on an orthogonal alkyne functionalized TAC-scaffold. *J. Pept. Sci*. *20*(4):235-239. DOI: 10.1002/psc.2624
21. Owsianka, A., Tarr, A. W., Juttla, V. S., *et al.* (2005) Monoclonal antibody AP33 defines a broadly neutralizing epitope on the hepatitis C virus E2 envelope glycoprotein. *J. Virol. 79*(11):11095-11104. DOI: 10.1128/JVI.79.17.11095-11104.2005
22. Tarr, A. W., Owsianka, A. M., Timms, J. M., *et al.* (2006) Characterization of the hepatitis C virus epitope defined by the broadly neutralizing monoclonal antibody AP33. *Hepatology. 43*(3):592-601. DOI: 10.1002/hep21088
23. Meola, A., Tarr, A. W., England, P., *et al.* (2015) Structural flexibility of a conserved antigenic region in hepatitis C virus glycoprotein E2 recognized by broadly neutralizing antibodies. *J. Virol. 89*(4): 2170-2181. DOI: 10.1128/JVI.02190-14
24. Keck, Z. Y., Xia, J., Wang, Y., *et al.* (2012) Human monoclonal antibodies to a novel cluster of conformational epitopes on HCV E2 with resistance to

neutralization escape in a genotype 2a isolate. *PLoS Pathog. 8*(4):e1002653. DOI: 10.1371/journal.ppat.1002653

25. Krey, T., Meola, A., Keck, Z. Y., *et al.* (2013) Structural basis of HCV neutralization by human monoclonal antibodies resistant to viral neutralization escape. *PLOS Pathog. 9*(5):e1003364. DOI: 10.1371/journal.ppat.1003364
26. Cowton, V. M., Singer, J. B., Gifford, R. J., *et al.* (2018) Predicting the effectiveness of hepatitis C virus neutralizing antibodies by bioinformatics analysis of conserved epitope residues using public sequence data. *Front Immunol. 9*:1470. DOI: 10.3389/fimmu.2018.01470
27. Vasiliauskaite, I., Owsianka, A., England, P., *et al.* (2017) Conformational flexibility in the immunoglobulin-like domain of the hepatitis C virus glycoprotein E2. *MBio. 8*(3):e00382-17. DOI: 10.1128/mBio.00382-17
28. Kong, L., Giang, E., Nieusma, T., *et al.* (2013) Hepatitis C virus E2 envelope glycoprotein core structure. *Science. 342*(6162):1090-1094. DOI: 10.1126/science.1243876
29. Opatz, T., Liskamp, R. M. J. (2001) A selectively deprotectable triazacyclophanescaffold for the construction of artificial receptors. *Org. Lett.* 3(22):3499–3502. DOI: 10.1021/oi0101741
30. Longin, O., Van de Langemheen, H., Liskamp, R. M. J. (2017) An orthogonally protected cyclotriveratrylene (CTV) as a highly pre-organized molecular scaffold for subsequent ligation of different cyclic peptides towards protein mimics. *Bioorg. Med. Chem. 25*(18):5008-5015. DOI:10.1016/j.bmc.2017.05.038
31. Longin, O., Hezwani, M., Van de Langemheen, H., *et al.* (2018) Synthetic antibody protein mimics of infliximab by molecular scaffolding on novel CycloTriVeratrilene (CTV) derivatives. *Org. Biomol. Chem. 16*(29):5254-5274. DOI: 10.1039/c8ob01104d
32. Werkhoven, P. R., Elwakiel, M., Meuleman, T. J., *et al.* (2016) Molecular construction of HIV-gp120 discontinuous epitope mimics by assembly of cyclic peptides on an orthogonal alkyne functionalized TAC-scaffold. *Org. Biomol. Chem. 14*(2):701-710. DOI: 10.1039/c5ob02014j
33. Meuleman, T. J., Dunlop, J. I., Owsianka, A. M., *et al.* (2018) Immobilization by surface conjugation of cyclic peptides for effective mimicry of the HCV-envelope E2 protein as a strategy toward synthetic vaccines. *Bioconjug. Chem. 29*(4):1091-1101. DOI: 10.1021/acs.bioconjchem.7b00755

34. Van de Langemheen, H., Korotkovs, V., Bijl, J., *et al.* (2017) Polar hinges as functionalized conformational constraints in (bi)cyclic peptides. *ChemBioChem. 18*(4):387-395. DOI: 10.1002/cbic.201600612
35. Meuleman, T. J., Cowton, V. M., Patel, A. H., *et al.* (*in press*) Improving the aqueous solubility of HCV-E2 glycoprotein epitope mimics by cyclization using polar hinges. *J. Pep. Sci. X*(X):XXX-XXX
36. Harris J.R., Markl, J. (1999) Keyhole limpet hemocyanin (KLH): A biomedical review. *Micron. 30*(6):597-623. DOI: 10.1016/S0968-4328(99)00036-0
37. Prentoe, J., Velázquez-Moctezuma, R., Augestad, E. H., *et al.* (2019) Hypervariable region 1 and N-linked glycans of hepatitis C regulate virion neutralization by modulating envelope conformations. *Proc. Natl. Acad. Sci. USA. 116*(20):10039-10047. DOI: 10.1073/pnas.1822002116
38. Sandomenico, A., Leonardi, A., Berisio, R., *et al.* (2016) Generation and characterization of monoclonal antibodies against a cyclic variant of hepatitis C virus E2 epitope 412-422. *J. Virol. 90*(7):3745-3759. DOI: 10.1128/jvi.02397-15
39. Pierce, B. G., Boucher, E. N., Piepenbrink, K. H., *et al.* Structure-based design of hepatitis C virus vaccines that elicit neutralizing antibodies responses to a conserved epitope. *J. Virol. 91*(20):e01032-17. DOI: 10.1128/jvi.01032-17
40. Bartosch, B., Dubuisson, J., Cosset, F. L. (2003) Infectious hepatitis C virus pseudo-particles containing functional E1-E2 envelope protein complexes. *J. Exp. Med. 197*(5):633-642. DOI: 10.1084/jem.20021756
41. Sandrin, V., Boson, B., Salmon, P., *et al.* (2002) Lentiviral vectors pseudotyped with a modified RD114 envelope glycoprotein show increased stability in sera and augmented transduction of primary lymphocytes and CD34+ cells derived from human and non-human primates. *Blood. 100*(3):823-832. DOI: 10.1182/blood-2001-11-0042
42. Ott, D. E. (1997) Cellular proteins in HIV virions. *Rev. Med. Virol. 7*(3):167-180. DOI: unavailable
43. Sung, V. M., Lai, M. M. (2002) Murine retroviral pseudo-type virus containing hepatitis B virus large and small surface antigens confers specific tropism for primary human hepatocytes: A potential liver-specific targeting system. *J. Virol. 75*(2):912-917. DOI: 10.1128/jvi.76.2.912-917.2002
44. Nègre, D., Duisit, G., Mangeot, P. E. (2002) Lentiviral vectors derived from simian immunodeficiency virus (SIV). *Curr. Top. Microbiol. Immunol. 261*:53-74. DOI: 10.1007/978-3-642-56114-6 3